

VERTICAL TRANSPORT AND DYNAMIC SIZE DISTRIBUTION OF
NEW BEDFORD HARBOR SEDIMENTS

A Thesis

by

STEPHANIE CAROL SANDERS

Submitted to the Office of Graduate Studies of
Texas A&M University
in partial fulfillment of the requirements for the degree of

MASTER OF SCIENCE

August 1990

Major Subject: Civil Engineering

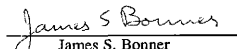
VERTICAL TRANSPORT AND DYNAMIC SIZE DISTRIBUTION OF
NEW BEDFORD HARBOR SEDIMENTS

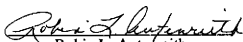
A Thesis


by

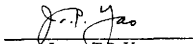
STEPHANIE CAROL SANDERS

Approved as to style and content by:


James S. Bonner
(Chair of Committee)


Robin L. Auterfreith
(Member)


Wayne R. Jordan
(Member)


James T.P. Yao
(Head of Department)

August 1990

ABSTRACT

Vertical Transport and Dynamic Size Distribution of
New Bedford Harbor Sediments. (August 1990)

Stephanie Carol Sanders, B.S., Texas A&M University;
M.S., Texas A&M University

Chair of Advisory Committee: Dr. James S. Bonner

A one dimensional particle transport model was developed to aid in the assessment of particle mediated transport of pollutants within the New Bedford Harbor Superfund Site. A mixed settling column was used to obtain vertical settling rates for cohesive particles under varying salinities, shear rates, particle concentrations, and particle types. The settling column was two meters in height and thirty centimeters in diameter. Impellers were placed down the length of the column and the mixing speed was computer controlled. The particles used in this column were obtained from three different locations within the New Bedford Harbor Superfund Site. Samples were analyzed on a Coulter Counter, AVC-80 Suspended Solids machine, and a HACH Model 2100A Turbidimeter. A vertical transport model, which included flocculation and floc breakup, was developed and calibrated with these laboratory data. Particle size distributions as well as total particle number and volume over time were produced and analyzed. Results show that particles will flocculate, and that shear rate has the greatest affect on settling. The lowest shear rate (10 sec^{-1}) produced the greatest settling velocity while higher shear rates (40 sec^{-1}) reduced the vertical transport of the particles. Salinity appeared to have an effect, but was overshadowed by the shear rates at which these tests were performed. Particle type showed no variation due to the similar properties between the sediments, and no conclusion could be drawn concerning concentration effect on settling velocity over the concentration range studied (10 to 80 mg/l).

The results will be used along with hydrodynamic data to assess the transport of particles resuspended by proposed dredging operations to remediate the underwater New Bedford Harbor Superfund Site.

DEDICATION

I would like to dedicate this thesis to my mother and father, Carolyn and Robert, and my brother, Jeff. Their belief in me often gave me much needed encouragement to complete my project. They were there for me in times of darkness and sunshine.

ACKNOWLEDGEMENT

I would like to thank Dr. Bonner for his continual support and guidance. His comments and suggestions were invaluable to me. I would also like to the Dr. Robin Autenrieth and Dr. Wayne Jordan for serving on my committee.

This research was conducted under USEPA Grant #CR-814257-01, "Study Of Processes Affecting Particle-Mediated Transport Of Hazardous Material In Marine Systems." Special thanks go to Dr. J.F. Paul for continual support of this project.

The list of appreciation to those who helped me technically is long. I am especially grateful to Sharon Ducharme for her friendship and ground breaking work on this project. Without her, progress would indeed be slow. Andy Ernest also deserves a special thanks for his programming and insight regarding modeling efforts. The road would definitely be long and hard without him. I would like to thank the following people for lending their technical help from time to time on my project; Mickey, Daniel, Cindy, Katrine, Lea, Terrell, Rob, Jeff, Carla, and Ravi.

The list of thanks would not be complete without including the friends that have supported me throughout my thesis work. I would like to thank Virginia Standefer for being not only a roommate for years on end, but also a best friend. I would also like to thank Tammy Nechita for her encouragement, much needed laughter, and invaluable friendship. Last, but not least, I would like to thank Emily McCreary for her support as a terrific friend and technical insight as a fellow grad student. I couldn't have survived grad school without all my friends at A&M!

TABLE OF CONTENTS

	Page
ABSTRACT.....	iii
DEDICATION.....	v
ACKNOWLEDGEMENT.....	vi
TABLE OF CONTENTS.....	vii
LIST OF TABLES.....	ix
LIST OF FIGURES.....	x
CHAPTER	
I INTRODUCTION.....	1
Problem Statement.....	1
Objectives.....	4
II LITERATURE REVIEW.....	6
Flocculation.....	6
Collisions.....	7
Brownian.....	8
Shear.....	8
Differential Settling.....	9
Floc Breakup.....	9
Settling Factors.....	13
Particle Type.....	13
Salinity.....	18
Particle Concentration.....	20
Shear Rate.....	22
III EXPERIMENTAL METHODS.....	28
Experimental Design.....	28
Instrumentation.....	31
Settling Column.....	32
Electronic Particle Counter.....	34
Suspended Solids and Turbidity.....	35
Density Meter.....	35
Experimental Procedures.....	36
Data Analysis.....	39
Initial Concentration Determination.....	39
Experimental Duplication.....	43

CHAPTER	Page
IV	MODEL DEVELOPMENT..... 44
	Model Framework..... 44
	Advection-Dispersion..... 49
	Flocculation..... 54
	Porosity..... 58
	Alpha and Dispersion as Size Dependant Parameters..... 60
	Resuspension..... 63
	Floc Breakup..... 65
	Correlation Coefficients..... 66
	Statistical Analysis..... 70
V	RESULTS AND DISCUSSION..... 72
	Observed and Predicted Results..... 72
	Particle Number Distribution..... 73
	Particle Volume Distribution..... 81
	Design 1: Variation of Concentraion..... 83
	Alpha..... 91
	Erosion..... 92
	Design 2: Variation of Shear and Salinity..... 94
	Alpha..... 102
	Erosion..... 103
	Design 3: Variation of Salinity and Particle Type... 106
	Alpha..... 106
	Erosion..... 107
	Resuspension..... 108
VI	SUMMARY AND CONCLUSIONS..... 111
	REFERENCES..... 113
	APPENDIX A..... 121
	APPENDIX B..... 126
	APPENDIX C..... 134
	APPENDIX D..... 157
	APPENDIX E..... 160
	APPENDIX F..... 259
	APPENDIX G..... 265
	VITA..... 266

LIST OF TABLES

TABLE	Page
1. 1 X 3 X 1 X 1 Concentration Design.....	30
2. 3 X 1 X 3 X 1 Shear and Salinity Design.....	31
3. 1 X 1 X 3 X 3 Particle Type and Salinity Design.....	31
4. Particle Reynolds Numbers.....	51
5. Analysis of Variance.....	71

LIST OF FIGURES

FIGURE	Page
1. New Bedford Harbor	2
2. Splitting of Particle of Size k	10
3. Erosion of Particle of Size k	11
4. Estimated Densities and Settling Velocities (Adapted from McCave, 1975).....	16
5. Densities from Logan and Hunt and McCave.....	17
6. Settling Velocities from Logan and Hunt and McCave.....	18
7. Alpha as a Function of Salinity for Clay Size Fraction of Pamlico Sediments (Adapted from Edzwald, et al. 1974).....	19
8. Variation of Particle Settling Velocity with Salinity (Adapted from Burt 1986).....	21
9. Settling Column Schematic from Ducharme 1989.....	33
10. Variation of Initial Particle Number Concentration with Particle Volume.....	41
11. Variation of Particle Number Concentration with Suspended Solids.....	42
12. Variation of Particle Volume Concentration with Suspended Solids.....	42
13. Particle Size Categories.....	46
14. Column Segments.....	47
15. Variation of Dispersion in Relation to Particle Size and Peclet Number.....	50

FIGURE	Page
16. Experiment 16: Heterogeneous Particle Size Distribution Observed with Shear of 10 sec^{-1} , Salinity of 15 ppt, Type A Sediment, and Suspended Solids of 40 mg/l at a depth of 34.4 cm.....	52
17. Experiment 16: Heterogeneous Particle Size Distribution Predicted with Shear of 10 sec^{-1} , Salinity of 15 ppt, Type A Sediment, and Suspended Solids of 40 mg/l at a depth of 34.4 cm (Advection-dispersion only).....	53
18. Experiment 16: Heterogeneous Particle Size Distribution Predicted with Shear of 10 sec^{-1} , Salinity of 15 ppt, Type A Sediment, and Suspended Solids of 40 mg/l at a depth of 34.4 cm.....	55
19. Experiment 8: Total Volume Observed and Predicted for Depths (a) 34.4 cm; (b) 70.2 cm; (c) 106.0 cm; and (d) 141.8 cm with G of 20 sec^{-1} and ∞ of 0.1.....	56
20. Experiment 5: Total Volume Observed and Predicted for Depths (a) 34.4 cm; (b) 70.2 cm; (c) 106.0 cm; and (d) 141.8 cm with G of 30 sec^{-1} and ∞ of 0.1.....	57
21. Experiment 6: Total Volume Observed and Predicted for Depths (a) 34.4 cm; (b) 70.2 cm; (c) 106.0 cm; and (d) 141.8 cm with G of 40 sec^{-1} and ∞ of 0.1.....	59
22. Experiment 16: Total Volume Observed and Predicted with ∞ 1-7 Equal to 0.05, 0.10, 0.15, 0.20, 0.25, 0.30, and 0.35, Respectively for Depths (a) 34.4 cm; (b) 70.2 cm; (c) 106.0 cm; and (d) 141.8 cm.....	61

FIGURE	Page
23. Experiment 16: Total Volume Observed and Predicted with $\infty 1.7$ Equal to 0.80, 0.80, 0.80, 0.85, 0.85, 0.90, and 0.90, Respectively for Depths (a) 34.4 cm; (b) 70.2 cm; (c) 106.0 cm; and (d) 141.8 cm.....	62
24. Experiment 21: Total Volume Observed and Predicted with $\infty 1.7$ Equal to 0.05, 0.10, 0.15, 0.20, 0.25, 0.30, and 0.35, Respectively for Depths (a) 34.4 cm; (b) 70.2 cm; (c) 106.0 cm; and (d) 141.8 cm.....	64
25. Experiment 20: Total Volume Observed and Predicted for Depths (a) 34.4 cm; (b) 70.2 cm; (c) 106.0 cm; and (d) 141.8 cm with G of 20 sec ⁻¹	67
26. Experiment 3: Total Volume Observed and Predicted for Depths (a) 34.4 cm; (b) 70.2 cm; (c) 106.0 cm; and (d) 141.8 cm with G of 30 sec ⁻¹	68
27. Experiment 21: Total Volume Observed and Predicted for Depths (a) 34.4 cm; (b) 70.2 cm; (c) 106.0 cm; and (d) 141.8 cm with G of 40 sec ⁻¹	69
28a. Experiment 7: Heterogeneous Particle Number-Based Observed Size Distribution with Shear of 20 sec ⁻¹ , Salinity of 15 ppt, Type A Sediment, and Suspended Solids of 10 mg/l at a Depth of 34.4 cm.....	74
28b. Experiment 7: Heterogeneous Particle Number-Based Observed Size Distribution with Shear of 20 sec ⁻¹ , Salinity of 15 ppt, Type A Sediment, and Suspended Solids of 10 mg/l at a Depth of 141.8 cm.....	74

FIGURE	Page
29a. Experiment 7: Heterogeneous Particle Number-Based Predicted Size Distribution with Shear of 20 sec ⁻¹ , Salinity of 15 ppt, Type A Sediment, and Suspended Solids of 10 mg/l at a Depth of 34.4 cm.....	75
29b. Experiment 7: Heterogeneous Particle Number-Based Predicted Size Distribution with Shear of 20 sec ⁻¹ , Salinity of 15 ppt, Type A Sediment, and Suspended Solids of 10 mg/l at a Depth of 141.8 cm.....	75
30a. Experiment 7: Heterogeneous Particle Volume-Based Observed Size Distribution with Shear of 20 sec ⁻¹ , Salinity of 15 ppt, Type A Sediment, and Suspended Solids of 10 mg/l at a Depth of 34.4 cm.....	76
30b. Experiment 7: Heterogeneous Particle Volume-Based Observed Size Distribution with Shear of 20 sec ⁻¹ , Salinity of 15 ppt, Type A Sediment, and Suspended Solids of 10 mg/l at a Depth of 141.8 cm.....	76
31a. Experiment 7: Heterogeneous Particle Volume-Based Predicted Size Distribution with Shear of 20 sec ⁻¹ , Salinity of 15 ppt, Type A Sediment, and Suspended Solids of 10 mg/l at a Depth of 34.4 cm.....	78
31b. Experiment 7: Heterogeneous Particle Volume-Based Predicted Size Distribution with Shear of 20 sec ⁻¹ , Salinity of 15 ppt, Type A Sediment, and Suspended Solids of 10 mg/l at a Depth of 141.8 cm.....	78

FIGURE	Page
32. Experiment 7: Total Particle Number Observed and Predicted for Depths (a) 34.4 cm; (b) 70.2 cm; (c) 106.0 cm; and (d) 141.8 cm with Shear of 20 sec ⁻¹ , Salinity of 15 ppt, Type A Sediment, and Suspended Solids of 10 mg/l.....	80
33a. Experiment 8: Heterogeneous Particle Number-Based Observed Size Distribution with Shear of 20 sec ⁻¹ , Salinity of 15 ppt, Type A Sediment, and Suspended Solids of 40 mg/l at a Depth of 34.4 cm.....	84
33b. Experiment 8: Heterogeneous Particle Number-Based Observed Size Distribution with Shear of 20 sec ⁻¹ , Salinity of 15 ppt, Type A Sediment, and Suspended Solids of 40 mg/l at a Depth of 141.8 cm.....	84
34a. Experiment 8: Heterogeneous Particle Volume-Based Observed Size Distribution with Shear of 20 sec ⁻¹ , Salinity of 15 ppt, Type A Sediment, and Suspended Solids of 40 mg/l at a Depth of 34.4 cm.....	85
34b. Experiment 8: Heterogeneous Particle Volume-Based Observed Size Distribution with Shear of 20 sec ⁻¹ , Salinity of 15 ppt, Type A Sediment, and Suspended Solids of 40 mg/l at a Depth of 141.8 cm.....	85
35a. Experiment 9: Heterogeneous Particle Number-Based Observed Size Distribution with Shear of 20 sec ⁻¹ , Salinity of 15 ppt, Type A Sediment, and Suspended Solids of 80 mg/l at a Depth of 34.4 cm.....	86

FIGURE	Page
35b. Experiment 9: Heterogeneous Particle Number-Based Observed Size Distribution with Shear of 20 sec ⁻¹ , Salinity of 15 ppt, Type A Sediment, and Suspended Solids of 80 mg/l at a Depth of 141.8 cm.....	86
36. Experiment 8: Total Particle Number Observed and Predicted for Depths (a) 34.4 cm; (b) 70.2 cm; (c) 106.0 cm; and (d) 141.8 cm with Shear of 20 sec ⁻¹ , Salinity of 15 ppt, Type A Sediment, and Suspended Solids of 40 mg/l.....	88
37. Experiment 7: Total Particle Volume Observed and Predicted for Depths (a) 34.4 cm; (b) 70.2 cm; (c) 106.0 cm; and (d) 141.8 cm with Shear of 20 sec ⁻¹ , Salinity of 15 ppt, Type A Sediment, and Suspended Solids of 10 mg/l.....	89
38. Experiment 8: Total Particle Volume Observed and Predicted for Depths (a) 34.4 cm; (b) 70.2 cm; (c) 106.0 cm; and (d) 141.8 cm with Shear of 20 sec ⁻¹ , Salinity of 15 ppt, Type A Sediment, and Suspended Solids of 40 mg/l.....	90
39. The Effect of Concentration on Alpha.....	91
40. The Effect of Particle Concentration on the Erosion Constant.....	93
41. The Effect of Particle Concentration on the Geometric Mean.....	93
42. The Effect of Particle Concentration on the Geometric Standard Deviation.....	94
43a. Experiment 18: Heterogeneous Particle Number-Based Observed Size Distribution with Shear of 20 sec ⁻¹ , Salinity of 15 ppt, Type A Sediment, and Suspended Solids of 40 mg/l at a Depth of 34.4 cm.....	95

FIGURE	Page
43b. Experiment 18: Heterogeneous Particle Number-Based Observed Size Distribution with Shear of 20 sec ⁻¹ , Salinity of 15 ppt, Type A Sediment, and Suspended Solids of 40 mg/l at a Depth of 141.8 cm.....	95
44a. Experiment 2: Heterogeneous Particle Number-Based Observed Size Distribution with Shear of 30 sec ⁻¹ , Salinity of 15 ppt, Type A Sediment, and Suspended Solids of 40 mg/l at a Depth of 34.4 cm.....	96
44b. Experiment 2: Heterogeneous Particle Number-Based Observed Size Distribution with Shear of 30 sec ⁻¹ , Salinity of 15 ppt, Type A Sediment, and Suspended Solids of 40 mg/l at a Depth of 141.8 cm.....	96
45a. Experiment 6: Heterogeneous Particle Number-Based Observed Size Distribution with Shear of 40 sec ⁻¹ , Salinity of 15 ppt, Type A Sediment, and Suspended Solids of 40 mg/l at a Depth of 34.4 cm.....	97
45b. Experiment 6: Heterogeneous Particle Number-Based Observed Size Distribution with Shear of 40 sec ⁻¹ , Salinity of 15 ppt, Type A Sediment, and Suspended Solids of 40 mg/l at a Depth of 141.8 cm.....	97
46a. Experiment 18: Heterogeneous Particle Volume-Based Observed Size Distribution with Shear of 20 sec ⁻¹ , Salinity of 15 ppt, Type A Sediment, and Suspended Solids of 40 mg/l at a Depth of 34.4 cm.....	99

FIGURE	Page
46b. Experiment 18: Heterogeneous Particle Volume-Based Observed Size Distribution with Shear of 20 sec ⁻¹ , Salinity of 15 ppt, Type A Sediment, and Suspended Solids of 40 mg/l at a Depth of 141.8 cm.....	99
47a. Experiment 2: Heterogeneous Particle Volume-Based Observed Size Distribution with Shear of 30 sec ⁻¹ , Salinity of 15 ppt, Type A Sediment, and Suspended Solids of 40 mg/l at a Depth of 34.4 cm.....	100
47b. Experiment 2: Heterogeneous Particle Volume-Based Observed Size Distribution with Shear of 30 sec ⁻¹ , Salinity of 15 ppt, Type A Sediment, and Suspended Solids of 40 mg/l at a Depth of 141.8 cm.....	100
48a. Experiment 6: Heterogeneous Particle Volume-Based Observed Size Distribution with Shear of 40 sec ⁻¹ , Salinity of 15 ppt, Type A Sediment, and Suspended Solids of 40 mg/l at a Depth of 34.4 cm.....	101
48b. Experiment 6: Heterogeneous Particle Volume-Based Observed Size Distribution with Shear of 40 sec ⁻¹ , Salinity of 15 ppt, Type A Sediment, and Suspended Solids of 40 mg/l at a Depth of 141.8 cm.....	101
49. The Effect of Shear and Salinity on Alpha.....	103
50. The Effect of Shear and Salinity on the Erosion Constant.....	104
51. The Effect of Shear and Salinity on the Geometric Standard Deviation.....	105
52. The Effect of Shear and Salinity on the Geometric Mean.....	106

FIGURE	Page
53. The Effect of Salinity and Particle Type on Alpha.....	107
54. The Effect of Salinity and Particle Type on the Erosion Constant.....	108
55. The Effect of Salinity and Particle Type on the Geometric Mean.....	109
56. The Effect of Salinity and Particle Type on the Geometric Standard Deviation.....	109
57. Shear and Salinity Affect on the Resuspension Constant.....	110
58. Resuspension Effect in the Column Based on Model Results.....	110

CHAPTER I

INTRODUCTION

PROBLEM STATEMENT

New Bedford Harbor, Massachusetts, an estuary of national concern, is located northeast of Narragansette Bay, just north of Buzzards Bay (Fig. 1). The Acushnet River serves as fresh water inflow to this narrow harbor that opens into Buzzards Bay. The harbor is considered a vertically well-mixed, shallow estuary (Teeter 1988). Salinity variation only occurs during heavy rains and can be as much as 18 ppt. The harbor has several constrictions, Coggeshal Street Bridge, Popes Island, and the hurricane barrier, that cause great deviation in currents while having little affect on tides (Teeter 1988). Because of discharge and dumping by adjacent industries, contamination has reached disastrous levels within the harbor.

Heavy metals and various organic chemicals are present in New Bedford Harbor bottom sediments with the upper one foot having the greatest contamination (Palermo, et al. 1988). Heavy metals such as cadmium, copper, chromium, iron, nickel, lead, and zinc have been detected in sediments throughout the harbor by Pruell, et al. (1989). Wade (1988) detected these same elements, but in differing concentrations. Organic chemicals such as chlorinated dibenzo-p-dioxins, chlorinated dibenzofurans, polyaromatic hydrocarbons (PAHs), and polychlorinated biphenyls (PCBs) have all been detected.

PCB concentrations in the sediments range from only a few parts per million (ppm) to over 100,000 ppm which exceeds the 50 ppm regulatory limit (Francingues, et al. 1988). The PCB concentration in the water column is in the parts per billion (ppb) range. Elutriate tests have shown concentrations of up to 0.22 mg/l which exceeds the marine water quality criteria of 0.01 mg/l (Averett 1988). Due to the hydrophobic nature of

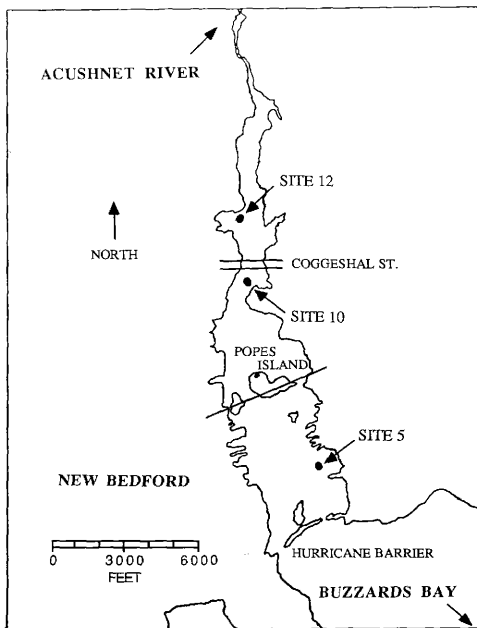


Fig. 1.- New Bedford Harbor

PCBs, contaminant sorption onto sediments, thus transport, is a high probability.

Sorption is greatly dependant on the type and size of particle within a system. Studies with Saginaw Bay sediments have shown that hexachlorobiphenyl (HCBP) adsorbs readily to sediments while adsorption to montmorillonite and kaolinite samples was weaker (Horzempa, et al. 1983). The difference in particle surface charge determines sorption rate. These surface charges can be greatly affected by organic sorption (Sholkovitz 1976). Sorbed organics can compose as much as 10% of the total sediment load (Humby 1975). These organics tend to "stick" particles together, thus forming a "new" particle (floc) of greater diameter. As surface area increases, so does the number of sorption sites. This is the main adsorption factor in coastal environments (Hiraizumi, et al. 1979).

Contaminants can also be released (desorbed). As particles flocculate in an estuary, desorption can occur. Mass transfer analysis predicts that after one half of the sorbate is sorbed (assuming loose surface sorption), collision-induced desorption becomes important (Mackay, et al. 1987). This limits the sorbed concentration to equal approximately that of the amount remaining in solution. Desorption can occur with organisms, but at a lower rate than that of adsorption. This has been seen with phytoplankton and zooplankton (Hiraizumi, et al. 1979). The organisms and sediments that sorb pollutants are consumed by larger organisms, thus the contaminant is distributed throughout the food chain.

In 1982, New Bedford Harbor, Massachusetts, was designated as a Federal Superfund site. The U.S. Army Corps of Engineers was enlisted in 1984 by the Environmental Protection Agency to report on the feasibility of remediation alternatives. All but one of the alternatives include dredging: 1) channelizing the Acushnet River north of the Coggeshall Street Bridge and capping contaminated sediments; 2) dredging contaminated sediments and placement in a side-lined containment site; 3) dredging the sediments and placement in a bottom and side lined containment site; 4) dredging

sediments and disposal on land; and 5) dredging contaminated and clean sediments, temporarily storing both, and placement in a constructed cell in the channel bottom with a cap of clean sediments (confined aquatic disposal, CAD) (Francingues, et al. 1988). Dredging activities increase turbidity (or the amount of sediment in the water column) through resuspension and spillage (Blokland 1989). Resuspension occurs from disturbance of the bottom or escape of gas from the sediments. Spillage occurs during the transport of the sediments from the bottom, overflow from hopper dredges, release of degassing water by the dredge, and pumping overboard of the lean mixture. The combination of dredging activities and estuary characteristics will determine the extent of sediment suspension and transport.

The vertical settling rates of sediments must be compared with vertical and horizontal hydrodynamic transport (advection and dispersion due to tides, winds, and currents). If the total vertical transport rate is much slower than the horizontal rate, sediments, thus contaminants, will reside in the flow and be transported away from the site. Fast settling particles will not remain suspended and will be concentrated near the site of resuspension. Vertical transport is governed by system hydrodynamics as well as particle characteristics such as density, size, and flocculation potential which all affect particle settling rates. The extent of both vertical and horizontal transport must be determined in order to accurately evaluate remediation techniques.

OBJECTIVES

The goal of this research is to determine the effect of environmental parameters (specific to New Bedford Harbor sediments) on vertical transport rates. These parameters will be laboratory controlled and include shear, salinity, particle concentration, and particle type effects. A model will be developed to describe vertical settling due to dispersion, advection, and flocculation. These vertical settling rates will be an integral part of a full-scale estuary model which incorporates hydrodynamic forces. The

determination of the extent of interactions between the above parameters on vertical settling will be achieved by completing the following objectives:

- 1) Define a particle characterization procedure for determining dynamic particle size distributions within a settling column.
- 2) Perform suspended solids, turbidity, and density tests to determine mass flux over space and time within the column.
- 3) Define particle settling velocities and dynamic size distributions based on four separate settling parameters; shear rate, salinity, particle type, and particle concentration within the system.
- 4) Assess the influence of flocculation processes on vertical transport of New Bedford Harbor sediments.
- 5) Determine the transport mechanisms by modeling the observed data with a one-dimensional transport model.

CHAPTER II

LITERATURE REVIEW

Sediments in an estuary originate from land sources (rivers, manmade structures, and dumping), oceanic sources (salinity currents, coastal wave action, and flood tides), and the estuary itself (erosion and marine life) (Humby 1975). Sediment transport occurs in three directions; large particles settle vertically (z), and smaller particles are horizontally transported in two directions (x and y). Typically some sediment is suspended in the water column at all times. This background of particles is referred to as the turbidity level for a given system. Dyer (1972) reports suspended solids measurements of 10 to 20 mg/l with particle diameters of 3 to 4 microns for many estuaries. Teeter (1988) gives a typical suspended solids level of 10 mg/l, with 40 mg/l for extreme conditions in New Bedford Harbor. The settling of particles is dependant on sediment type, particle concentration, salinity, and shear present in a system. If conditions are favorable, large aggregates can form which settle relatively fast. Particle aggregation is a well documented phenomenon; Brun-Cottan (1976), Edzwald (1974), Humby (1975), Hunt (1984), Krank (1975), Lavelle (1988), Lick (1982), Luck (1970), and McCave (1975). While enhancing settling velocities, aggregation (flocculation) complicates the prediction of particle size distributions and settling velocities because of continual formation and breakup. The following sections describe flocculation (collision and breakup) and settling factors important to settling velocity determination.

FLOCCULATION

The term flocculation is often used interchangeably with aggregation. Flocculation occurs when two or more particles adhere to form a larger particle. Formation of a larger particle yields higher settling velocities due to increased diameter. The importance of this

can be seen with Stokes equation:

$$V_s = \frac{g(\rho_p - \rho_l)d^2}{18\mu} \quad (1)$$

where d is particle diameter, g is acceleration due to gravity, ρ_l is liquid density, ρ_p is particle density, μ is viscosity, and V_s is settling velocity. The use of this equation requires quantification of particle density and diameter which can be difficult for flocculent systems due to continual floc breakup and reformation. Collision of particles must be quantified before an accurate density or diameter can be determined for modeling purposes.

Collisions

The number of collisions between i and j size particles (N_{ij}) can be defined in terms of particle number concentrations (n_i and n_j) and a collision frequency function β as described by:

$$N_{ij} = \beta(d_i, d_j) n_i n_j \quad (2)$$

where β is a function of particle diameter. The number of k size particles formed by i and j size particles (assuming binary collisions only) is:

$$\frac{dn_k}{dt} = 0.5 \sum_{i+j=k} \beta(d_i, d_j) n_i n_j - n_k \sum_{i=1} \beta(d_i, d_j) n_i \quad (3)$$

where the first term accounts for formation of k size particles and is divided by two because the summation counts the collision twice (Swift and Friedlander 1964). α is the collision efficiency factor which is dependant on ionic strength, pH, temperature, and other factors that affect particle surface charge (Lawler 1979). The second term represents the loss of k size particles due to collisions. The collision frequency function must be experimentally determined for a given system due to its dependance on particle size, chemistry, and transport mechanism. Flocculation is governed by three collision mechanisms, Brownian motion, shear, and differential settling. Depending on reactor

conditions (ie. shear, sample, or media), one or more mechanism may dominate. The following three sections describe the three collision frequency functions according to Lawler (1979).

Brownian

Under conditions of high particle concentration (greater than 10 g/l) and low or no shear, Brownian motion (perikinetic flocculation) gains importance (Krone 1978). Brownian motion is temperature dependant and allows for collisions based on molecular movement. This type of motion is predominantly for particles of less than one micron in diameter. The collision frequency function (in terms of particle volume rather than diameter) due to Brownian motion can be described by:

$$\beta(v_i, v_j) = \frac{2\kappa T}{3\mu} \left(\frac{1}{v_i^{1/3}} + \frac{1}{v_j^{1/3}} \right) (v_i^{1/3} + v_j^{1/3}) \quad (4)$$

where κ is Boltzmann's constant, T is temperature, and v is the volume of i and j size particles. For monodispersed systems ($v_i=v_j$), this equation can be simplified:

$$\beta_m = \frac{8\kappa T}{3\mu} \quad (5)$$

This type of collision produces a weak floc that is easily broken by any change in the surrounding fluid (Krone 1978).

Shear

The transport mechanism of shear (orthokinetic flocculation) can be characterized in terms of laminar or turbulent flow. The frequency of collisions due to laminar shear forces on a spherical particle can be described by:

$$\beta(v_i, v_j) = \frac{1}{\pi} (v_i^{1/3} + v_j^{1/3})^3 \frac{du}{dz} \quad (6)$$

where du/dz is the local velocity gradient. As seen by this equation, as the aggregate grows, the frequency of collision increases. The aggregates formed from shear are spherical in shape (Krone 1978).

Under turbulent shear conditions, the local velocity gradient is expressed in terms of turbulent energy dissipation:

$$\beta(v_i, v_j) = \frac{1}{\pi} (v_i^{1/3} + v_j^{1/3})^3 \left(\frac{\epsilon_d}{\nu} \right)^{0.5} \quad (7)$$

where ϵ_d is the turbulent energy dissipation and ν is the kinematic viscosity (μ/ρ). Particles smaller than fluid eddies will be affected by this turbulence. These aggregates are formed from particles rotating in opposite directions, thus the bonds are very strong (Krone 1978). As the turbulence increases, even strong bonds may be broken. Floc breakup depends on system chemistry and shear conditions and will be discussed in a subsequent section. A dynamic equilibrium will eventually be reached (ie. particles are breaking and reforming into the same size) (Boadway 1978). The time required to reach a dynamic equilibrium depends on chemistry and hydrodynamics of the system (Montgomery 1985).

Differential Settling

Particles may also collide vertically during the settling process. This occurs due to the variety of settling velocities present in a heterogeneous or flocculent system. Collisions due to differential settling are described by:

$$\beta(v_i, v_j) = \left(\frac{6}{\pi} \right)^{1/3} \frac{g}{12\mu} (\rho_p - \rho_l) (v_i^{1/3} + v_j^{1/3})^3 (v_i^{1/3} - v_j^{1/3}) \quad (8)$$

This collision mechanism is also important for highly concentrated suspensions and is most effective for large particles. Differential settling also gains importance in heterogeneous systems and under low shear conditions (Montgomery 1985). Due to low shear conditions, the flocs produced tend to be ragged, weak, and low density (Krone 1978).

Floc Breakup

Aggregates may also breakup which will affect the resulting size distribution, thus settling velocities in a system. Under highly viscous conditions and laminar flow, the

breakup of flocs formed from cohesionless, spherical particles has been observed (Kao and Mason 1975; Powell and Mason 1982). A spherical cluster initially forms and soon begins to elongate. Peripheral particles are then stripped away from the parent cluster. The aggregate radius becomes a function of shear, time, and initial radius:

$$(r_0^3 - r_a^3) = k_b G t_s \quad (9)$$

where r_0 is the initial radius, r_a is the aggregate radius, k_b is a rate constant, G is the shear rate, and t_s is shearing time. These flocs will eventually disintegrate into primary particles.

Floc breakup can also be expressed in the form of splitting and erosion. Pressure differences can cause splitting, the rupture of a floc into daughter fragments (Fig. 2). Turbulence within a system can cause erosion of small clusters or primary particles from a parent floc (Pandya and Spielman 1983; Lu and Spielman 1985) (Fig. 3). A combination of these mechanisms can be used to describe particle size distributions within a system.

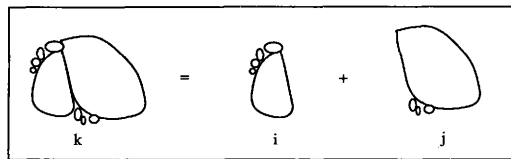
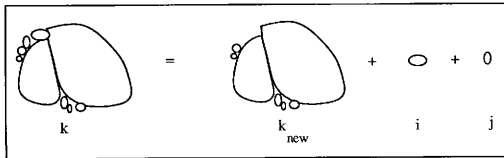


Fig. 2.- Splitting of Particle of Size k

Fig. 3.- Erosion of Particle of Size k

Pandya and Spielman's (1982) floc population balance equation incorporates both splitting and erosion in turbulent flow, but neglects reflocculation of daughter flocs:

$$\frac{\partial n(v,t)}{\partial t} = \int v_d(\bar{v}) g(v) n(\bar{v},t) P_s(v, \bar{v}) d\bar{v} - g(v) n(v,t) \quad (10)$$

$$+ \int v_e(\bar{v}) n(\bar{v},t) P_e(v, \bar{v}) d\bar{v} - \frac{\partial}{\partial v} \left[\left(\frac{dv}{dt} \right)_e n(v,t) \right]$$

The first term of the equation represents the formation of daughter flocs due to floc splitting, and the second term represents the loss of the parent floc where:

$$v_d(\bar{v}) = 2 + k_l [v_{\text{parent}}^P] \quad (10a)$$

$$g(v) = k_2 v_{\text{parent}}^m \quad (10b)$$

$$P_s(v, \bar{v}) = \frac{1}{\sigma_s(\bar{v}) \sqrt{2\pi}} \exp \left[- \frac{[v - \bar{v}_s(\bar{v})]^2}{2\sigma_s^2(\bar{v})} \right] \quad (10c)$$

represent the average number of daughter flocs $v_d(\bar{v})$, the splitting frequency $g(v)$ which is dependant on parent floc size, and the normal fragment probability distribution

$P_s(v, \bar{v})$, respectively. The third term in Eq. 10 represents the "new" particles formed by floc erosion, and the fourth term describes the shrinkage of the parent floc volume due

to erosion where:

$$q_e(\bar{v}) = \bar{k}G \quad (10d)$$

$$P_e(v) = \frac{1}{v\sqrt{2\pi \ln \sigma_{ge}}} \exp \left[\frac{-(\ln v - \ln \bar{v}_{ge})^2}{2 \ln^2 \sigma_{ge}} \right] \quad (10e)$$

$$-\left(\frac{dv}{dt}\right)_e = \frac{\bar{k} \int_{\bar{v}}^v P_e(\bar{v}) d\bar{v}}{\int_0^v P_e(\bar{v}) d\bar{v}} G \quad (10f)$$

represent the rate of formation of erosion fines $q_e(\bar{v})$, the log-normal probability distribution of eroded particles $P_e(v)$, and the instantaneous rate of change of parent floc volume due to erosion $-(dv/dt)_e$, respectively. The third term in Eq. 10 describes the "new" particles formed due to erosion, and the last term represents the shrinkage of the parent floc volume.

The splitting frequency varies with floc diameter to the first power. Experiments with Kaolin-hydrous ferric-oxide flocs in a sheared batch reactor show that the splitting frequency function varies to the 0.71 power of the shear rate and to the 0.33 power of the parent floc volume (Pandya and Spielman 1983). The average number of daughter flocs produced is 2.5. The mean and standard deviation are at a fixed ratio to one another and are independent of shear rate or parent size.

Lu and Spielman (1985) have performed experiments with kaolinite and polymer solutions. Both breakage (Eq. 10) and flocculation (Eq. 3) are accounted for in this model. The collision frequency function is expressed in terms of turbulent energy dissipation (Eq. 7). The splitting frequency is proportional to the product of the shear rate and parent floc volume. The decrease of parent floc volume due to erosion is proportional to the product of the shear rate and the mean particle volume of erosion fines. For a given shear rate, a maximum stable floc size occurs over time.

Akers, et al. (1987) performed experiments with monosized (0.97 micron) particles. The particles were introduced into a tube and driven by a plunger to and from inside of the tube. Pressure differences cause splitting, but this is limited. For a given flow condition, an equilibrium size distribution is reached. Beyond this time, no splitting occurs and a simple frequency function fails.

SETTLING FACTORS

Flocculation and breakup have been shown to be an important factor in transport of estuarine sediments. Shear, salinity, particle type, and particle concentration are four interrelated parameters that affect flocculation rate and extent. In order to predict sediment transport in an estuary, the effect of these parameters must be quantified in terms of particle settling velocity.

Particle Type

The type of particle in a system will affect settling velocity. For example, comparison of sludge studies at the same shear rate with variation only in sludge type and water temperature indicates that removal rates will vary depending on particle type (Hunt and Pandya 1984). Particle characteristics such as mineralogy, organic content, size, and density will affect settling.

An example of mineralogical effect on flocculation can be seen by comparing flocculation rates for clays. Illite and kaolinite flocculate quicker than montmorillonite at low salinities (Burton 1980). Settling velocities for illite and kaolinite are higher than those for montmorillonite (Dyer 1972). The higher velocity is attributed to flocculation. Also, similar stability trends are noted by Edzwald, et al. (1974). However, Krank (1975) finds no evident differences in floc behavior between quartz, feldspar, or clay. In natural systems, organics may cover up crystal faces of a particle thus masking mineralogical effects.

The presence of organics can greatly increase settling velocities. Organics can compose as much as 40% of a particle (McCave 1975). Meade (1972) records values of 10 to 20%. Luck (1970) demonstrates on video (in the field) that organic slimes are present and form aggregates with sediments. While organics have a lower specific gravity than sediments, the settling velocity is increased due to an increased diameter. A sample mixture of 50% organic and 50% inorganic has a faster settling velocity than a sample that is purely organic or inorganic (Krank 1984). The presence of carbohydrates (0.0005 to 1.0 g/l) can increase settling velocities by up to 25% (Dyer 1972). Krank (1984) proposes that there is an optimal organic to inorganic ratio that will produce settleable macroflocs, the rest staying in suspension.

Particle size has a large effect on settling velocity. For particles less than 4-5 microns, settling according to Stokes Law becomes insignificant (Brun-Cottan 1976). These small particles are likely to be horizontally advected, while large aggregates will settle to the seafloor. Aggregation occurs in upper layers, and these aggregates are rapidly lost to the seabed (McCave 1975). The size of cohesive particles (clay and silt) is under 60 microns. Floc sizes are usually in the range of 5 to 50 microns. Determination of particle size can become complicated due to aggregation. Particles are constantly moving from one size category to another due to formation and breakup. Even so, the size distribution of particles in a flocculating system remains fairly constant (Krank 1980). This is because the flocs in the distribution are made from particles of all sizes. Experimental measurement of floc diameter is difficult due to various floc strengths. Sampling may break or form flocs thus tainting values of in situ sizes and densities (Lawler 1979).

The density of a particle will affect settling, but the extent of it's effect depends on the assumptions made in order to determine exact values. For instance, if a particle is considered as a solid sphere, the density is greater than that of an aggregate. But, the greater density does not necessarily out weigh the effects of an increased diameter due to flocculation. To apply models to predict settling velocities, simplifications must be made.

A constant density can be assumed or a porosity function may be included. Depending on system dynamics, a constant density value may sufficiently describe settling velocity. Density can be determined experimentally by measurement with a pycnometer, calibrated density gradients, a density meter, or a similar device. Back calculation of density from Stokes law using laboratory settling velocities is another method of density determination. Particle density can be represented as a constant value or as a function that varies with porosity.

Density can be assigned a constant value based on experimental measurement of actual density or by the definition of a function to describe density. Boadway (1978) and Krone (1978) both express aggregate density as a function of solids concentration:

$$\rho_a = \frac{C}{F\rho_p}(\rho_p - \rho_1) + \rho_1 \quad (11)$$

where ρ_s is aggregate density, C is total suspended solids, and F' is the volume fraction of particle. The floc density varies with floc size and solids concentration. As particles aggregate, water is trapped thus lowering the effective density of the "new" particle.

McCave (1975) assumes a 60/40 mineral/organic mixture to calculate the density of each particle size. The mineral and organic densities are assumed to be 2.5 and 1.03 g/cm³, respectively. The effective density ($\Delta\bar{\rho}$) is defined as the difference between particle wet bulk density ($\bar{\rho}$) and fluid density (ρ_1). The following mass balance relationships were used to calculate effective densities:

$$v_{om}\rho_{om} + v_w\rho_w = \bar{\rho}v_{tot} \quad (12a)$$

$$v_{om} + v_w = v_{tot} = 1 \quad (12b)$$

Using a primary particle density of 1.591 g/cm³, McCave (1975) estimates floc effective densities in the range of 1.056 to 1.25 g/cm³. Figure 4 is a plot of particle settling velocity (based on Stokes law) and corresponding particle wet bulk density taken from McCave (1975, Table 2).

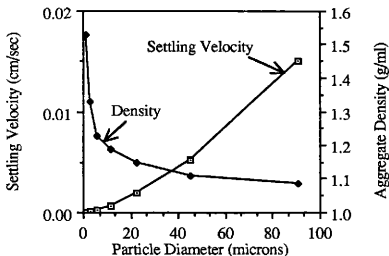


Fig. 4.- Estimated Densities and Settling Velocities (Adapted from McCave 1975)

The density decreases slightly, but these changes are small in comparison to the increase in diameter. The settling velocity is based on the square of the diameter. As particles grow, settling velocity increases as a function of diameter. Dyer (1972) finds that for particles with a density of 2.6 g/cm^3 , the floc density can range from 1.27 to 1.8 g/cm^3 and decreases with increasing size.

As aggregates grow, more water is entrained within their structure. The result is a dynamic density depending on floc porosity. Effective floc density and floc diameter can be plotted as a straight line on a logarithmic scale (Tambo and Watanabe 1979b). The floc density function can be expressed in terms of two empirical constants:

$$\rho_e = \rho_a - \rho_w = \frac{a}{\left(\frac{d_f}{1}\right)^{K_p}} \quad (13)$$

where d_f is the floc diameter ($d_f/1 \text{ cm}$ is dimensionless), and a and K_p are constants. The experimental apparatus consists of a flocculator with a quiescent settling tube attached below. The time required for a single floc to settle 5 cm is recorded, and the floc diameter

is measured with a camera. The density is then back-calculated using a modified Stokes equation. Under these conditions, coagulants and pH alter effective floc density while shear rates (40 to 80 rev/min in the flocculator), flocculent aids, and alkalinity have negligible effects on the floc density function.

Logan and Hunt (1987) use the floc density function and empirical values, but they are expressed in terms of porosity:

$$(1 - P) = B d_f^{-d} \quad (14)$$

where P is porosity, B and d are empirical constants, and d_f is floc diameter. Tambo and Watanabe's (1979a) Fig. 14 was used to choose a d of -1.6, and a porosity of 0.4 was chosen in order to yield a value of 8.0 for B. These values yield a porosity of 0.995 for a 100 micron floc composed of one micron particles. This falls within the range of 0.66 to 0.999 as reported by several other authors (Logan and Hunt 1987, Table 1.0). Porosities for diatom flocs of diameters 7 to 22 mm range from 0.99931 to 0.99984 (Logan and Alldredge 1989). A comparison of McCave's (1975) and Logan and Hunt's (1987) methods are presented in Figs. 5 and 6. The porosity function was used with comparable solid densities as used by McCave and plotted with McCave's results.

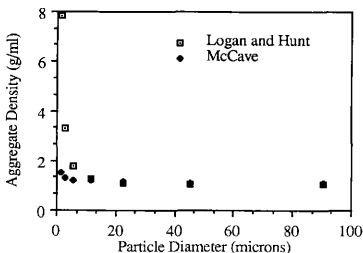


Fig. 5.- Densities from Logan and Hunt and McCave

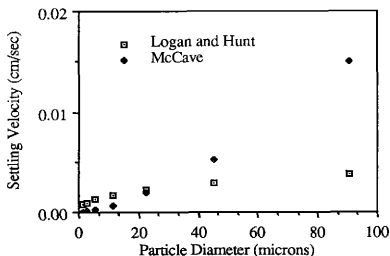


Fig. 6.- Settling Velocities from Logan and Hunt and McCave

As seen in Fig. 5, the aggregate density is extremely high for particles less than three microns. This occurs due to negative porosities generated by Eq. 14. Therefore, the use of the porosity function for small sizes is limited. The resulting settling velocity (Fig. 6) calculated by using the porosity to calculate aggregate density is fairly constant. The larger aggregates approach a porosity of almost 99% which seems to decrease settling much more than assuming a solid density.

Salinity

Due to its effect on flocculation potential and fluid density, salinity will also alter settling velocities. Salinity gradients can be formed in estuaries, but because New Bedford Harbor is considered well-mixed, salinity effects on particle attraction is of the most importance (Dyer 1979). As ionic strength increases, the double layer surrounding a particle is compressed. This compression results in a decreased zeta potential which enhances coagulation. The amount of ions required for sufficient compression depends on ionic strength as well as particle type (Montgomery 1985).

Krank (1984) and Edzwald, et al. (1974) both demonstrate the importance of destabilization to sediment transport. According to Edzwald, et al. (1974), the rate of coagulation will increase with increasing salinity. This is seen by increasing alpha values

for increasing salinity in a 2 liter mixed reactor ($G = 52.3 \text{ sec}^{-1}$) using Palminico Sound sediments (Fig.7). Lavelle (1988) finds that the presence of seawater increases the size distribution peak from 4 to 7 microns. The salt water also exhibits a narrower size distribution than that of fresh water. Hahn's (1970) experiments with montmorillonite in a continuous flow reactor show that settling velocity does increase with ionic strength.

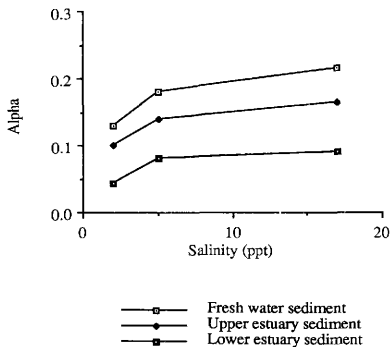


Fig. 7.- Alpha as a Function of Salinity for Clay Size Fraction of Pamlico Sediments
(Adapted from Edzwald, et al. 1974)

The effect of salinity under field conditions may be overshadowed by hydrodynamic conditions involving turbulent flow (Humby 1975). Teeter (1988) claims that salinity has the greatest effect only between 0 and 4 ppt, thus salt fluctuations in the estuary are virtually unimportant. A field study utilizing an Owen tube shows no observable effect on settling velocity due to salinity variation (Burt 1986). It is postulated that flocculation potential due to salinity becomes unimportant due to the long time periods a particle resides in the estuary. Salinity affects the speed of flocculation rather than its extent. Settling velocity for differing salinities is plotted for various initial particle concentration values by Burt (1986) (taken from data collected by Owen, Allersma, and Krone) (Fig. 8). Small slopes exist at small concentrations, thus salinity does not have a great effect on settling velocity. In almost all cases the slope decrease occurs after approximately 5 ppt. As the concentration increases, the slopes increase thus showing a greater salinity dependence.

Particle Concentration

As seen with Burt's examination, particle concentration has a large effect on settling velocity. Faisst (1978) has performed settling experiments on varying dilutions of sludge in seawater. Sedimentation velocity increases with increasing solids content. Flocculation enhanced by an increased solids concentration is hypothesized to be the cause for increased settling velocities. Because these studies were performed in a quiescent settling column, the concentration effect is more apparent. Studies performed under sheared conditions exhibit increased settling velocities with increasing concentration (Fig. 8). The effect of concentration can be described by various equations depending on "low", "intermediate", and "high" concentration levels.

An empirical expression is derived by Hunt and Pandya (1984) that depicts particle

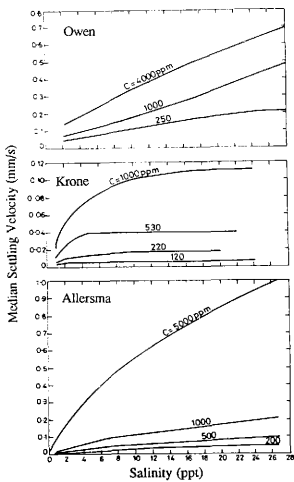


Fig. 8.- Variation of Particle Settling Velocity with Salinity (Adapted from Burt 1986)

settling as second order dependent on particle concentration as follows:

$$\frac{dc}{dt} = -bc^2 \quad (15)$$

where c is total suspended particle mass per fluid volume, and b is the rate parameter depending on fluid and particle characteristics. Low particle concentration prevents a large number of particle contacts, thus settling is discrete. Intermediate concentrations between the range of 10-200 mg/l to 2,000-75,000 mg/l can promote settling (Teeter 1988). Extremely high concentrations may hinder settling due to an increase in viscosity (Lawler 1979). Krone (from Mehta 1986) defines the "critical" concentrations to be less than 300 ppm for low concentrations, between 300 to 10,000 ppm for intermediate concentrations, and greater than 10,000 ppm for high concentrations.

Farley and Morel (1986) implement an additive power law to describe concentration effects:

$$\frac{dc}{dt} = -B_{ds}c^3 - B_{sh}c^2 - B_b c^{1.4} \quad (16)$$

In this equation B represents a rate coefficient for differential settling (ds), shear (sh), and Brownian (b). Only one coagulation method is assumed dominant for a given mass concentration. Differential settling dominates for high concentrations, shear at intermediate concentrations, and Brownian at low concentrations. Montgomery (1985) states that Brownian motion is more important under high particle concentration conditions. The possibility exists that differential settling has a greater impact on particle settling than Brownian motion for systems of high particle concentrations. The power law fits well for quiescent data. Hunt and Pandya's (1984) data (collected under shear conditions) is also described accurately with this power law (neglecting Brownian motion).

Shear Rate

Many laboratory studies have been performed under quiescent conditions to determine particle settling velocity; Lavelle (1988), Farley and Morel (1986), Faisst (1978), and

Krank (1980). However, these studies give little insight to processes pertinent to particle settling in field conditions due to the absence of turbulence. Most environments will have some degree of turbulence which can promote bottom resuspension, flocculation, and perhaps floc breakup. Resuspension acts as a source of sediments, thus particle concentrations near the bottom are increased. The resulting viscosity may be great enough to hinder settling to appreciable levels. By decreasing the settling velocity, contaminants have a greater probability of transport to other areas of the environment. Flocculation and floc breakup can act together to affect settling velocity. Without shear, differential settling is the mechanism for particle aggregation. The addition of shear introduces an additional means of particle contact described by the flow conditions. In order to better understand settling processes in the environment, shear has been incorporated in laboratory studies by using viscometers, impellers in a mixing vessel, or flumes. A variety of methods have been developed to measure and mathematically represent shear.

Shear can be classified based on the type of flow in a system, laminar, transitional, or turbulent. Laminar flow follows a distinct pattern and can be described with stream lines. When laminar flow begins to become unstable, the resulting flow is termed transitional. Turbulent flow is fully unstable and characterized by irregular fluctuations in flow velocity. Turbulent flow can further be classified as steady or unsteady. Steady flows can be represented by a constant average velocity over time, while the average velocity for an unsteady flow varies over time (Shames 1982). The Reynolds number is a dimensionless ratio used to categorize the flow. The ratio is density, velocity, and length divided by viscosity. The critical Reynolds number can be used to classify flow in proximity to any object, therefore the values used in the ratio depend on the system in question (ie. particles, flat plates, pipe flow, etc.). Likewise, different critical Reynolds numbers exist for these systems. In determining particle settling velocity, classification is

necessary in order to make assumptions on drag determination which affects particle settling velocities.

The shear produced in a system must be measured in order to provide accurate fluid and particle velocities. The equation for root mean square (rms) velocity gradient (G) can be presented as:

$$G = \sqrt{\frac{P}{\mu v}} \quad (17)$$

where P is power input determined by the speed of the impeller times 2π times the torque divided by 60. Another way of expressing G is in terms of power dissipation per unit mass:

$$G = \sqrt{\frac{\bar{\epsilon}}{\nu}} \quad (18)$$

where $\bar{\epsilon}$ is the average power dissipation per unit mass. The use of G is questioned by several authors (Cleasby 1984; Glasgow 1986). In deriving Eq. 17 and 18, the shear stress is assumed to be a function of absolute viscosity:

$$\tau = \mu \frac{\partial v}{\partial n} \quad (19)$$

as derived from Newton's viscosity law where $\partial v / \partial n$ represents G. Total shear stress can also be expressed in terms of molecular and eddy viscosity:

$$\tau = (\mu + \epsilon_v) \frac{d\bar{u}}{dn} \quad (20)$$

where ϵ_v is the coefficient of eddy viscosity. In highly turbulent systems, absolute viscosity is not as important as eddy viscosity. The root mean velocity gradient and average total velocity can be expressed as:

$$\left(\bar{u}^2\right)^{1/2} = \frac{C_c \omega D^2}{\left(T_d^2 H\right)^{1/3}} \quad (21)$$

where C_c is a correlating constant in the x, y, and z directions, T_d is the tank diameter, H is the liquid depth, D is the impeller diameter, and ω is the impeller rotational speed

(Cleasby 1984). This study indicates viscosity independence for large particles. In turbulent systems, eddies of various sizes exist. The size of the eddy determines the size of particle affected by the eddy. Local shear within an eddy may greatly exceed that averaged throughout the system. Flocculation and breakup in a system may be vastly different than that predicted based on an average velocity gradient.

Oldshue (1983) shows that for the same G value, different impellers will require different times to reach minimum turbidity. Blade shape will determine the size and quantity of eddies induced into the flow. These eddies may serve to bring particles together or tear them apart depending on the length of the eddy relative to particle diameter. Glasgow (1986) measures dissipation along a turbine-type impeller blade. Dissipation decreases as the distance increases from the shaft. The local dissipation exceeds the mean dissipation for the reactor.

For a given impeller speed, the energy input increases depending on reactor and impeller geometry (Mhaisalkar 1986). Typically, the turbulence is quantified by power input. Krank (1984) performs studies by shaking a sample on a shaker table. The results show a change in particle size distributions with increased turbulence, but shear can only be quantified in terms of shaking speed or excursions per second. This allows for relative turbulence comparison only. For a flocculent suspension, the aggregate settling velocity increases with increasing shear rate (Hunt and Pandya 1984). At some point, shear rates can become too high to promote settling. Lavelle et al. (1988) shows that as shear is increased, smaller flocs or flocs of lower density are produced. Cleasby (1984) represents the turbulent energy spectrum as $(\bar{\epsilon})^{2/3}$.

Shear rates in a system may be sufficiently strong enough to resuspend sediments that have reached the bottom boundary. Resuspension can also be referred to as erosion or entrainment and occurs in two forms (Mehta 1986). Surface or particle-particle erosion results from breakage of particle bonds due to turbulence near the bottom boundary. This type of erosion is prevalent in areas of moderate tides and low particle concentrations.

Mass or bulk erosion is the second form of erosion. Failure along a plane under the bed surface causes a mass of sediments to erode. This condition occurs under severe wave or scour conditions and for areas of high particle concentration.

While no predictive model exists for bed erosion, empirical methods have been implemented. Sheng (1986) presents an empirical form used by numerous authors to describe the erosion rate (E):

$$E = M(\tau_b - \tau_c) \quad (22)$$

where M is an erosion rate constant, τ_b is the bottom shear stress, and τ_c is the critical shear stress necessary for erosion. The critical shear stress depends on factors such as sediment water content, bed density, bed history, temperature, organic content, and aggregate strength. Typical values for M are 1×10^{-6} to 2×10^{-5} sec/cm, and values for τ_c range from 0.2 to 20 dyne/cm² (Sheng 1986).

Results from flume studies show that erosion and deposition of cohesive sediments does not occur simultaneously (Parthenaides 1986). A given flow will hold a specific amount of the total suspended sediment in suspension. The amount of sediment retained in suspension is not dependant on the total sediment concentration, but is a function of the bed shear stress. Fluid salinity and bed consolidation time affect resuspension rates for cohesive sediments.

Fukuda and Lick (1980) express deposition (D_e) and entrainment in the following form:

$$q_s = E - D_e = E - \beta_e C \quad (23)$$

where q_s is the net sediment flux, and β_e is the coefficient of proportionality. The equilibrium or steady state concentration (C_{eq}) is expressed as E/β_e . Shear stress and sediment water content affect entrainment rates and equilibrium concentrations. As the bulk sediment water increases linearly, the entrainment rate and equilibrium concentration increase logarithmically. The same relationships exist for shear near critical shear stress

values. Entrainment rates and equilibrium concentrations increase (for a given water content and shear stress) as the clay content increases and the median particle size decreases. Lick (1982) extends these studies. Entrainment experiments show that particle size variation is important to entrainment rates in that the amount of sediment available for resuspension at a given shear stress is finite. Also, the available sediments are continuously entrained and deposited. A specific fraction that is deposited is not readily resuspended, and a superficial layer exists that is readily suspended.

As previously discussed, the interaction of salinity, particle type, shear, and particle concentration all affect settling velocity. Salinity and particle type define charges that affect alpha. Particle size directly affects settling velocity as seen in Stokes equation. The size of a particle also indirectly affects collisions between particles depending on eddy size. Shear and particle concentration often determine collision rate and the extent of resuspension. In order to analyze data in regards to which interactions are most important, all of the above factors must be investigated and incorporated into a model.

CHAPTER III

EXPERIMENTAL METHODS

Over the years, many settling studies have been performed under a variety of conditions. The type of samples used in these columns are as diversified as are the settling columns used. These columns differ in height, diameter, type of sampling ports, and hydrodynamic characteristics. Settling velocity will change in accordance with sample type and settling conditions. Salinity, shear rate, particle concentration, and particle type are very important parameters that may alter particle settling rates. These parameters were arranged in a factorial framework outlining specific experiments to be performed. An electronic particle counter, suspended solids instrument, and turbidimeter were used to measure New Bedford Harbor particle size distributions and mass within the settling column developed by Ducharme (1989).

EXPERIMENTAL DESIGN

The most efficient method to investigate four parameters, shear rate, salinity, particle concentration, and particle type, is that of factorial design. The parameters are termed factors in the experimental design. Factorial designs allow the determination of interactions between factors over a wide range of conditions (ie. various shear rates, salinities, particle concentrations, or particle types). For example, salinity represents one factor and salinity values of 5, 15, and 30 ppt represent 3 levels. As the number of factors and levels increase, so does the accuracy of the calculation of interaction between factors. Factorial designs may be used to plan future work by determining the most significant factor interactions (John and Quenouille 1977).

Parameters may be investigated in detail or a cursory examination may be performed with factorial designs. The purpose of investigation for this work is to determine the

pertinent parameters to be more closely investigated in future studies. For a factorial design involving four factors and three levels, $3 \times 3 \times 3 \times 3 = 3^4 = 81$ experiments are necessary. Each experiment requires approximately one week to complete, therefore the factorial design must be adjusted to fit a reasonable time frame. A fractional factorial design requires $3^{4-1} = 27$ experiments which would require approximately eight months for completion. The next alternative involves sacrificing close investigation of one factor. Concentration was chosen to be represented in only three experiments due the extensive characterization of concentration effects by previous authors (Faisst 1978, Hunt and Pandya 1984, Teeter 1988, and Farley and Morel 1986). Based on this decision, the experimental framework was structured as a series of three factorial designs with an emphasis placed on shear, salinity, and particle type.

Particle concentration, shear rate and salinity, and particle type and salinity were varied within Experimental Design 1, 2, and 3, respectively. Table 1 represents a simple $1 \times 3 \times 1 \times 1$ design to determine concentration effects at only one level of the remaining factors. A $3 \times 1 \times 3 \times 1$ (or 3^2) design broken into 3 blocks of various salinities was used to determine shear and salinity interactions (Table 2). Particle type and salinity interactions can be determined from the 3^2 design with blocks of particle type in Table 3. The third block in Table 3 is comprised of experiments 18, 19, and 20 from Table 2. This reduces the number of experiments thus time required while retaining the integrity of the experimental framework. The experiments were numbered in the manner in which they were performed. Randomization was used to alleviate any systematic errors in performing the experiment. Duplication was demonstrated with experiments 2 and 7. Only one other duplication was necessary due to previous validation work on the settling column designed by Ducharme (1989). This experiment was chosen at random and will be discussed in a following section.

The sediments used in these experiments were taken from New Bedford Harbor and are classified as organic silts and clays (OH and OL) with silty sands (SM) (Wade 1988).

The hot spot site (location with PCB concentrations as high as 10,000 mg/l) is slightly higher in clay content, and the specific gravity of the sediments tested was 2.5. The exact particle concentrations used within the column were defined based on preliminary electronic particle counter tests and literature values. The three particle types are denoted as A, B, and C. Type A originated from Site 5 (Fig. 1) and had a PCB concentration of 6.1 ppm. Type B, with approximately 30 ppm PCB concentration, was taken from Site 10. Type C, which contains the highest PCB concentration of all the samples (300 ppm), was taken from Site 12 (Pruell, et al. 1989). The shear rate and salinity values were selected based on typical estuary conditions and are defined in the following tables.

Table 1.- 1 X 3 X 1 X 1 Concentration Design

Experiment Number	Shear Rate (1/sec)	Particle Concentration (mg/l)	Salinity (ppt)	Particle Type
7	20	10	15	A
8	20	40	15	A
9	20	80	15	A

Table 2.- 3 X 1 X 3 X 1 Shear and Salinity Design

Experiment Number	Shear Rate (1/sec)	Particle Concentration (mg/l)	Salinity (ppt)	Particle Type
19	20	40	5	A
1	30	40	5	A
17	40	40	5	A
18	20	40	15	A
2	30	40	15	A
6	40	40	15	A
20	20	40	30	A
3	30	40	30	A
21	40	40	30	A

Table 3.- 1 X 1 X 3 X 3 Particle Type and Salinity Design

Experiment Number	Shear Rate (1/sec)	Particle Concentration (mg/l)	Salinity (ppt)	Particle Type
10	20	40	5	B
11	20	40	15	B
12	20	40	30	B
13	20	40	5	C
14	20	40	15	C
15	20	40	30	C
18	20	40	5	A
19	20	40	15	A
20	20	40	30	A

INSTRUMENTATION

The above experiments were performed in a mixed settling column and various instruments were used to analyze the samples. An electronic particle counter was used in

order to examine the changes in particle size distributions over time. Suspended solids and turbidity measurements were taken to verify trends in the size distribution data. The settling column did have the capability of *in situ* measurement of particle settling through the use of photocells, but only physical samples were analyzed and reported based on the need for investigation of particle size distributions. The following sections describe the experimental apparatus used in this investigation: settling column, particle sizing apparatus, suspended solids machine, turbidity meter, and density meter.

Settling Column

The two meter settling column was designed and validated by Ducharme (1989). This column is a 38.1 cm diameter PVC pipe with a wall thickness of 1.27 cm (Fig. 9). A hollow glass shaft with PVC impellers is rotated by a motor which is computer controlled. The speed is monitored and studies have been performed to determine the hydrodynamics of this system in terms of shear rate (G) for this system at varying motor speeds (Ducharme 1989). Ten sampling ports are spaced approximately 15.24 cm apart down the length of the column. These ports are made of 3 mm glass tubing with a 1 mm inner diameter and extend inward one half the radius of the column. Samples were extracted from one half the radius of the column rather than at the wall. In addition to sampling ports, ten sets of sensors (photocells) are also spaced down the length of the column. Particles passing a sensor impede light that is transmitted from a corresponding light-emitting diode (LED). This attenuation is directly related to the concentration of particles. The resulting voltage change was continuously recorded and fed into a computer data file. This data was not analyzed based on the need for detailed particle size distribution data. The samples drawn from the column were analyzed using an electronic particle counter, an AVC-80 Suspended Solids Machine, and a HACH Model 2100A Turbidimeter.

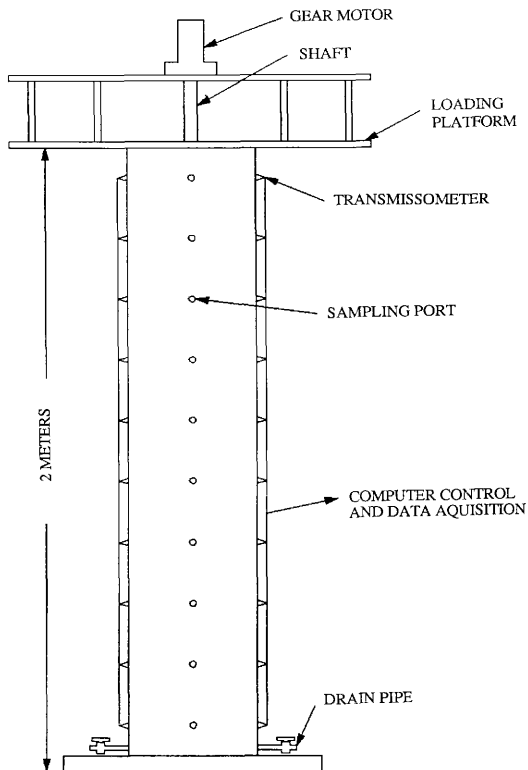


Fig. 9.- Settling Column Schematic from Ducharme 1989

Electronic Particle Counter

Samples of approximately 50 ml were drawn at given time intervals during each study. An electronic particle counter (Coulter Counter, Coulter Electronics Limited) was used to analyze the samples to determine a dynamic size distribution. The particle counter counts the number of particles in a given sample volume based on electrical impedance. In these studies, a 140 micron aperture was used which is accurate over a particle size range of 2.8 to 84 microns. In a natural system particles less than 2 microns in diameter exist. A smaller aperture would count a considerable amount of these particles, but aperture clogging is a problem. The New Bedford Harbor sediments are highly flocculant and a larger aperture is necessary to accommodate large flocs. A manometer setting was used which siphons exactly 2000 microliters of the 50 ml sample for analysis. The coincidence correction indicates the possibility of two or more particles passing through the aperture at the same time and must be less than 20%. Based on coincidence limit, the maximum concentration within the column with no dilution was determined. This was accomplished by testing samples of varying concentrations. By using a concentration that required no dilution, sampling error was reduced.

In designing the experiment, reproducibility of particle numbers within a sample was a main concern. This reproducibility relied heavily on the aperture siphoning a completely mixed suspension. With the flocculent nature of the particles, typical mixing in the sample chamber to achieve a homogeneous suspension altered particle diameters. Also, the probability of particles settling in the sample container before measurement was of great concern. When allowed to settle, the particles tended to stick together which increased the possibility of experimental error. With this in mind, the use of polyvinyl pyrrolidone (PVP) was investigated in order to suspend particles for measurement (Appendix B). PVP is a viscous medium often used to suspend biological materials for analysis. An experiment was performed to test the effect of PVP versus no PVP, stirring versus no stirring, and waiting versus no waiting (Appendix B). The results showed

that the benefits of PVP were limited and outweighed by the cost and effort in implementing its use. When the samples were allowed to stand for one hour before analysis, the flocs tended to stick together yielding high diameters. Stirring the sample provided a means for flocculation and floc breakup which also changed particle diameters. The best solution was the immediate placement of the sampling beaker into the Coulter sampling stand and measurement without stirring. This required constant supervision and analysis of samples.

Suspended Solids and Turbidity

Suspended solids and turbidity tests were also performed with column samples. The procedure outlined in Standard Methods (1985) was used initially to measure suspended solids (Appendix B). Test runs were made to determine the amount of sample needed in order to obtain detectable suspended solids and turbidity. With the arrival of a Suspended Solids Machine (CEM, Corp. AVC-80), a new procedure for measuring suspended solids was adopted (Appendix B). This new method gave consistently lower results than the previous method. Sand tests were performed to verify the use of the new procedure for following experiments. (Some experiments are therefore lacking suspended solids measurements.) The turbidity was determined by extracting 20 ml of the suspended solid sample (prior to suspended solid determination) and placing it in the sample chamber of a HACH Model 2100A Turbidimeter. The resulting measurement was then recorded.

Density Meter

A Mettler/Paar Digital Density Meter was used to measure sediment density. This device can measure densities from 1.08 to 3.0 g/ml with six places of accuracy. The device consists of a DMA 602 measuring cell and a DMA 60 meter. A Neslab Endocal 150 Cool Flow and a Neslab Exacal-100UHP Constant Temperature Bath were connected to the apparatus to maintain the desired temperature within ± 0.5 °C. Temperature variations as small as 0.1 °C can affect density.

The density meter measures the period of oscillation of a glass measuring cell which contains the sample. This measurement can then be used to calculate density. First, the calibration constant (k_d) must be determined. For a given temperature, the period of oscillation for air and water was recorded. The calibration constant was calculated using:

$$k_d = \frac{(\rho_{\text{water}} - \rho_{\text{air}})}{(T_{\text{water}}^2 - T_{\text{air}}^2)} \quad (24)$$

where the density of air and water were found in density tables and T represents the recorded period. The sediment sample (of known concentration) was then injected into the cell and the period recorded. The bulk density of the sample (ρ_b) was calculated using:

$$\rho_b = (T_b^2 - T_{\text{water}}^2)k_d + \rho_{\text{water}} \quad (25)$$

The particle density was then calculated using:

$$\frac{1}{\rho_p} = \left[\frac{\left(\frac{1}{\rho_s} - \frac{1}{\rho_l} \right)}{C} \right] + \frac{1}{\rho_s} \quad (26)$$

where C is the known sediment concentration. The density of the New Bedford Harbor sediments was determined to be 1.7 g/ml.

EXPERIMENTAL PROCEDURES

Procedures were developed to reproduce the initial conditions outlined in Tables 1, 2, and 3 for shear, salinity, and particle concentration. To produce the exact shear required, the speed of the impeller was monitored with the use of the computer as previously described. The shear rate is reported with 4% error for Design 1 and 10% error for Designs 2 and 3. The salt water was artificially made with Instant Ocean (Aquarium Systems, Mentor, Ohio). Approximately 220 l of distilled water were added to the column. The desired amount of Instant Ocean was then added and air mixed for one hour. The air was then stopped and the shaft rotations started immediately.

The reproduction of the desired particle concentration was difficult due to the high water content of the sediment samples. The procedure developed for duplicating particle concentrations involved preparing samples in an identical manner and monitoring initial particle number counts. The suspended solids values reported were obtained from analyzing data after the experiments were performed. The samples taken from the harbor were refrigerated at all times. Type A was delivered in a 30 gallon drum and was mixed and separated into separate containers as described in Ducharme (1989). Type B and type C were delivered in a 10 liter container and two 5 liter containers, respectively. Both of these were mixed before extracting samples. All three types were wet sediments, and the following procedure was developed to determine the maximum particle concentration within the particle counter limit that would require no sample dilution (thus reducing time and error).

The approximate concentration needed by the electronic particle counter was determined by trial and error. A good initial estimate was made, and a sample was added to the column. The sample was measured using the electronic particle counter and several dilutions were necessary before acceptable readings were achieved. The approximate maximum sediment concentration for the column that would require no dilution for particle counter readings was back calculated, and a new trial run was performed. When the desired results were achieved, the samples were then prepared identically.

To prepare samples of the same concentration, a 1 liter sample was mixed and allowed to settle overnight. The concentrated sediment was then mixed and 50 ml aliquots were measured and placed into 250 ml Erlenmeyer flasks. The flask was then filled with 15 ppt Instant Ocean which would allow for easier sample addition to the column when under tight time constraints. The flask was labeled, sealed with aluminum foil, and capped. Nine flasks were prepared at the same time from the same sample which reduced error due to variations in water content. All samples were then refrigerated.

In order to insure that the experiments were performed at the desired initial concentration, the first samples taken during an experiment were analyzed using the electronic particle counter. The criteria for 40 mg/l concentration was that the initial number count must fall between 89,000 and 111,000 per 2000 microliters which allows for 20% error. The high initial value was necessary to accurately track decreasing number of particles over time. The 80 mg/l study was conducted by doubling the amount of sample added to the column in the 40 mg/l studies. The samples extracted during the study were then diluted by one fourth using 15 ppt salt water (the same salinity as in the column). The approximately one fourth the amount of sample used in the 40 mg/l studies was used for the 10 mg/l experiments. Suspended solids measurements were not feasible to use as a criteria because of the time involved (ie. ten minutes would be required for analysis between critical initial measurements). The time between samples for initial readings must be reduced as much as possible due to the continual settling of the particles. In order to achieve an accurate measure of initial concentration throughout the column, initial measurements must be as quick as possible. Suspended solids measurements (using a suspended solids machine) require approximately ten minutes to perform. Particle counts can be taken in half this time, therefore particle numbers taken from the electronic particle counter were used to set the criteria for initial concentration verification during an experiment. Particle volumes did not seem to be as constant as number and consequently were not examined for the initial concentration verification during an experiment. After the experiments were performed, the suspended solids data and the volume data were used to find a relationship to express the concentration in mg/l and the corresponding error. The results are presented in the data analysis section.

All studies started under completely mixed conditions. (The exact procedure for performing the experiments is outlined in Appendix B.) This was achieved by air mixing the sediments in the column. After two minutes of vigorous mixing, the air was stopped and shaft rotations were immediately started. The order and times at which samples were

taken is outlined in Appendix B, Table B2. The sampling order was staggered over space and time to reduce the amount of samples necessary while maintaining the integrity of the experiment. Approximately 100 samples were taken for measurement in the electronic particle counter and 50 samples for the AVC-80 Suspended Solids Machine and HACH Turbidimeter. The samples extracted represent a 2% decrease in column volume over the entire study. The continuous experiments lasted from 10 to 22 hours.

DATA ANALYSIS

The data analysis consisted of comparing the interaction between the experimental parameters. A model was developed to produce predicted results based on transport mechanisms pertinent to these studies and will be discussed in the following chapter. The observed and predicted size distributions were compared visually and through the use of correlation coefficients. In drawing conclusions based upon comparison, the errors involved in reproducing the initial conditions (ie. particle concentration, salinity, etc.) must be determined. The initial concentration (particle number concentration in the model and suspended solids values in Tables 1, 2, and 3) was an averaged value from sampling ports 3, 7, and 10. The particle concentration increased slightly with depth as the particles were continually settling over the sampling time period of approximately 20 minutes. The error associated with this procedure was approximately 5%. The ability to reproduce experimental conditions and results is necessary to accurately compare results within each experimental design.

Initial Concentration Determination

The total particle number and volume concentration averages for the initial time were examined in terms of their correlation (Fig. 10). A high correlation would be expected because particle volume is calculated from particle number, but the resulting correlation was low. Total particle volume within a given size category was calculated by assuming the particle is a sphere (Appendix B). The resulting volume is multiplied by the number

of particles counted. Due to porosity and uneven floc shape, the particle number and volume is easily misrepresented. Calibration of the electronic particle counter requires the measurement of electronic pulse height and width. Spheres are used for calibration, thus the pulse width for flocs may be uncalibrated (Treweek and Morgan 1977). Also, a highly porous particle may be counted as several particles rather than just one. Experimental studies have shown that the electronic particle counter has less accuracy in counting flocs than in sizing flocs (Lawler 1979). As the floc passes through the aperture, it may be counted more than once. With highly flocculant systems, the correlation between total particle number and volume concentration will most likely be less than zero.

The suspended solids data were used along with the particle size distribution data to define initial concentration within the column in terms of mg/l for the five experiments with no suspended solids measurement due to a change in method of measurement as previously discussed. Originally, a correlation was attempted between initial averages of total particle number, volume and suspended solids (Appendix B, Figs. B1 and B2). The correlation coefficients was low. The initial suspension contained many small particles not yet flocculated. Therefore, the suspended solids did not indicate the number of particles within the system. Treweek and Morgan (1980) observed that before flocculation 90 % of the turbidity level is attributed to particles less than two microns in diameter. After flocculation 80 % of the turbidity is attributed to particles greater than two microns in diameter. The total particle number or volume concentration can not be correlated linearly for initial distributions due to presence of many small particles which represent zero suspended solids. The background count of the settling column appears to be upwards of 30,000 particles per ml when the data is extrapolated. Actual measurements indicated levels of 8,000 or less (7 % or less). The total particle number and volume concentration for all data were then correlated with suspended solids (Figs.

11 and 12). The correlation is slightly higher and the y-intercept is near zero due to the inclusion of flocs and increased number of data points.

The determination of the suspended solids is important only when labeling or discussing the experimental conditions in relation to field studies. Kavanaugh, et al. (1980) finds a poor correlation between suspended solids and particle number concentration. The technique of drying and weighing used to obtain suspended solids measurements is vastly different from the use of electrical impedance used to determine particle number and volume. Microscopic particles counted by the electronic particle counter may be filtered out of samples measured for suspended solids. Treweek and Morgan (1980) finds no direct relationship between particle number concentration and turbidity. Significant changes in particle size distribution were detected without corresponding changes in turbidity levels. The particle number and volume concentration determined with the electronic particle counter yields valuable size distribution data pertinent to flocculation determination and is therefore of most interest to this research.

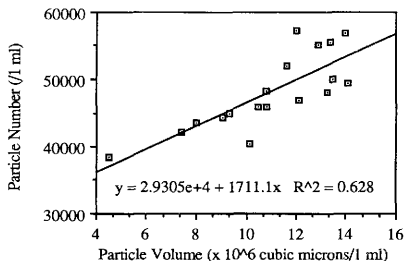


Fig. 10.- Variation of Initial Particle Number Concentration with Particle Volume

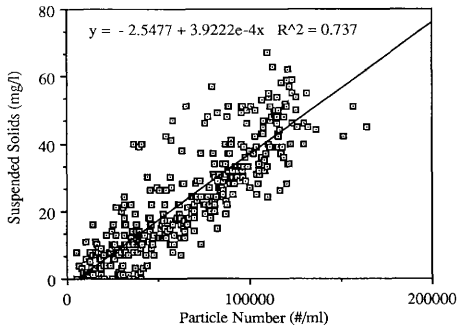


Fig. 11.- Variation of Particle Number Concentration with Suspended Solids

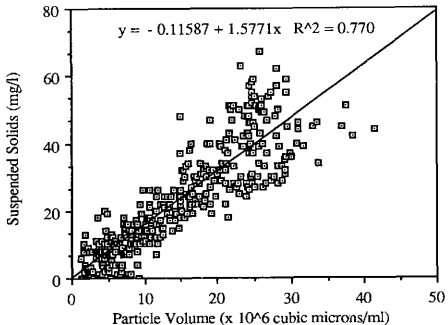


Fig. 12.- Variation of Particle Volume Concentration with Suspended Solids

Initial concentration in the column can be reported in terms of mg/l by using the linear relationship in Fig. 11. However, this is not recommended when viewing the value obtained for the correlation coefficient. Five experiments had no suspended solids values due to the change of suspended solids measurement. The suspended solids values varied up to five percent when measured. The median concentration of 40 mg/l has an error of $\pm 20\%$. Eighty percent of the experiments were within a 20% error for a particle concentration of 40 mg/l. The relative difference between a concentration of 10 mg/l and 40 mg/l is 75%. The relative difference between a concentration of 80 mg/l and 40 mg/l is 50%. The significance placed on any conclusion regarding concentration effects should be cautious. Concentrations of higher suspended solids concentrations must be investigated for more sound conclusions. To reduce confusion when examining the experimental designs, the concentration is represented as 10, 40, and 80 mg/l for Design 1 and 40 mg/l for Designs 2 and 3.

Experimental Duplication

Experiments 2 and 8 were duplicated at random with experiments 5 and 18, respectively. These experiments were performed under the same conditions and simulated using the identical model parameters. Experiments 2 and 5 differed by less than 1% in terms of initial particle number concentration and 3% in terms of particle volume concentration. Experiments 8 and 18 differed by 6% in terms of initial particle number and 13% in terms of particle volume concentration. The initial conditions were duplicated with enough accuracy to yield the same observed and predicted results. The fit of the data was expressed in terms of a correlation coefficient between observed and predicted results (described in the following section). The correlation coefficient for experiments 2 and 5 differed by 0.024 and 0.003 for the mean total particle volume and number, respectively. The correlation coefficients for experiments 8 and 18 differed by 0.024 and 0.007 for mean total particle volume and number, respectively. The fit of the data was achieved for both duplicate sets with less than 2% difference in correlation.

CHAPTER IV

MODEL DEVELOPMENT

To model particle size distributions, total particle number, and total volume within the column, a generic modeling framework was implemented to allow modular addition of transport mechanisms. This framework consisted of a basic advection-dispersion equation, boundary conditions, input of initial conditions, and definition of segments. A Runge-Kutta routine was used to solve the differential equations. The observed and predicted values were compared visually to arrive at a good initial estimate. A parameter estimation routine was then used to better estimate parameters in the model. Various mechanisms, such as a density function, floc breakup, and resuspension, were added individually in order to fit the experimental data. To analyze the fit of the final model iteration, correlation coefficients for observed versus predicted values were computed. A statistical analysis was performed to determine the interaction of shear, salinity, and particle type.

MODEL FRAMEWORK

Experimental procedures can incorporate a number of mechanisms, such as advection, dispersion, erosion, and flocculation, into a transport model. Perhaps the simplest model is of advection and dispersion only. Advection is the movement of material from one location to another (Chapra and Reckhow 1983). For vertical transport, advection was only considered in one direction (z). Dispersion (dilution due to fluid mixing) was considered only in the z direction. The mixing region insured that no horizontal variation in concentration existed. The advection-dispersion equation is as follows:

$$\frac{\partial c}{\partial t} = D_z \frac{\partial^2 c}{\partial z^2} - v_z \frac{\partial c}{\partial z} \quad (27)$$

where c is particle number concentration, D_z is dispersion in the vertical direction, and v_z is the vertical settling velocity. The vertical settling velocity is expressed as Stokes (Eq. 1) with no hydrodynamic influences such as fluid convection.

Subscripts can be added to incorporate heterogeneity, thus creating a separate equation for each particle category:

$$\frac{\partial c_k}{\partial t} = D_z \frac{\partial^2 c_k}{\partial z^2} - v_{z_i} \frac{\partial c_k}{\partial z} \quad (28)$$

where k represents particle size and ranges from 1 to n (n being the number of size categories) (Ernest et al. 1990). The electronic particle counter divides the particles into 256 size categories, therefore requiring 256 state equations to model the system. The run time of the model would be from 3 to 8 hours under these conditions. The original 256 size categories were condensed into eight categories in order to decrease model run time (outlined in Appendix C). The eight size categories are pictured in Figure 13. The categories were chosen on a log basis. Many small particles are present in this system, therefore more resolution was needed at small particle sizes. The computational time for the resulting eight equations was on the order of minutes. The dilution factor for the particle counter was also input into the program in order to obtain particle number concentration per 1 ml. The observed files (particle number concentration per ml of sample tested) were linked together along with the corresponding time of sample. Particle diameter and volume were calculated as outlined in Appendix B).

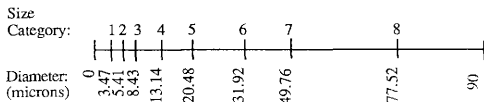


Fig. 13.- Particle Size Categories

To apply the model, boundary conditions and segment lengths must be chosen for the system. The top boundary is described by a no flux condition:

$$D_z \frac{\partial c}{\partial z} = v_z \quad (29)$$

This reflective boundary allows nothing to escape from the top of the column. The bottom boundary is described as advective:

$$D_z \frac{\partial c}{\partial z} = 0 \quad (30)$$

The advective flux equals the dispersive flux. Some particles are allowed to settle out of the system at the bottom boundary.

A finite segment approach was used to solve the above equations (Chapra and Reckhow 1983; Thomann 1972). This approach computes the mass balance across segments that are completely mixed. The column was divided into a series of horizontal segments (Fig. 14). The sediment flux into a segment was described by examining the boundary at $i-1$ and i , and the flux out was expressed at the i and $i+1$ boundary. The particle concentration at the boundary was expressed as a combination of concentrations in adjoining segments. Weighting factors were used to accomplish this:

$$c_{i-1,i} = \phi_{i-1,i} c_{i-1} + \theta_{i-1,i} c_i \quad (31a)$$

$$c_{i,i+1} = \phi_{i,i+1} c_i + \theta_{i,i+1} c_{i+1} \quad (31b)$$

where ϕ and θ are weights obtained by:

$$\phi_{ij} = \frac{l_i}{l_j + l_i} \quad (31c)$$

$$\theta_{ij} = 1 - \frac{l_i}{l_j + l_i} \quad (31d)$$

where l_i is the length of segment i . The weighting factors (Eqs. 31a and 31b) can be substituted into the advective dispersive equation (Eq. 27) to yield:

$$\begin{aligned} V_i \frac{dc_i}{dt} = & Q_{i-1,i}(\phi_{i-1,i}c_{i-1} + \theta_{i-1,i}c_i) - Q_{i,i+1}(\phi_{i,i+1}c_i + \phi_{i,i+1}c_{i+1}) \\ & + E'_{i-1,i}(c_{i-1,i} - c_i) + E'_{i,i+1}(c_{i+1} - c_i) \end{aligned} \quad (32)$$

where V_i is the volume of the section, Q_i is the flow, and E' is equal to the dispersion coefficient times the cross sectional area divided by the mean segment length.

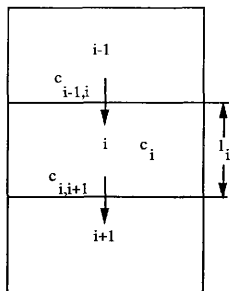


Fig. 14.- Column Segments

The column was divided into fifty equal segment lengths, and a central differencing scheme was implemented across these segments. The number of segments necessary depended on the sensitivity of the model. Sensitivity can be characterized in terms of stability or numerical dispersion (Chapra and Reckhow 1983). Spatially centered

differencing schemes may yield unstable solutions if the physical dispersion is equal to zero. Static instability occurs when inappropriate differencing techniques are implemented, and dynamic instability is a result of performing computations over an erroneously long time period. Dynamic instability can be alleviated with the use of smaller time steps at the expense of model run time. Numerical dispersion is important when the physical dispersion in a system is small. To account for the effects of numerical dispersion, the segment lengths may be shortened, or the numerical dispersion can be subtracted from the physical dispersion. The use of fifty equal segments and appropriate time steps (Appendix C) assured model stability and minimal numerical dispersion. The first and last segment served to satisfy boundary condition equations. (Only data from sampling ports 2 through 9 were used for parameter estimation purposes to reduce any possible boundary effects of the column).

A first order Runge-Kutta routine was used to solve Eq. 32. Although the Runge-Kutta routine could be increased up to fifth order, a first order approximation was chosen due to run time constraints. The run time for the parameter estimation routine (described in the following paragraph) varied from 10 to 48 hours on a VAX 3100 single user system. The most appropriate values for the parameters were determined, and then the model was used to produce concentration profiles in a matter of minutes.

A parameter estimation algorithm, PARMEST, was used to find the best fitting parameters of each experiment (Bonner, et al. 1990; Ernest, et al. 1990). The specific parameters depend on the equations used. The estimation routine minimized the variation between model and experimental data. As with any least squares technique, the variation is termed the residual function and is defined as the sum of the squares of the differences between experimental and model data. The residual (S_r) was expressed as a function of dispersion only:

$$S_r(D_z) = \sum_{i=1}^n (C_{\text{pred},i} - C_{\text{obs},i})^2 \quad (33)$$

where C_{pred} is the predicted or model concentration, and C_{obs} is the experimental concentration. A similar equation was formulated as a function of settling velocity (Ernest et al. 1990). The residual function was minimized by taking its derivative and setting the resulting equation equal to zero, for example:

$$DS_r(D_z) = \frac{\partial S_r}{\partial D_z} = 2 \sum_{i=1}^n \left[(C_{\text{pred},i} - C_{\text{obs},i}) \frac{\partial C_{\text{pred},i}}{\partial D_z} \right] = 0 \quad (34)$$

Because the model equation used in this case is nonlinear, numerical methods were implemented to find the solution (or root) of the normal equation. A variety of methods such as secant, Newton, Gauss-Newton, and Newton-Rahpson exist to provide solutions and should be chosen case specific. For most experiments, the full Newton method was used. This method converged relatively quickly, but some instability occurred when the initial parameter estimates were far from values necessary to describe the system. The Newton-Rahpson method was then used for these experiments. The solution was an optimal set of parameter(s) for a given data set. These optimal values were then used in the transport model to achieve theoretical particle concentrations over time and space.

ADVECTION-DISPERSION

The advection-dispersion equation (Eq. 32) was first used to describe particle size distributions in the settling column. The dispersion coefficient was assumed to be hydrodynamic only. The Peclet number can be used to characterize the importance of advection and dispersion, and is calculated by:

$$Pe = \frac{V_s H}{d_p} \quad (35)$$

where H is the water depth (200 cm) and d_p is the particle diameter (cm). Peclet numbers were calculated for dispersion values ranging from 1.0 to 10.0 using particles with an

effective density of 1.7 g/ml and diameters of 2 to 90 microns (Fig. 15). Small Peclet numbers ($\ll 1$) indicate highly dispersive systems (ie. the column is completely mixed over time), and large Peclet numbers ($\gg 1$) denote advective dominant systems (Chapra and Reckhow 1983). As seen by Fig. 15, particles less than 20 microns fall near the dispersive dominant region, and increasing diameters along with increasing dispersion coefficients fall in the advective dominant region.

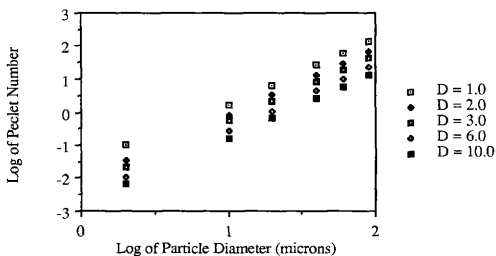


Fig. 15. - Variation of Dispersion in Relation to Particle Size and Peclet Number

The settling velocity was assumed to follow Stokes Law. Reynolds numbers were calculated to validate this assumption using:

$$Re = \frac{\rho V_s l}{\mu} \quad (36)$$

where l is length scale (diameter of particle or impeller). The particle Reynolds numbers (Table 4) were well under the critical value of 2.0 for laminar settling. The impeller Reynolds numbers ranged from 71 to 274 for G values of 10 to 40 sec^{-1} , respectively. According to tests with an eight blade turbine (Oldshue 1983), these values fall upwards of the laminar flow regime and ranges to the transitional flow zone. Under transitional

conditions, the flow is most likely turbulent near the impellers and laminar in further regions.

Table 4.- Particle Reynolds Numbers

Particle Diameter (microns)	Stokes Velocity (cm/s)	Particle Reynolds Number
3.47	4.58E-4	1.58E-5
5.41	1.11E-3	5.99E-5
8.43	2.70E-3	2.27E-4
13.14	6.56E-3	8.58E-6
20.48	1.59E-2	3.25E-3
31.92	3.87E-2	1.23E-2
49.76	9.39E-2	4.65E-2
77.52	2.30E-1	1.80E-1

Model simulations were performed using the advection-dispersion equation. Dynamic particle size distributions were produced and compared to experimental observations. Figure 16 depicts the change in observed particle volume concentration over time at a depth of 34.4 cm within the column. As seen by the decrease in the particle size distribution, the mass in the column dropped rapidly during the first two hours. At approximately 13 hours, the particle volume concentration reached near zero levels for all size categories. The size distributions predicted by the model indicated a much lower mass loss rate. In figure 17, the predicted particle size distribution decreased little over time. Only a slight disappearance of particles in the 32 and 50 micron particle size categories was predicted. To increase the mass loss rate, flocculation was incorporated to account for increasing settling velocities.

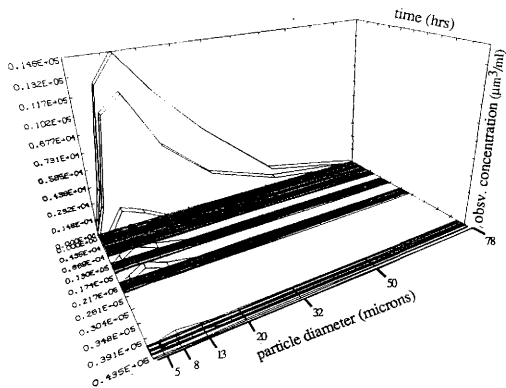


Fig. 16.- Experiment 16: Heterogeneous Particle Size Distribution Observed with Shear of 10 sec^{-1} , Salinity of 15 ppt, Type A Sediment, and Suspended Solids of 40 mg/l at a Depth of 34.4 cm

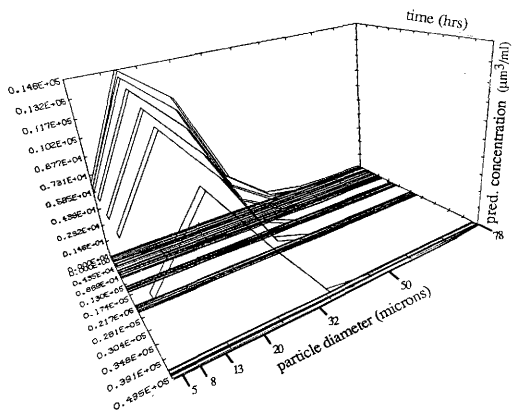


Fig. 17.- Experiment 16: Heterogeneous Particle Size Distribution Predicted with Shear of 10 sec⁻¹, Salinity of 15 ppt, Type A Sediment, and Suspended Solids of 40 mg/l at a Depth of 34.4 cm (Advection-dispersion only)

FLOCCULATION

Additional terms (Eq. 3) were added to account for the formation of flocs:

$$\frac{\partial c_k}{\partial t} = D_z \frac{\partial^2 c_k}{\partial z^2} - v_z \frac{\partial c_k}{\partial z} + \frac{1}{2} \sum_{i+j=k}^{\infty} \beta(v_i, v_j) c_i c_j - \sum_{i=1}^{\infty} \beta(v_i, v_j) c_i \quad (37)$$

The beta term is expressed as an addition of shear (Eq. 6) and differential settling (Eq. 7). Only binary collisions were assumed. The new particle created was placed in the corresponding category which could in turn be flocculated. The addition of flocculation greatly improved model prediction of the particle size distribution. As previously discussed, the observed particle size distributions indicated mass loss over time as seen by decreasing particle number concentration (Fig. 16). The pure advective-dispersive model indicated little to no mass loss within the settling column (Fig. 17). In Figure 18, the model improvement due to the addition of flocculation terms can be seen by the decrease in particle number concentration over time.

The addition of flocculation did increase settling velocities, but the model fit was progressively worse for experiments conducted under higher shear conditions. Total particle number and total particle volume (the addition of the number or volume of particles measured in the eight particle size categories at a given time and location) were examined as well as the individual size distributions previously presented in 3-D. The discrepancy between observed and predicted total particle volume was the greatest, therefore was closely examined when evaluating model results. Figure 19 depicts total particle volume over time at four depths for a shear rate of 20 sec⁻¹. The model fits well at the top 34 cm of the settling column, but an over prediction of particle settling rate is apparent from a depth of 70 cm to the bottom of the settling column. When the shear rate is increased to 30 sec⁻¹, particle settling rates are under predicted at the top and over predicted at the bottom (Fig. 20). According to observed results, the mass loss rate throughout the settling column drops drastically when the shear rate is increased to 40 sec⁻¹. The model over predicts particle settling at the top, and under predicts settling rates at the

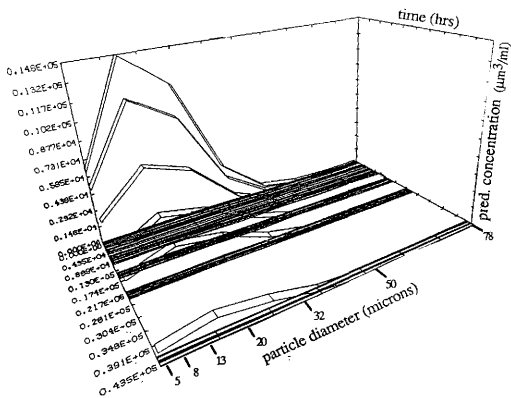


Fig. 18.- Experiment 16: Heterogeneous Particle Size Distribution Predicted with Shear of 10 sec⁻¹, Salinity of 15 ppt, Type A Sediment, and Suspended Solids of 40 mg/l at a Depth of 34.4 cm

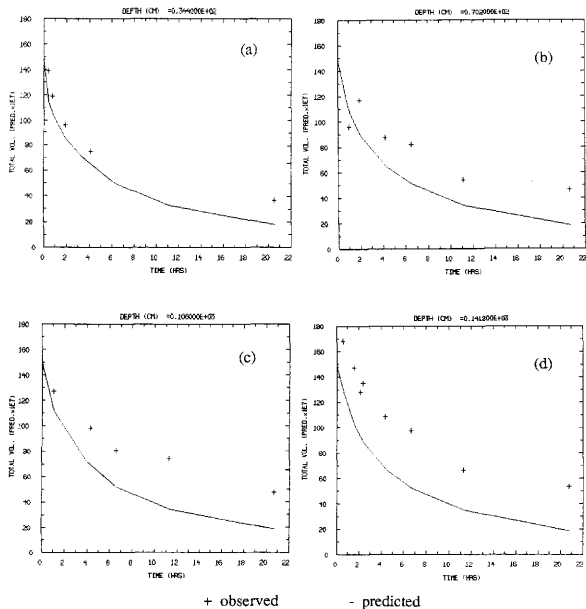


Fig. 19.- Experiment 8: Total Volume Observed and Predicted for Depths (a) 34.4 cm; (b) 70.2 cm; (c) 106.0 cm; and (d) 141.8 cm with G of 20 sec⁻¹ and ∞ of 0.1

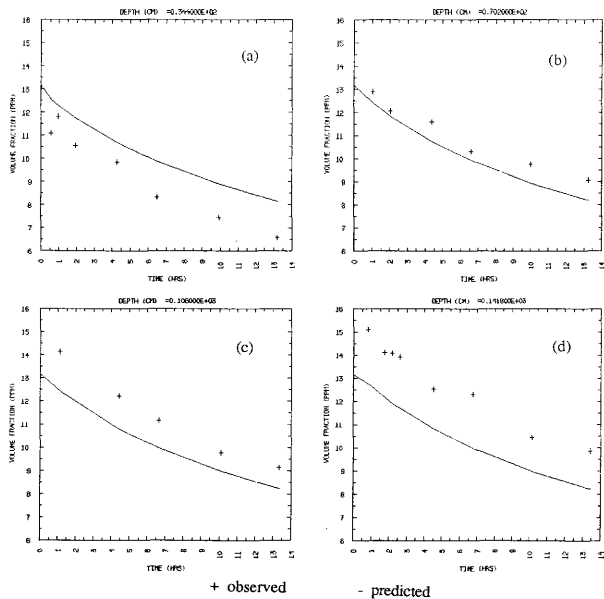


Fig. 20.- Experiment 5: Total Volume Observed and Predicted for Depths (a) 34.4 cm; (b) 70.2 cm; (c) 106.0 cm; and (d) 141.8 cm with G of 30 sec^{-1} and ∞ of 0.1

bottom (Fig. 21). For high shear rates, the particles remained in suspension longer than model predictions. To account for this discrepancy, the addition of porosity was investigated.

POROSITY

As sediments aggregate, water is entrained in the floc. The resulting settling velocity increases, but less than that expected based on increased particle diameters alone. The change in particle density due to water entrainment causes the unexpectedly lower settling velocities. If the porosity can be determined, the new particle density can be calculated. The porosity of the new particle (P_{new}) can be expressed as the volume of the voids (V_{vnew}) divided by the volume of the solids (V_{snew}):

$$P_{new} = \frac{V_{vnew}}{V_{snew}} = \frac{V_{vi} + V_{vj} + V_{eij}}{V_{si} + V_{sj}} \quad (38)$$

where the volume of the voids is expressed as the sum of the volume of the voids of particle size i (V_{vi}) and j (V_{vj}) and the volume of entrained water (V_{eij}) as a result of the collision. The volume of the solids is simply the addition of the volume of particle size i (V_{si}) and j (V_{sj}). The volume of the voids can be expressed as:

$$V_v = \left(\frac{P}{1+P} \right) V_T \quad (39a)$$

and the volume of the solids can be expressed as:

$$V_s = \left(\frac{1}{1+P} \right) V_T \quad (39b)$$

where V_T is the total volume of the new particle. The volume of the new particle is:

$$V_{new} = V_i + V_j + V_{cij} \quad (40)$$

where the volume can be expressed in terms of particle diameter (assuming a spherical particle). Using Eq. 11, Eq. 26 (expressed in terms of diameter) was substituted into Eq. 29 to yield a function (F):

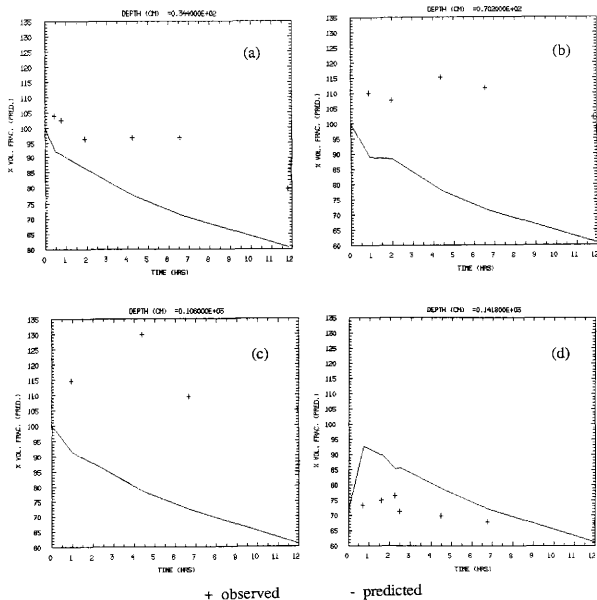


Fig. 21.- Experiment 6: Total Volume Observed and Predicted for Depths (a) 34.4 cm; (b) 70.2 cm; (c) 106.0 cm; and (d) 141.8 cm with G of 40 sec⁻¹ and ∞ of 0.1

$$F = \frac{\pi}{6} d_{\text{new}}^3 - B d_{\text{new}}^{-d} R_{ij} - 2 R_{ij} \quad (41)$$

where d_{new} is the new particle diameter, and R_{ij} represents the volume in terms of a porosity function (Appendix D). The function was numerically solved to yield the new diameter which was used to calculate the new density and volume needed for Stokes settling velocity calculations.

A constant B value of 8.0 was used in the model and the d_{new} value was estimated. Initial estimates for d_{new} less than 1.0 failed. Other estimates greater than one were simulated and had little to no effect on the particle size distribution. The right shifted peak present in the observed size distributions could not be reproduced. Instead, the peak remained shifted to the left. For particle diameters under three microns, the porosity function yields negative porosities. The resulting aggregate density can be as great as 8.0 as seen in Fig. 5. Limits must be implemented to account for porosity of small diameter particles.

ALPHA AND DISPERSION AS SIZE DEPENDENT PARAMETERS

Alpha and dispersion were both allowed to vary as a function of particle size. Varying the dispersion coefficient did not improve the solution fit to the observed data. Therefore, the dispersion coefficient was represented as only one lump parameter.

Alpha was subscripted for each particle size category. This allowed a difference in collision potential between small and large particles. The porosity term was represented with $B = 8.0$ and $d = 1.6$. Experiment 16, the lowest shear rate (10 sec⁻¹), is presented as an example. Alpha values ranging from 0.05 to 0.3 were used for the model predictions in Figure 22. By using alpha values ranging from 0.8 to 0.9, the over prediction of particle settling rates in Figure 22 was cut by one half (Fig. 23). Both ranges of alpha were used to predict total particle volume for the highest shear rate (40 sec⁻¹), and almost identical results were obtained. The model prediction using alpha values ranging from

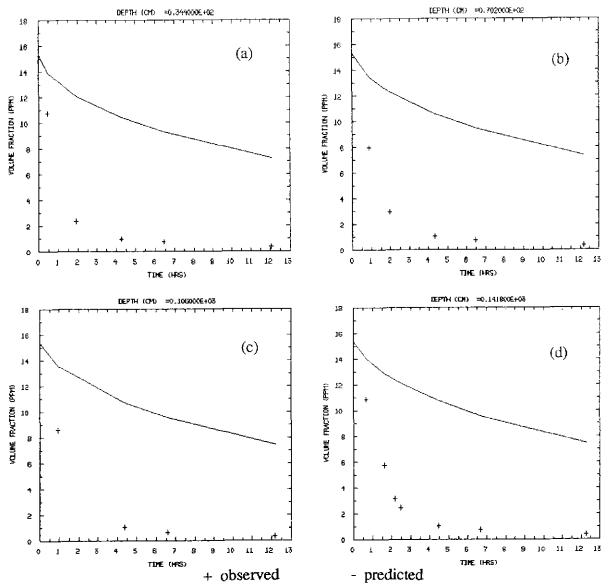


Fig. 22.- Experiment 16: Total Volume Observed and Predicted with $\omega_{c 1-7}$ Equal to 0.05, 0.10, 0.15, 0.20, 0.25, 0.30, and 0.35, Respectively for Depths (a) 34.4 cm; (b) 70.2 cm; (c) 106.0 cm; and (d) 141.8 cm

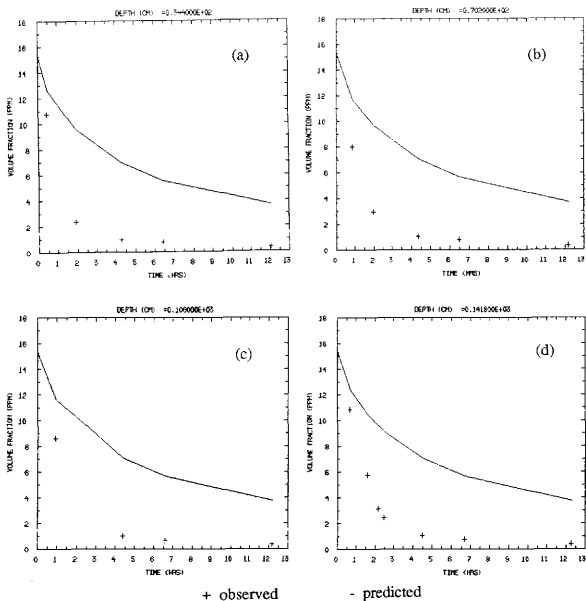


Fig. 23.- Experiment 16: Total Volume Observed and Predicted with $\alpha_{c 1-7}$ Equal to 0.80, 0.80, 0.80, 0.85, 0.85, 0.90, and 0.90, Respectively for Depths (a) 34.4 cm; (b) 70.2 cm; (c) 106.0 cm; and (d) 141.8 cm

0.05 to 0.3 are presented in Figure 24. The model over predicted particle settling rates throughout the settling column. Apparently, flocculation is not the only mechanism important to particle transport within the settling column. Resuspension and floc breakup are two processes which may be significant. First, the particles could be settling rapidly, but the apparent decrease in settling velocity could really be a resuspension of the particles. Second, the flocs may be breaking apart which would reduce settling velocity through decreased particle diameters.

RESUSPENSION

Because mass was still being retained within the water column and this phenomena increased with shear rate, a resuspension term was added. The concentration in the column was too low for a sediment bed to form at the bottom of the settling column. However, a decay factor was added to allow particles to be carried upward: The resuspension velocity (V_B) is a function of settling velocity:

$$V_B = \frac{V_s}{K_R + V_s} V_s \quad (42)$$

where K_R is a resuspension constant. The resuspension constant obtained was on the order of 1.0×10^{-6} . This value is extremely small and was not significant. The implementation of the questionable porosity function may attribute to this conclusion.

The addition of the above combination of parameters (flocculation, porosity, subscription of alpha, and resuspension) was not successful. Floc breakup was then investigated as a possible solution. Flocs can break up thus decreasing mean diameters and consequently settling velocity. After reviewing the performance of previous mechanisms, a combination of flocculation (one alpha), floc breakage due to erosion, and resuspension (present due to high shear rates) was implemented.

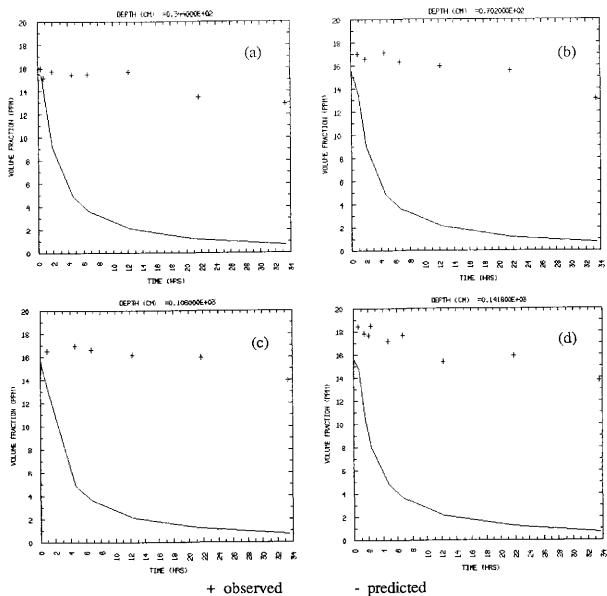


Fig. 24.- Experiment 21: Total Volume Observed and Predicted with $\alpha_{c1.7}$ Equal to 0.05, 0.10, 0.15, 0.20, 0.25, 0.30, and 0.35, Respectively for Depths (a) 34.4 cm; (b) 70.2 cm; (c) 106.0 cm; and (d) 141.8 cm

FLOC BREAKUP

For modeling purposes, floc erosion rather than floc splitting was implemented. Floc splitting occurs mostly due to pressure differences and was therefore not taken into account. Also, by neglecting splitting, the parameters necessary to evaluate are reduced from six to three which constrains the solution of the model and reduces parameter estimation time by one half. The equation for erosion is taken from Eq. 10:

$$\frac{\partial n(v,t)}{\partial t} = \int_v^{\infty} q_e(\bar{v}) n(\bar{v}, t) P_e(v, \bar{v}) d\bar{v} - \frac{\partial}{\partial v} \left[\left(\frac{dv}{dt} \right)_e n(v, t) \right] \quad (43)$$

where:

$$q_e(\bar{v}) = \bar{k}G \quad (43a)$$

and

$$P_e(v) = \frac{1}{v\sqrt{2\pi \ln \sigma_{ge}}} \exp \left[\frac{-(\ln v - \ln \bar{v}_{ge})^2}{2 \ln^2 \sigma_{ge}} \right] \quad (43b)$$

and

$$-\left(\frac{dv}{dt} \right)_e = \frac{\bar{k} \int_v^{\infty} P_e(\bar{v}) d\bar{v}}{\int_0^v P_e(\bar{v}) d\bar{v}} G \quad (43c)$$

represent the rate of formation of erosion fines $q_e(\bar{v})$, the probability distribution of eroded particles $P_e(v)$, and the instantaneous rate of change of parent floc volume due to erosion $-(dv/dt)_e$, respectively. The size distribution is considered to be log-normal with σ_{ge} as the geometric standard deviation and \bar{v}_{ge} as the geometric mean, both of which are independent of parent floc size (Lu and Spielman 1985).

Floc erosion was implemented by substituting Eq. 43a and Eq. 43c into Eq. 43 and expressing the resulting equation as summations:

$$\frac{\partial n_k}{\partial t} = \sum_{j=k+1}^N P_{e_{k,j}} n_j G_k - \sum_{j=1}^{k-1} P_{e_{j,k}} n_k G_k \quad (44)$$

where the first term represents the formation of particles due to erosion, and the second term represents the loss of the parent size particle. The model parameters are the erosion constant, geometric mean, and geometric standard deviation which are used to calculate the size distribution. The above model (flocculation, floc breakup due to erosion, and resuspension) fit observed data reasonably well and was used as the transport equation to describe all experiments. The predicted total particle volume shows little discrepancy from observed values at shear rates of 20 sec⁻¹ (Fig.25). As shear rate is increased to 30 sec⁻¹, the model slightly over predicts particle settling rates throughout the top 100 cm, and the fit improves for the bottom half of the column (Fig. 26). The model followed this same trend for shear rates of 40 sec⁻¹ with the over prediction being slightly greater (Fig. 27). Even though the model results show a discrepancy in total particle volume at higher shear rates (G of 30 and 40 sec⁻¹), the predictions are very accurate in terms of total particle number and 3-D particle number and volume size distributions as seen by the predicted and observed correlation coefficients (Appendix E, Table E4). Computation and interpretation of correlation coefficients will be discussed in the following section.

CORRELATION COEFFICIENTS

The model results and experimental data were compared statistically by using correlation coefficients. The basic formula for computation of the correlation coefficient (R) is as follows (Holman and Gajda 1984):

$$R = \left[1 - \frac{\sigma_{y,x}^2}{\sigma_y^2} \right]^{0.5} \quad (45)$$

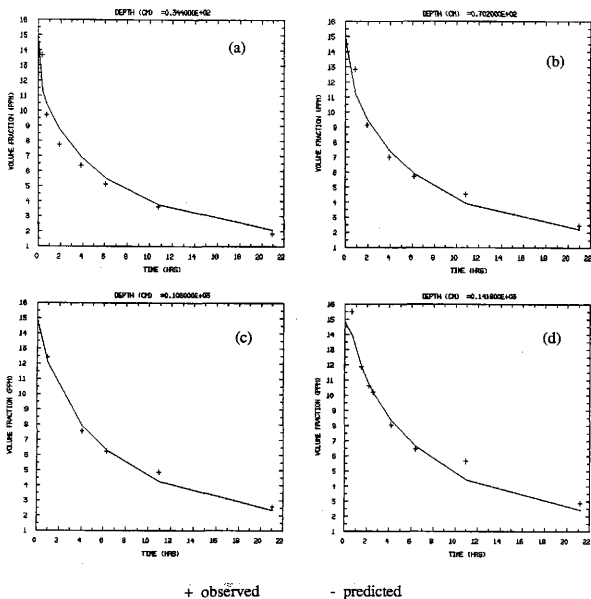


Fig. 25.- Experiment 20: Total Volume Observed and Predicted for Depths (a) 34.4 cm; (b) 70.2 cm; (c) 106.0 cm; and (d) 141.8 cm with G of 20 sec⁻¹

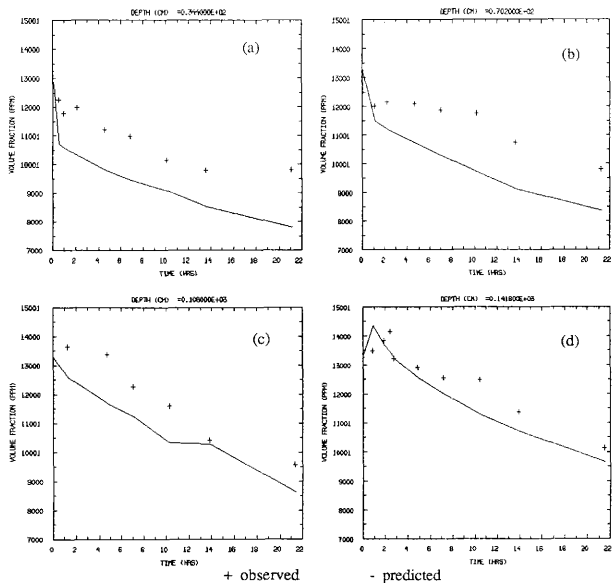


Fig. 26.- Experiment 3: Total Volume Observed and Predicted for Depths (a) 34.4 cm; (b) 70.2 cm; (c) 106.0 cm; and (d) 141.8 cm with G of 30 sec^{-1}

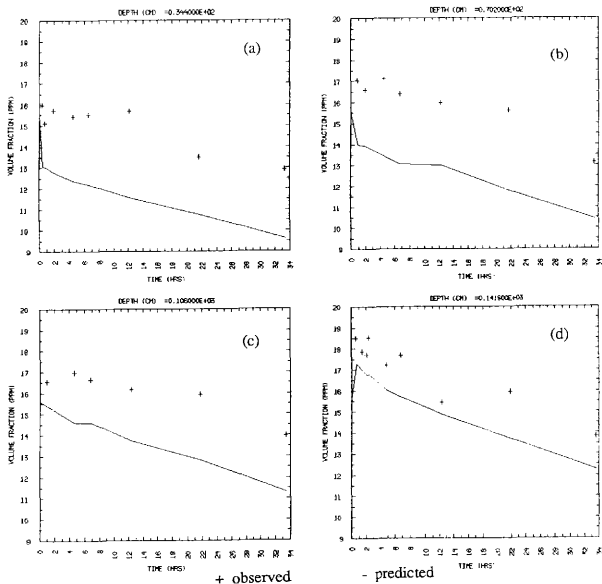


Fig. 27.- Experiment 21: Total Volume Observed and Predicted for Depths (a) 34.4 cm; (b) 70.2 cm; (c) 106.0 cm; and (d) 141.8 cm with G of 40 sec⁻¹

where

$$\sigma_y = \left[\frac{\sum_{i=1}^n (y_i - y_m)^2}{n-1} \right]^{0.5} \quad (45a)$$

and

$$\sigma_{y,x} = \left[\frac{\sum_{i=1}^n (y_i - y_{ic})^2}{n-2} \right]^{0.5} \quad (45b)$$

where y_i is the actual value of y observed, y_{ic} is the computed y , and y_m is the mean y . The correlation coefficients were computed based on total particle number, total particle volume, particle number, and particle volume (for a given time) by replacing the y with particle number and particle volume, respectively. The total number and volume correlation give an indication of fit throughout the column at a given time. The number and volume correlations indicate the fit based on individual points in space and time. The model predicted particle number concentration (the volume was computed from number values), therefore the correlation coefficient for total number is slightly higher in most cases than that for volume. The estimation routine (PARMEST) was run until the correlation coefficient for number concentration was greater than 0.90. Any further accuracy would not be feasible due to model run time (which exceeded 48 hours in some cases).

STATISTICAL ANALYSIS

The model parameters for Design 2 and 3 were analyzed to determine the main interactions between factors and their significance. First, a two-way table of total yields was constructed (John and Quenouille 1977). For example, in Experimental Design 2 the two-way table consists of blocks (salinity) along one axis and treatments (shear rate) along the other. The alpha values are then placed correspondingly in the table and totals

for all columns and rows are calculated (Appendix F). The main interactions were computed by dividing the sum of the squares of the treatment by the mean sum of the squares. An analysis of variance is then performed by completing the following table (John and Quenouille 1977):

Table 5.- Analysis of Variance

	Degrees of freedom, d.f.	Sum of squares, s.s.	Mean of squares, m.s.
Blocks	$b-1$	s.s.B	$s.s.B/(b-1)$
Treatments	$t-1$	s.s.T	$s.s.T/(t-1)$
Residual	$(b-1)(t-1)$	differencing	$diff./((b-1)(t-1))$
Total	$bt-1$	s.s.x	

where b and t represent the number of blocks and treatments, respectively. The sum of the squares of x was computed by summing the squares of the parameter under investigation and subtracting the mean square of the column totals. The sum of the squares for the block and treatments was computed by subtracting the mean square of the column totals from the mean sum of the squares of the block and treatment totals. The variance ratio was computed as the mean sum of the squares for the treatments divided by the mean sum of the squares of the residual. Using the corresponding degrees of freedom $[(t-1)/(b-1)(t-1)]$, a 5 % level of significance was chosen from Table A.2 in John and Quenouille (1977). The variance ratio computed from experimental data must exceed the 5 % level of significance in order for the differences in the parameter between the treatments (ie. shear rate) to be significant.

CHAPTER V

RESULTS AND DISCUSSION

The observed and predicted particle size distributions in terms of number and volume were examined to determine the effects of shear, salinity, particle type, and particle concentration on the vertical transport of New Bedford Harbor sediments. In all experiments, two recurrent phenomena were observed: a sudden drop in observed particle number at a depth of 34.4 cm (contrary to predicted results); and an absence of particles in the 77 micron particle category of predicted particle volume distributions (contrary to observed results). The observed and predicted particle size distribution, total particle volume, and total particle number plots are presented and discussed in relation to the three experimental designs outlined in Chapter 3: concentration, shear and salinity, and salinity and particle type variation. The resulting model parameters, alpha, erosion constant, geometric mean, geometric standard deviation, and resuspension constant, for each experimental design are presented and discussed as well as the statistical interactions and significance between experimental factors.

OBSERVED AND PREDICTED RESULTS

The observed particle number distributions closely resembled those predicted except for two distinct phenomena. One trend present in all observed data is a sudden drop in particle number at a depth of 34.4 cm during the first hour of the experiment. The predicted particle numbers decrease at the same rate throughout the column. Another phenomena can be seen in the particle volume distributions. For experiments in which the observed volume distributions present particles in the 77 micron size category, these large particles are absent in predicted volume distributions.

Particle Number Distribution

The observed number distribution at the top (depth of 34.4 cm) shows that particles settled faster initially than predicted for all experiments. The observed distribution at a depth of 34.4 cm (Fig. 28a) drops rapidly over the first two hours while the distribution at a depth of 141.8 (Fig. 28b) drops at a consistent rate. The predicted number distributions decrease at the same rate throughout the column (Fig. 29). Possible explanations for the phenomena observed at the top of the settling column include: boundary effects at the top of the column, floc shape, or the flocculation process itself.

Boundary effects at the top of the column that are not accounted for in the model may indirectly affect flocculation. Dye studies have shown that no advective currents are present at the top of the column (Ducharme 1989). However, the turbulence (size of eddies) may be different at the top of the column due to the boundary presented by the water surface. The model does not incorporate any variation of turbulence based on spatial locations. The predicted size distributions are similar throughout the depth of the column (Fig. 29) while the observed distributions for the top of the column vary from those at greater depths (Fig. 28). Turbulence can affect the probability of particle contacts as determined by eddy size or the shape of flocs.

Large eddies will only be effective in colliding large particles, and small particles are brought into contact by smaller eddies (Cleasby 1984). If the boundary effects at the top of the column are sufficient to produce smaller eddies, particle contact would be enhanced causing flocculation into larger particles. These large particles would have increased settling velocities which would decrease the mass in the system. The rapid decrease in observed number distributions (Fig. 28a) and shifted volume distribution (Fig. 30a) appears to support this explanation. Figure 28a shows a drastic decrease in particle number during the first two hours at a depth of 34.4 cm. Particle volume (Fig. 30a) decreases also, but at a slower rate. As seen in the volume distribution, large particles are present at all times.

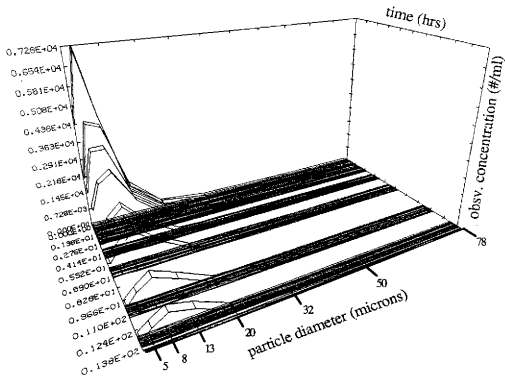


Fig. 28a.- Experiment 7: Heterogeneous Particle Number-Based Observed Size Distribution with Shear of 20 sec⁻¹, Salinity of 15 ppt, Type A Sediment, and Suspended Solids of 10 mg/l at a Depth of 34.4 cm

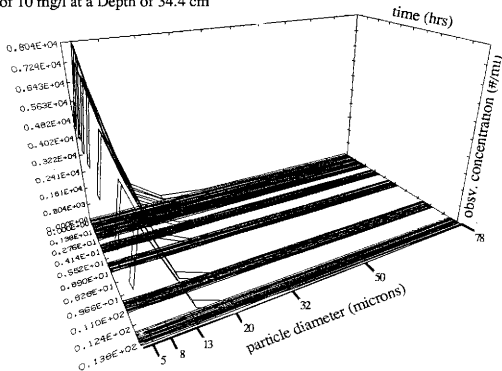


Fig. 28b.- Experiment 7: Heterogeneous Particle Number-Based Observed Size Distribution with Shear of 20 sec⁻¹, Salinity of 15 ppt, Type A Sediment, and Suspended Solids of 10 mg/l at a Depth of 141.8 cm.

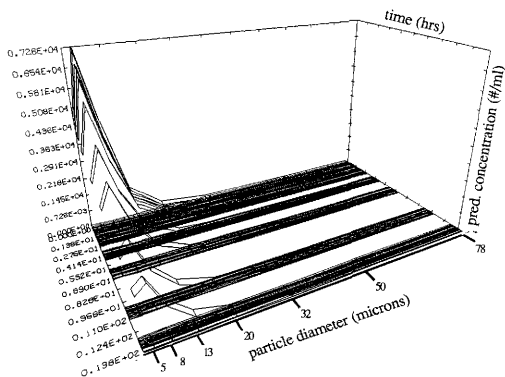


Fig. 29a.- Experiment 7: Heterogeneous Particle Number-Based Predicted Size Distribution with Shear of 20 sec⁻¹, Salinity of 15 ppt, Type A Sediment, and Suspended Solids of 10 mg/l at a Depth of 34.4 cm

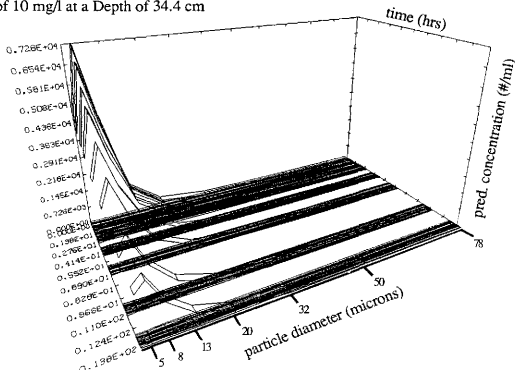


Fig. 29b.- Experiment 7: Heterogeneous Particle Number-Based Predicted Size Distribution with Shear of 20 sec⁻¹, Salinity of 15 ppt, Type A Sediment, and Suspended Solids of 10 mg/l at a Depth of 141.8 cm

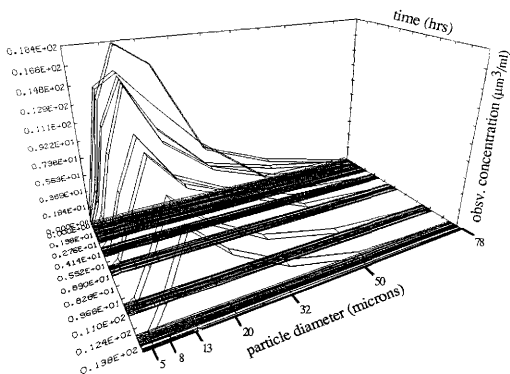


Fig. 30a.- Experiment 7: Heterogeneous Particle Volume-Based Observed Size Distribution with Shear of 20 sec^{-1} , Salinity of 15 ppt, Type A Sediment, and Suspended Solids of 10 mg/l at a Depth of 34.4 cm

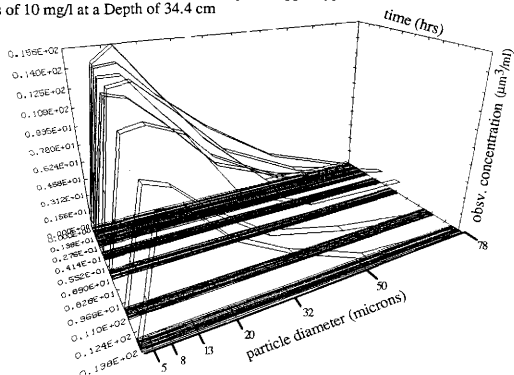


Fig. 30b.- Experiment 7: Heterogeneous Particle Volume-Based Observed Size Distribution with Shear of 20 sec^{-1} , Salinity of 15 ppt, Type A Sediment, and Suspended Solids of 10 mg/l at a Depth of 141.8 cm

As seen in by the particle number distribution (Fig. 28a), most of the particles are approximately 10 microns in diameter, but the size of particles containing the greatest volume is 20 microns (Fig. 30a). The observed number distribution appears to decrease, but actually the volume is shifted to the larger particles. No large particles (77 micron) are present in the predicted distribution (Fig. 31a). The presence of many small particles and absence of particle volume in large particle categories in predicted distributions may indicate under prediction of alpha and/or an over prediction of floc breakup. A higher alpha would decrease particle numbers and increase volume in the large size category. A decrease in floc breakup would preserve the large particles created by flocculation. Perhaps the shear rate should be represented in a different manner, such as incorporating eddy size, at the top of the column.

Based on eddy size, Cleasby (1984) suggests the use of two shear values. For particles with diameters less than Kolmogoroff microscale eddy size, the aggregation rate is suggested to be represented by Eq. 18 (Oldshue 1983). The aggregation rate for larger particles is recommended to be proportional to the cube root of the mean eddy viscosity squared. The root mean square velocity gradient (G) is viscosity dependent and does not include eddy viscosity. Small particles are viscosity dependent as opposed to large particles which are independent of viscosity effects, thus the use of shear representation dependent on particle size is suggested. Glasgow and Kim (1986) also suggests compartmentalizing shear due to the inadequacy of G in describing pertinent local turbulence. The behavioral difference according to particle size can also be seen by examination of Peclet numbers. Based on particle Peclet numbers, with dispersion values ranging from 1.0 to 6.0, particles less than 20 microns are dispersive dominant and larger particles are advective dominant (Chap. 4, Fig. 15). Perhaps shear should be represented as a function based on particle size.

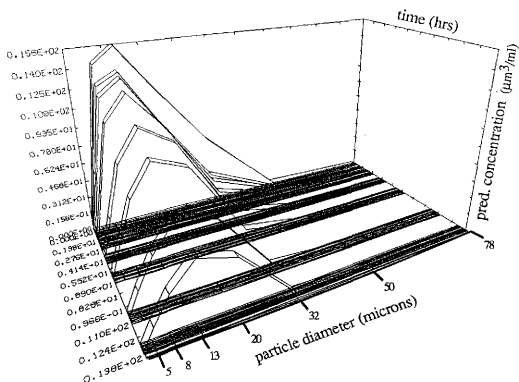


Fig. 31a.- Experiment 7: Heterogeneous Particle Volume-Based Predicted Size Distribution with Shear of 20 sec^{-1} , Salinity of 15 ppt, Type A Sediment, and Suspended Solids of 10 mg/l at a Depth of 34.4 cm

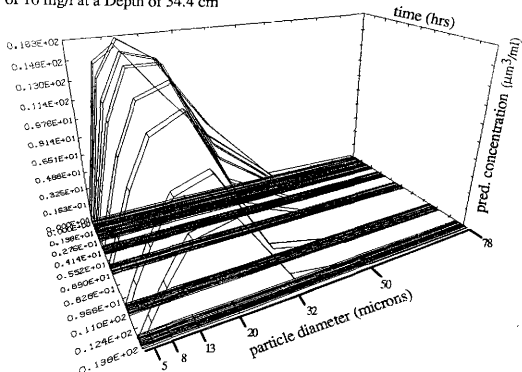


Fig. 31b.- Experiment 7: Heterogeneous Particle Volume-Based Predicted Size Distribution with Shear of 20 sec^{-1} , Salinity of 15 ppt, Type A Sediment, and Suspended Solids of 10 mg/l at a Depth of 141.8 cm

Depending on the hydrodynamics, flocs may vary in shape which will in turn affect particle settling velocities (Powell and Mason 1982). Experiments using cohesive polystyrene spheres show that under sheared conditions, flocs were deformed first into an ellipsoid and then further elongated into a cylinder. Ultimately, necking occurred as the cylinder was further stretched, and small clusters of particles were broken away from the parent floc. Particle shape determines the drag coefficient and can alter particle settling velocity by a factor of two. The forces acting on a particle can be represented as:

$$\frac{4}{3}\pi r^3 \rho_s g - \frac{4}{3}\pi r^3 \rho_l g - \frac{C_D \pi r^2 \rho_l v^2}{2} = 0 \quad (46)$$

where the terms represent gravitational force, buoyant force, and drag force, respectively.

This expression can be solved for the terminal settling velocity of the particle:

$$V_T = \left[\frac{4Dg(\rho_s - \rho_l)}{3C_D \rho_l} \right]^{1/2} \quad (47)$$

For particle Reynolds numbers less than 2.0, laminar settling described by Stokes law can be applied (Oldshue 1983). The coefficient of drag (for $Re < 200,000$) can therefore be represented as:

$$C_{D,cylinder} = 1.0 + 10.0(Re)^{-0.67} \quad (48)$$

$$C_{D,sphere} = \frac{24}{Re} + \frac{6}{1 + \sqrt{Re}} + 0.4 \quad (49)$$

for cylinders and spheres, respectively (Gerhart and Gross 1985). Based on the particle Reynolds numbers, laminar conditions applied locally around the particle. Under these conditions, the drag coefficient for a sphere is up to eight times greater than that for a cylinder. The resulting velocity for a cylindrical shaped particle is twice that of a sphere. The aggregates resulting from flocculation are assumed spherical in the model. Considering the possibility of cylindrical shaped particles, the model would tend to under predict settling velocities at the top of the column which is indeed the case (Fig. 32a). In

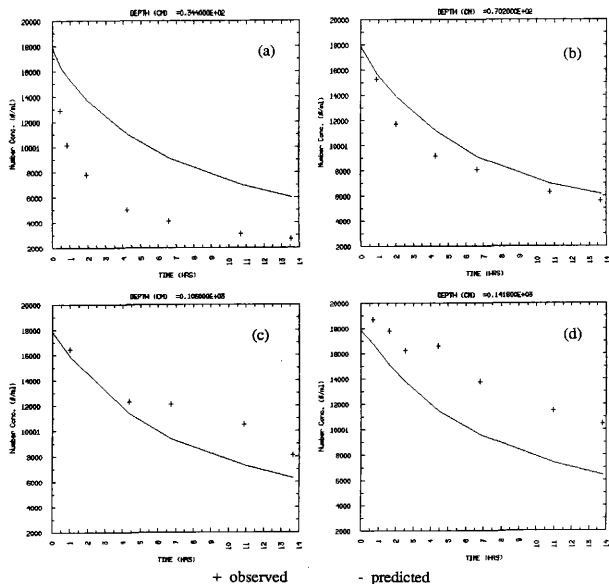


Fig. 32.- Experiment 7: Total Particle Number Observed and Predicted for Depths (a) 34.4 cm; (b) 70.2 cm; (c) 106.0 cm; and (d) 141.8 cm with Shear of 20 sec⁻¹, Salinity of 15 ppt, Type A Sediment, and Suspended Solids of 10 mg/l

the model the drag coefficient is represented as $24/Re$ as defined in Stokes law. This is a typical representation for settling particles and the resulting difference from Eq. 49 is not great. The above theory is based on local conditions only, thus the validity is questionable.

The flocculation process in itself may be the answer to the seemingly greater increase in settling velocity at the top of the column. As particles flocculate, a great number of small particles produce one large particle. The presence of the large particle is not as obvious as the sudden disappearance of many small particles, thus the settling velocity appears to drastically increase. The mass available to enter the top segment is limited which also yields the appearance of increased settling velocities. Sediment entering segment two is limited by the amount of sediment present in segment one. The sediments in segment one will flocculate and settle to segment two. After all the sediments have passed segment one, no new segments are available for flocculation, thus the obvious decrease in particle number at the top of the column. The bottom of the column does not display this sudden decrease in particle numbers due to the continual settling of particles through the length of the settling column. The flocculation process is the most likely explanation for the seemingly higher settling velocities at the top of the column.

Particle Volume Distribution

The observed and predicted particle volume decrease over time, but the distributions retain their initial shape (Fig. 30 and 31). The basic difference between observed and predicted distributions is the absence of larger particles over time in the predicted distributions. For all experiments in which particles in the 77 micron category are present after one hour, the observed data indicates that these particles are present throughout all time (Fig. 30a and 30b). Large particles (77 microns) are absent in predicted size distributions (Fig. 31a and 31b). Increased porosity or the choice of size categories are two possible explanations for this discrepancy. The constant density assumed in the model may allow the particles to settle faster in predicted results rather than observed

results. As aggregates are formed, water is entrained within their structure thus lowering density (Boadway 1978; Krone 1978). From figure 6, assuming a solid density of 1.1 g/ml, the lower density due to porosity will slow settling velocity as much as 64% a 77 micron particle. Porosity can be incorporated to account for water entrainment, but this increases the complexity of the model. One additional parameter must be estimated by the model, thus run time is increased and a unique solution is sacrificed. Also, particle history must be accounted for in regards to density changes. Two particles of the same size may have different densities (ie. one is a primary particle and one is an aggregate). To keep track of every particle diameter would require a very large data base or a sophisticated algorithm. The level of model improvement due to the addition of porosity may not warrant the increased complexity necessary to incorporate porosity.

The choice of size categories for the model must also be taken into consideration when drawing conclusions concerning large particle diameters. The raw particle size data was divided into 256 size categories by the electronic particle counter. This data was then condensed into eight categories by choosing upper and lower limits on a log scale and representing only the mean size in the model. Particle sizing is very important to processes previously described: eddy and particle interaction is size dependant; particle radius determines the probability of collision; and settling velocity is dependant on particle diameter. A system with 256 sizes of particles may behave differently than one with only eight sizes. The model attempts to reproduce observed results that cover a wide range of sizes with only eight size categories. The goodness of fit of the model is compared with a condensed version of the observed data. The upper and lower limits of the size category are small for small particle diameters (<20 microns), but larger particles (49 to 90 microns) are grouped into one large category (77 micron). The relative error (ie. relative difference between lower and upper particle diameters) involved for each size category is 23%. However, once the maximum stable particle size has been reached, it will be consistently presented higher or lower than it's true value. Also, erosion of some

particles may be unaccounted for due to category averaging. A particle may be eroded, but the size change may not be great enough to warrant a change in category. Erosion may be underpredicted which will in turn affect settling velocities.

The average settling velocity for all particles at a given time may be under or over predicted depending on the placement of particles in the last two size categories. For example, the error involved in under or over predicting settling velocity is magnified with the large range for the 77 micron category. The velocity calculations are based on the median size of 77 microns. This represents a possible 33 to 39 % error in velocity calculations. The discrepancy between observed and predicted volume is most likely a combination of porosity and particle size representation.

The results from the experiments were examined in terms of concentration, shear and salinity, and particle type and salinity variation as defined by experimental Designs 1, 2, and 3, respectively (Tables 1, 2, and 3). The previously discussed trends in particle number and volume distributions are present in all experiments. The variation between individual experimental factors will be discussed in the following sections.

DESIGN 1: VARIATION OF CONCENTRATION

Particle concentration was varied in the three experiments as outlined by Table 1. Experiments for initial concentrations of 10 and 40 mg/l (experiments 7 and 8) exhibited the same dynamic size distribution in observed particle size distributions. The peaks in number distributions were shifted slightly to the right of median values throughout time (Fig. 28 and 33). The volume distribution was normally distributed throughout time (Fig. 30 and 34). The 80 mg/l study (experiment 9) exhibited distributions with mean particle sizes much smaller than those in the 10 and 40 mg/l studies (Fig. 35). No particles less than 30 microns were present in observed data for all depths sampled in the column, therefore this is probably the result of sample preparation. Sediments obtained

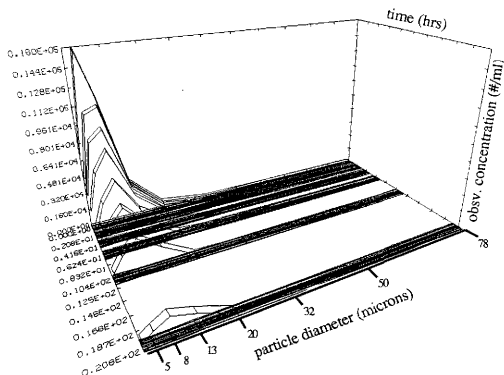


Fig. 33a.- Experiment 8: Heterogeneous Particle Number-Based Observed Size Distribution with Shear of 20 sec⁻¹, Salinity of 15 ppt, Type A Sediment, and Suspended Solids of 40 mg/l at a Depth of 34.4 cm

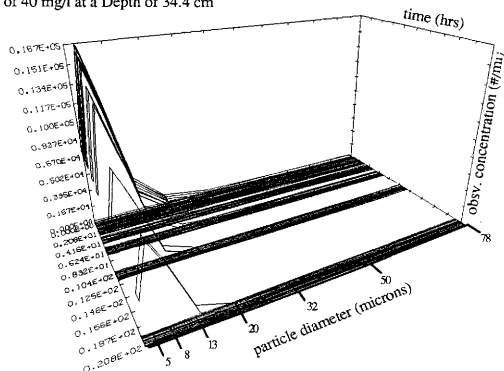


Fig. 33b.- Experiment 8: Heterogeneous Particle Number-Based Observed Size Distribution with Shear of 20 sec⁻¹, Salinity of 15 ppt, Type A Sediment, and Suspended Solids of 40 mg/l at a Depth of 141.8 cm

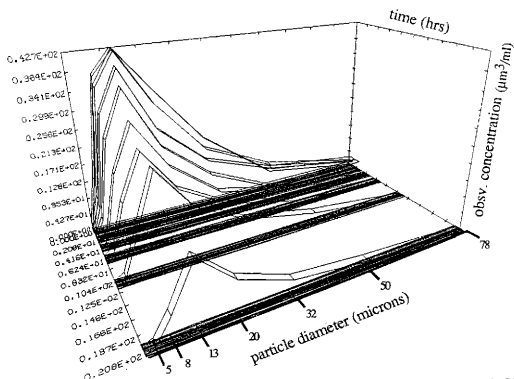


Fig. 34a.- Experiment 8: Heterogeneous Particle Volume-Based Observed Size Distribution with Shear of 20 sec^{-1} , Salinity of 15 ppt, Type A Sediment, and Suspended Solids of 40 mg/l at a Depth of 34.4 cm

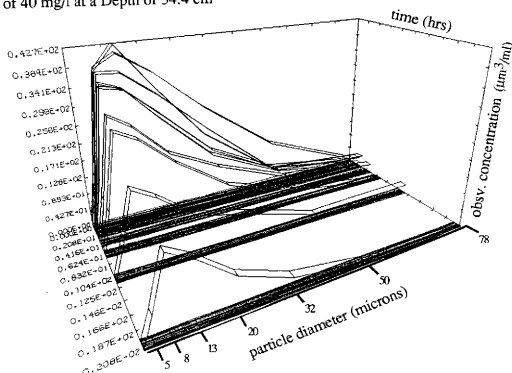


Fig. 34b.- Experiment 8: Heterogeneous Particle Volume-Based Observed Size Distribution with Shear of 20 sec^{-1} , Salinity of 15 ppt, Type A Sediment, and Suspended Solids of 40 mg/l at a Depth of 141.8 cm

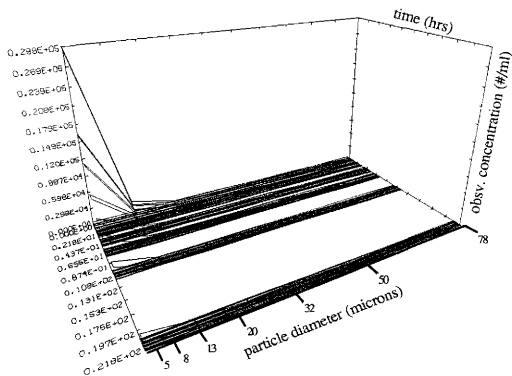


Fig. 35a.- Experiment 9: Heterogeneous Particle Number-Based Observed Size Distribution with Shear of 20 sec⁻¹, Salinity of 15 ppt, Type A Sediment, and Suspended Solids of 80 mg/l at a Depth of 34.4 cm

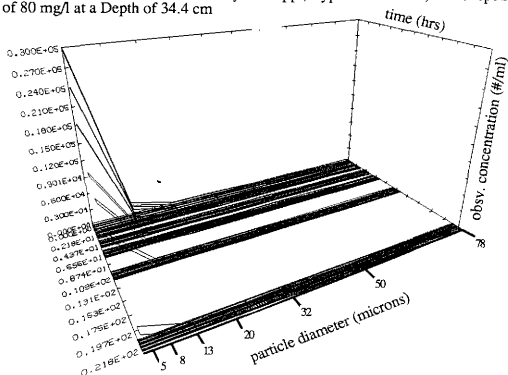


Fig. 35b.- Experiment 9: Heterogeneous Particle Number-Based Observed Size Distribution with Shear of 20 sec⁻¹, Salinity of 15 ppt, Type A Sediment, and Suspended Solids of 80 mg/l at a Depth of 141.8 cm

from New Bedford Harbor were thoroughly mixed. The samples extracted for used in the settling column were shaken to allow for a representative size distribution. For this experiment, a representative sample was not collected. This error is the result of improper mixing or handling of the sample. Due to the above variation in initial distributions of experiments 7, 8, and 9, any conclusions concerning concentration variation must be guarded. However, this variation in initial size distribution can give some insight as to the model performance.

The absence of large particles (77 micron category) in model predictions can be seen in the correlation between model and observed results. The correlation coefficient is above 0.9 for particle size distributions and total volume within the column (Appendix E, Table E4). The size distribution correlations compare each predicted and observed distribution over space and time. Upon visual comparison, this correlation may at first seem too high (Fig. 32 and 36). Approximately five hundred data points were analyzed for particle number and volume. Comparison over such a large number of data points contributes to higher correlations. The total number and volume correlations were the result of analyzing approximately sixty data points. The goodness of fit is more sensitive to each data point when only half the number of points is involved. The correlation for total volume exceeded that of total number and can be seen in Fig. 37 and 38. The correlation coefficient for total number is above 0.9 only for experiment 9. The model predicted the size distributions in experiment 9 more accurately than those in experiments 7 and 8. This can be seen visually in the size distributions and statistically by the high correlation coefficients. The failure to predict the formation of particles in the 40 to 90 micron category in experiment 7 and 8 may be the key to the low correlation in total number. The observed and predicted distributions can be visually examined for trends, but model parameters may give insight as to the processes actually affecting the distribution.

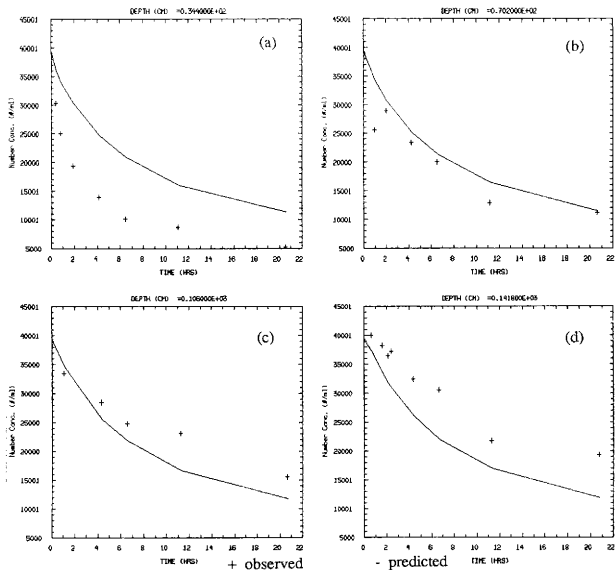


Fig. 36.- Experiment 8: Total Particle Number Observed and Predicted for Depths (a) 34.4 cm; (b) 70.2 cm; (c) 106.0 cm; and (d) 141.8 cm with Shear of 20 sec⁻¹, Salinity of 15 ppt, Type A Sediment, and Suspended Solids of 40 mg/l

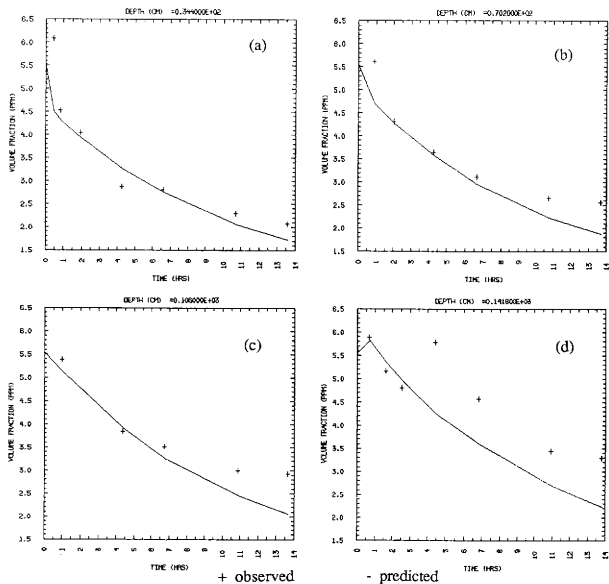


Fig. 37.- Experiment 7: Total Particle Volume Observed and Predicted for Depths (a) 34.4 cm; (b) 70.2 cm; (c) 106.0 cm; and (d) 141.8 cm with Shear of 20 sec⁻¹, Salinity of 15 ppt, Type A Sediment, and Suspended Solids of 10 mg/l

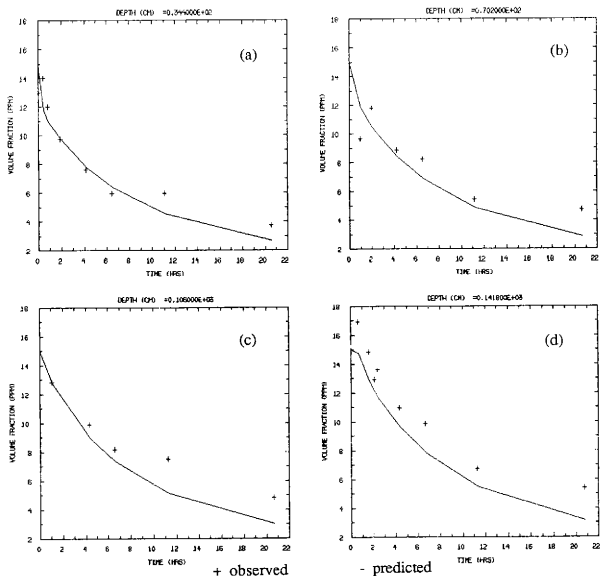


Fig. 38.- Experiment 8: Total Particle Volume Observed and Predicted for Depths (a) 34.4 cm; (b) 70.2 cm; (c) 106.0 cm; and (d) 141.8 cm with Shear of 20 sec⁻¹, Salinity of 15 ppt, Type A Sediment, and Suspended Solids of 40 mg/l

Alpha

Alpha describes the efficiency of collisions and ranges from 0 to 1.0 (1.0 for all collisions being effective). The alpha values for all experiments varied between 0.0457 and 0.254 (Appendix E, Table E1). Alpha values decreased with increasing concentration (Fig. 39). The concentrations used in all experiments were below 100 mg/l. Typically for low concentrations (less than 300 mg/l), settling is considered discrete due to the improbability of particle contacts based on particle radius (Krone 1978). According to the model results flocculation does occur. Shear rate promotes flocculation for low concentration conditions, whereas under quiescent conditions no flocculation would occur. The apparent decrease in alpha with concentration can only be compared with the 10 and 40 mg/l experiments. The mean particle size in the 80 mg/l experiment was much smaller than that in the other two experiments. No valid conclusion regarding particle concentration effects can be made based on comparison between only two experiments.

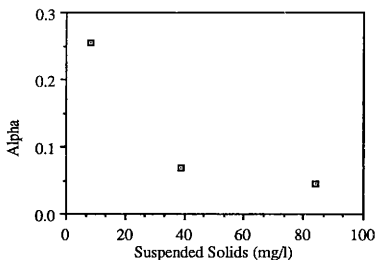


Fig. 39.- The Effect of Concentration on Alpha

Erosion

The model parameters used to describe erosion were the erosion constant, geometric mean, and geometric standard deviation. The erosion constant describes the rate of formation of erosion fines and is dependant on system chemistry only (Pandya and Spielman 1982; Lu and Spielman 1985). The erosion constant decreases with increasing suspended solid concentrations (Fig. 40). Perhaps the increased concentration enhances particle collisions which are effective in eroding particles. The efficiency of collisions would decrease which can be seen by alpha values in Figure 39.

The geometric mean and standard deviation describes the log-normal size distribution of eroded particles. The geometric mean of the eroded particle size distribution varied from 53 to 190 cubic microns (Fig. 41). This corresponds to geometric mean particle diameters of 4.66 to 7.13 microns. The standard deviation varied from 1.38 to 9.72 (Fig. 42). The geometric mean values for size distributions in literature vary from 25 to 30 cubic microns (Pandya and Spielman 1982) and from 4 to 5 microns (Lu and Spielman 1985) for particle volume and diameter, respectively. Literature values for geometric standard deviations are 3.4 (Pandya and Spielman 1982) and vary from 3 to 7 (Lu and Spielman 1985). The magnitude of difference between literature and experimental values is again attributed to the difference in scope of experimental conditions. The geometric mean decreases with increasing concentration, but no trend is apparent for the standard deviation. Based on the theory that increased concentration promotes erosion, the mean size would decrease with increasing concentration.

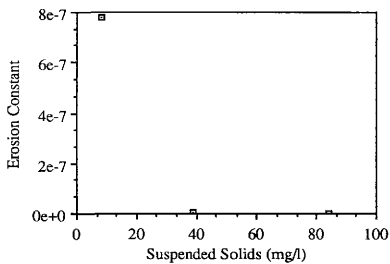


Fig. 40.- The Effect of Particle Concentration on the Erosion Constant

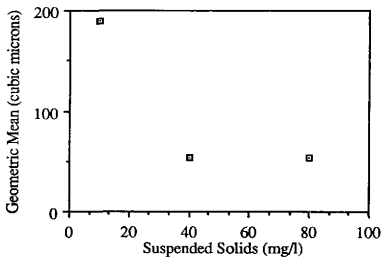


Fig. 41.- The Effect of Particle Concentration on the Geometric Mean

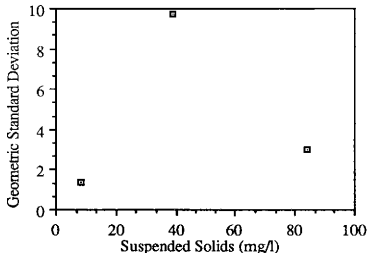


Fig. 42.- The Effect of Particle Concentration on the Geometric Standard Deviation

DESIGN 2: VARIATION OF SHEAR AND SALINITY

Shear and salinity were investigated under three conditions (Table 2). The changes in size distribution in terms of salinity variation were relatively small. Shear exhibited the greatest effect on particle settling, and will be discussed in greater detail. Total number and volume correlation between observed and model results became increasingly worse with increased shear rates (Appendix E, Table E4). At a shear rate of 20 sec^{-1} , the particle number concentration was decreased by 90 % after 21 hours (Fig. 43a and 43b). The particles remained in suspension longer as shear was increased from 30 to 40 sec^{-1} . At shear rates of 30 and 40 sec^{-1} , the particle number concentration decreased by 60 % after the first 12 hours (Figs. 44 and 45, respectively). For a shear of 30 sec^{-1} , the particle number concentration decreased by another 10 % at 21 hours. The particle number concentration did not decrease more than 60 % for a shear rate of 40 sec^{-1} . The observed volume distributions indicate the presence of large particles throughout time. At a shear rate of 20 sec^{-1} , the particle volume indicates that particles are present throughout all size

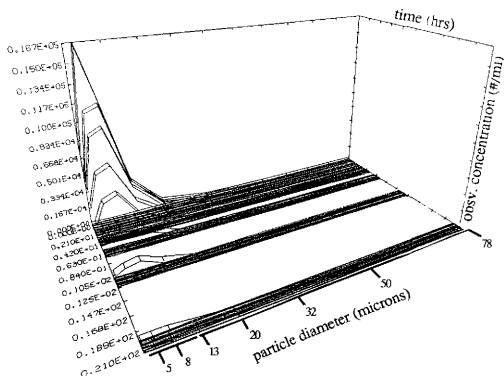


Fig. 43a.- Experiment 18: Heterogeneous Particle Number-Based Observed Size Distribution with Shear of 20 sec⁻¹, Salinity of 15 ppt, Type A Sediment, and Suspended Solids of 40 mg/l at a Depth of 34.4 cm

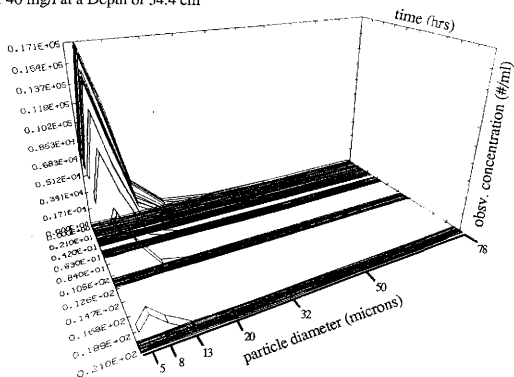


Fig. 43b.- Experiment 18: Heterogeneous Particle Number-Based Observed Size Distribution with Shear of 20 sec⁻¹, Salinity of 15 ppt, Type A Sediment, and Suspended Solids of 40 mg/l at a Depth of 141.8 cm

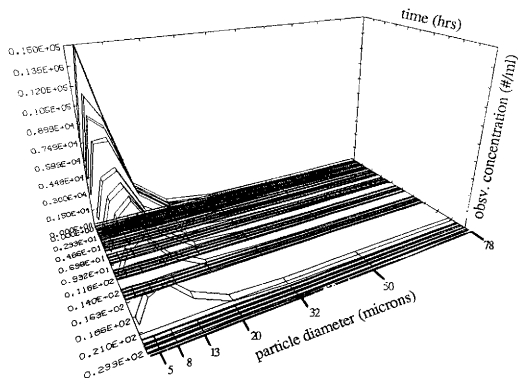


Fig. 44a.- Experiment 2: Heterogeneous Particle Number-Based Observed Size Distribution with Shear of 30 sec^{-1} , Salinity of 15 ppt, Type A Sediment, and Suspended Solids of 40 mg/l at a Depth of 34.4 cm

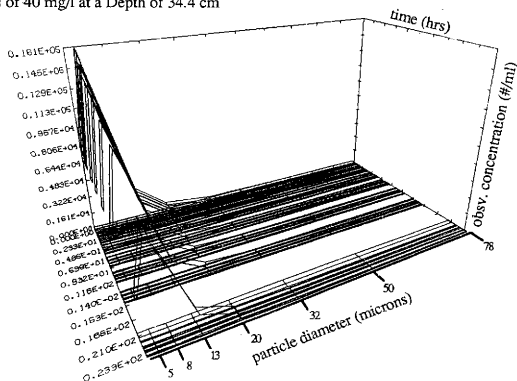


Fig. 44b.- Experiment 2: Heterogeneous Particle Number-Based Observed Size Distribution with Shear of 30 sec^{-1} , Salinity of 15 ppt, Type A Sediment, and Suspended Solids of 40 mg/l at a Depth of 141.8 cm

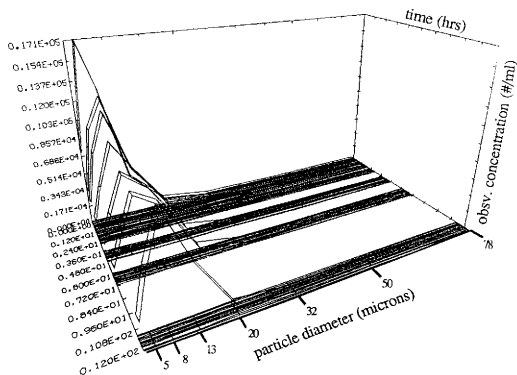


Fig. 45a.- Experiment 6: Heterogeneous Particle Number-Based Observed Size Distribution with Shear of 40 sec^{-1} , Salinity of 15 ppt, Type A Sediment, and Suspended Solids of 40 mg/l at a Depth of 34.4 cm

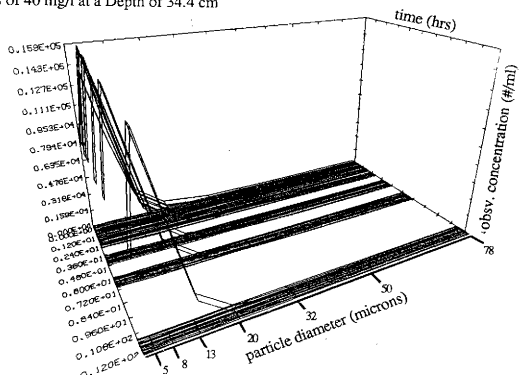


Fig. 45b.- Experiment 6: Heterogeneous Particle Number-Based Observed Size Distribution with Shear of 40 sec^{-1} , Salinity of 15 ppt, Type A Sediment, and Suspended Solids of 40 mg/l at a Depth of 141.8 cm

categories during the first six hour of the experiment (Fig. 46). As shear increased, the volume of particles in the last category increased. At a shear of 30 sec^{-1} , particle volume can be observed throughout all size categories over a 23 hour time period (Fig. 47). As the shear was increased to 40 sec^{-1} , the particle volume was further increased (Fig. 48). Several reasons exist: decrease in particle density due to water entrainment, an increase in the maximum erodible size, eddy viscosity effects, or particle shape.

Lavelle et al. (1988) has found that smaller flocs or flocs of lower density are produced as shear is increased. Due to the presence of large particles as seen in volume distributions, lower floc density seems a more likely explanation in this case. The larger particles may have lower settling velocities, thus the particle would remain in suspension longer. The lower settling velocity would be the result of a decrease in density due to water entrainment. As stated previously, density decrease due to an increased porosity is more visible in larger particles. The model assumed a constant density for all particles. The absence of large particles in model predictions may be due to these particles settling out of suspension.

Another possibility is the increase in particle maximum erodible size. The flocculation rate in the column increases with G to continually produce large particles. Floc breakup may also occur, but is overshadowed by the aggregation rate. Flocs have a maximum erodible size (ie. flocculation and floc breakup will affect all sizes of particles, but a maximum particle size exists and is defined by system conditions). Perhaps this size increases with shear. Based on observed data, a possibility exists that flocculation and/or floc breakup of large particles is under predicted in model results. An increased α would allow small particles to aggregate and constantly provide new large particles which are absent in predicted size distributions.

Another possibility for the differences between observed and predicted particles in the larger size categories is the treatment of viscosity. As previously discussed, eddies of a

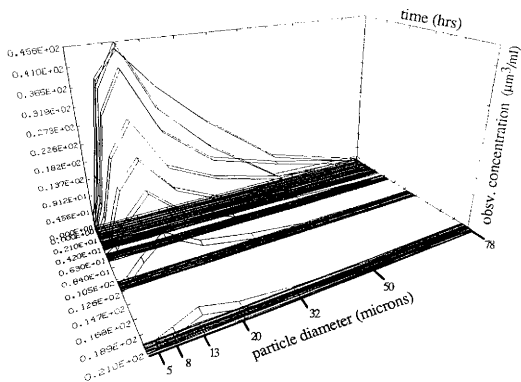


Fig. 46a.- Experiment 18: Heterogeneous Particle Volume-Based Observed Size Distribution with Shear of 20 sec^{-1} , Salinity of 15 ppt, Type A Sediment, and Suspended Solids of 40 mg/l at a Depth of 34.4 cm

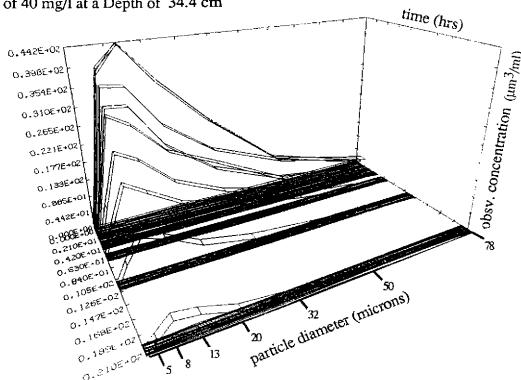


Fig. 46b.- Experiment 18: Heterogeneous Particle Volume-Based Observed Size Distribution with Shear of 20 sec^{-1} , Salinity of 15 ppt, Type A Sediment, and Suspended Solids of 40 mg/l at a Depth of 141.8 cm

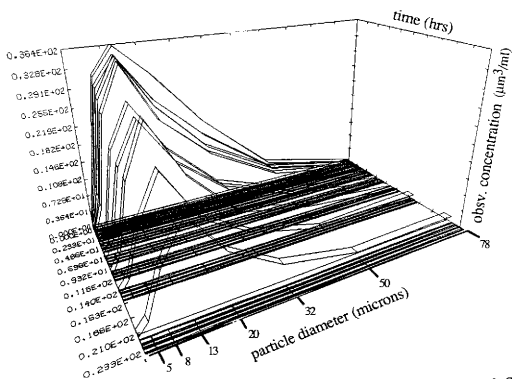


Fig. 47a.- Experiment 2: Heterogeneous Particle Volume-Based Observed Size Distribution with Shear of 30 sec^{-1} , Salinity of 15 ppt, Type A Sediment, and Suspended Solids of 40 mg/l at a Depth of 34.4 cm

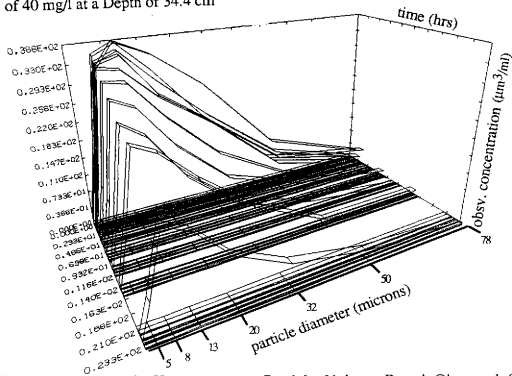


Fig. 47b.- Experiment 2: Heterogeneous Particle Volume-Based Observed Size Distribution with Shear of 30 sec^{-1} , Salinity of 15 ppt, Type A Sediment, and Suspended Solids of 40 mg/l at a Depth of 141.8 cm

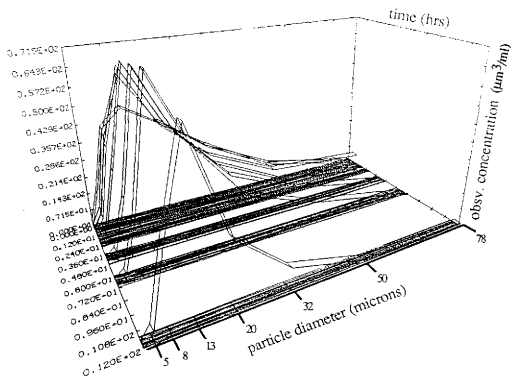


Fig. 48a.- Experiment 6: Heterogeneous Particle Volume-Based Observed Size Distribution with Shear of 40 sec⁻¹, Salinity of 15 ppt, Type A Sediment, and Suspended Solids of 40 mg/l at a Depth of 34.4 cm

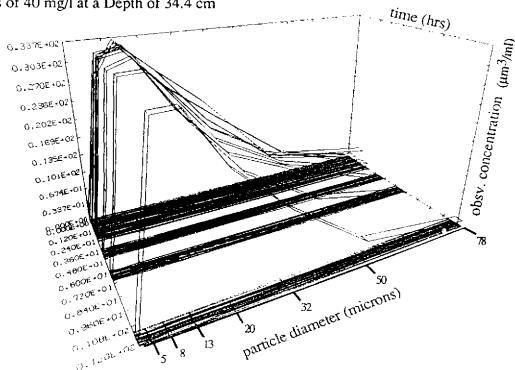


Fig. 48b.- Experiment 6: Heterogeneous Particle Volume-Based Observed Size Distribution with Shear of 40 sec⁻¹, Salinity of 15 ppt, Type A Sediment, and Suspended Solids of 40 mg/l at a Depth of 141.8 cm

particular size will only affect particles of a given size. Perhaps the larger particles should be treated in terms of eddy viscosity. The distribution of eddy sizes may change with increasing G . The increase of G may increase the number of small eddies. These small eddies may promote the contact of small particles, thus large particles are constantly formed. The model makes no distinction between size in terms of shear, therefore perhaps the flocculation has been under predicted.

The increase of G may affect the particle shape. The flocs formed under high shear conditions must have strong bonds in order to avoid splitting and erosion. Krone (1978) reports that spherical shaped aggregates are formed under sheared conditions. However, the sheared conditions were not described. This finding is contrary to Powell and Mason (1982). Perhaps the difference is due to the use of possible turbulent conditions by Krone as opposed to the laminar shear conditions used by Powell and Mason. The formation of spherical particles would yield a lower settling velocity than for a cylindrical particle as previously discussed. The model assumes spherical particles, thus the formation of spherical particles in the column with increasing shear does not explain the differences in observed and predicted volume distributions. The conditions in the column varied from Powell and Mason's, but the possibility of elongated particles can not be totally disregarded. The elongation of particles with increasing shear would yield higher settling velocities for predicted distributions. Perhaps this would explain model under predictions in the large categories. However, small particles would also be affected to a smaller degree.

Alpha

The shear rate variation in experimental Design 2 seemed to have the greatest effect on alpha. An extra experiment was performed at a shear rate of 10 sec^{-1} and a salinity of 15 ppt in order to investigate the trend in model results. Based on model results, as shear increased the alpha values tapered off and neared zero (Fig. 49). The chance of a particle contacting another may be increased by increasing shear rates, but the efficiency of the

collision may be reduced. The reduction in efficiency is represented by lower alpha values. However, the observed size distributions indicate an increase in alpha and/or lower settling velocities for large particles. Perhaps the predicted decrease in alpha is a reflection of the model's inadequate treatment of large particles.

Calculation of the main interactions (Appendix F), reveals that salinity does have an effect on alpha though it is not as great as that of shear rate. The change in alpha due to salinity was significant only at low shear (10 sec⁻¹). This follows trends presented in Fig. 7 (Burt 1986). The rate of mean particle settling velocity was greater for low salinities than high salinities. The high alpha present at low salinity reflects greater flocculation, thus increased settling velocities for low salinities.

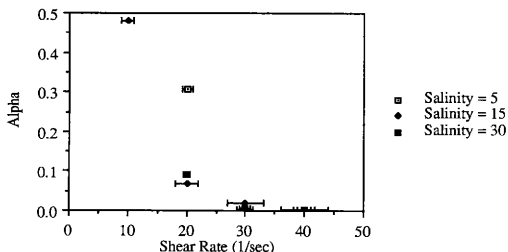


Fig. 49.- The Effect of Shear and Salinity on Alpha

Erosion

The erosion constant was found to slightly decrease for experimental design 2 (Fig. 50). Statistical analysis showed very small interactions for shear and salinity (Appendix F). Shear exceeded the 5 % level of significance for Design 2. The slight decrease in the erosion constant is also found in Pandya and Spielman (1982). Kaolinite values for the

erosion constant are reported as $6.0E-3$ to $8.0E-3$ (Lu and Spielman 1985) and $0.95E-5$ to $1.14E-5$ (Pandya and Spielman 1982). These values (obtained over a range of shear rates) are independent of shear rate. The order of magnitude of difference between Lu and Spielman's (1985) and Pandya and Spielman's (1982) values and experimental values (4.23×10^{-9} to 1.66×10^{-11}) is due to the difference in experimental conditions (ie. 2 m water column compared to a 14.5 l cylinder) and mechanisms used in the model to obtain the erosion parameters. Flocculation was not accounted for in Pandya and Spielman's (1982) model, rather particles were flocculated previous to the experiment and only breakup was studied. As with alpha, increasing shear rates seem to decrease the parameter. Perhaps the decrease in rate of formation in erosion fines and increase in the geometric mean is a means to predict the larger particle sizes present in volume distributions.

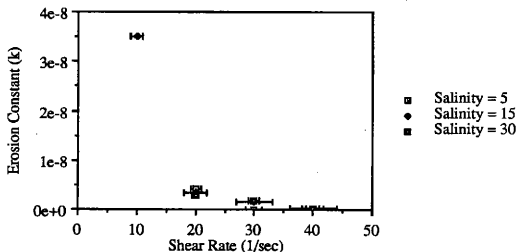


Fig. 50.- The Effect of Shear and Salinity on the Erosion Constant

Shear rate has a small statistical significance for the geometric mean and standard deviation (Appendix F). The mean and standard deviation increases slightly with increasing shear rate in Design 2 (Fig. 51 and 52). As the shear rate is increased,

stronger flocs are subject to breakage and the resulting particle size distribution of eroded particles shifts to the right. This accounts for the increase in mean particle diameter. The possibility of increased flocculation rates with shear would yield larger particles which would in turn increase the eroded diameter. The standard deviation increases with shear and indicates a wider range of eroded particle sizes with increasing shear. The mean and standard deviation in Design 3 decreases slightly with increasing salinity, but no salinity effects appear in Design 2.

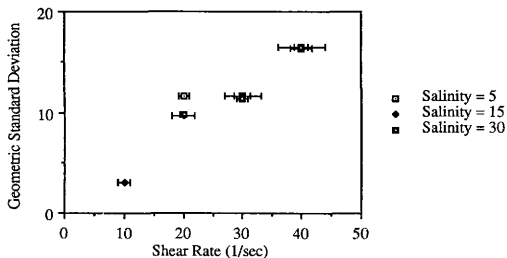


Fig. 51.- The Effect of Shear and Salinity on the Geometric Standard Deviation

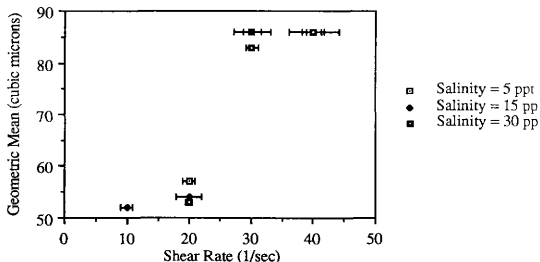


Fig. 52.- The Effect of Shear and Salinity on the Geometric Mean

DESIGN 3: VARIATION OF SALINITY AND PARTICLE TYPE

Salinity and particle type were varied under three conditions. Particle type seemed to have no effect on particle settling for the samples tested in these experiments. Salinity affected transport only slightly. The observed data for the various salinities were similar in all cases. The experiments were performed with a G of 20 sec^{-1} . The effect of salinity was probably overshadowed by this shear rate. Lower values of G (such as the experiment previously mentioned with a G of 10 sec^{-1}) would probably enhance the effect of salinity. The observed volume distributions drop suddenly after approximately two hours. The predicted volume distributions have a more steady rate of particle settling.

Alpha

Design 3 exhibited virtually no variation of alpha with particle type. Alpha values obtained for Type A, B, and C sediment are identical (Fig. 53). The sediments throughout the harbor are classified as organic silts and clays with silty sands (Wade 1988). The total organic carbon content (TOC) only varies from 4.12 percent at the

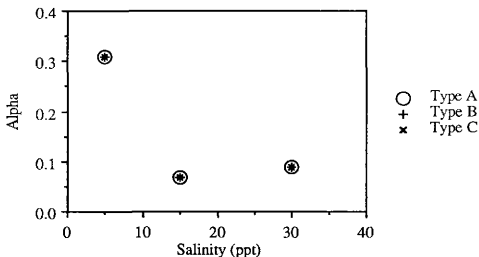


Fig. 53.- The Effect of Salinity and Particle Type on Alpha

mouth of the harbor to 11.3 percent at the upper most end (Pruell, et al. 1988). The sediment samples tested seem to be similar enough in content to warrant no variation in alpha due to particle type. Distinct areas of the harbor may have unusually high clay or organic content at levels to sufficiently affect alpha, but these were not represented in the samples tested.

Although no interaction was found for type, salinity was found to be the main interaction (Appendix F). As salinity increased, alpha decreased and leveled off. Again, this follows trends presented in Burt (1986). All experiments for Design 3 were carried out at a shear rate of 20 sec⁻¹. As seen in Design 2, salinity effects may be overshadowed at this shear rate.

Erosion

The erosion constant decreases slightly for particle type and salinity variations, experimental design 3 (Fig. 54). Statistical analysis showed very small interactions for Constant salinity and particle type (Appendix F). Salinity exceeded the 5 % level of

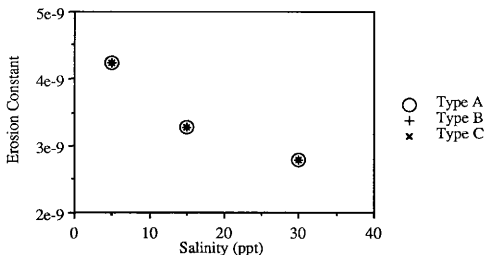


Fig. 54.- The Effect of Salinity and Particle Type on the Erosion Constant

significance for Design 3. The range of difference in erosion constant for salinity values was $3.0E-9$ to $4.3E-9$. Salinity has a small statistical significance on the geometric mean (Appendix F). The mean and standard deviation in Design 3 decreases slightly (Fig. 55 and 56). Again, salinity seems to be overshadowed by shear rate. The slight decrease could be attributed to lower flocculation rates at increased salinities (Fig. 53). With the decrease in probability of formation of large particles, the mean erosion size would tend to decrease.

RESUSPENSION

The resuspension constant describes the effect of resuspension on the bottom boundary of the column, and was not great enough to significantly affect particle transport within the settling column. Design 2, shear and salinity variation, indicated some interaction through statistical analysis (Appendix F), but a trend was not apparent (Fig. 57). Particle velocity at the bottom of the column was computed using resuspension coefficients obtained from the model. Resuspension coefficients ranged from $0.78E-6$

to $0.34E-9$ for experiments in all three designs. The settling velocity and the resuspension velocity was equal at the bottom (Fig. 58). For such small resuspension constants, only particles less than 1 micron would be affected. The resuspension constant must be on the order of $1.0E-3$ for (particle sizes of 2 to 90 microns) for resuspension to be a significant mechanism.

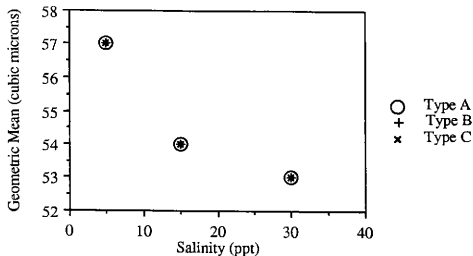


Fig. 55.- The Effect of Salinity and Particle Type on the Geometric Mean

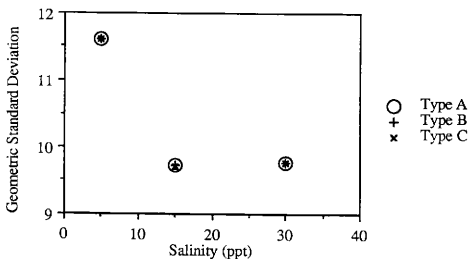


Fig. 56.- The Effect of Salinity and Particle Type on the Geometric Standard Deviation

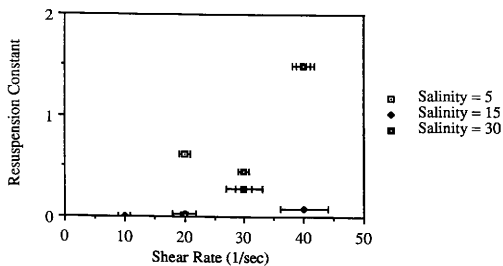


Fig. 57. - Shear and Salinity Effect on the Resuspension Constant

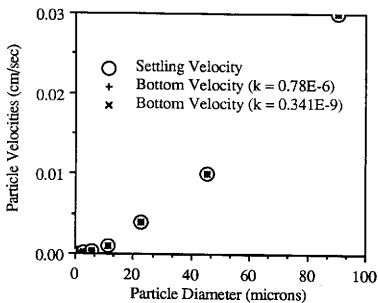


Fig. 58. -Resuspension Effect in the Column Based on Model Results

CHAPTER VI

SUMMARY AND CONCLUSIONS

Settling studies were performed with New Bedford Harbor bottom sediments in a two meter settling column. The effects of particle concentration, shear rate, salinity, and particle type on dynamic particle size distributions were investigated with the use of three factorial designs. The first design was used to determine the variation between 10, 40, and 80 mg/l particle concentrations within the settling column. No conclusive results were obtained. The second design was used to examine affects of shear rate, 10, 20, 30, and 40 sec⁻¹, and salinity, 5, 15, and 30 ppt, on dynamic particle size distributions. At low shear rates the particles settled relatively fast. Higher shear rates held particles in suspension. Almost no variation in particle settling due to salinity differences was observed. The third design was used to investigate the affects of the salinity variations previously described and also particle type, taken from three locations within the harbor.

A one dimensional advective-dispersive model was used to describe dynamic particle size distributions. Flocculation, floc breakup, and resuspension terms were used to describe particle transport. Flocculation was described with the use of a collision efficiency factor, alpha, unique to each experiment. Floc break up was described as particle erosion, and three coefficients, erosion, geometric mean, and geometric standard deviation, were determined for each experiment. Resuspension was represented as a constant and applied to the bottom boundary. Dynamic particle number and volume size distributions were generated by the model and compared with observed results by computing a correlation coefficient. The correlation between model and observed data was above 0.90 for most cases.

The hydrodynamics in the column are such that flocs are formed, but decreased diameter due to erosion at high shear rates maintains particles in suspension. The

observed and predicted results indicate that flocculation and floc breakup are important processes in particle transport. From observed results, the presence of large particles throughout time indicates that aggregation is occurring. The model must incorporate floc breakup to adequately reproduce observed particle distributions. Shear seemed to have the greatest effect on transport parameters. As shear increases, the particles remain in suspension. This phenomena is most likely due to an increased particle porosity.

The sediment settling rates are on the order of one day for a depth of 2 m at relatively high shear conditions. When compared to tidal cycles of 12 hours for New Bedford Harbor, the settling rates are much slower. The sediment will most likely be held in suspension long enough to be transported by tides, currents, or vertical mixing cycles. These results from this research imply that when turbulent conditions exist within New Bedford Harbor (ie. during dredging operations or tidal action), bottom sediments will be held in suspension and/or resuspended, thus increasing the transport of contaminated sediments to other areas of the harbor.

Conclusions:

1. Over the range of shear rates tested, the particles remain in suspension longer as shear rate increases.
2. Over the range of salinities tested, high salinities decrease particle collision efficiency.
3. The particle types tested in this research exhibit no significant differences in particle transport parameters.
4. Based on model results, New Bedford Harbor sediments are flocculant and can be described with flocculation and floc breakup parameters.
5. Floc breakup was adequately described in the model by three constants: erosion constant, geometric mean particle diameter, and geometric standard deviation.
6. Simple resuspension has no effect on particle transport in the studies conducted in this research.

REFERENCES

- Akers, R.J., Rushton, A.G., and Stenhouse, J.I.T. (1987). "Floc Breakage: The Dynamic Response of the Particle Size Distribution in a Flocculated Suspension to a Step Change in Turbulent Energy Dissipation." Chem. Eng. Sci., 42(4), 787-798.
- Averett D.E. (1988) "Characterization and Elutriate Testing of Acushnet River Estuary Sediment," Report 3 of 12, New Bedford Harbor Superfund Project: Acushnet River Estuary Engineering Feasibility Study Series, Technical Report EL-88-15, U.S. Army Engineer Waterways Experiment Station, Vicksburg, Miss.
- Blokland, T. (1989). "Determination of Dredging-Induced Turbidity." Tera Et. Aqua, 1,13-23.
- Boadway, J. D. (1978). "Dynamics of Growth and Breakage of Alum Floc in Presence of Fluid Shear." J. Environ. Eng. Div., ASCE, 104 (EE5), 901-915.
- Bonner, J. S., Ernest, A. N., Ducharme, S. L., and Autenrieth, R. L. (1990). "Parameterizing Models for Contaminated Sediment Transport." Transport and Transformation of Contaminants Near the Sediments-Water Interface, Springer-Verlag, Berlin, in press.
- Brun-Cottan, J. C. (1976). "Stokes Settling and Dissolution Rate Model for Marine Particles as a Function of Size Distribution." J. Geophys. Res., 81(9), 1601-1606.
- Burt, T. N. (1986). "Field Settling Velocities of Estuary Muds." Estuarine Cohesive Sediment Dynamics, Springer-Verlag, Berlin, 126-149.
- Chapra, S.C. and Reckhow, K.H. (1983). Engineering Approaches for Lake Management. Volume 2: Mechanistic Modeling. Butterworth Publishers, Boston.
- Cleasby, J. L. (1984). "Is Velocity Gradient a Valid Turbulent Flocculation Parameter?" J. Environ. Eng., ASCE, 110(5), 875-897.
- Coulter Electronics Limited. (1986). "Fine Particle Application Notes for Coulter Counters." Coulter Electronics Limited, Luton, Beds., England.
- Ducharme, S. L. (1989). "Design and Validation of a Settling Column for Particle Transport Studies," thesis presented to Texas A&M University at College Station, Texas, in partial fulfillment of the requirements for the degree of Master of Science.
- Dyer, K. R. (1979). "Estuaries and Estuarine Sedimentation." Estuarine Hydrography and Sedimentation, Cambridge University Press, Cambridge, 1-18.
- Dyer, K. R. (1972). "Sedimentation in Estuaries." The Estuarine Environment, Applied Science Publishers LTD, London, 10-32.
- Edzwald, J. K., Upchurch, J. B., and O'Melia, C. R. (1974). "Coagulation in Estuaries." Environ. Sci. Technol., 8(1), 58-63.

- Ernest A. N. S., Bonner, J. S., and Autenrieth, R. L. (1990). "Model Parameter Estimation Approach for Predicting Particle Transport." J. Environ. Eng., ASCE, reviewed and resubmitted.
- Faisst, W. K. (1978). "Characterization of Particles in Digested Sewage Sludge." Particulates in Water: Characterization, Fate Effects and Removal, American Chemical Society, Washington, D.C., 259-282.
- Farley, K. J. and Morel, F. M. M. (1986). "Role of Coagulation in the Kinetics of Sedimentation." Environ. Sci. Technol., 20(2), 187-195.
- Francingues, N.R., Jr., Averett, D.E. and Otis, M.J. (1988). "Study Overview," Report 1 of a series, New Bedford Harbor Superfund Project: Acushnet River Estuary Engineering Feasibility Study Series, Technical Report EL-88-15, US Army Engineer Waterways Experiment Station, Vicksburg, Miss.
- Fukuda, M.K. and Lick, W. (1980). "The Entrainment of Cohesive Sediments in Freshwater." J. Geophys. Res., 85, 2813-2824.
- Gerhart, P.M. and Gross, R.J. (1985). Fundamentals of Fluid Mechanics. Addison-Wesley Publishing Company, Reading, Ma.
- Glasgow, L. A. and Kim, Y. H. (1986). "Characterization of Agitation Intensity in Flocculation Processes." J. Environ. Eng., ASCE, 112(6), 1158-1163.
- Hahn, H. H. and Stumm, W. (1970). "The Role of Coagulation in Natural Waters." Am. J. of Sci., 268, 354-368.
- Hiraizumi, Y., Takahashi, M. and Nishimura, H. (1979). "Adsorption of Polychlorinated Biphenyl onto Sea Bed Sediment, Marine Plankton, and Other Adsorbing Agents." Environ. Sci. Technol., 13, 580-584.
- Holman, J. P., and Gajda, W. J., Jr. (1984). Experimental Methods for Engineers. McGraw-Hill Book Co., New York.
- Horzempa, L.M. and Di Toro, D.M. (1983). "The Extent of Reversibility of Polychlorinated Biphenyl Adsorption," Wat. Res., 17, 851-859.
- Humby, E. J. and Dunn, J. N. (1975). "Sedimentary Processes Within Estuaries and Tidal Inlets," Pollution Criteria for Estuaries. John Wiley and Sons, New York, 6.1-6.13.
- Hunt, J. R. and Pandya, J. D. (1984). "Sewage Sludge Coagulation and Settling in Seawater," Environ. Sci. Technol., 18(2), 119-121.
- John, J. A. and Quenouille, M. H. (1977). Experiments: Design and Analysis. Charles Griffin & Company LTD, London.
- Kao, S.V. and Mason, S.G. (1975). "Dispersion of Particles by Shear." Nature, 253, 619-621.
- Kavanaugh, M.C., Tate, K.C., Trussell, A.R., Trussell, R.R., and Treweek G. (1980). "Use of Particle Size Distribution Measurements for Selection and Control of Solid/Liquid

Separation Processes," Particulates in Water. American Chemical Society, Washington, D.C., 312-327.

Kranck, K. (1986). "Settling Behavior of Cohesive Sediment," Estuarine Cohesive Sediment Dynamics. Springer-Verlag, Berlin, 151-169.

Kranck, K. (1984). "The Role of Flocculation in the Filtering of Particulate Matter in Estuaries," The Estuary as a Filter. Academic Press, Orlando, FL, 159-175.

Kranck, K. (1980). "Experiments on the Significance of Flocculation in the Settling of Fine-grained Sediment in Still Water." Can. J. Earth Sci., 17, 1517-1526.

Kranck, K. (1975). "Sediment Deposition From Flocculated Suspensions." Sedimentology, 22, 111-123.

Krone, R. B. (1978). "Aggregation of Suspended Particles in Estuaries," Estuarine Transport Processes. University of South Carolina Press, Columbia, SC, 177-190.

Lavelle, J. W., Ozturgut, E., Baker, E. T., Tennant, D. A. and Walker, S. L. (1988). "Settling Speeds of Sewage Sludge in Seawater." Environ. Sci. Technol., 22(10), 1201-1207.

Lawler, D.F. (1979). "A Particle Approach to Thickening.", Ph.D. Dissertation, Dept. of Environmental Sciences and Engineering, University of North Carolina at Chappel Hill, Chappel Hill, North Carolina.

Lick, W. (1982). "Entrainment, Deposition, and Transport of Fine-grained Sediments in Lakes." Hydrobiol., 91, 31-40.

Logan, B.E. and Alldredge, A.L. (1989). "Potential for Increased Nutrient Uptake by Flocculating Diatoms," Mar. Biol., 101, 443-450.

Logan, B.E. and Hunt, J.R. (1987). "Advantages to Microbes of Growth in Permeable Aggregates in Marine Systems." Limnol. Oceanogr., 32(5), 1034-1048.

Lu, C.F. and Spielman, L.A. (1985). "Kinetics of Floc Breakage and Aggregation in Agitated Liquid Suspensions." J. Coll. Interface Sci., 103(1), 95-.

Luck, G. (1970). "Observation of Sediment Motion by Underwater-television." Coastal Engr. Conf. Proc., 2, 687-708.

Mackay, D. and Powers, B. (1987). "Sorption of Hydrophobic Chemicals from Water: A Hypothesis for the Mechanism of the Particle Concentration Effect." Chemosphere, 16, 745-757.

McCave, I. N. (1975). "Verticle Flux of Particles in the Ocean." Deep-Sea Res., 22, 491-502.

Meade, R. H. (1972). "Transport and Deposition of Sediments in Estuaries," Environmental Framework of Coastal Plain Estuaries. Memoir 133, Geological Society of America, Inc., Boulder, Colorado, 91-120.

- Mehta, A. J. (1986). "Characterization of Cohesive Sediment Properties and Transport Processes in Estuaries," Estuarine Cohesive Sediment Dynamics. Springer-Verlag, Berlin, 290-325.
- Mhaisalkar, V. A., Paramasivam, R. and Bhole, A. G. (1986). "An Innovative Technique for Determining Velocity Gradient in Coagulation-flocculation Process." Wat. Res., 20(10), 1307-1314.
- Montgomery, J. M. Consulting Engrs., Inc. (1985). Water Treatment Principles and Design. John Wiley & Sons, Inc., New York.
- Oldshue, J.Y. (1983). Fluid Mixing Technology, McGraw-Hill Publications Co., New York.
- Palermo, M.R. and Pankow, V.R. (1988). "Evaluation of Dredging and Dredging Control Technologies" Report 10 of 12, New Bedford Harbor Superfund Project: Acushnet River Estuary Engineering Feasibility Study Series, Technical Report E-88-15, US Army Engineer Waterways Experiment Station, Vicksburg, Miss.
- Pandya, J.D. and Spielman, L.A. (1983). "Floc Breakage in Agitated Suspensions: Effect of Agitation Rate," Chem. Eng. Sci., 38, 12, 1983-1992.
- Pandya, J.D. and Spielman, L.A. (1982). "Floc Breakage in Agitated Suspensions: Theory and Data Processing Strategy." J. Coll. Interface Sci., 90(2), 517-.
- Parthenaides, E. (1986). "A Fundamental Framework for Cohesive Sediment Dynamics." Estuarine Cohesive Sediment Dynamics. Springer-Verlag, Berlin, 219-250.
- Powell, R.L. and Mason, S.G. (1982). "Dispersion by Laminar Flow." A.I.Ch.E. Journal, 28, 2, 286-293.
- Pruell, et al., EPA laboratory results, Narragansette, Rhode Island, unpublished work (1989).
- Shames, I.H. (1982). Mechanics of Fluids. McGraw-Hill Book Company, New York.
- Sheng, Y.P. (1986). "Modeling Bottom Boundary Layer and Cohesive Sediment Dynamics in Estuarine and Coastal Waters," Estuarine Cohesive Sediment Dynamics. Springer-Verlag, Berlin, 360-400.
- Sholkovitz, E. R. (1976). "Flocculation of Dissolved Organic and Inorganic Matter During the Mixing of River Water and Seawater." Geochim. Cosmochim. Acta, 40, 831-845.
- Standard Methods for the Examination of Water and Wastewater 16th edition, (1985), APHA, AWWA, WPCF editors., American Public Health Assoc., Washington D.C.
- Swift, D.L. and Friedlander, S.K. (1964). "Coagulation of Hydrosols by Brownian Motion and Laminar Shear Laws." J. Coll. Sci., 19, 621-647.
- Tambo, N. and Watanabe, Y. (1979a). "Physical Aspect of Flocculation Process- I. Fundamental Treatise." Water Res., 13, 429-439.

Tambo, N. and Watanabe, Y. (1979b). "Physical Characteristics of Floccs- I. The Flocc Density Function and Aluminium Flocc." Water Res., 13, 409-419.

Teeter, A. M. 1988. "Sediment and Contaminant Hydraulic Transport Investigations" Report 2 of 12, New Bedford Harbor Superfund Project: Acushnet River Estuary Engineering Feasibility Study Series, Technical Report E-88-15, US Army Engineer Waterways Experiment Station, Vicksburg, Miss.

Thomann, R.V. (1972). System Analysis and Water Quality Management. McGraw-Hill Book Company, New York.

Treweek, G.P. and Morgan, J.J. (1980). "Prediction of Suspension Turbidities from Aggregate Size Distribution," Particulates in Water, American Chemical Society, Washington, D.C., 328-349.

Treweek, G. P. and Morgan, J. J. (1977). "Size Distribution of Flocculated Particles: Applications of Electronic Particle Counters.", Environ. Sci. Technol., 11(7), 707-714.

Wade, R. 1988. "Settling and Chemical Clarification Tests" Report 7 of 12, New Bedford Harbor Superfund Project: Acushnet River Estuary Engineering Feasibility Study Series, Technical Report E-88-15, US Army Engineer Waterways Experiment Station, Vicksburg, Miss.

SUPPLEMENTAL SOURCES CONSULTED

- Allersma, E. (1982). "Mud in Estuaries and Along Coasts." Intl. Sym. on River Sed., Beijing, China, Pub. no. 270, 663-685.
- Amirtharajah, A. and Trusler, S. L. (1986). "Destabilization of Particles by Turbulent Rapid Mixing." J. Environ. Eng., ASCE, 112(6), 1085-1108.
- Argaman, Y. and Kaufman, W.J. (1970). "Turbulence and Flocculation." J. Sanit. Eng., ASCE, 96(SA2), 223-239.
- Bedford, K. W. and Babajimopoulos, C. (1977). "Verticle Diffusivities in Areally Averaged Models." J. Environ. Eng. Div., ASCE, 103(EE1), 113-125.
- Box, G. E., Hunter, W. G., and Hunter J. S. (1978). Statistics for Experiemnts: An Introduction to Design, Data Analysis, and Model Building. John Wiley & Sons, New York.
- Camp, T.R. and Stein, P.C. (1943). "Velocity Gradients and Internal Work in Fluid Motion." J. Boston Soc. Civil Eng., 30(4), 219-237.
- Carder, K.L., Steward, R.G. and Betzer, P.R. (1982). "In Situ Holographic Measurements of the Sizes and Settling Rates of Oceanic Particulates." J. Geophys. Res., 87(C8), 5681-5685.
- Cornwell, D.A., Bishop, M.M. (1983). "Determining Velocity Gradients in Laboratory and Full-scale Systems." Resear. Technol. J. AWWA, 9, 470-475.
- Cox, C. M., Deursen, P. P., and Verhoevan, F. A. (1986). "The Relevant Soil Properties of Dredging Silt." Dredg. Port Construc., 8, 39-45.
- Donaghay, P. L. and Klos, E. (1985). "Physical, Chemical and Biological Responses to Simulated Wind and Tidal Mixing in Experimental Marine Ecosystems." Mar. Ecol. Prog. Ser., 26, 35-45.
- Egolf, C. B. and McCabe, W. L. (1937) "Rate of Sedimentation of Flocculated Particles." Am. Institute of Chem. Engrs. Transactions, 33, 620-642.
- Friedlander, S. K. (1977). Smoke, Dust, and Haze. John Wiley & Sons, New York.
- Friedlander, S. K. (1960). "Similarity Considerations for the Particle-Size Spectrum of a Coagulating, Sedimenting Aerosol." J. Meteorol., 17(5), 479-483.
- Gadd, G. E. (1965). "Turbulence Damping and Drag Reduction Produced by Certain Additives in Water." Nature, 206(4983), 463-467.
- Gibbs, R. J. (1982). "Floc Breakage during HIAC Light-Blocking Analysis." Environ. Sci. Technol., 16(5), 298-299.
- Hannah, S. A., Cohen J. M., and Robeck, G. G. (1967). "Measurement of Floc Strength by Particle Counting." J. AWWA, 843-858.

- Hunt, J. R. (1982). "Self-Similar Particle-Size Distributions During Coagulation: Theory and Experimental Verification." J. Fluid Mech., 122, 169-185.
- Hunt, J. R. (1978). "Prediction of Oceanic Particle Size Distributions from Coagulation and Sedimentation Mechanisms," Particulates in Water: Characterization, Fate Effects and Removal. American Chemical Society, Washington, D.C. 243-257.
- Jenkinson, I. R. (1986). "Oceanographic Implications of Non-newtonian Properties Found in Phytoplankton Cultures." Nature, 323, 6087, 435-437.
- Jerlov, N. G. (1959). "Maxima in the Vertical Distribution of Particles in the Sea." Deep-Sea Res., 5, 173-184.
- Johnson, B. H. (1980). "Discussion of Mathematical Models for Computing the Physical Fate of Solids Released in Open Water During Dredging or Dredged Material Disposal," Contaminants and Sediments, Vol. 1. Ann Arbor Science Pub, Inc., Ann Arbor, MI, 331-348.
- Kang, S.W., Sheng, Y.P. and Lick, W. (1982). "Wave Action and Bottom Shear Stresses in Lake Erie." J. Great Lakes Res., 8(3), 482-494.
- Koh, R. C. Y. (1982). "Initial Sedimentation of Waste Particulates Discharged from Ocean Outfalls." Environ. Sci. Technol., 16(11), 757-763.
- Krone, R. B. (1986). "The Significance of Aggregate Properties to Transport Processes," Estuarine Cohesive Sediment Dynamics. Springer-Verlag, Berlin, 66-84.
- Liu, H. (1977). "Predicting Dispersion Coefficient of Streams." J. Environ. Eng. Div., ASCE, 103(EE1), 59-69.
- McCave, I. N. (1979). "Suspended Sediment," Estuarine Hydrography and Sedimentation. Cambridge University Press, Cambridge, London, 131-185.
- Mehta, A. J. and Partheniades, E. (1975). "An Investigation of the Depositional Properties of Flocculated Fine Sediments." J. Hydraulic Res., 13(4), 361-381.
- Morton, R. W. (1972). "Spatial and Temporal Distribution of Suspended Sediment in Narragansett Bay and Rhode Island Sound," Environmental Framework of Coastal Plain Estuaries. Memoir 133, Geological Society of America, Inc., Boulder, Colorado, 131-141.
- Owen, M. W. (1971). "The Effect of Turbulence on the Settling Velocities of Silt Flocs." Int. Assoc. Hydraul. Res., Congr., Proc., 14, 4, 27-32.
- Reich, I. and Vold, R. D. (1959). "Flocculation-Deflocculation in Agitated Suspensions." J. Physic. Chem., 63, 1497-1501.
- Schroeder, P. R. and Shields, F. D., Jr. (1983). "Chemical Clarification of Dredged Material." J. Environ. Eng., ASCE, 109(2), 414-427.
- Schubel, J. R. (1972). "Distribution and Transportation of Suspended Sediment in Upper Chesapeake Bay," Environmental Framework of Coastal Plain Estuaries. Memoir 133, Geological Society of America, Inc., Boulder, Colorado, 151-167.

Schubel, J. R. (1971). "Tidal Variation of the Size Distribution of Suspended Sediment at a Station in the Chesapeake Bay Turbidity Maximum." Netherlands J. of Sea Res., 5 (2), 252-266.

Spielman, L.A. (1970). "Viscous Interactions in Brownian Coagulation." J. Coll. Interface Sci., 33(4), 562.

Sverdrup, H.U., Johnson, M.W. and Fleming, R.H. (1970). The Oceans. Their Physics, Chemistry, and General Biology. Prentice-Hall, Inc., New Jersey.

Tambo, N. and Hozumi, H. (1979). "Physical Aspect of Flocculation Process- II. Contact Flocculation." Wat. Res., 13, 441.

Tambo, N. and Hozumi, H. (1979). "Physical Characteristics of Flocs- II. Strength of Flocc." Wat. Res., 13, 421-427.

Teeter, A.M. and Pankow, W. (1989) "Deposition and Erosion Testing on the Composite Dredged Material Sediment Sample from New Bedford Harbor, Massachusetts" Final Report, New Bedford Harbor Superfund Project: Acushnet River Estuary Engineering Feasibility Study Series, Technical Report HL-89-11, US Army Engineer Waterways Experiment Station, Vicksburg, Miss.

Teeter, A. M. (1984). "Vertical Transport in Fine-grained Suspension and Newly-deposited Sediment," Estuarine Cohesive Sediment Dynamics. Springer-Verlag, Berlin, 170-191.

Turk, J. T. (1980). "Applications of Hudson River Basin PCB-transport Studies," Contaminants and Sediments, Vol. 1. Ann Arbor Science Pub., Inc., Ann Arbor, MI, 171-183.

Uhl, V.W. and Gray, J.B. (1967). Mixing Theory and Practice, Vol II. Academic Press, Inc., Orlando.

APPENDIX A

NOTATION

The following symbols are used in this paper:

a	=	empirical constant;
B_b	=	rate coefficient for Brownian;
B_{ds}	=	rate coefficient for differential settling;
B_{sh}	=	rate coefficient for shear;
B	=	empirical constant;
$-b$	=	rate parameter for particle settling;
C	=	total suspended solids concentration;
C_c	=	correlating constant;
C_{eq}	=	equilibrium concentration;
c_i	=	particle number concentration of size i particles;
C_{pred}	=	predicted particle concentration;
C_{obs}	=	observed particle concentration;
D	=	impellor diameter;
D_e	=	deposition;
D_z	=	verticle dispersion;
d	=	particle diameter;
$-d$	=	empirical constant for the porosity function;
$d_{k,i,j}$	=	particle diameters of size $k, i,$ and $j,$ respectively;
d_f	=	floc diameter ($df/1$ is dimensionless);
d_p	=	particle diameter;
du/dz	=	velocity gradient;
dv/dt	=	instanaeous rate of change of parent floc volume due to;
E	=	erosion rate;

E	=	dispersion coefficient times the cross sectional area divided by the mean segment length;
F	=	porosity function;
F'	=	volume fraction of particles;
G	=	shear rate;
g	=	acceleration due to gravity;
$g(v)$	=	splitting frequency;
H	=	water depth;
K_1	=	empirical coefficient;
K_2	=	empirical splitting frequency coefficient;
K_C	=	calibration constant;
K_P	=	empirical constant;
K_R	=	resuspension constant;
k	=	Boltzmann's constant;
\bar{k}	=	erosion rate coefficient;
k_d	=	calibration constant;
l	=	length scale;
M	=	erosion rate coefficient;
N_{ij}	=	number of collisions between particles i and j ;
$n_{k,i,j}$	=	number concentration of particles size k , i , and j , respectively;
P	=	porosity;
P_{new}	=	porosity of new particle;
P_e	=	probability distribution of eroded particles;
P_s	=	fragment size distribution;
Pe	=	Peclet number;
P'	=	power;

Q_i	=	flow through segment i ;
q_e	=	rate of formation of erosion fines;
q_s	=	net sediment flux;
R	=	correlation coefficient;
R_{ij}	=	particle volume in terms of a porosity function;
Re	=	Reynolds number;
r_a	=	aggregate radius;
$r_{k,i,j}$	=	radius of particles k , i , and j , respectively;
r_o	=	initial particle radius;
S_r	=	residual;
T	=	temperature;
T_d	=	Tank diameter;
T_x	=	period of oscillation subscripted respectively;
t	=	time;
t_s	=	shearing time;
V_B	=	Bottom velocity;
V_r	=	resuspension velocity;
V_s	=	settling velocity;
V_T	=	total particle volume;
V_z	=	verticle settling velocity;
v_e	=	volume of entrained water;
$\overline{v_{ge}}$	=	geometric mean of erosion product size distribution;
$v_{k,i,j}$	=	volume of particles of size k , i , j , respectively;
v_l	=	liquid volume;
v_{om}	=	volume of organic and mineral;

v_{tot}	=	total particle volume;
v_s	=	volume of solids;
v_v	=	volume of the voids;
v_w	=	volume of entrained water;
$y_{i,ic,m}$	=	observed, predicted, and mean data point, respectively;
∞	=	collision efficiency factor;
β	=	collision frequency;
β_e	=	coefficient of proportionality;
$\bar{\epsilon}$	=	average power dissipation per unit mass;
ϵ_d	=	turbulent energy dissipation;
ϵ_v	=	coefficient of eddy viscosity;
ν	=	kinematic viscosity;
ν_d	=	average number of daughter flocs;
$\bar{\rho}$	=	particle wet bulk density;
$\overline{\Delta\rho}$	=	effective density;
ρ_a	=	aggregate density;
ρ_b	=	particle wet bulk density;
ρ_e	=	effective density;
ρ_l	=	liquid density;
ρ_{om}	=	organic/mineral density;
ρ_p	=	particle density;
ρ_w	=	density of water;
σ_{ge}	=	geometric standard deviation of erosion product distribution;
σ_s	=	standard deviation of fragment size distribution due to splitting;

$\sigma_{y,x}$ = variables used in calculating correlation coefficients;

τ = shear stress;

τ_b = bottom shear stress;

τ_c = critical erosion shear stress;

μ = viscosity;

ω = impellor rotational speed;

θ_i = weighting factor;

ϕ_i = weighting factor;

APPENDIX B
EXPERIMENTAL PROCEDURES

COULTER COUNTER

Analysis of the Use of PVP

Table B1.- Mean Particle Diameters (microns) from Testing the Use of PVP

NO PVP		PVP	
STIRRED SAMPLES:		STIRRED SAMPLES:	
Waiting	20.95	Waiting	16.71
No Waiting	16.97	No Waiting	15.32
QUIESCENT SAMPLES:		QUIESCENT SAMPLES:	
Waiting	19.27	Waiting	18.05
No Waiting	16.53	No Waiting	15.05

Calculation of Volume Based on Particle Numer:

(Reference Manual for the Coulter Multisizer, Coulter Electronics Limited, England, May 1987.)

First, the size of each channel (1-256) is calculated in terms of particle diameter (microns) by:

$$(1) \quad d = d_{256} (2^{1/50})^U$$

Where:

$$(2) \quad d_{256} = \frac{K_c}{\sqrt[3]{I \cdot G}}$$

$$(3) \quad U = 256 \left(\frac{x}{256} - 1 \right)$$

K_c is the calibration constant for a given experiment, I is the current (taken from the Multisizer), G is the gain (also from the Multisizer), and x is the channel of interest. The volume is assumed spherical and calculated by:

$$(4) \quad V = \frac{\pi d^3}{6}$$

The number of particles within one channel is multiplied by the volume of one particle as calculated above. This is repeated for each channel to yield the volume distribution.

SUSPENDED SOLIDS MEASUREMENT

Total Suspended Solids Dried at 103-105°C

(Standard Methods, 209 C.)

Preparation:

- 1) Place a glass-fiber filter (wrinkle side up) in a Gooch crucible.
- 2) Apply a vacuum and wash three times with 20 ml of distilled water.
- 3) Dry at 103 to 105°C for 1 hour.
- 4) Cool in a desiccator, remove, and weigh (mg).
- 5) Repeat the above until a constant weight (or loss of <0.5 mg) is achieved between weighings.
- 6) Store in a desiccator and weigh before using.

Sample Measurement:

- 1) Apply vacuum and wet filter with distilled water.
- 2) Filter sample, wash three times with 10 ml of distilled water, and continue suction for three minutes.
- 3) Dry for 1 hour (103 to 105°C), cool in desiccator, and weigh (mg) until the weight loss is < 4% of the previous weight.

Calculation of Suspended Solids (mg/l):

(dried filter and residue - dried filter) X 1000

sample volume, ml

Suspended Solids Machine

CEM Corporation, AVC-80 Suspended Solids Machine

(12203 Burgoyne, Houston, TX 77077, (713)531-7928)

Preparation:

- 1) Place a glass-fiber filter (wrinkle side up) in a filter apparatus.
- 2) Apply a vacuum and wash three times with 20 ml of distilled water.
- 3) Place in "oven" and microwave six minutes to dry.
- 4) Tare the balance to zero.

Sample:

- 1) Remove the filter from the oven and place in filter apparatus.
- 2) Apply vacuum, wet filter, add sample, and wash three times with 10 ml of distilled water.
- 3) Place in "oven" enter sample volume and set time for six minutes (or until weigh fluctuations cease).
- 4) Record the displayed suspended solids reading.

EXPERIMENTAL PROCEDURE

Preparation (one day before the scheduled study):

- 1) Clean column by filling half way, air mixing, and rinsing five times.
- 2) Clean approximately 60 beakers (150 ml).
- 3) Prepare disks for the Coulter counter and data sheets (Coulter and SS data).
- 4) Prepare 1000 ml Instant Ocean at the desired concentration for use in the Coulter counter. (Filter the saltwater twice.)
- 5) Prepare labels for sample beakers.

Study procedure:

- 1) Fill clean column with distilled water and turn on air.
- 2) Weigh desired amount of salt.
- 3) Pour salt into column.
- 4) Turn on LEDs and close doors to loading platform.
- 5) While the column is being air mixed for approximately one hour, start up the Coulter counter:
 - * clean aperture
 - * put the desired concentration of saltwater in the fill jar
 - * take a saltwater reading (assuming the Coulter counter has been calibrated previously as outline in the Coulter manual)
 - * take a sample from port 3 and record particle number and volume
 - * repeat for port 7
- 6) Warm up motor:
 - * turn air off, open doors on loading platform
 - * connect motor
 - * start program (gwbasic, load"mainall8", run)
 - * test run 5 times for 200 sec each (check that the shaft is turning properly)
 - * close doors
 - * run a blank for 300 sec
 - * set computer time to 0:00:00 (under system)
 - * start program again and set up initial conditions (ready to hit return and start shaft immediately after sediments are added)
- 7) Turn air on, open doors.
- 8) Shake up sediment sample, pour into column, and set a timer for 2 minutes.
- 9) When timer sounds, turn off air and immediately hit return on computer to start

Table B2.- Sample Extraction Time Table

Down: Consecutive samples (approximately 10 minutes apart)

Across: Sample times in hours

Port	0	0.4	0.8	1.4	1.9	2.4	3.8	4.3	6.1	6.6	11.1	11.6	20.6	21.1
1	●		●		●	●		●		●		●		●
2	●			●		●	●		●		●		●	
3			●		●			●		●		●		●
4	●	●		●		●	●		●		●		●	
5	●		●		●			●		●		●		●
6	●	●		●	●		●		●		●		●	
7		●		●		●		●		●		●		●
8	●		●				●		●		●		●	
9	●	●		●		●		●		●		●		●
10		●	●		●		●		●		●		●	

the shaft.

10)

When study is over, hit control break to stop the program (only when the shaft

pauses in between rotations), type system (in order to close the files), unplug motor, and turn off LEDs.

SUSPENDED SOLIDS AND TURBIDITY DATA

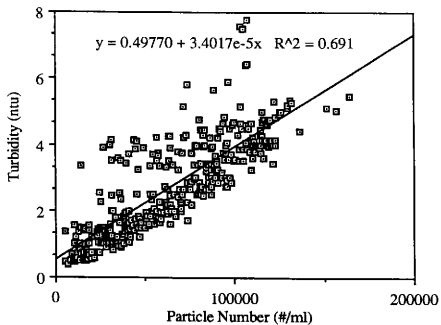


Fig. B1. - Variation of Particle Number Concentration with Turbidity

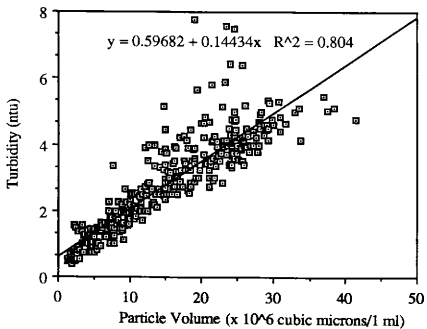


Fig. B2. - Variation of Particle Volume Concentration with Turbidity

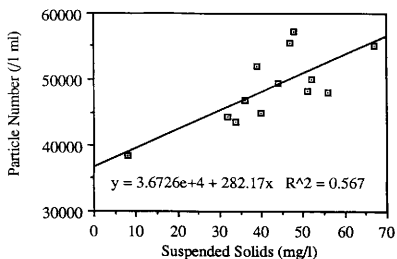


Fig. B4. - Variation of Suspended Solids with Initial Particle Number Concentration

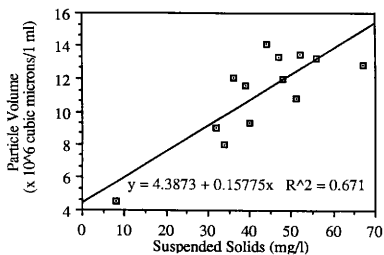


Fig. B5. - Variation of Initial Suspended Solids with Particle Volume

APPENDIX C
MODEL CODE


```

C=====
C      PROGRAM TO EXECUTE FINITE SEGMENT MODEL FRAMEWORK
C
C      THE FOLLOWING MODEL FRAMEWORK WAS DEVELOPED BY
C      ANDREW ERNEST AT TEXAS A&M UNIVERSITY.
C
C      THE DIFFERENTIAL EQUATIONS WERE A COLLABORATION
C      BETWEEN:
C
C              ANDREW ERNEST
C              STEPHANIE SANDERS
C              JAMES BONNER
C=====
PROGRAM PEMOD
INCLUDE 'MODEL.PAR'
INCLUDE 'OBSERV.CMN'
CHARACTER*40 CINPUT,FILIN,FILOUT,FILPAR,FILREP
EXTERNAL CINPUT
EXTERNAL IINPUT
EXTERNAL DINPUT
IRE = 5
IWR = 6
ISAM = 17
IFIL = 18
IPAR = 19
IREP = 20
C----- READ IN OBSERVED DATA
OPEN(IRE,FILE='SYS$INPUT',STATUS='OLD')
OPEN(IWR,FILE='SYS$OUTPUT',STATUS='OLD')
FILIN = CINPUT('INPUT DATA FILE NAME',IRE,IWR)
FILOUT = CINPUT('OUTPUT DATA FILE NAME',IRE,IWR)
FILREP = CINPUT('OUTPUT REPORT FILE NAME',IRE,IWR)
IEST = IINPUT('ESTMATE PAR.? [0/1/2/3/4]',IRE,IWR)
CLOSE(IRE)
CLOSE(IWR)
CALL RDOBS(ISAM,FILIN)
CALL PSETUP
IF(IEST.NE.0) THEN
  TOL = DINPUT('TOLERANCE',IRE,IWR)
  NMAX = IINPUT('NMAX',IRE,IWR)
  IF(IEST.EQ.1) THEN
    ITMX = IINPUT('ITMX',IRE,IWR)
    CALL NEWTNR(NMAX,ITMX,TOL)
  ENDIF
  IF(IEST.EQ.2) THEN
    CALL GAUSSN(NMAX,TOL)
  ENDIF
  IF(IEST.EQ.3) THEN
    CALL NEWTON(NMAX,TOL)
  ENDIF
  IF(IEST.EQ.4) THEN
    IP = IINPUT('IP',IRE,IWR)

```

```
    CALL NEWTN1(IP,NMAX,TOL)
  ENDIF
ENDIF
C    CALL WROBS(IFIL,FILOUT)
CALL SIMULA
CALL PEOUT(IFIL,FILOUT)
CALL PEREPT(IREP,FILREP)
STOP
END
```

```

C=====
C THIS ROUTINE DEFINES THE FIRST ORDER ORDINARY DIFFERENTIAL
C EQUATIONS TO BE SOLVED
C=====
SUBROUTINE DFDT
INCLUDE 'MODEL.PAR'
INCLUDE 'MODEL.CMN'
INCLUDE 'COEFF.CMN'
DO 10 IN=1,NSTATE
C--- TOP BOUNDARY: DISP*dc/dx = VEL*C
  I = 1
  J = 1
  K = 1
  AIM1I = ZL(K)/(ZL(K-1) + ZL(K))
  A1P1 = ZL(K+1)/(ZL(K+1) + ZL(K))
  BIM1I = 1.0 - AIM1I
  B1P1 = 1.0 - A1P1
  QIM1I = VEL(IN)/ZL(K)
  Q1P1 = VEL(IN)/ZL(K)
  EIM1I = 2.0*DISP(IN)/(ZL(K-1)*ZL(K) + ZL(K)*ZL(K))
  E1P1 = 2.0*DISP(IN)/(ZL(K)*ZL(K) + ZL(K+1)*ZL(K))
  DCDT(IN,I,J,K) =
C & + QIM1I*(AIM1I*C(IN,I,J,K-1) + BIM1I*C(IN,I,J,K))
  & - Q1P1*(A1P1*C(IN,I,J,K) + B1P1*C(IN,I,J,K+1))
C & + EIM1I*(C(IN,I,J,K-1) - C(IN,I,J,K))
  & + E1P1*(C(IN,I,J,K+1) - C(IN,I,J,K))
C--- INTERIOR SEGMENTS
  DO 20 I=1,NUMI
  DO 20 J=1,NUMJ
  DO 20 K=2,NUMK - 1
  AIM1I = ZL(K)/(ZL(K-1) + ZL(K))
  A1P1 = ZL(K+1)/(ZL(K+1) + ZL(K))
  BIM1I = 1.0 - AIM1I
  B1P1 = 1.0 - A1P1
  QIM1I = VEL(IN)/ZL(K)
  Q1P1 = VEL(IN)/ZL(K)
  EIM1I = 2.0*DISP(IN)/(ZL(K-1)*ZL(K) + ZL(K)*ZL(K))
  E1P1 = 2.0*DISP(IN)/(ZL(K)*ZL(K) + ZL(K+1)*ZL(K))
  DCDT(IN,I,J,K) =
  & + QIM1I*(AIM1I*C(IN,I,J,K-1) + BIM1I*C(IN,I,J,K))
  & - Q1P1*(A1P1*C(IN,I,J,K) + B1P1*C(IN,I,J,K+1))
  & + EIM1I*(C(IN,I,J,K-1) - C(IN,I,J,K))
  & + E1P1*(C(IN,I,J,K+1) - C(IN,I,J,K))
20 CONTINUE
C--- BOTTOM BOUNDARY: DISP*dc/dx = 0
  I = 1
  J = 1
  K = NUMK
  AIM1I = ZL(K)/(ZL(K-1) + ZL(K))
  A1P1 = ZL(K+1)/(ZL(K+1) + ZL(K))
  BIM1I = 1.0 - AIM1I
  B1P1 = 1.0 - A1P1
  QIM1I = VEL(IN)/ZL(K)

```

```

QIIP1 = VEL(IN)/ZL(K)*VEL(IN)/(VKRES+VEL(IN))
EIM11 = 2.0*DISP(IN)/(ZL(K-1)*ZL(K) + ZL(K)*ZL(K))
DCDT(IN,I,J,K) =
&   + QIM11*(AIM11*C(IN,I,J,K-1) + BIM11*C(IN,I,J,K))
&   - QIIP1*C(IN,I,J,K)
&   + EIM11*(C(IN,I,J,K-1) - C(IN,I,J,K))
10  CONTINUE
C
C---- FLOCCULATION TERMS
C
C     ACCUMULATE PARTICLE GENERATION AND LOSS TERMS
C
DO 30 I=1, NUMI
DO 30 J=1, NUMJ
DO 30 K=1, NUMK
C
DO 30 IL=1, NSTATE
C
DO 30 JL=IL, NSTATE
C
C     RATE OF LOSS OF PARTICLES OF SIZE JL AS A RESULT OF EROSION
C     TO FORM
C     PARTICLES OF SIZE IL
C
ELOSS = DKE*PRE(IL,JL)*C(JL,I,J,K)
C
C     KL IS THE NEW SIZE PARTICLE FORMED
C
KL = ISIZ(IL,JL)
C
C     RATE OF LOSS OF PARTILCES OF SIZE IL AND JL AS A RESULT OF A
C     SUCCESSFUL COLLISION BETWEEN IL AND JL TO FORM KL
C
PLOSS = ALPHA(KL)*BETA(IL,JL)*C(JL,I,J,K)*C(IL,I,J,K)
C
C     RATE OF FORMATION OF PARTICLE SIZE KL AS A RESULT OF A
C     SUCCESSFUL COLLISION BETWEEN IL AND JL
C
PGENKL = FRAC(IL,JL)*PLOSS
C
C     ACCUMULATE PARTICLE GENERATION AND LOSS TERMS IN
C     APPROPRIATE
C     PARTICLE CATEGORIES
C
DCDT(KL,I,J,K) = DCDT(KL,I,J,K) + PGENKL
DCDT(IL,I,J,K) = DCDT(IL,I,J,K) - PLOSS
DCDT(JL,I,J,K) = DCDT(JL,I,J,K) - PLOSS
DCDT(IL,I,J,K) = DCDT(IL,I,J,K) + ELOSS*VOL(JL)/VOL(IL)
DCDT(JL,I,J,K) = DCDT(JL,I,J,K) - ELOSS
C
30  CONTINUE
RETURN
END

```

```

*****
*   4TH ORDER RUNGE-KUTTA ROUTINE SOLVES COUPLED DIFFERENTIAL
*
*   EQUATIONS SIMTANOUSLY.
*
*****
FUNCTION RUNGE
INCLUDE 'MODEL.PAR'
INCLUDE 'MODEL.CMN'
DATA ICOUNT1/0/
C
  ICOUNT1 = ICOUNT1 + 1
  GOTO(100,200,300,400,500) ICOUNT1
C
C   ..... PASS 1 .....
C
100  CONTINUE
     RUNGE = 1
     RETURN
C
C   ..... PASS 2 .....
C
200  CONTINUE
C
DT = DTMAX
DO 5 IS=1,NSTATE
DO 5 I=1,NUMI
DO 5 J=1,NUMJ
DO 5 K=1,NUMK
  IF(C(IS,I,J,K).EQ.0.0D0) THEN
    RTMP = DTMAX
  ELSEIF(DCDT(IS,I,J,K).LT.0.0D0.AND.C(IS,I,J,K).GT.0.0D0) THEN
    RTMP = - C(IS,I,J,K)/DCDT(IS,I,J,K)/SF
  ELSEIF(DCDT(IS,I,J,K).GT.0.0D0.AND.C(IS,I,J,K).GT.0.0D0) THEN
    RTMP = DTMAX
  ELSEIF(DCDT(IS,I,J,K).LT.0.0D0.AND.C(IS,I,J,K).LT.0.0D0) THEN
    RTMP = DTMIN
  ELSEIF(DCDT(IS,I,J,K).GT.0.0D0.AND.C(IS,I,J,K).LT.0.0D0) THEN
    RTMP = DTMAX
  ELSE
    RTMP = DTMAX
  ENDIF
  DT = MIN(DT,RTMP)
5   CONTINUE
  DT = MAX(DT,DTMIN)
  DT = MIN(DT,DTMAX)
  DT = MIN(DT,(TNEXT - TYME))
C   WRITE(*,1000) TYME, TLAST,DT
C
  ALF = 0.5
  IF(1ORDER.EQ.3) THEN
    RUNGE = 1
    GO TO 10

```

```

ELSEIF(IORDER.EQ.2) THEN
  ICOUNT1 = 3
  RUNGE = 1
  GOTO 10
ELSE
  ICOUNT1 = 0
  RUNGE = 0
  ALF = 1.0
ENDIF
10  CONTINUE
   DO 20 L = 1, NSTATE
   DO 20 I = 1, NUMI
   DO 20 J = 1, NUMJ
   DO 20 K = 1, NUMK
     SAVEY(L,I,J,K) = C(L,I,J,K)
     PHI(L,I,J,K) = DCDT(L,I,J,K)
C(L,I,J,K) = SAVEY(L,I,J,K) + ALF*DT*DCDT(L,I,J,K)
20  CONTINUE
     TYME = TYME + ALF*DT
RETURN
C
C   ..... PASS 3 .....
C
300 CONTINUE
   DO 30 L = 1, NSTATE
   DO 30 I = 1, NUMI
   DO 30 J = 1, NUMJ
   DO 30 K = 1, NUMK
     PHI(L,I,J,K) = PHI(L,I,J,K) + 2.0*DCDT(L,I,J,K)
     C(L,I,J,K) = SAVEY(L,I,J,K) + 0.5*DT*DCDT(L,I,J,K)
30  CONTINUE
     RUNGE = 1
RETURN
C
C   ..... PASS4 .....
C
400 CONTINUE
   IF(IORDER.EQ.3) THEN
     RUNGE = 1
     GOTO 35
   ELSE
     ICOUNT1 = 0
     RUNGE = 0
   ENDIF
35  CONTINUE
   DO 40 L=1,NSTATE
   DO 40 I=1, NUMI
   DO 40 J=1, NUMJ
   DO 40 K=1, NUMK
     PHI(L,I,J,K) = PHI(L,I,J,K) + 2.0*DCDT(L,I,J,K)
     C(L,I,J,K) = SAVEY(L,I,J,K) + DT*DCDT(L,I,J,K)
40  CONTINUE
     TYME = TYME + 0.5*DT

```

```
      RETURN
C
C      ..... PASS 5 .....
C
500   CONTINUE
      DO 50 L=1, NSTATE
      DO 50 I=1, NUMI
      DO 50 J=1, NUMJ
      DO 50 K=1, NUMK
         C(L,I,J,K) = SAVEY(L,I,J,K)
      &  +(PHI(L,I,J,K) + DCDT(L,I,J,K))*DT/6.0
50   CONTINUE
      ICOUNT1=0
      RUNGE = 0
      RETURN
C
1000  FORMAT(+ TYME ':',E12.6,' OF ',E12.6,' DT ':',E12.6)
      END
```

```

C=====
C  RUNGE-KUTTA INTEGRATION OF SYSTEM OF 1ST ORDER ORDINARY
C  DIFFERENTIAL EQUATIONS.
C  UPON ENTRY, THE ARGUMENTS CONTAIN LOCATIONS AND TIMES AT
C  WHICH MODEL VALUES ARE DESIRED.
C  CALLS INTEGER FUNCTION RUNGE SUBROUTINE DFDT
C=====
SUBROUTINE MODEL(PMD,PRED,XPRED,YPRED,ZPRED,TPRED,ISPRED,
& NPRED,NUMPRD,NPAR)
INCLUDE 'MODEL.PAR'
INCLUDE 'MODEL.CMN'
EXTERNAL RUNGE
DIMENSION
PRED(NUMPRD),XPRED(NUMPRD),YPRED(NUMPRD),ZPRED(NUMPRD)
DIMENSION TPRED(NUMPRD),PMD(NPAR)
INTEGER ISPRED(NUMPRD)
C---- SET UP GRID
CALL GENGRD(PRED,XPRED,YPRED,ZPRED,TPRED,ISPRED,NPRED)
C---- READ INPUT PARAMETERS
CALL RDPAR(PMD,NPAR)
C---- INITIALIZE TIME AND PREDICTION COUNTER
TYME = TFIRST
NPRED = 0
C---- BEGIN ITERATIONS
DO 10 IT=1,NUMT
  TNEXT = TT(IT)
  30 CONTINUE
  IF(TYME.EQ.TNEXT) THEN
C---- PRINT OUT IF TYME = TT(IT)
  CALL
WROUT(PRED,XPRED,YPRED,ZPRED,TPRED,ISPRED,NPRED,NUMPRD)
  GOTO 10
ENDIF
C---- CALL RUNGE-KUTTA IVP SOLVER
20 K1 = RUNGE()
C---- WHENEVER K1=1 CALCULATE DERIVATIVE VALUES
IF (K1.EQ.1) THEN
C---- CALCULATE DERIVATIVES FOR ALL STATE VARIABLES
CALL DFDT
C---- NOW DO THE NEXT PASS OF THE RUNGE - KUTTA.
GOTO 20
ELSE
GOTO 30
ENDIF
10 CONTINUE
C---- TIME HAS EXPIRED
RETURN
END

```



```

C=====
C   ROUTINE TO READ IN INITIAL CONDITIONS AND SET UP FINITE
C   SEGMENT GRID LIMITS. SET UP INVARIANT COEFFICIENTS.
C=====
SUBROUTINE RDOBS(IRE,FILIN)
INCLUDE 'MODEL.PAR'
INCLUDE 'COEFF.CMN'
CHARACTER*(*) FILIN
CHARACTER*80 SAMFIL
CHARACTER*20 PNA
REAL*4 VPARTS
DIMENSION PAR(10)
EXTERNAL VPARTS
EXTERNAL DINPUT
C=====
C---- SET UP OBSERVATIONS
C
RHOP = DINPUT('RHOP',5,6)
DISPER = DINPUT('DISPERSION COEFFICIENT [CM/S^2]',5,6)
VELGRA = DINPUT('VELOCITY GRADIENT [1/S]',5,6)
PAR(1) = DINPUT('ALPHA',5,6)
PAR(2) = DINPUT('K SQUIGGLE',5,6)
PAR(3) = DINPUT('VGE',5,6)
PAR(4) = DINPUT('SGE',5,6)
PAR(5) = DINPUT('VKRES',5,6)
IO = 0
OPEN(IRE,FILE=FILIN,STATUS='OLD')
READ(IRE,*) NSTATE
DO 10 IS=1,NSTATE
  READ(IRE,*) VLO(IS),VOL(IS),VUP(IS)
10  CONTINUE
20  CONTINUE
  READ(IRE,*,END=40) CO,XO,YO,ZO,TO,IS,WO
  IO = IO + 1
  CALL PEOBS(CO,XO,YO,ZO,TO,WO,IS,IO)
c write(*,999) CO,XO,YO,ZO,TO,IS,WO,io
c 999 format('+',5(1x,e9.3),1x,i4,1x,e9.3,1x,i4)
GOTO 20
40  CONTINUE
CLOSE(IRE)
C=====
C---- ASSIGN PARAMETER VALUES
C
PLO = 0.0
PUP = 10.0
DELP = 1.0E-2
CALL PEPAR(PLO,PUP,DELP,PAR(1),'ALPHA',1)
PLO = 0.0
PUP = 1.0
DELP = 1.0E-2
CALL PEPAR(PLO,PUP,DELP,PAR(2),'K SQUIGGLE',2)
PLO = 0.0
PUP = 1.0

```

```
DELP = 1.0E-2
CALL PEPAR(PLO,PUP,DELP,PAR(3),'VGE',3)
PLO = 1.1
PUP = 100.0
DELP = 1.0E-2
CALL PEPAR(PLO,PUP,DELP,PAR(4),'SGE',4)
PLO = 0.0
PUP = 10.0
DELP = 1.0E-2
CALL PEPAR(PLO,PUP,DELP,PAR(5),'VKRES',5)
NP = 5
C=====
CALL PENUM(NP,IO)
C=====
RETURN
END
```

```

C=====
C   ROUTINE TAKES THE C,X,Y,Z,T & IS VECTORS SUPPLIED BY THE
C   CALLING PROGRAM AND GENERATES A X,Y,Z FINITE SEGMENT
C   GRID, A VECTOR OF TIMES FOR OUTPUT AND THE INITIAL
C   CONCENTRATION PROFILE.
C=====
SUBROUTINE GENGRD(CV,XV,YV,ZV,TV,ISV,N)
  INCLUDE 'MODEL.PAR'
  INCLUDE 'MODEL.CMN'
  DIMENSION CV(N),XV(N),YV(N),ZV(N),TV(N)
  INTEGER ISV(N)
C----  FIND UPPER AND LOWER LIMITS
  NSTATE = 0
  TFIRST = DMAX
  TLAST = DMIN
  XFIRST = DMAX
  XLAST = DMIN
  YFIRST = DMAX
  YLAST = DMIN
  ZFIRST = DMAX
  ZLAST = DMIN
  DO 10 I=1,N
    NSTATE = MAX(NSTATE,ISV(I))
    TFIRST = MIN(TFIRST,TV(I))
    TLAST = MAX(TLAST,TV(I))
    XFIRST = MIN(XFIRST,XV(I))
    XLAST = MAX(XLAST,XV(I))
    YFIRST = MIN(YFIRST,YV(I))
    YLAST = MAX(YLAST,YV(I))
    ZFIRST = MIN(ZFIRST,ZV(I))
    ZLAST = MAX(ZLAST,ZV(I))
  10  CONTINUE
C---  ADD TERMS TO XX,YY,ZZ,TT
  NUMI = 1
  NUMJ = 1
  NUMK = 1
  NUMT = 1
  XX(NUMI) = XFIRST
  YY(NUMJ) = YFIRST
  ZZ(NUMK) = ZFIRST
  TT(NUMT) = TFIRST
  20  CONTINUE
C----  X-DISTANCE
  IF(NUMI.GT.NTI) STOP 'NTI EXCEEDED'
  IF(NUMJ.GT.NTJ) STOP 'NTJ EXCEEDED'
  IF(NUMK.GT.NTK) STOP 'NTK EXCEEDED'
  IF(NUMT.GT.NTT) STOP 'NTT EXCEEDED'
  IF((XX(NUMI).NE.XLAST)) THEN
    NUMI = NUMI + 1
    XX(NUMI) = XLAST
  ENDIF
C----  Y-DISTANCE
  IF((YY(NUMJ).NE.YLAST)) THEN

```

```

    NUMJ = NUMJ + 1
    YY(NUMJ) = YLAST
  ENDIF
C---- Z-DISTANCE
  IF((ZZ(NUMK).NE.ZLAST)) THEN
    NUMK = NUMK + 1
    ZZ(NUMK) = ZLAST
  ENDIF
C---- TIME
  IF((TT(NUMT).NE.TLAST)) THEN
    NUMT = NUMT + 1
    TT(NUMT) = TLAST
  ENDIF
C---- LOOP OVER ALL OBSERVATIONS
  DO 30 I=1,N
    IF((XV(I).LT.XX(NUMI)).AND.(XV(I).GT.XX(NUMI-1)))THEN
      XX(NUMI) = XV(I)
    ENDIF
C---- Y-DISTANCE
    IF((YV(I).LT.YY(NUMJ)).AND.(YV(I).GT.YY(NUMJ-1))) THEN
      YY(NUMJ) = YV(I)
    ENDIF
C---- Z-DISTANCE
    IF((ZV(I).LT.ZZ(NUMK)).AND.(ZV(I).GT.ZZ(NUMK-1))) THEN
      ZZ(NUMK) = ZV(I)
    ENDIF
C---- TIME
    IF((TV(I).LT.TT(NUMT)).AND.(TV(I).GT.TT(NUMT-1))) THEN
      TT(NUMT) = TV(I)
    ENDIF
  30 CONTINUE
  IF((XX(NUMI).EQ.XLAST).AND.(YY(NUMJ).EQ.YLAST)
    & .AND.(ZZ(NUMK).EQ.ZLAST).AND.(TT(NUMT).EQ.TLAST)) GOTO 40
  GOTO 20
  40 CONTINUE
C---- GENERATE SEGMENT LENGTHS
C---- X-DISTANCE
  XL(1) = ABS(XX(2) - XX(1))
  XL(0) = XL(1)
  XX(0) = XX(1) - XL(1)
  DO 50 IX=2,NUMI-1
    XL(IX) = ABS(XX(IX+1) - XX(IX-1))/2.0D0
  50 CONTINUE
  XL(NUMI) = ABS(XX(NUMI) - XX(NUMI-1))
  XL(NUMI+1) = XL(NUMI)
  XX(NUMI+1) = XX(NUMI) + XL(NUMI)
C---- Y-DISTANCE
  YL(1) = ABS(YY(2) - YY(1))
  YL(0) = YL(1)
  YY(0) = YY(1) - YL(1)
  DO 60 IY=2,NUMJ-1
    YL(IY) = ABS(YY(IY+1) - YY(IY-1))/2.0D0
  60 CONTINUE

```

```

YL(NUMJ) = ABS(YY(NUMJ) - YY(NUMJ-1))
YL(NUMJ+1) = YL(NUMJ)
YY(NUMJ+1) = YY(NUMJ) + YL(NUMJ)
C---- Z-DISTANCE
ZL(1) = ABS(ZZ(2) - ZZ(1))
ZL(0) = ZL(1)
ZZ(0) = ZZ(1) - ZL(1)
DO 70 IZ=2,NUMK-1
  ZL(IZ) = ABS(ZZ(IZ+1) - ZZ(IZ-1))/2.0D0
70  CONTINUE
ZL(NUMK) = ABS(ZZ(NUMK) - ZZ(NUMK-1))
ZL(NUMK+1) = ZL(NUMK)
ZZ(NUMK+1) = ZZ(NUMK) + ZL(NUMK)
C---- SET UP INITIAL CONDITIONS
DO 80 IS=1,NSTATE
DO 80 IX=1,NUMI
DO 80 IY=1,NUMJ
DO 80 IZ=1,NUMK
  C(IS,IX,IY,IZ) = FINTRP(CV,XV,YV,ZV,TV,ISV,N,XX(IX),YY(IY),
    & ZZ(IZ),TFIRST,IS)
C  WRITE(*,2000) XX(IX),YY(IY),ZZ(IZ),TFIRST,C(IS,IX,IY,IZ),IS
80  CONTINUE
2000  FORMAT(5(1X,E12.6),1X,I4)
C=====
C  WRITE(*,1000) NSTATE,NUMI,NUMJ,NUMK,NUMT
1000  FORMAT(' NSTATE ',I3,/
  & ' NUMI ',I3,/
  & ' NUMJ ',I3,/
  & ' NUMK ',I3,/
  & ' NUMT ',I3)
RETURN
END

```

```

=====
C      ROUTINE TO WRITE OUT INITIAL CONDITIONS AND SET UP FINITE
C      SEGMENT GRID LIMITS. SET UP INVARIANT COEFFICIENTS.
=====
C      SUBROUTINE WROBS(IRE,FILIN)
C      INCLUDE 'MODEL.PAR'
C      INCLUDE 'COEFF.CMN'
C      CHARACTER*(*) FILIN
C      CHARACTER*80 SAMFIL
C      CHARACTER*40 PN1,PN2
=====
C----- SET UP OBSERVATIONS
C      CALL PENUM(2,IO)
C
C      XO = 1.0
C      YO = 1.0
C      ZO = 1.0
C      IS = 1
C      IO = 0
C      OPEN(IRE,FILE=FILIN,STATUS='OLD')
C10     CONTINUE
C      READ(IRE,*,END=20) TO,CO
C      IO = IO + 1
C      CALL PEOBS(CO,XO,YO,ZO,TO,IS,IO)
C      GOTO 10
C20    CONTINUE
C      CLOSE(IRE)
=====
C----- ASSIGN PARAMETER VALUES
C
C----- RATE
C      CALL POPAR(PL1,PU1,DP1,P1,PN1,1)
C
=====
C----- SETUP INVARIANT COEFFICIENTS
C
C      RETURN
C      END

```

```

=====
C
C   SUBROUTINE TO READ MODEL PARAMETERS
C
C=====
C   SUBROUTINE RDPAR(PMD,NPAR)
C   INCLUDE 'MODEL.PAR'
C   INCLUDE 'MODEL.CMN'
C   INCLUDE 'COEFF.CMN'
C   DIMENSION PMD(NPAR)
C=====
C----  SETUP INVARIANT COEFFICIENTS
C
C   ISIZ(I,J)   CONTAINS THE CATEGORY IN WHICH THE NEW
C               PARTICLE FORMED BY A SUCCESSFUL COLLISION
C               OF I AND J C WILL BE.
C
C   FRAC(I,J)   CONTAINS THE NUMBER OF PARTICLES IN CATEGORY
C               ISIZ(I,J) CREATED BY A SUCCESSFUL COLLISION OF I
C               AND J.
C
C   BETA(I,J)   CONTAINS THE FREQUENCY OF COLLISIONS BETWEEN
C
C               PARTICLES OF SIZE I AND J
C
C   G           VELOCITY GRADIENT (1/SEC)
C
C   GRAV        ACCELERATION DUE TO GRAVITY (CM/SEC**2)
C
C   RHOS        DENSITY OF PARTICLES (G/CM^3)
C
C   RHOL        DENSITY OF LIQUID (G/CM^3)
C
C   DMU         VISCOSITY OF LIQUID (G/CM S)
C
C   PRE(I,J)    CONTAINS THE FREQUENCY OF EROSIONS OF
C               PARTICLE SIZE
C               J TO FORM PARTICLE SIZE I
C
C   DKE         EROSION EFFICIENCY ?
C
C   SGE         GEOMETRIC STANDARD DEVIATION OF DISTRIBUTION
C               CREATED AS A RESULT OF EROSION
C
C   VGE         GEOMETRIC MEAN OF DISTRIBUTION CREATED AS
C               A RESULT OF EROSION
C=====
C   G = VELGRA
C   GRAV = 981.0
C   DMU = 1.04E-2
C   RHOS = 1.7
C   RHOL = 1.0
C
C----  ALPHA
C

```

```

DO 100 IP=1,NSTATE
  ALPHA(IP) = PMD(1)
100  CONTINUE
C
DKE = PMD(2)
VGE = PMD(3)
SGE = PMD(4)
VKRES = PMD(5)
C
SUM = 0.0
DO 5 I=1,NSTATE
C   SUM = SUM + PE(VOL(I),SGE,VGE)*(VUP(I) - VLO(I))
  SUM = SUM + PE(VOL(I),SGE,VGE)*VOL(I)
C   WRITE(*,'(1X,I4,3(1X,E12.6))') I,SUM,PE(VOL(I),SGE,VGE),VOL(I)
  5   CONTINUE
  IF(SUM.EQ.0.0) SUM = 1.0
C
DO 6 I=0,NSTATE
DO 6 J=0,NSTATE
  PRE(I,J) = 0.0
  6   CONTINUE
C
DO 10 I=1,NSTATE
  DISP(I) = DISPER
  DIAMI = (6.0DO*VOL(I)/PI)**(0.3333333333333333)
  VEL(I) = (GRAV*(RHOP - RHOL)*DIAMI**2)/(18.0*DMU)
  DO 10 J=1,NSTATE
    IF(J.GT.I) THEN
C     PRE(I,J) = G*PE(VOL(I),SGE,VGE)*(VUP(I) - VLO(I))/SUM
      PRE(I,J) = G*PE(VOL(I),SGE,VGE)*VOL(I)/SUM
    ELSE
      PRE(I,J) = 0.0
    ENDIF
  10  CONTINUE
C   TTO = 0.0
C   DO 15 I=1,NSTATE
C     WRITE(*,*) PE(VOL(I),SGE,VGE),PRE(I,5)/G,I
C     TTO = TTO + PRE(I,5)/G
C15  CONTINUE
C   WRITE(*,*) TTO
C=====
DIFFC = (((6.0/PI)**(0.3333333333333333))*
&        (GRAV/(12.0*DMU))*(RHOP - RHOL)
  GOP = G/PI
DO 50 I=1,NSTATE
  DIAMI = (6.0*VOL(I)/PI)**(0.3333333333333333)
  VOL3I = VOL(I)**(0.3333333333333333)
  DO 50 J = 1, NSTATE
    DIAMJ = (6.0*VOL(J)/PI)**(0.3333333333333333)
    VOL3J = VOL(J)**(0.3333333333333333)
    VOLIJ = (VOL3I + VOL3J)**3
    BETA(I,J) = 0.0
    BETA(I,J) = BETA(I,J) + GOP*VOLIJ

```



```

      BETA(I,J) = BETA(I,J) +
&      DIFFC*VOLIJ*ABS(VOL3I - VOL3J)
      VOLNEW = VOL(I) + VOL(J)
      DO 60 K = NSTATE,1,-1
      DIAMK = (6.0*VOL(K)/PI)**(0.3333333333333333)
      IF(VOLNEW.GE.VLO(K)) THEN
      ISIZ(I,J) = K
      FRAC(I,J) = VOLNEW/VOL(K)
      GOTO 50
      ENDIF
60      CONTINUE
50      CONTINUE
C=====
C---- DEFINE ORDER OF RUNGE - KUTTA
      IORDER = 1
C---- DEFINE SPECIFIED TIME STEP
      DTMAX = 3600.0
      DTMIN = 0.1
      SF = 10.0
C=====
      RETURN
      END
      FUNCTION PE(V,SGE,VGE)
C=====
C      FUNCTION TO EVALUATE RESULTING DISTRIBUTION DUE TO
C      EROSION
C      V      PARTICLE VOLUME
C      SGE    GEOMETRIC STANDARD DEVIATION
C      VGE    GEOMETRIC MEAN
C=====
      PARAMETER (PI = 3.1415926536)
      PE = EXP(- (LOG(V) - LOG(VGE))**2 / (2.0*LOG(SGE)**2) )
      &      / (V*SQRT(2.0*PI)*LOG(SGE))
      RETURN
      END

```

```

C=====
C  SUBROUTINE TO WRITE OUTPUT
C=====
      SUBROUTINE WROUT(PRED,XPRED,YPRED,ZPRED,TPRED,ISPRED,
&      NPRED,NUMPRD)
      INCLUDE 'MODEL.PAR'
      INCLUDE 'MODEL.CMN'
      INCLUDE 'COEFF.CMN'
      DIMENSION
      PRED(NUMPRD),XPRED(NUMPRD),YPRED(NUMPRD),ZPRED(NUMPRD)
      DIMENSION TPRED(NUMPRD)
      INTEGER ISPRED(NUMPRD)
      IF(NPRED.EQ.0) TOTV0 = 0.0
      TOTV = 0.0
      DO 10 IS=1,NSTATE
      DO 10 IX=1,NUMI
      DO 10 IY=1,NUMJ
      DO 10 IZ=1,NUMK
      NPRED = NPRED + 1
      TOTV = TOTV + C(IS,IX,IY,IZ)*VOL(IS)*XL(IX)*YL(IY)*ZL(IZ)
      PRED(NPRED) = C(IS,IX,IY,IZ)
      XPRED(NPRED) = XX(IX)
      YPRED(NPRED) = YY(IY)
      ZPRED(NPRED) = ZZ(IZ)
      TPRED(NPRED) = TYME
      ISPRED(NPRED) = IS
10      CONTINUE
      IF(TOTV0.EQ.0.0) TOTV0 = TOTV
      TOTV = TOTV/TOTV0
C      WRITE(*,100) TYME,TOTV
100     FORMAT('+','TIME:',E9.3,' FRACTION REMAINING:',E9.3)
      RETURN
      END

```

```

C=====
C   PARAMETER STATEMENTS USED TO DEFINE NAMED CONSTANTS
C   USED IN DIMENSIONING ARRAYS.
C       NTS   NUMBER OF PERMISSIBLE STATE EQUATIONS
C       NTI   NUMBER OF PERMISSIBLE SEGMENTS IN X - DIR.
C       NTJ   NUMBER OF PERMISSIBLE SEGMENTS IN Y - DIR.
C       NTK   NUMBER OF PERMISSIBLE SEGMENTS IN Z - DIR.
C       NTT   NUMBER OF PERMISSIBLE TIME STEPS
C       DMAX  LARGEST DOUBLE PRECISION NUMBER
C       DMIN  SMALLEST DOUBLE PRECISION NUMBER
C       PI    PI
C       NTOBS TOTAL PERMISSIBLE NUMBER OF
C            OBSERVATIONS
C       NTPAR TOTAL PERMISSIBLE NUMBER OF PARAMETERS
C=====
IMPLICIT REAL*8 (A-H,O-Z)
  PARAMETER (NTS=10,NTI=2,NTJ=2,NTK=11,NTT=100)
  PARAMETER (NTALL = NTS*NTI*NTJ*NTK)
PARAMETER (DMAX = 1.0D30, DMIN = -1.0E30)
PARAMETER (PI = 3.1415926536)
PARAMETER (NTOBS = 2600)
PARAMETER (NTPAR = 10)

```

```

C=====
C   COMMON BLOCK FOR FINITE SEGMENT MODEL FRAMEWORK
C=====
C   INTEGER RUNGE
C   C   ARRAY CONTAINING VALUES OF THE STATE
C   VARIABLES AT ALL SEGMENTS AT THE CURRENT
C   TIME STEP. STARTS OFF CONTAINING INITIAL
C   CONDITIONS.
C   DCDT ARRAY CONTAINING THE VALUES OF THE
C   DERIVATIVES OF ALL THE STATE VARIABLES AT ALL
C   SEGMENTS AT THE CURRENT TIME STEP.
C   XL   SEGMENT LENGTH IN X-DIRECTION
C   YL   SEGMENT LENGTH IN Y-DIRECTION
C   ZL   SEGMENT LENGTH IN Z-DIRECTION
C   XX   DISTANCE TO CENTER OF SEGMENT IN X-DIRECTION
C   YY   DISTANCE TO CENTER OF SEGMENT IN Y-DIRECTION
C   ZZ   DISTANCE TO CENTER OF SEGMENT IN Z-DIRECTION
C   TT   TIMES AT WHICH OUTPUT IS REQUIRED
C   DTMAX   MAXIMUM TIME STEP SIZE
C   DTMIN   MINIMUM TIME STEP SIZE
C   TYME   CURRENT MODEL TIME.
C   NSTATE   NUMBER OF STATE EQUATIONS.
C   NUMI   NUMBER OF SEGMENTS IN X - DIRECTION.
C   NUMJ   NUMBER OF SEGMENTS IN Y - DIRECTION.
C   NUMK   NUMBER OF SEGMENTS IN Z - DIRECTION.
C   PHI   ARRAY OF INCREMENT FUNCTIONS FOR ALL STATE
C   EQUATIONS AT ALL SEGMENTS :
C   C(I+1) = PHI(I)*H + C(I).
C   SAVEY   TEMPORARY ARRAY USED TO HOLD THE
C   VALUES OF
C   THE STATE VARIABLES DURING RUNGE - KUTTA
C   PASSES.
C   IORDER   ORDER OF THE RUNGE - KUTTA INTEGRATION :
C   1   EULER'S METHOD
C   2   MODIFIED EULER
C   3   FOURTH ORDER RUNGE - KUTTA.
C   TOL   SYSTEM TOLERANCE.
COMMON /RK/ C(0:NTS,0:NTI,0:NTJ,0:NTK)
COMMON /RK/ DCDT(0:NTS,0:NTI,0:NTJ,0:NTK)
COMMON /RK/ XL(0:NTI),XX(0:NTI)
COMMON /RK/ YL(0:NTJ),YY(0:NTJ)
COMMON /RK/ ZL(0:NTK),ZZ(0:NTK)
COMMON /RK/ TT(0:NTT),TNEXT
COMMON /RK/ XFIRST,XLAST
COMMON /RK/ YFIRST,YLAST
COMMON /RK/ ZFIRST,ZLAST
COMMON /RK/ TFIRST,TLAST
COMMON /RK/ DTMIN,DTMAX,SF,TYME
COMMON /RK/ NSTATE,NUMI,NUMJ,NUMK,NUMT
COMMON /RK/ PHI(NTS,NTI,NTJ,NTK),SAVEY(NTS,NTI,NTJ,NTK)
COMMON /RK/ IORDER,TOL

```

```
C=====
C   COMMON BLOCK CONTAINING THE MODEL COEFFICIENTS
C=====
COMMON /COEFF/ VOL(NTS),VEL(NTS),DISP(NTS)
COMMON /COEFF/ VLO(NTS),VUP(NTS)
COMMON /COEFF/ BETA(0:NTS,0:NTS),ALPHA(NTS)
COMMON /COEFF/ ISIZ(0:NTS,0:NTS),FRAC(0:NTS,0:NTS)
COMMON /COEFF/ PRE(0:NTS,0:NTS),SGE, VGE, DKE, VKRES
COMMON /COEFF/ G,GRAV, RHOP, RHOS, RHOL, DMU, DISPER,VELGRA
```

```

C=====
C   COMMON BLOCK CONTAINING OBSERVED OR INPUT
C   CONCENTRATIONS AND LOCATION.
C
C       OBS  VECTOR OF OBSERVED VALUES
C       XOBS VECTOR OF X-LOCATIONS
C       YOBS VECTOR OF Y-LOCATIONS
C       ZOBS VECTOR OF Z-LOCATIONS
C       TOBS VECTOR OF TIMES
C       ISOBS VECTOR OF STATE VARIABLE NUMBER
C       NOBS NUMBER OF OBSERVATIONS
C       PLO  PARAMETER LOWER LIMIT
C       PUP  PARAMETER UPPER LIMIT
C       P    STARTING PARAMETER VALUE / INITIAL GUESS 1
C       PO   STARTING PARAMETER VALUE / INITIAL GUESS 0
C       PIN  ARRAY TO CONTAIN INPUT PARAMETER VALUES
C       PC   CURRENT PARAMETER VALUE
C       PNAME PARAMETER NAME
C       NPAR NUMBER OF PARAMETERS
C=====
REAL*8 OBS,XOBS,YOBS,ZOBS,TOBS
CHARACTER*40 PNAME
COMMON /OBSERV/
OBS(NTOBS),XOBS(NTOBS),YOBS(NTOBS),ZOBS(NTOBS)
COMMON /OBSERV/ TOBS(NTOBS),ISOBS(NTOBS)
COMMON /OBSERV/ NOBS
COMMON /OBSERV/ PLO(NTPAR),PUP(NTPAR),P(NTPAR),PO(NTPAR)
COMMON /OBSERV/ PIN(NTPAR),PC(NTPAR),PNAME(NTPAR)
COMMON /OBSERV/ NPAR

```

APPENDIX D
POROSITY DERIVATION

DERIVATION OF PARTICLE DIAMETER BASED ON POROSITY:

Given:

$$(1) \quad V_{\text{new}} = V_i + V_j + V_{\text{cij}}$$

$$(2) \quad P_{\text{new}} = \frac{V_{\text{vnew}}}{V_{\text{snew}}} = \frac{V_{\text{vi}} + V_{\text{vj}} + V_{\text{eij}}}{V_{\text{si}} + V_{\text{sj}}}$$

$$(3) \quad V_v = \left(\frac{P}{1+P}\right)V_T$$

$$(4) \quad V_s = \left(\frac{1}{1+P}\right)V_T$$

$$(5) \quad P_i = 1 - Bd_i^{-d}$$

$$(6) \quad V_i = \frac{\pi d_i^3}{6}$$

Substitute eqn (6) into eqn (1):

$$(7) \quad \frac{\pi d_{\text{new}}^3}{6} = V_i + V_j + V_{\text{cij}}$$

Let:

$$(8) \quad \phi_i = \frac{P_i}{1+P_i}$$

Substitute eqn (5) and eqn (8) into eqn (2):

$$(9) \quad 1 - Bd_{\text{new}}^{-d} = \frac{\phi_i V_i + \phi_j V_j + V_{\text{eij}}}{(1-\phi_i)V_i + (1-\phi_j)V_j}$$

$$(10) \quad \Rightarrow V_{\text{cij}} = (1 - Bd_{\text{new}}^{-d})[(1-\phi_i)V_i + (1-\phi_j)V_j] - \phi_i V_i - \phi_j V_j$$

Substitute eqn (7) into eqn (10):

$$(11) \quad \frac{\pi d_{\text{new}}^3}{6} = (1 - Bd_{\text{new}}^{-d})[(1-\phi_i)V_i + (1-\phi_j)V_j] + (1-\phi_i)V_i + (1-\phi_j)V_j$$

Let:

$$(12) \quad R_{ij} = [(1 - \phi_i)V_i + (1 - \phi_j)V_j]$$

Substitute eqn (12) into eqn (11):

$$(13) \quad \frac{\pi d_{new}^3}{6} = -Bd_{new}^{-d}R_{ij} + 2R_{ij}$$

$$(14) \quad \Rightarrow F = \frac{\pi d_{new}^3}{6} - Bd_{new}^{-d}R_{ij} + 2R_{ij}$$

$$(15) \quad \Rightarrow F' = \frac{3\pi d_{new}^2}{6} + d \text{ superscript } Bd_{new}^{-(d+1)}R_{ij}$$

Numerically solve for d_{new} using eqn (14) and (15).

APPENDIX E
EXPERIMENTAL AND MODEL RESULTS

Table E1.-Experimental Design 1: Concentration Variation

Modeling Parameter	Exp. 7 C = 10 mg/l	Exp. 8 C = 40 mg/l	Exp. 9 C = 80 mg/l
Alpha	0.254	0.0683	0.0457
Erosion constant	0.780E-6	0.327E-8	0.341E-9
Geometric mean	0.190E-9	0.542E-10	0.533E-10
Geo. standard deviation	1.383	9.72	3.005
Resuspension constant	0.089	0.025	0.341E-5

Table E2.- Experimental Design 2: Salinity and Shear Variation

Salinity of 5 ppt	Exp. 19 G = 20	Exp. 1 G = 30	Exp. 17 G = 40
Alpha Erosion constant	0.308	0.0018	0.0047
Geometric mean	0.423E-8	0.166E-10	0.163E-9
Geo. standard deviation	57	86	86
Resuspension constant	11.6	11.6	16.4
	0.6148	0.272	1.49
Salinity of 15 ppt	Exp. 18 G = 20	Exp. 2 G = 30	Exp. 6 G = 40
Alpha Erosion constant	0.0683	0.0185	0.0047
Geometric mean	0.327E-8	0.166E-8	0.163E-9
Geo. standard deviation	54	86	86
Resuspension constant	9.72	11.62	16.47
	0.025	0.272	0.0769
Salinity of 30 ppt	Exp. 20 G = 20	Exp. 3 G = 30	Exp. 21 G = 40
Alpha Erosion constant	0.09	0.008	0.00467
Geometric mean	0.279E-8	0.174E-8	0.163E-9
Geo. standard deviation	53	83	86
Resuspension constant	9.76	11.43	16.41
	0.0175	0.444	1.49

Table E3.- Experimental Design 3: Salinity and Particle Type Variation

Particle Type A	Exp. 19 I = 5	Exp. 18 I = 15	Exp. 20 I = 30
Alpha Erosion constant	0.308	0.068	0.0899
Geometric mean	0.423E-8	0.327E-8	0.279E-8
Geo. standard deviation	57	54	53
Resuspension constant	11.6	9.72	9.76
	0.6148	0.0250	0.0175
Particle Type B	Exp. 10 I = 5	Exp. 11 I = 15	Exp. 12 I = 30
Alpha Erosion constant	0.308	0.068	Missing Data
Geometric mean	0.423E-8	0.327E-8	
Geo. standard deviation	57	54	
Resuspension constant	11.6	9.72	
	0.0061	0.0250	
Particle Type C	Exp. 13 I = 5	Exp. 14 I = 15	Exp. 15 I = 30
Alpha Erosion constant	0.308	0.068	0.0899
Geometric mean	0.423E-8	0.327E-8	0.279E-8
Geo. standard deviation	57	54	53
Resuspension constant	11.6	9.70	9.76
	0.0061	0.025	0.0175

Table E4.- Observed and Predicted Correlation Coefficients

<u>Experiment</u>	<u>Number</u>	<u>Volume</u>	<u>Tot. Num</u>	<u>Tot. Vol.</u>
1	0.958	0.960	0.434	0.633
2	0.946	0.916	0.725	0.890
3	0.942	0.948	0.534	0.668
5	0.943	0.937	0.632	0.866
6	0.917	0.900	0.377	-0.854
7	0.926	0.926	0.755	0.926
8	0.953	0.947	0.841	0.927
9	0.976	0.972	0.940	0.967
10	0.956	0.947	0.898	0.977
11	0.940	0.803	0.727	0.800
13	0.946	0.946	0.894	0.971
14	0.968	0.949	0.917	0.975
15	0.972	0.921	0.868	0.970
16	0.966	0.898	0.959	0.946
17	0.896	0.910	0.591	-0.378
18	0.960	0.923	0.900	0.951
19	0.969	0.937	0.939	0.970
20	0.969	0.946	0.907	0.984
21	0.903	0.876	0.630	-2.390

* Particle number and volume concentration correlation is between observed and predicted data that encompasses each data point (~ 500 points) taken throughout an experiment (over space, time, and particle size). Total particle number and volume concentration correlation is between observed and predicted data that is comprised of approximately 60 data points taken over space and time. The total of particle number or volume concentration is calculated over all size categories at a given time to yield one data point to be used in the correlation procedure.

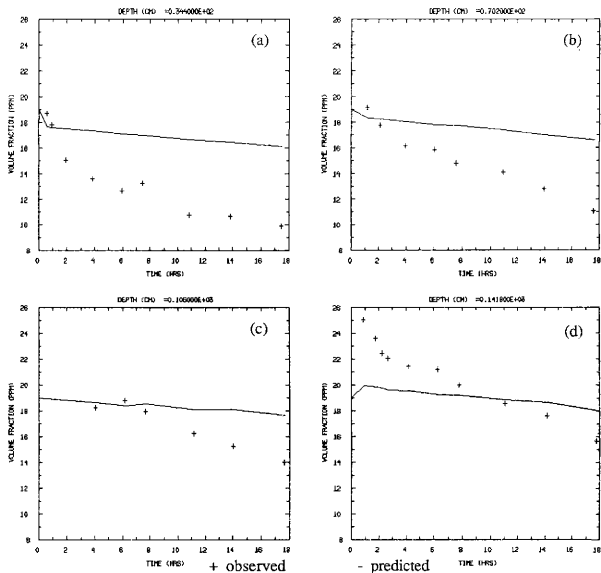


Fig. E2.- Experiment 1: Total Particle Volume Observed and Predicted for Depths (a) 34.4 cm; (b) 70.2 cm; (c) 106.0 cm; and (d) 141.8 cm with Shear of 30 sec⁻¹, Salinity of 5 ppt, Type A Sediment, and Suspended Solids of 40 mg/l.

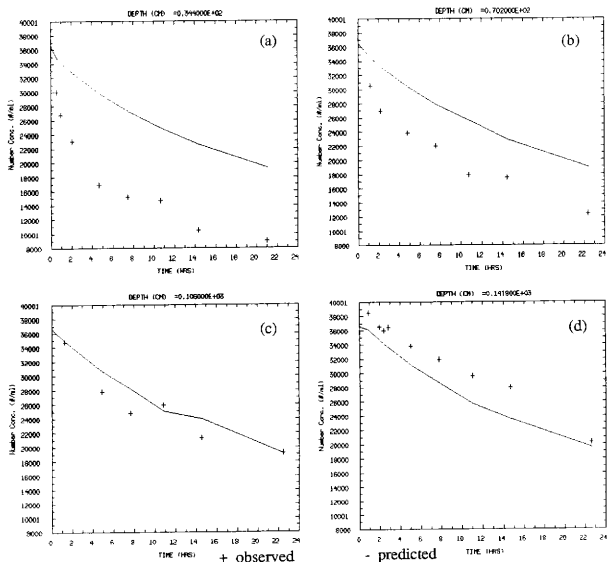


Fig. E3.- Experiment 2: Total Particle Number Observed and Predicted for Depths (a) 34.4 cm; (b) 70.2 cm; (c) 106.0 cm; and (d) 141.8 cm with Shear of 30 sec⁻¹, Salinity of 15 ppt, Type A Sediment, and Suspended Solids of 40 mg/l.

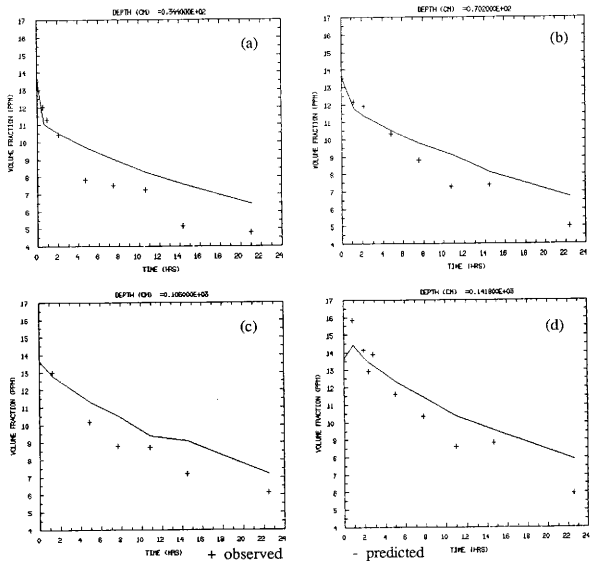


Fig. E4.- Experiment 2: Total Particle Volume Observed and Predicted for Depths (a) 34.4 cm; (b) 70.2 cm; (c) 106.0 cm; and (d) 141.8 cm with Shear of 30 sec⁻¹, Salinity of 15 ppt, Type A Sediment, and Suspended Solids of 40 mg/l.

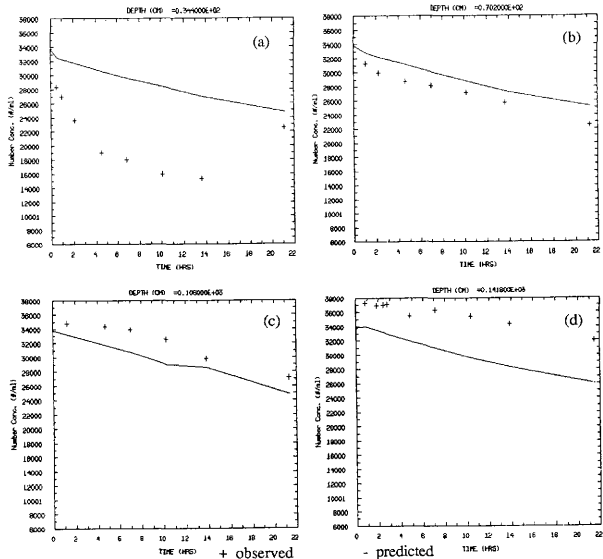


Fig. E5.- Experiment 3: Total Particle Number Observed and Predicted for Depths (a) 34.4 cm; (b) 70.2 cm; (c) 106.0 cm; and (d) 141.8 cm with Shear of 30 sec⁻¹, Salinity of 30 ppt, Type A Sediment, and Suspended Solids of 40 mg/l.

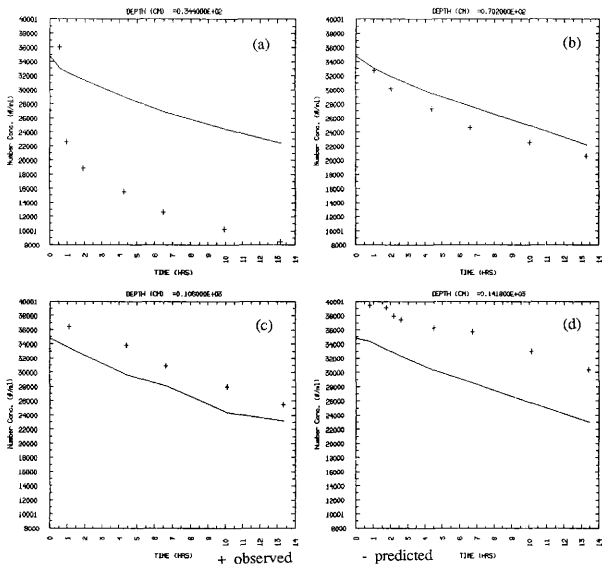


Fig. E6.- Experiment 5: Total Particle Number Observed and Predicted for Depths (a) 34.4 cm; (b) 70.2 cm; (c) 106.0 cm; and (d) 141.8 cm with Shear of 30 sec⁻¹, Salinity of 15 ppt, Type A Sediment, and Suspended Solids of 40 mg/l.

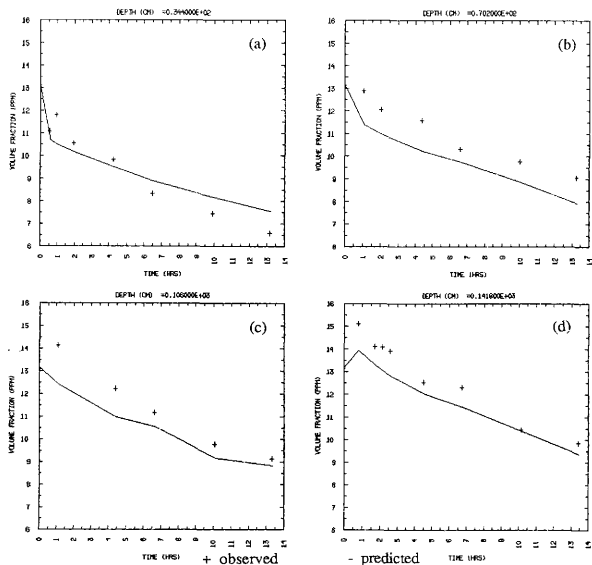


Fig. E7.- Experiment 5: Total Particle Volume Observed and Predicted for Depths (a) 34.4 cm; (b) 70.2 cm; (c) 106.0 cm; and (d) 141.8 cm with Shear of 30 sec⁻¹, Salinity of 15 ppt, Type A Sediment, and Suspended Solids of 40 mg/l.

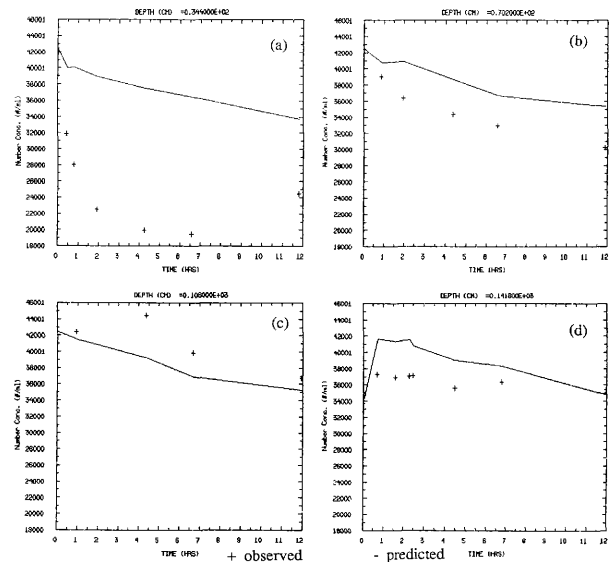


Fig. E8.- Experiment 6: Total Particle Number Observed and Predicted for Depths (a) 34.4 cm; (b) 70.2 cm; (c) 106.0 cm; and (d) 141.8 cm with Shear of 40 sec⁻¹, Salinity of 15 ppt, Type A Sediment, and Suspended Solids of 40 mg/l.

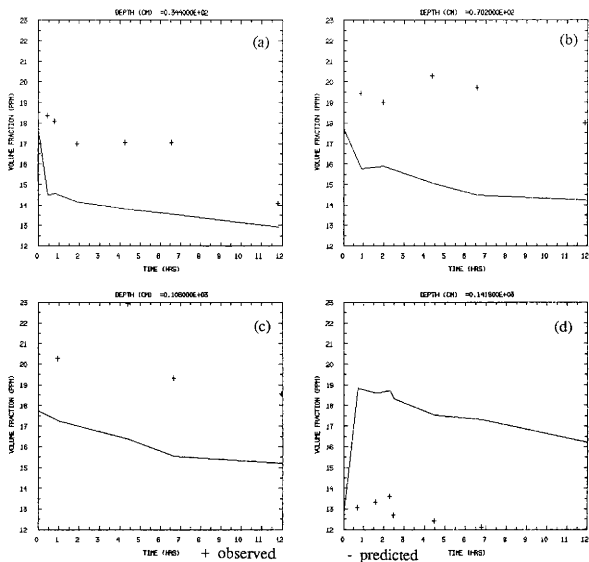


Fig. E9.- Experiment 6: Total Particle Volume Observed and Predicted for Depths (a) 34.4 cm; (b) 70.2 cm; (c) 106.0 cm; and (d) 141.8 cm with Shear of 40 sec⁻¹, Salinity of 15 ppt, Type A Sediment, and Suspended Solids of 40 mg/l.

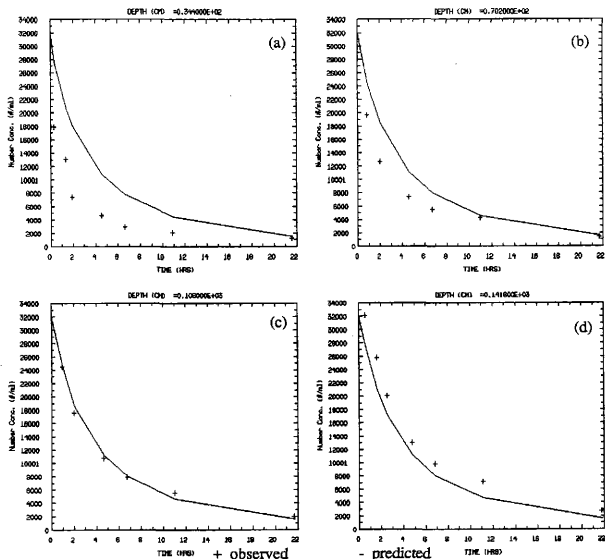


Fig. E10.- Experiment 9: Total Particle Number Observed and Predicted for Depths (a) 34.4 cm; (b) 70.2 cm; (c) 106.0 cm; and (d) 141.8 cm with Shear of 20 sec⁻¹, Salinity of 15 ppt, Type A Sediment, and Suspended Solids of 80 mg/l.

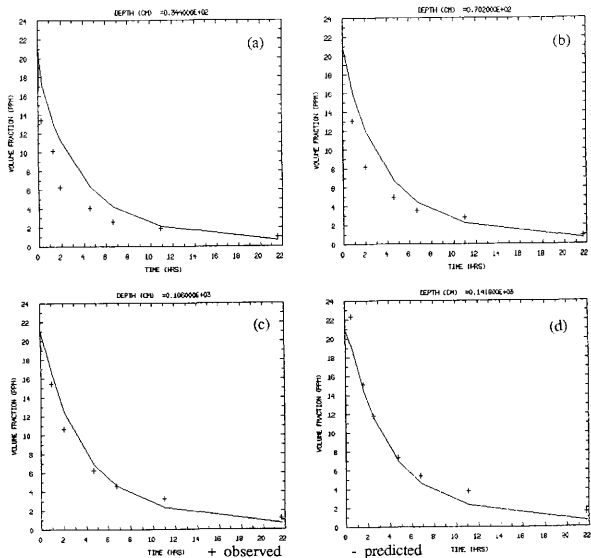


Fig. E11.- Experiment 9: Total Particle Volume Observed and Predicted for Depths (a) 34.4 cm; (b) 70.2 cm; (c) 106.0 cm; and (d) 141.8 cm with Shear of 20 sec⁻¹, Salinity of 15 ppt, Type A Sediment, and Suspended Solids of 80 mg/l.

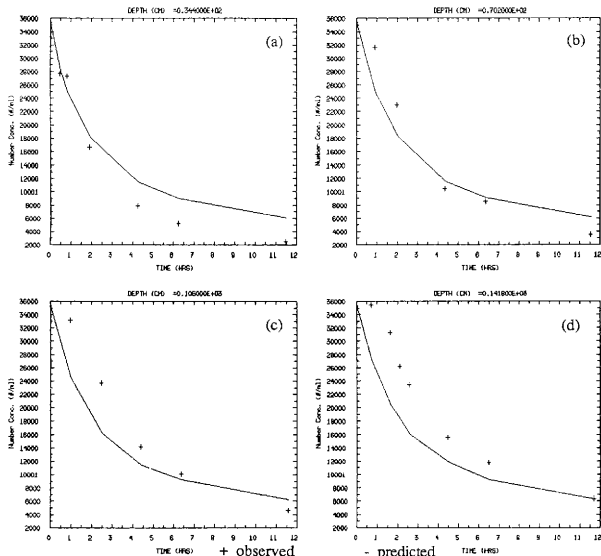


Fig. E12.- Experiment 10: Total Particle Number Observed and Predicted for Depths (a) 34.4 cm; (b) 70.2 cm; (c) 106.0 cm; and (d) 141.8 cm with Shear of 20 sec⁻¹, Salinity of 5 ppt, Type B Sediment, and Suspended Solids of 40 mg/l.

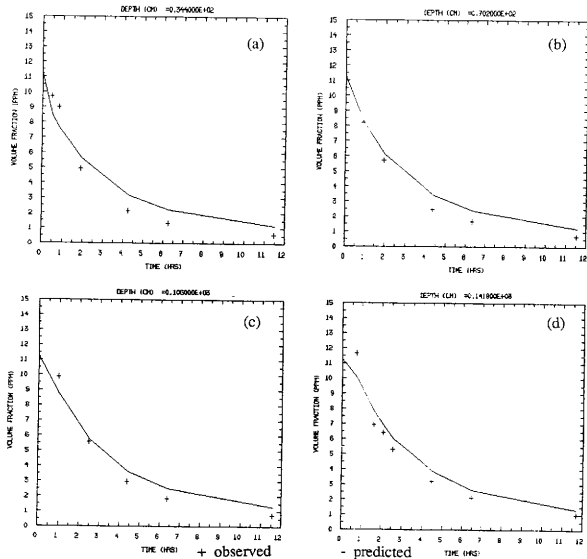


Fig. E13.- Experiment 10: Total Particle Volume Observed and Predicted for Depths (a) 34.4 cm; (b) 70.2 cm; (c) 106.0 cm; and (d) 141.8 cm with Shear of 20 sec⁻¹, Salinity of 5 ppt, Type B Sediment, and Suspended Solids of 40 mg/l.

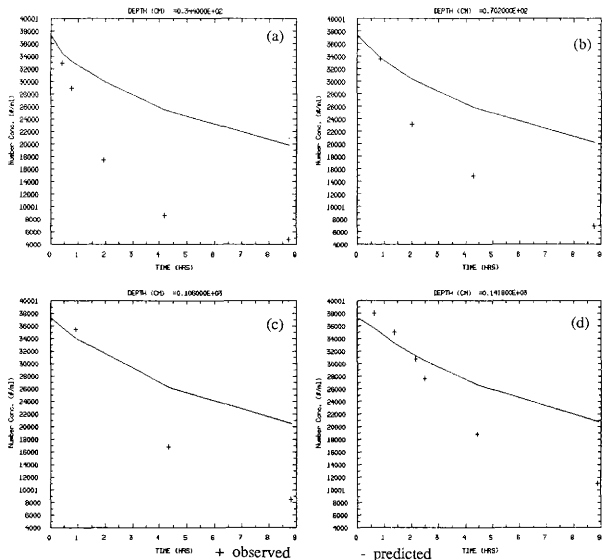


Fig. E14.- Experiment 11: Total Particle Number Observed and Predicted for Depths (a) 34.4 cm; (b) 70.2 cm; (c) 106.0 cm; and (d) 141.8 cm with Shear of 20 sec⁻¹, Salinity of 15 ppt, Type B Sediment, and Suspended Solids of 40 mg/l.

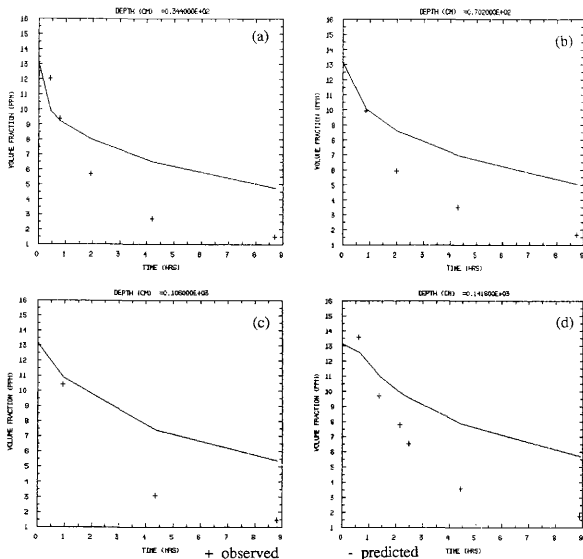


Fig. E15.- Experiment 11: Total Particle Volume Observed and Predicted for Depths (a) 34.4 cm; (b) 70.2 cm; (c) 106.0 cm; and (d) 141.8 cm with Shear of 20 sec⁻¹, Salinity of 15 ppt, Type B Sediment, and Suspended Solids of 40 mg/l.

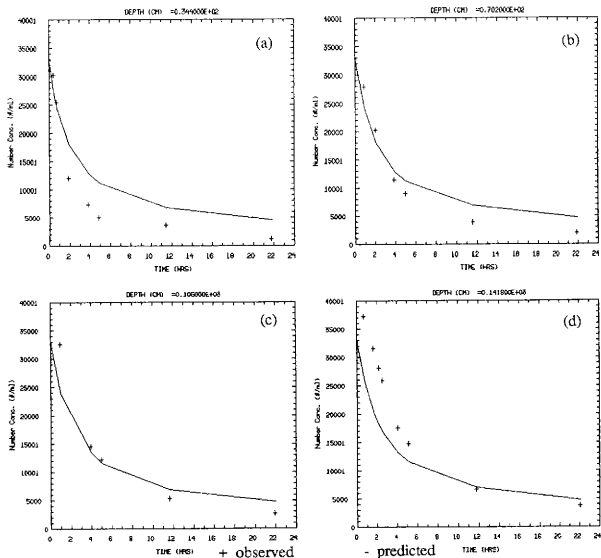


Fig. E16.-- Experiment 13: Total Particle Number Observed and Predicted for Depths (a) 34.4 cm; (b) 70.2 cm; (c) 106.0 cm; and (d) 141.8 cm with Shear of 20 sec⁻¹, Salinity of 5 ppt, Type C Sediment, and Suspended Solids of 40 mg/l.

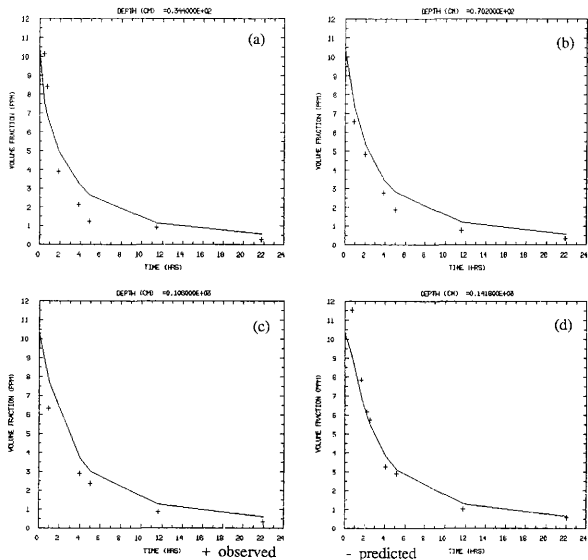


Fig. E17.- Experiment 13: Total Particle Volume Observed and Predicted for Depths (a) 34.4 cm; (b) 70.2 cm; (c) 106.0 cm; and (d) 141.8 cm with Shear of 20 sec⁻¹, Salinity of 5 ppt, Type C Sediment, and Suspended Solids of 40 mg/l.

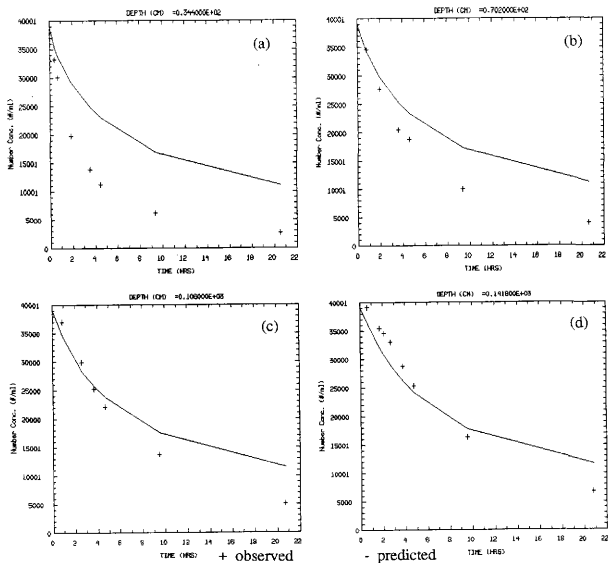


Fig. E18.- Experiment 14: Total Particle Number Observed and Predicted for Depths (a) 34.4 cm; (b) 70.2 cm; (c) 106.0 cm; and (d) 141.8 cm with Shear of 20 sec⁻¹, Salinity of 15 ppt, Type C Sediment, and Suspended Solids of 40 mg/l.

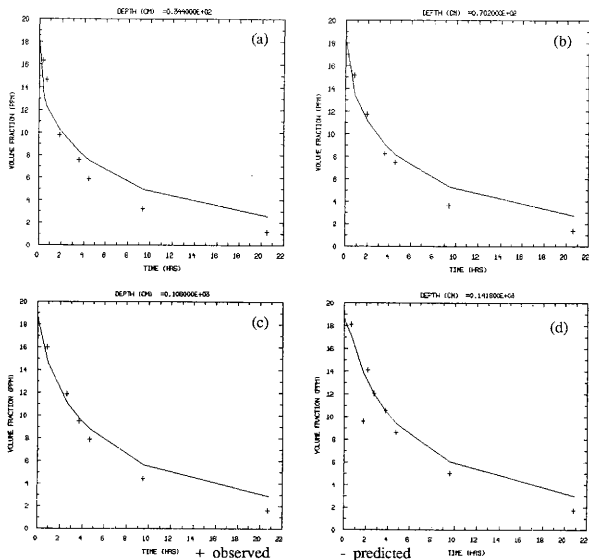


Fig. E19.- Experiment 14: Total Particle Volume Observed and Predicted for Depths (a) 34.4 cm; (b) 70.2 cm; (c) 106.0 cm; and (d) 141.8 cm with Shear of 20 sec⁻¹, Salinity of 15 ppt, Type C Sediment, and Suspended Solids of 40 mg/l.

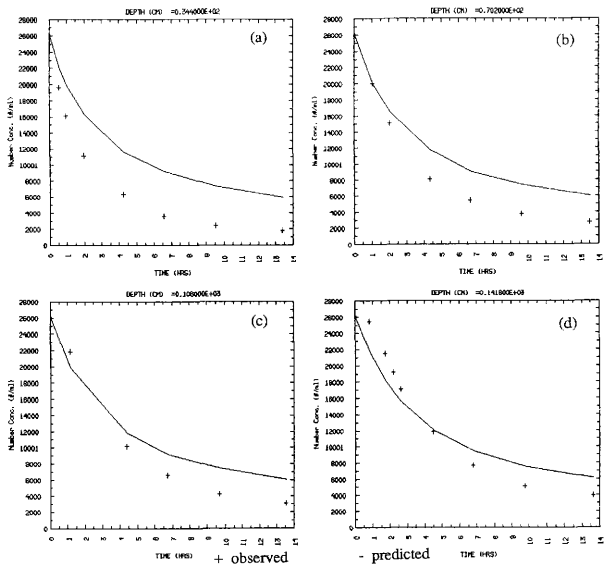


Fig. E20.- Experiment 15: Total Particle Number Observed and Predicted for Depths (a) 34.4 cm; (b) 70.2 cm; (c) 106.0 cm; and (d) 141.8 cm with Shear of 20 sec⁻¹, Salinity of 30 ppt, Type C Sediment, and Suspended Solids of 40 mg/l.

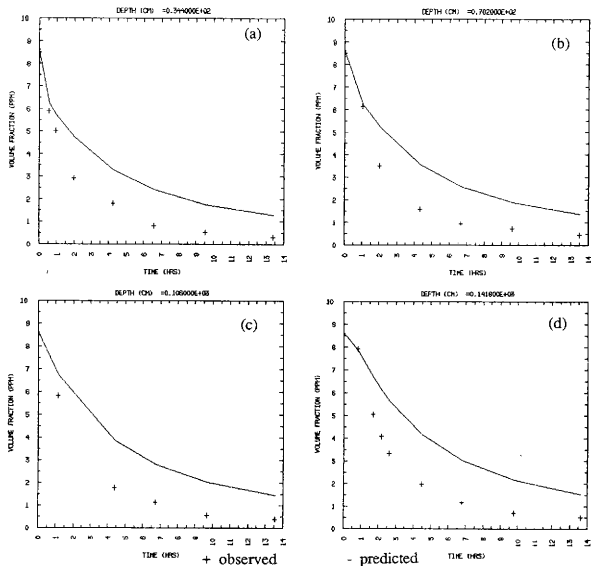


Fig. E21.- Experiment 15: Total Particle Volume Observed and Predicted for Depths (a) 34.4 cm; (b) 70.2 cm; (c) 106.0 cm; and (d) 141.8 cm with Shear of 20 sec⁻¹, Salinity of 30 ppt, Type C Sediment, and Suspended Solids of 40 mg/l.

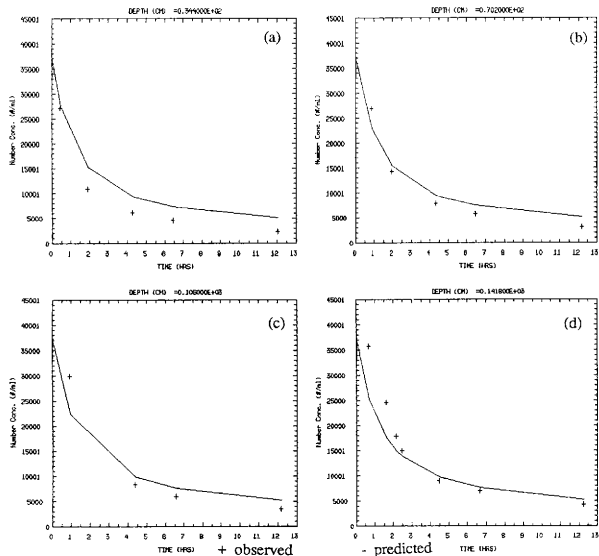


Fig. E22.- Experiment 16: Total Particle Number Observed and Predicted for Depths (a) 34.4 cm; (b) 70.2 cm; (c) 106.0 cm; and (d) 141.8 cm with Shear of 10 sec^{-1} , Salinity of 15 ppt, Type A Sediment, and Suspended Solids of 40 mg/L.

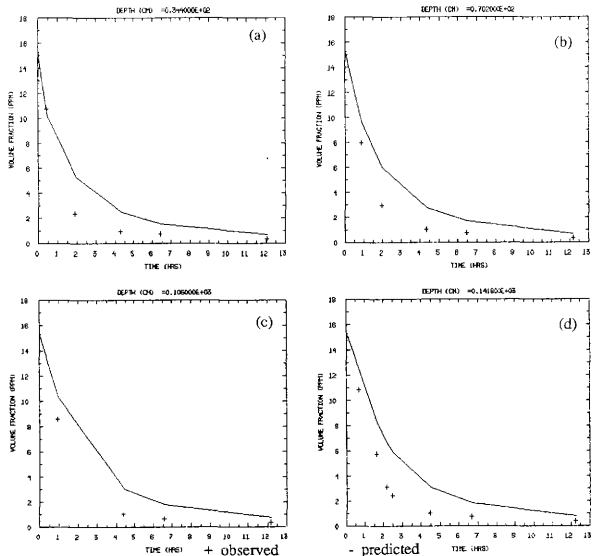


Fig. E23.- Experiment 16: Total Particle Volume Observed and Predicted for Depths (a) 34.4 cm; (b) 70.2 cm; (c) 106.0 cm; and (d) 141.8 cm with Shear of 10 sec^{-1} , Salinity of 15 ppt, Type A Sediment, and Suspended Solids of 40 mg/l .

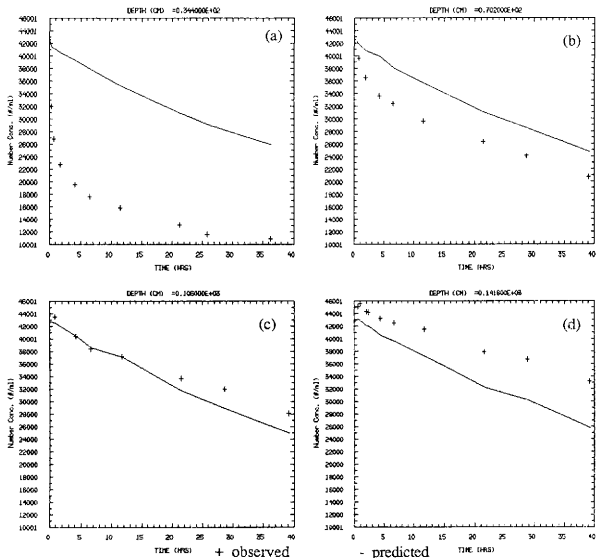


Fig. E24.- Experiment 17: Total Particle Number Observed and Predicted for Depths (a) 34.4 cm; (b) 70.2 cm; (c) 106.0 cm; and (d) 141.8 cm with Shear of 40 sec⁻¹, Salinity of 5 ppt, Type A Sediment, and Suspended Solids of 40 mg/l.

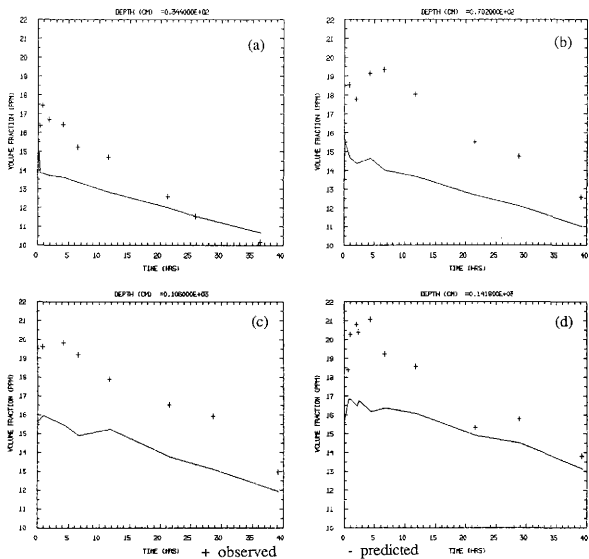


Fig. E25.- Experiment 17: Total Particle Volume Observed and Predicted for Depths (a) 34.4 cm; (b) 70.2 cm; (c) 106.0 cm; and (d) 141.8 cm with Shear of 40 sec^{-1} , Salinity of 5 ppt, Type A Sediment, and Suspended Solids of 40 mg/l .

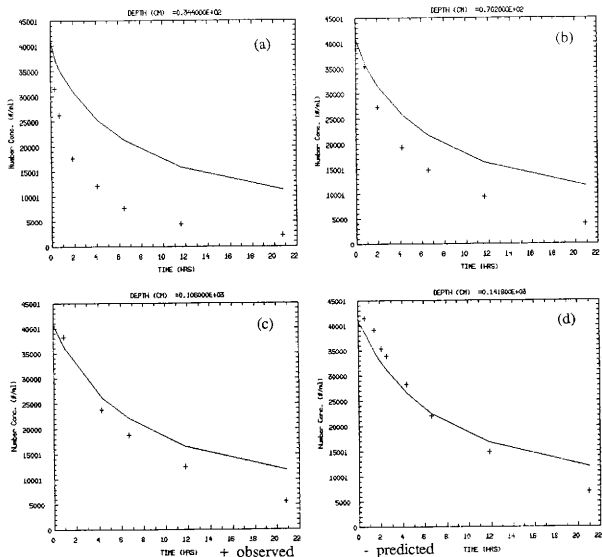


Fig. E26.- Experiment 18: Total Particle Number Observed and Predicted for Depths (a) 34.4 cm; (b) 70.2 cm; (c) 106.0 cm; and (d) 141.8 cm with Shear of 20 sec⁻¹, Salinity of 5 ppt, Type A Sediment, and Suspended Solids of 40 mg/l.

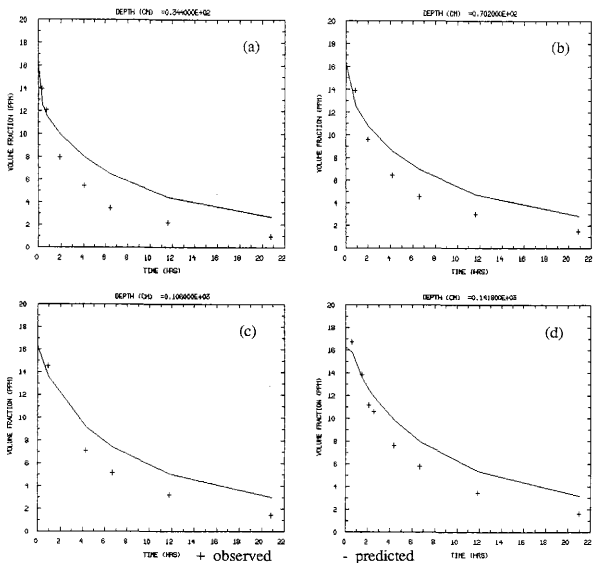


Fig. E27.- Experiment 18: Total Particle Volume Observed and Predicted for Depths (a) 34.4 cm; (b) 70.2 cm; (c) 106.0 cm; and (d) 141.8 cm with Shear of 20 sec⁻¹, Salinity of 5 ppt, Type A Sediment, and Suspended Solids of 40 mg/l.

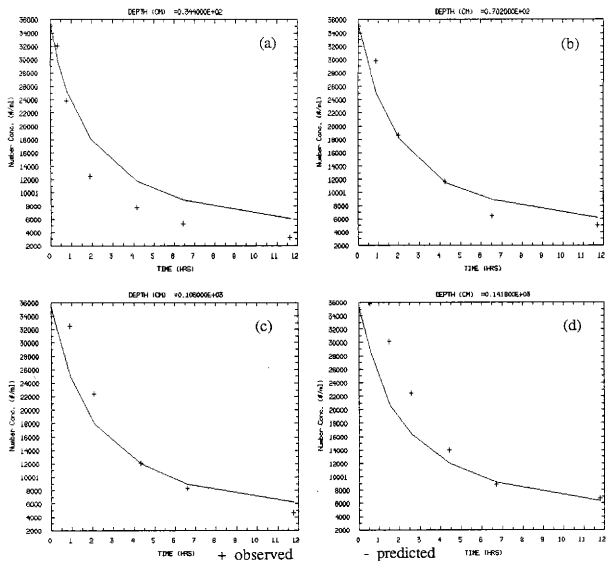


Fig. E28.- Experiment 19: Total Particle Number Observed and Predicted for Depths (a) 34.4 cm; (b) 70.2 cm; (c) 106.0 cm; and (d) 141.8 cm with Shear of 20 sec⁻¹, Salinity of 15 ppt, Type A Sediment, and Suspended Solids of 40 mg/l.

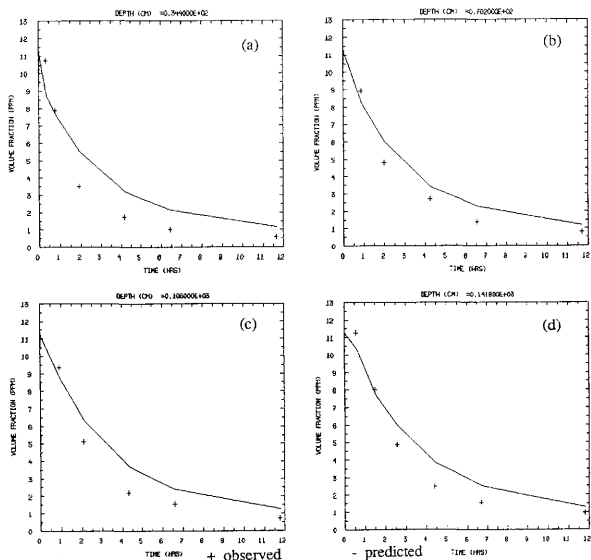


Fig. E29.- Experiment 19: Total Particle Volume Observed and Predicted for Depths (a) 34.4 cm; (b) 70.2 cm; (c) 106.0 cm; and (d) 141.8 cm with Shear of 20 sec⁻¹, Salinity of 15 ppt, Type A Sediment, and Suspended Solids of 40 mg/l.

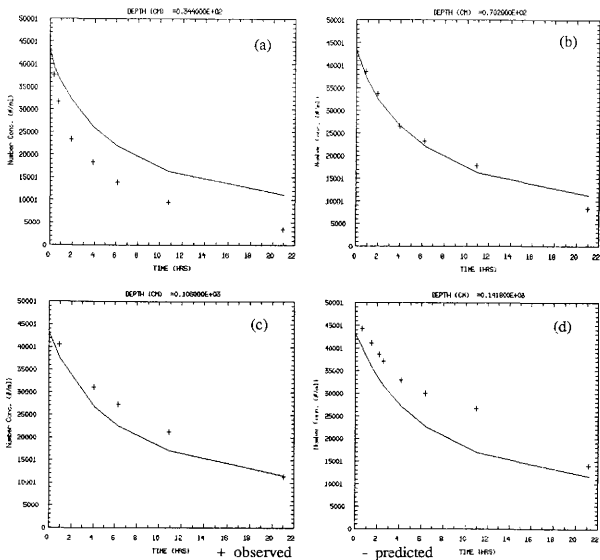


Fig. E30.- Experiment 20: Total Particle Number Observed and Predicted for Depths (a) 34.4 cm; (b) 70.2 cm; (c) 106.0 cm; and (d) 141.8 cm with Shear of 20 sec^{-1} , Salinity of 30 ppt, Type A Sediment, and Suspended Solids of 40 mg/L.

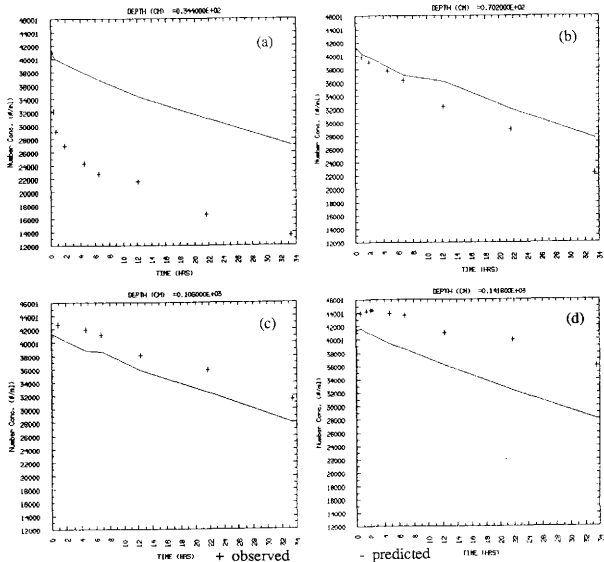


Fig. E31.- Experiment 21: Total Particle Number Observed and Predicted for Depths (a) 34.4 cm; (b) 70.2 cm; (c) 106.0 cm; and (d) 141.8 cm with Shear of 40 sec⁻¹, Salinity of 30 ppt, Type A Sediment, and Suspended Solids of 40 mg/l.

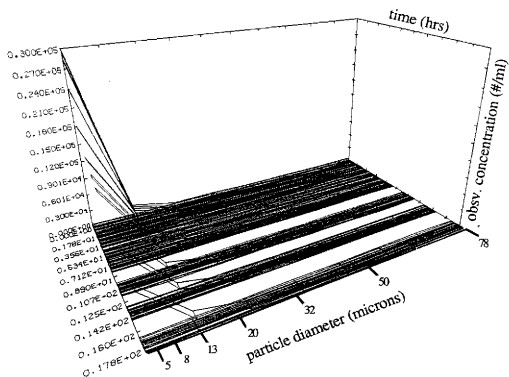


Fig. E32a.- Experiment 1: Heterogeneous Particle Number-Based Observed Size Distribution with Shear of 30 sec⁻¹, Salinity of 5 ppt, Type A Sediment, and Suspended Solids of 40 mg/l at a Depth of 34.4 cm.

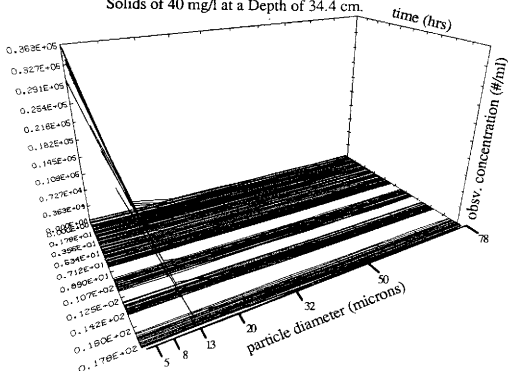


Fig. E32b.- Experiment 1: Heterogeneous Particle Number-Based Observed Size Distribution with Shear of 30 sec⁻¹, Salinity of 5 ppt, Type A Sediment, and Suspended Solids of 40 mg/l at a Depth of 141.8 cm.

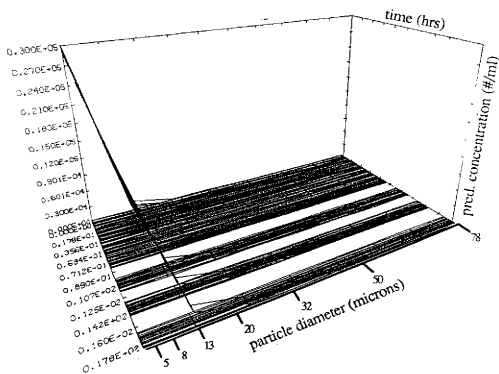


Fig. E33a.- Experiment 1: Heterogeneous Particle Number-Based Predicted Size Distribution with Shear of 30 sec⁻¹, Salinity of 5 ppt, Type A Sediment, and Suspended Solids of 40 mg/l at a Depth of 34.4 cm.

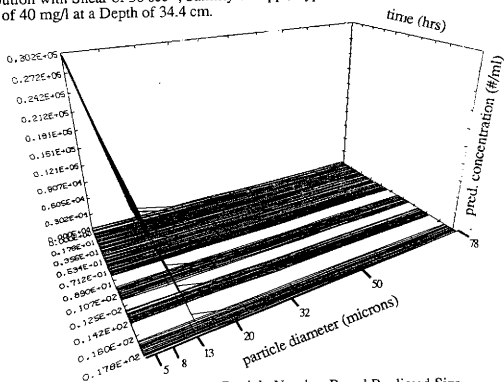


Fig. E33b.- Experiment 1: Heterogeneous Particle Number-Based Predicted Size Distribution with Shear of 30 sec⁻¹, Salinity of 5 ppt, Type A Sediment, and Suspended Solids of 40 mg/l at a Depth of 141.8 cm.

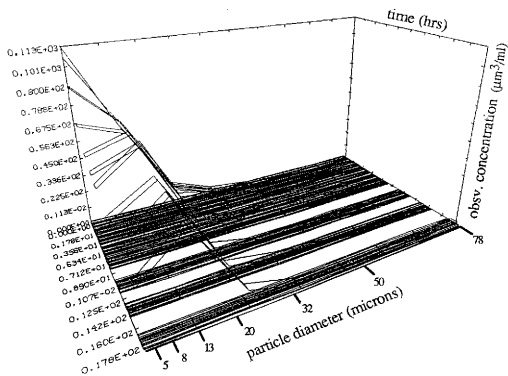


Fig. E34a.- Experiment 1: Heterogeneous Particle Volume-Based Observed Size Distribution with Shear of 30 sec⁻¹, Salinity of 5 ppt, Type A Sediment, and Suspended Solids of 40 mg/l at a Depth of 34.4 cm.

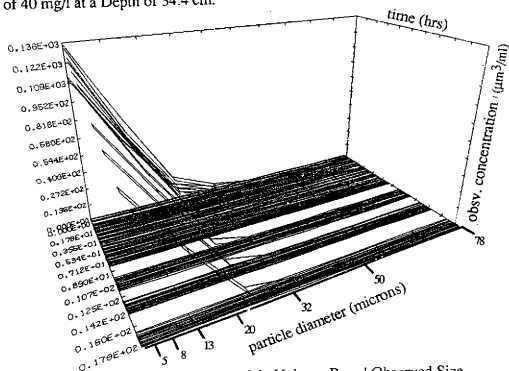


Fig. E34b.- Experiment 1: Heterogeneous Particle Volume-Based Observed Size Distribution with Shear of 30 sec⁻¹, Salinity of 5 ppt, Type A Sediment, and Suspended Solids of 40 mg/l at a Depth of 141.8 cm.

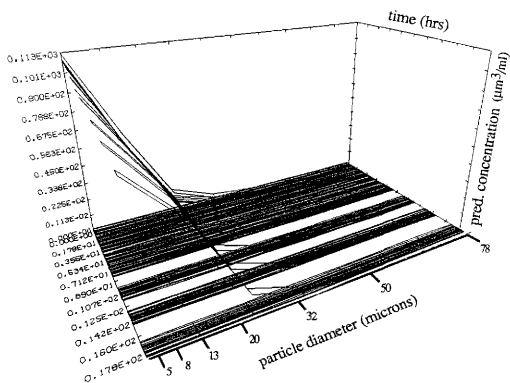


Fig. E35a.- Experiment 1: Heterogeneous Particle Volume-Based Predicted Size Distribution with Shear of 30 sec⁻¹, Salinity of 5 ppt, Type A Sediment, and Suspended Solids of 40 mg/l at a Depth of 34.4 cm.

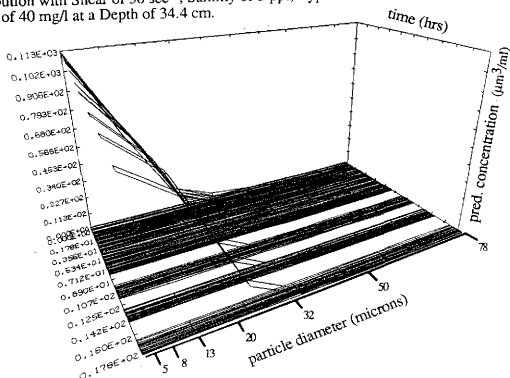


Fig. E35b.- Experiment 1: Heterogeneous Particle Volume-Based Predicted Size Distribution with Shear of 30 sec⁻¹, Salinity of 5 ppt, Type A Sediment, and Suspended Solids of 40 mg/l at a Depth of 141.8 cm.

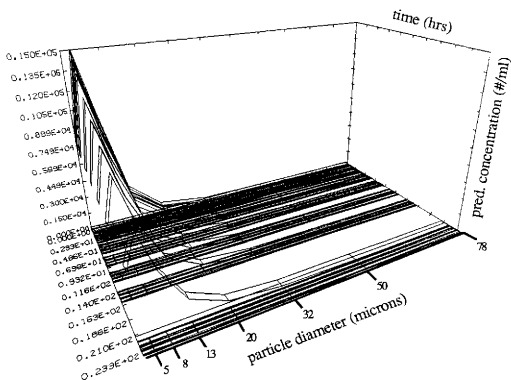


Fig. E36a.- Experiment 2: Heterogeneous Particle Number-Based Predicted Size Distribution with Shear of 30 sec^{-1} , Salinity of 15 ppt, Type A Sediment, and Suspended Solids of 40 mg/l at a Depth of 34.4 cm.

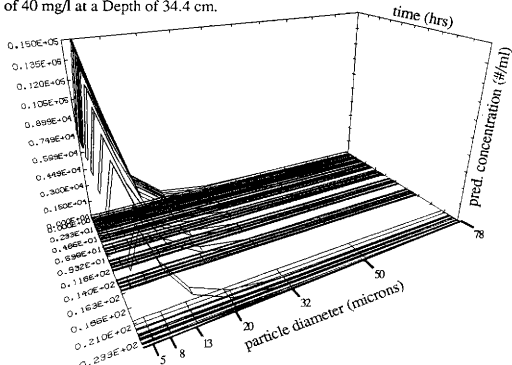


Fig. E36b.- Experiment 2: Heterogeneous Particle Number-Based Predicted Size Distribution with Shear of 30 sec^{-1} , Salinity of 15 ppt, Type A Sediment, and Suspended Solids of 40 mg/l at a Depth of 141.8 cm.

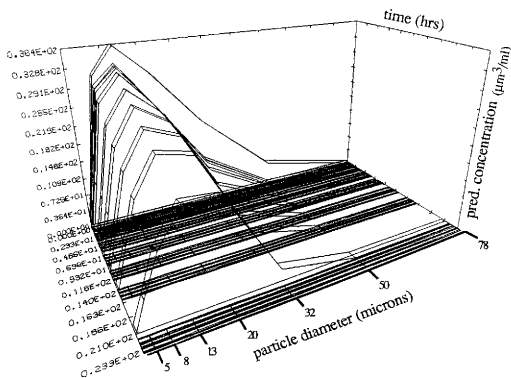


Fig. E37a.- Experiment 2: Heterogeneous Particle Volume-Based Predicted Size Distribution with Shear of 30 sec⁻¹, Salinity of 15 ppt, Type A Sediment, and Suspended Solids of 40 mg/l at a Depth of 34.4 cm.

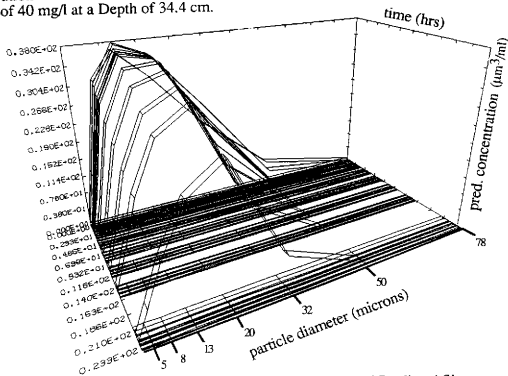


Fig. E37b.- Experiment 2: Heterogeneous Particle Volume-Based Predicted Size Distribution with Shear of 30 sec⁻¹, Salinity of 15 ppt, Type A Sediment, and Suspended Solids of 40 mg/l at a Depth of 141.8 cm.

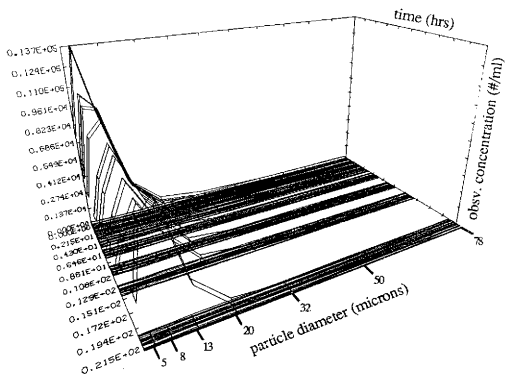


Fig. E38a.- Experiment 3: Heterogeneous Particle Number-Based Observed Size Distribution with Shear of 30 sec⁻¹, Salinity of 30 ppt, Type A Sediment, and Suspended Solids of 40 mg/l at a Depth of 34.4 cm.

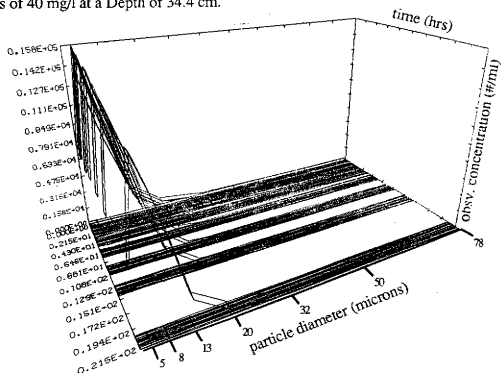


Fig. E38b.- Experiment 3: Heterogeneous Particle Number-Based Observed Size Distribution with Shear of 30 sec⁻¹, Salinity of 30 ppt, Type A Sediment, and Suspended Solids of 40 mg/l at a Depth of 141.8 cm.

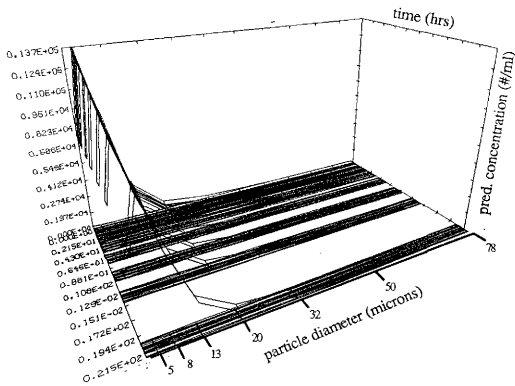


Fig. E39a.- Experiment 3: Heterogeneous Particle Number-Based Predicted Size Distribution with Shear of 30 sec⁻¹, Salinity of 30 ppt, Type A Sediment, and Suspended Solids of 40 mg/l at a Depth of 34.4 cm.

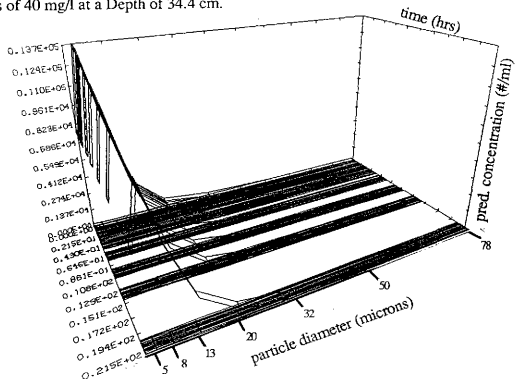


Fig. E39b.- Experiment 3: Heterogeneous Particle Number-Based Predicted Size Distribution with Shear of 30 sec⁻¹, Salinity of 30 ppt, Type A Sediment, and Suspended Solids of 40 mg/l at a Depth of 141.8 cm.

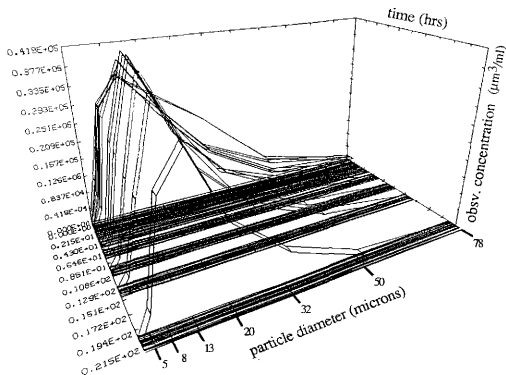


Fig. E40a.- Experiment 3: Heterogeneous Particle Volume-Based Observed Size Distribution with Shear of 30 sec-1, Salinity of 30 ppt, Type A Sediment, and Suspended Solids of 40 mg/l at a Depth of 34.4 cm.

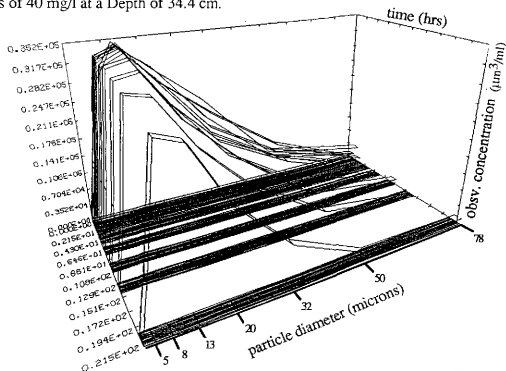


Fig. E40b.- Experiment 3: Heterogeneous Particle Volume-Based Observed Size Distribution with Shear of 30 sec-1, Salinity of 30 ppt, Type A Sediment, and Suspended Solids of 40 mg/l at a Depth of 141.8 cm.

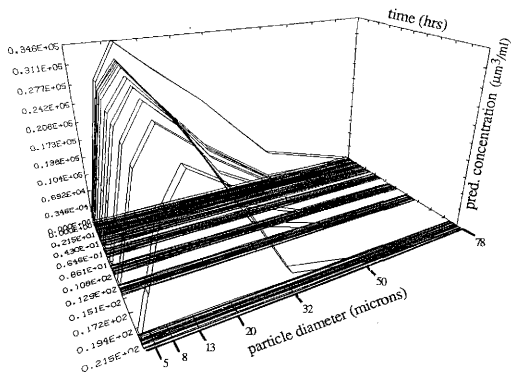


Fig. E41a.- Experiment 3: Heterogeneous Particle Volume-Based Predicted Size Distribution with Shear of 30 sec^{-1} , Salinity of 30 ppt, Type A Sediment, and Suspended Solids of 40 mg/l at a Depth of 34.4 cm.

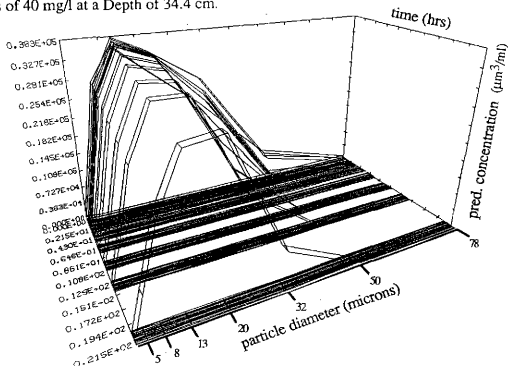


Fig. E41b.- Experiment 3: Heterogeneous Particle Volume-Based Predicted Size Distribution with Shear of 30 sec^{-1} , Salinity of 30 ppt, Type A Sediment, and Suspended Solids of 40 mg/l at a Depth of 141.8 cm.

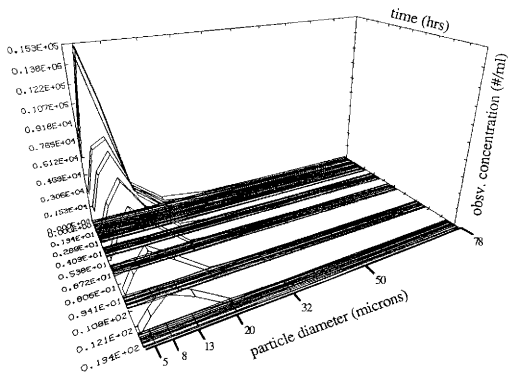


Fig. E42a.- Experiment 5: Heterogeneous Particle Number-Based Observed Size Distribution with Shear of 30 sec⁻¹, Salinity of 15 ppt, Type A Sediment, and Suspended Solids of 40 mg/l at a Depth of 34.4 cm.

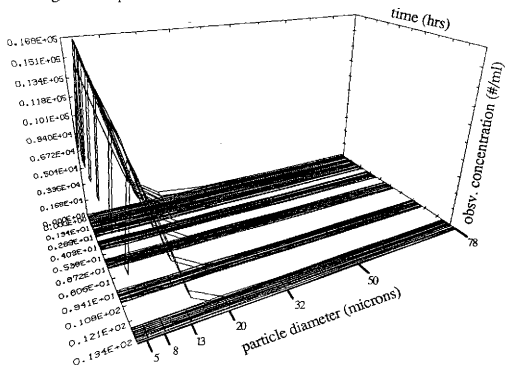


Fig. E42b.- Experiment 5: Heterogeneous Particle Number-Based Observed Size Distribution with Shear of 30 sec⁻¹, Salinity of 15 ppt, Type A Sediment, and Suspended Solids of 40 mg/l at a Depth of 141.8 cm.

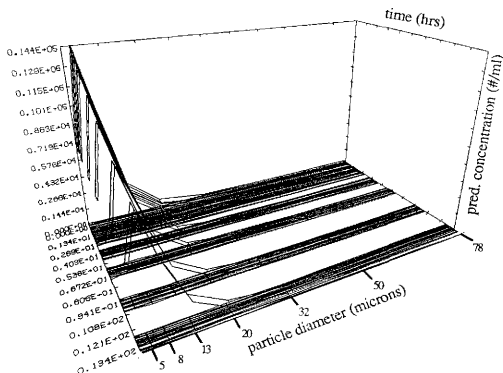


Fig. E43a.- Experiment 5: Heterogeneous Particle Number-Based Predicted Size Distribution with Shear of 30 sec⁻¹, Salinity of 15 ppt, Type A Sediment, and Suspended Solids of 40 mg/l at a Depth of 34.4 cm.

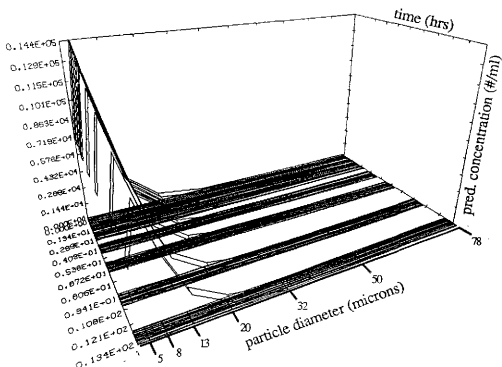


Fig. E43b.- Experiment 5: Heterogeneous Particle Number-Based Predicted Size Distribution with Shear of 30 sec⁻¹, Salinity of 15 ppt, Type A Sediment, and Suspended Solids of 40 mg/l at a Depth of 141.8 cm.

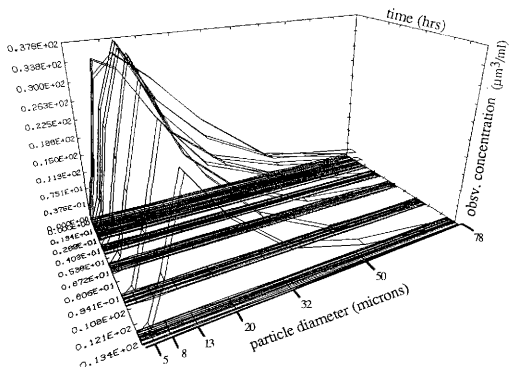


Fig. E44a.- Experiment 5: Heterogeneous Particle Volume-Based Observed Size Distribution with Shear of 30 sec⁻¹, Salinity of 15 ppt, Type A Sediment, and Suspended Solids of 40 mg/l at a Depth of 34.4 cm.

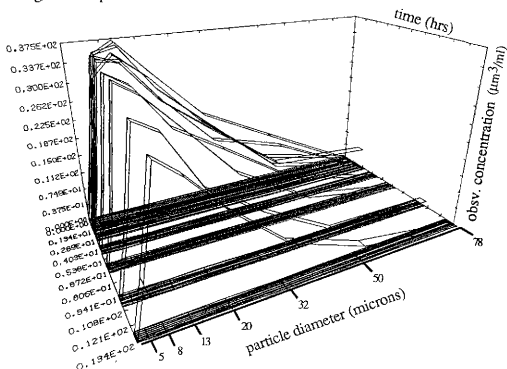


Fig. E44b.- Experiment 5: Heterogeneous Particle Volume-Based Observed Size Distribution with Shear of 30 sec⁻¹, Salinity of 15 ppt, Type A Sediment, and Suspended Solids of 40 mg/l at a Depth of 141.8 cm.

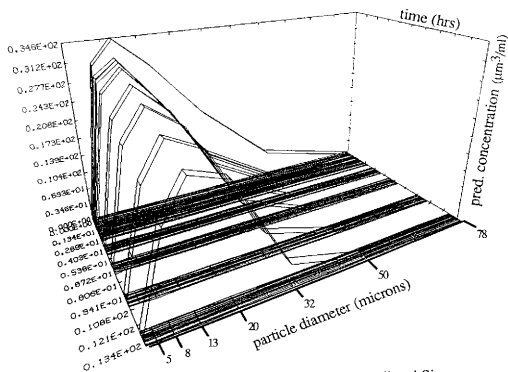


Fig. E45a.- Experiment 5: Heterogeneous Particle Volume-Based Predicted Size Distribution with Shear of 30 sec^{-1} , Salinity of 15 ppt, Type A Sediment, and Suspended Solids of 40 mg/l at a Depth of 34.4 cm.

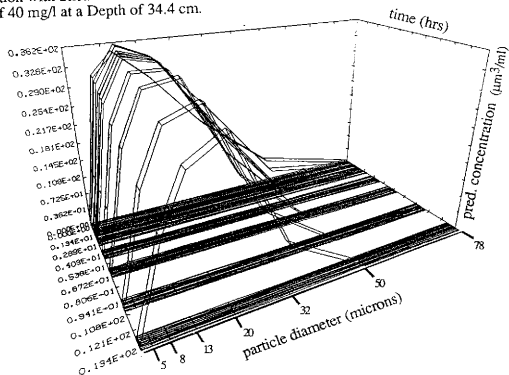


Fig. E45b.- Experiment 5: Heterogeneous Particle Volume-Based Predicted Size Distribution with Shear of 30 sec^{-1} , Salinity of 15 ppt, Type A Sediment, and Suspended Solids of 40 mg/l at a Depth of 141.8 cm.

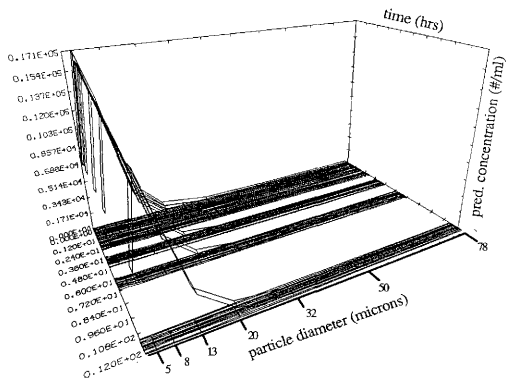


Fig. E46a.- Experiment 6: Heterogeneous Particle Number-Based Predicted Size Distribution with Shear of 40 sec⁻¹, Salinity of 15 ppt, Type A Sediment, and Suspended Solids of 40 mg/l at a Depth of 34.4 cm.

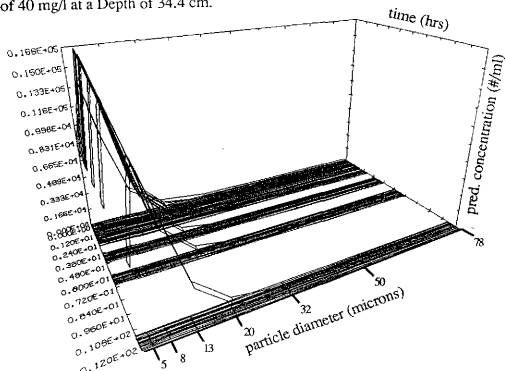


Fig. E46b.- Experiment 6: Heterogeneous Particle Number-Based Predicted Size Distribution with Shear of 40 sec⁻¹, Salinity of 15 ppt, Type A Sediment, and Suspended Solids of 40 mg/l at a Depth of 141.8 cm.

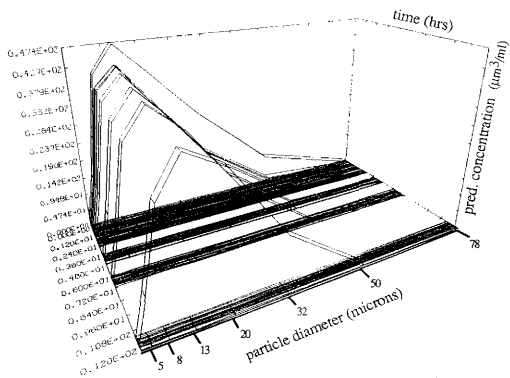


Fig. E47a.- Experiment 6: Heterogeneous Particle Volume-Based Predicted Size Distribution with Shear of 40 sec^{-1} , Salinity of 15 ppt, Type A Sediment, and Suspended Solids of 40 mg/l at a Depth of 34.4 cm.

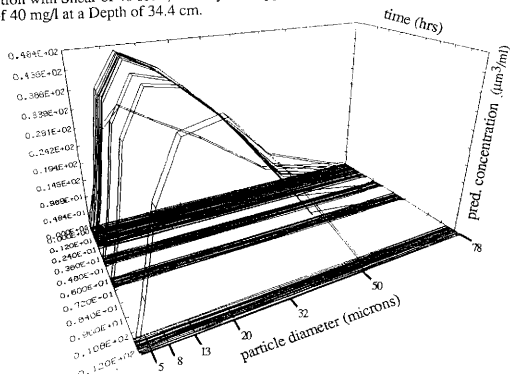


Fig. E47b.- Experiment 6: Heterogeneous Particle Volume-Based Predicted Size Distribution with Shear of 40 sec^{-1} , Salinity of 15 ppt, Type A Sediment, and Suspended Solids of 40 mg/l at a Depth of 141.8 cm.

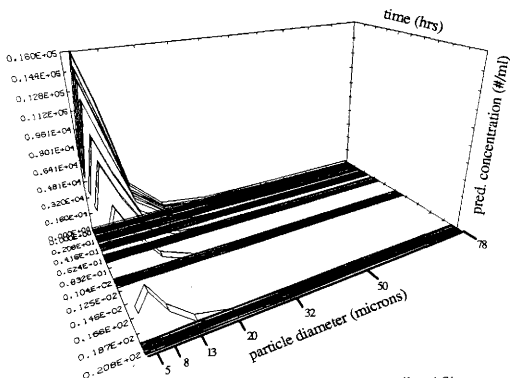


Fig. E48a.- Experiment 8: Heterogeneous Particle Number-Based Predicted Size Distribution with Shear of 20 sec⁻¹, Salinity of 15 ppt, Type A Sediment, and Suspended Solids of 40 mg/l at a Depth of 34.4 cm.

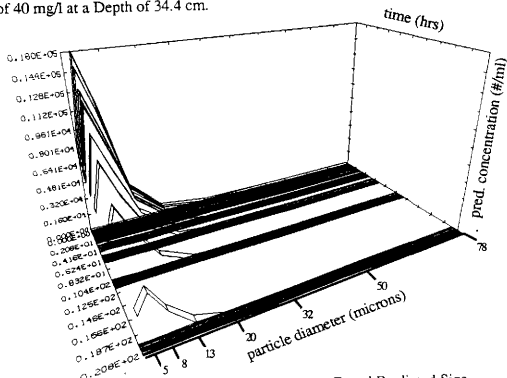


Fig. E48b.- Experiment 8: Heterogeneous Particle Number-Based Predicted Size Distribution with Shear of 20 sec⁻¹, Salinity of 15 ppt, Type A Sediment, and Suspended Solids of 40 mg/l at a Depth of 141.8 cm.

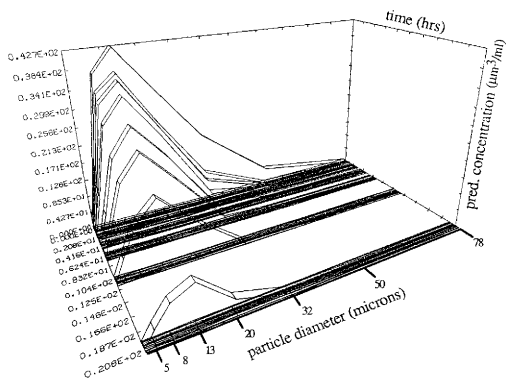


Fig. E49a.- Experiment 8: Heterogeneous Particle Volume-Based Predicted Size Distribution with Shear of 20 sec⁻¹, Salinity of 15 ppt, Type A Sediment, and Suspended Solids of 40 mg/l at a Depth of 34.4 cm.

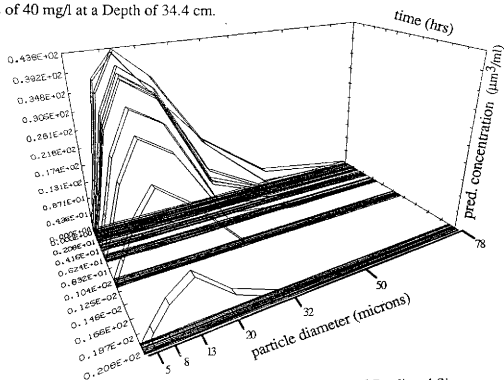


Fig. E49b.- Experiment 8: Heterogeneous Particle Volume-Based Predicted Size Distribution with Shear of 20 sec⁻¹, Salinity of 15 ppt, Type A Sediment, and Suspended Solids of 40 mg/l at a Depth of 141.8 cm.

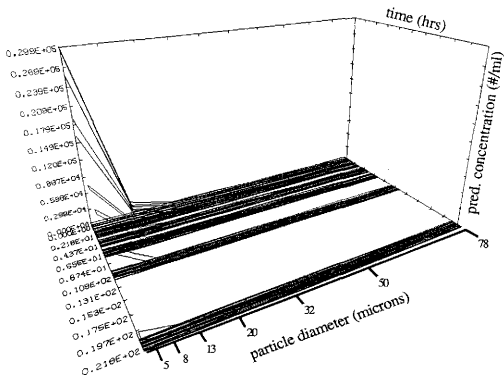


Fig. E50a.- Experiment 9: Heterogeneous Particle Number-Based Predicted Size Distribution with Shear of 20 sec⁻¹, Salinity of 15 ppt, Type A Sediment, and Suspended Solids of 80 mg/l at a Depth of 34.4 cm.

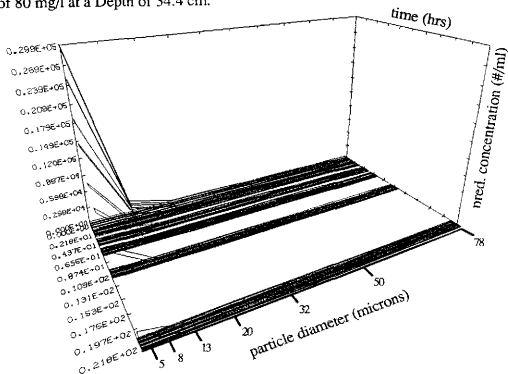


Fig. E50b.- Experiment 9: Heterogeneous Particle Number-Based Predicted Size Distribution with Shear of 20 sec⁻¹, Salinity of 15 ppt, Type A Sediment, and Suspended Solids of 80 mg/l at a Depth of 141.8 cm.

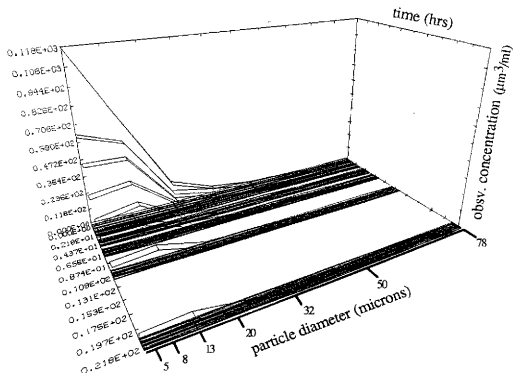


Fig. E51a.- Experiment 9: Heterogeneous Particle Volume-Based Observed Size Distribution with Shear of 20 sec^{-1} , Salinity of 15 ppt, Type A Sediment, and Suspended Solids of 80 mg/l at a Depth of 34.4 cm.

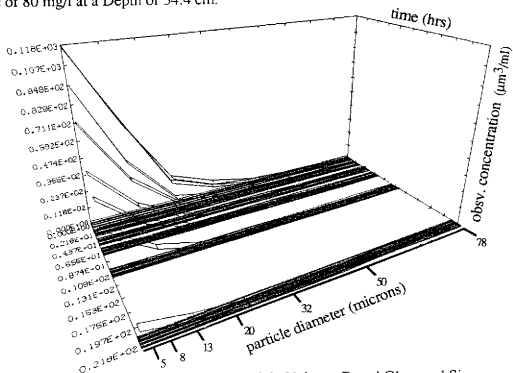


Fig. E51b.- Experiment 9: Heterogeneous Particle Volume-Based Observed Size Distribution with Shear of 20 sec^{-1} , Salinity of 15 ppt, Type A Sediment, and Suspended Solids of 80 mg/l at a Depth of 141.8 cm.

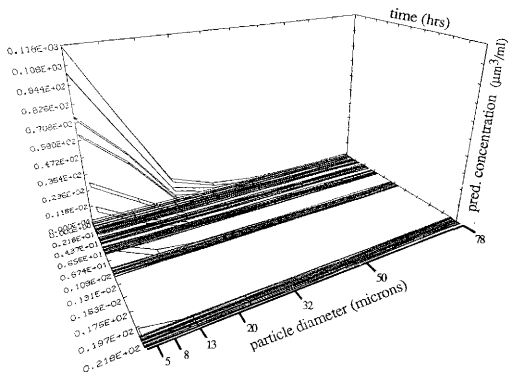


Fig. E52a.- Experiment 9: Heterogeneous Particle Volume-Based Predicted Size Distribution with Shear of 20 sec⁻¹, Salinity of 15 ppt, Type A Sediment, and Suspended Solids of 80 mg/l at a Depth of 34.4 cm.

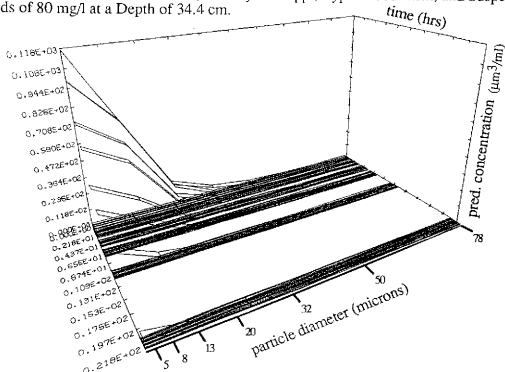


Fig. E52b.- Experiment 9: Heterogeneous Particle Volume-Based Predicted Size Distribution with Shear of 20 sec⁻¹, Salinity of 15 ppt, Type A Sediment, and Suspended Solids of 80 mg/l at a Depth of 141.8 cm.

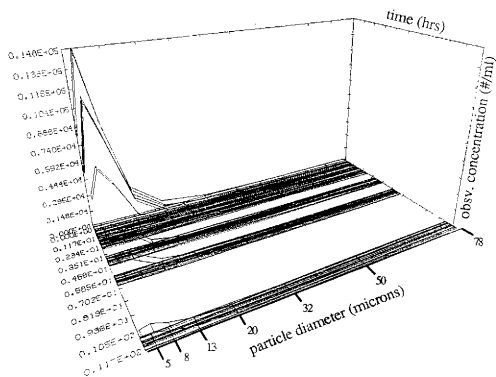


Fig. E53a.- Experiment 10: Heterogeneous Particle Number-Based Observed Size Distribution with Shear of 20 sec⁻¹, Salinity of 5 ppt, Type B Sediment, and Suspended Solids of 40 mg/l at a Depth of 34.4 cm.

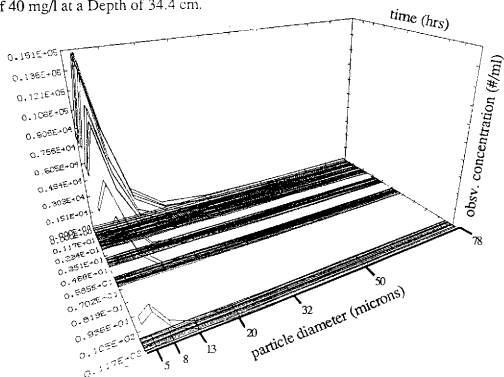


Fig. E53b.- Experiment 10: Heterogeneous Particle Number-Based Observed Size Distribution with Shear of 20 sec⁻¹, Salinity of 5 ppt, Type B Sediment, and Suspended Solids of 40 mg/l at a Depth of 141.8 cm.

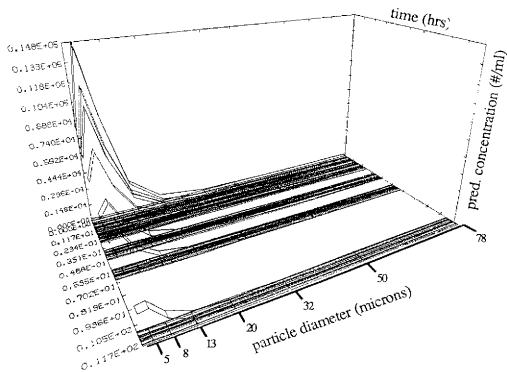


Fig. E54a.- Experiment 10: Heterogeneous Particle Number-Based Predicted Size Distribution with Shear of 20 sec⁻¹, Salinity of 5 ppt, Type B Sediment, and Suspended Solids of 40 mg/l at a Depth of 34.4 cm.

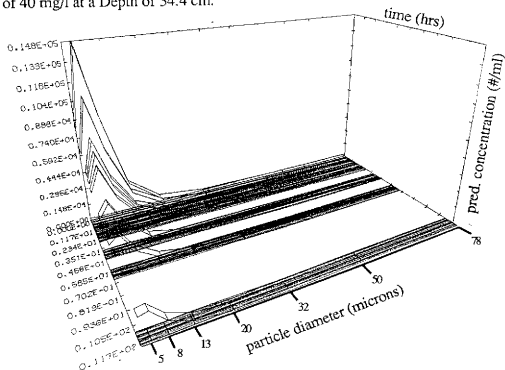


Fig. E54b.- Experiment 10: Heterogeneous Particle Number-Based Predicted Size Distribution with Shear of 20 sec⁻¹, Salinity of 5 ppt, Type B Sediment, and Suspended Solids of 40 mg/l at a Depth of 141.8 cm.

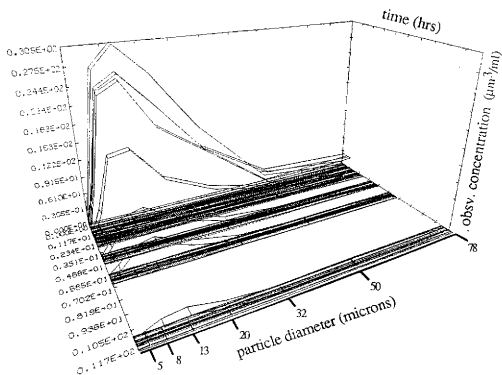


Fig. E55a.- Experiment 10: Heterogeneous Particle Volume-Based Observed Size Distribution with Shear of 20 sec^{-1} , Salinity of 5 ppt, Type B Sediment, and Suspended Solids of 40 mg/l at a Depth of 34.4 cm.

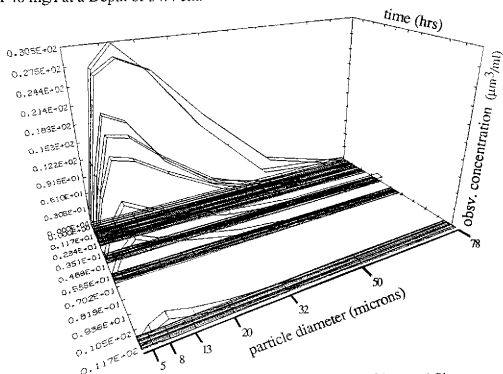


Fig. E55b.- Experiment 10: Heterogeneous Particle Volume-Based Observed Size Distribution with Shear of 20 sec^{-1} , Salinity of 5 ppt, Type B Sediment, and Suspended Solids of 40 mg/l at a Depth of 141.8 cm.

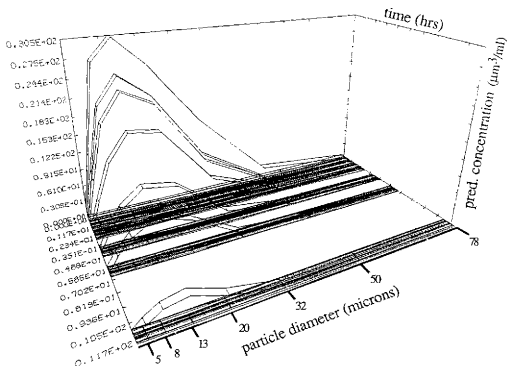


Fig. E56a.- Experiment 10: Heterogeneous Particle Volume-Based Predicted Size Distribution with Shear of 20 sec⁻¹, Salinity of 5 ppt, Type B Sediment, and Suspended Solids of 40 mg/l at a Depth of 34.4 cm.

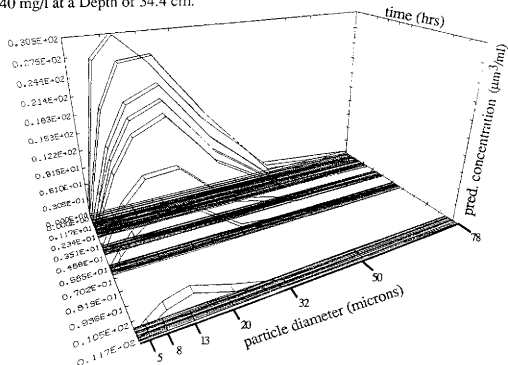


Fig. E56b.- Experiment 10: Heterogeneous Particle Volume-Based Predicted Size Distribution with Shear of 20 sec⁻¹, Salinity of 5 ppt, Type B Sediment, and Suspended Solids of 40 mg/l at a Depth of 141.8 cm.

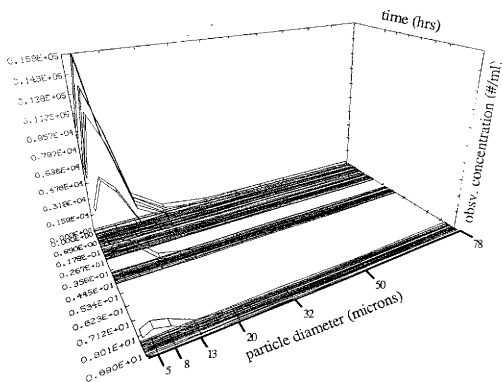


Fig. E57a.- Experiment 11: Heterogeneous Particle Number-Based Observed Size Distribution with Shear of 20 sec^{-1} , Salinity of 15 ppt, Type B Sediment, and Suspended Solids of 40 mg/l at a Depth of 34.4 cm.

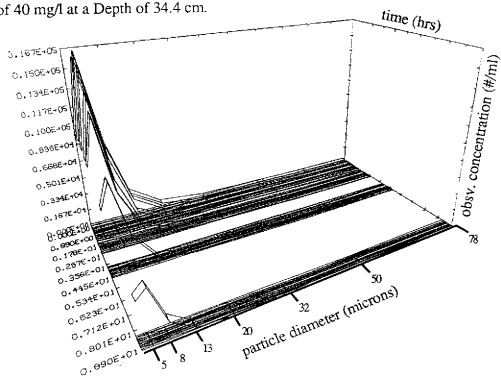


Fig. E57b.- Experiment 11: Heterogeneous Particle Number-Based Observed Size Distribution with Shear of 20 sec^{-1} , Salinity of 15 ppt, Type B Sediment, and Suspended Solids of 40 mg/l at a Depth of 141.8 cm.

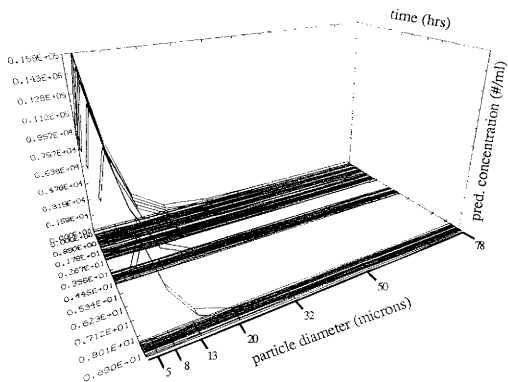


Fig. E58a.- Experiment 11: Heterogeneous Particle Number-Based Predicted Size Distribution with Shear of 20 sec⁻¹, Salinity of 15 ppt, Type B Sediment, and Suspended Solids of 40 mg/l at a Depth of 34.4 cm.

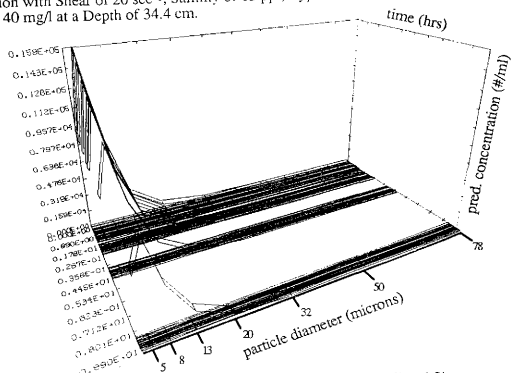


Fig. E58b.- Experiment 11: Heterogeneous Particle Number-Based Predicted Size Distribution with Shear of 20 sec⁻¹, Salinity of 15 ppt, Type B Sediment, and Suspended Solids of 40 mg/l at a Depth of 141.8 cm.

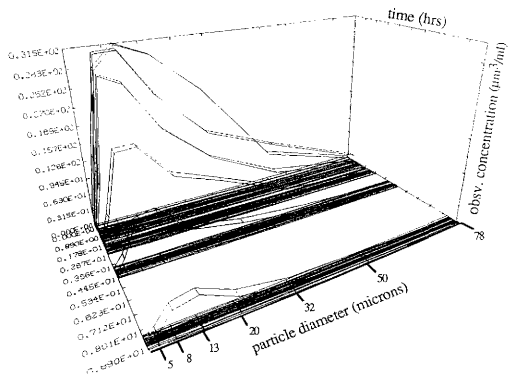


Fig. E59a.- Experiment 11: Heterogeneous Particle Volume-Based Observed Size Distribution with Shear of 20 sec⁻¹, Salinity of 15 ppt, Type B Sediment, and Suspended Solids of 40 mg/l at a Depth of 34.4 cm.

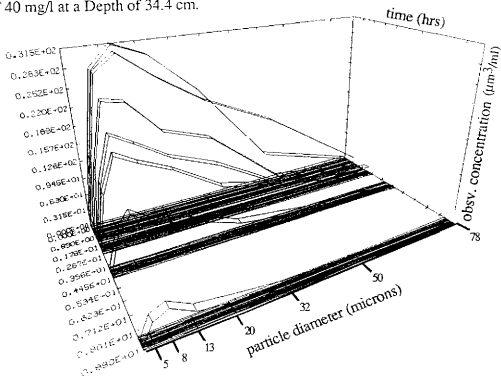


Fig. E59b.- Experiment 11: Heterogeneous Particle Volume-Based Observed Size Distribution with Shear of 20 sec⁻¹, Salinity of 15 ppt, Type B Sediment, and Suspended Solids of 40 mg/l at a Depth of 141.8 cm.

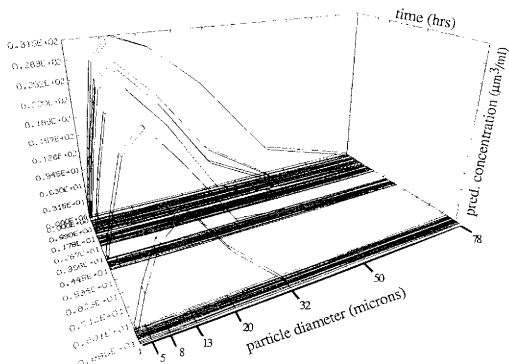


Fig. E60a.- Experiment 11: Heterogeneous Particle Volume-Based Predicted Size Distribution with Shear of 20 sec⁻¹, Salinity of 15 ppt, Type B Sediment, and Suspended Solids of 40 mg/l at a Depth of 34.4 cm.

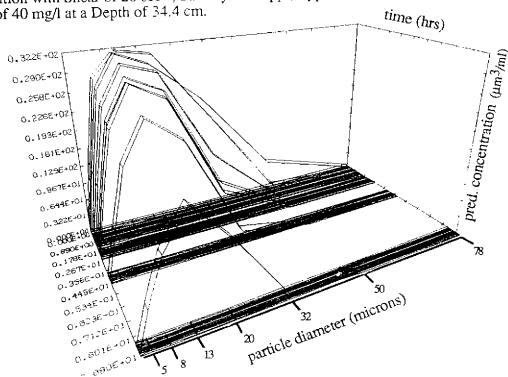


Fig. E60b.- Experiment 11: Heterogeneous Particle Volume-Based Predicted Size Distribution with Shear of 20 sec⁻¹, Salinity of 15 ppt, Type B Sediment, and Suspended Solids of 40 mg/l at a Depth of 141.8 cm.

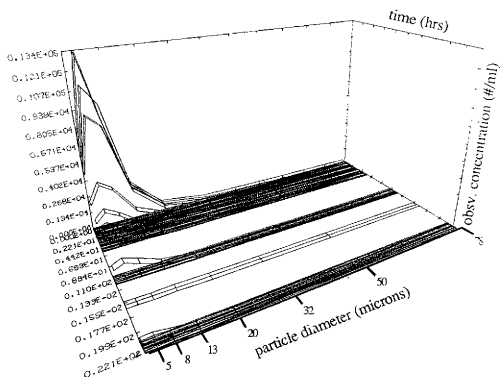


Fig. E61a.- Experiment 13: Heterogeneous Particle Number-Based Observed Size Distribution with Shear of 20 sec⁻¹, Salinity of 5 ppt, Type C Sediment, and Suspended Solids of 40 mg/l at a Depth of 34.4 cm.

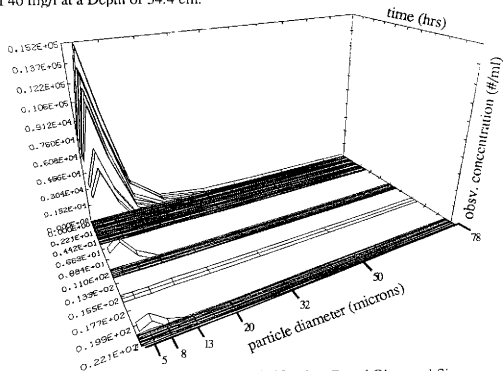


Fig. E61b.- Experiment 13: Heterogeneous Particle Number-Based Observed Size Distribution with Shear of 20 sec⁻¹, Salinity of 5 ppt, Type C Sediment, and Suspended Solids of 40 mg/l at a Depth of 141.8 cm.

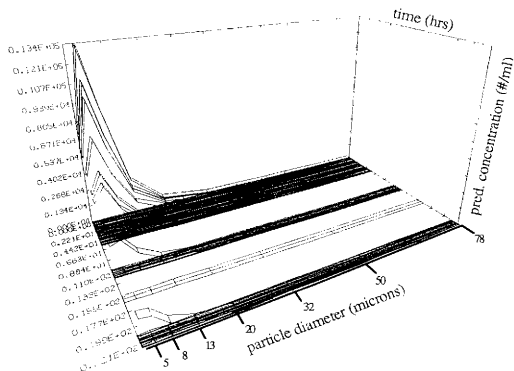


Fig. E62a.- Experiment 13: Heterogeneous Particle Number-Based Predicted Size Distribution with Shear of 20 sec⁻¹, Salinity of 5 ppt, Type C Sediment, and Suspended Solids of 40 mg/l at a Depth of 34.4 cm.

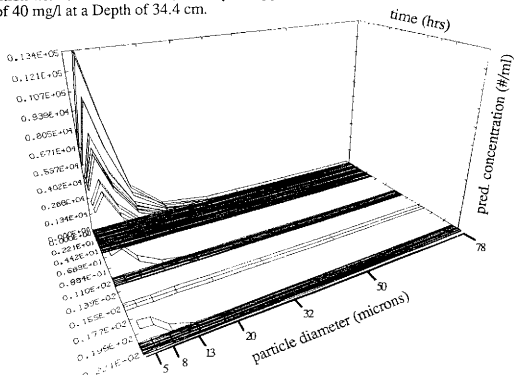


Fig. E62b.- Experiment 13: Heterogeneous Particle Number-Based Predicted Size Distribution with Shear of 20 sec⁻¹, Salinity of 5 ppt, Type C Sediment, and Suspended Solids of 40 mg/l at a Depth of 141.8 cm.

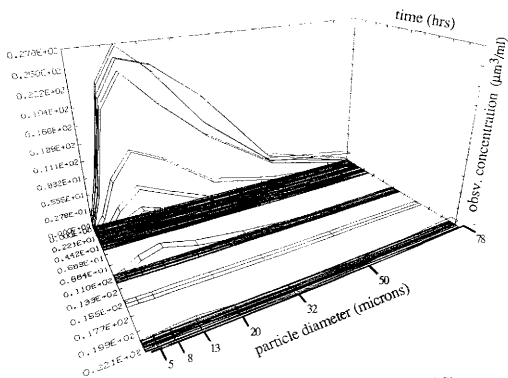


Fig. E63a.- Experiment 13: Heterogeneous Particle Volume-Based Observed Size Distribution with Shear of 20 sec⁻¹, Salinity of 5 ppt, Type C Sediment, and Suspended Solids of 40 mg/l at a Depth of 34.4 cm.

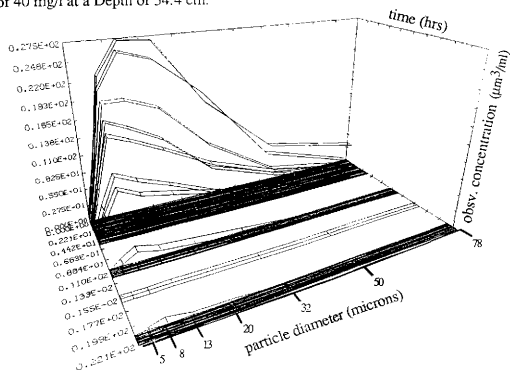


Fig. E63b.- Experiment 13: Heterogeneous Particle Volume-Based Observed Size Distribution with Shear of 20 sec⁻¹, Salinity of 5 ppt, Type C Sediment, and Suspended Solids of 40 mg/l at a Depth of 141.8 cm.

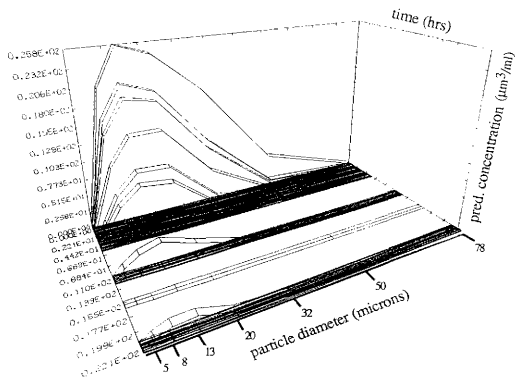


Fig. E64a.- Experiment 13: Heterogeneous Particle Volume-Based Predicted Size Distribution with Shear of 20 sec⁻¹, Salinity of 5 ppt, Type C Sediment, and Suspended Solids of 40 mg/l at a Depth of 34.4 cm.

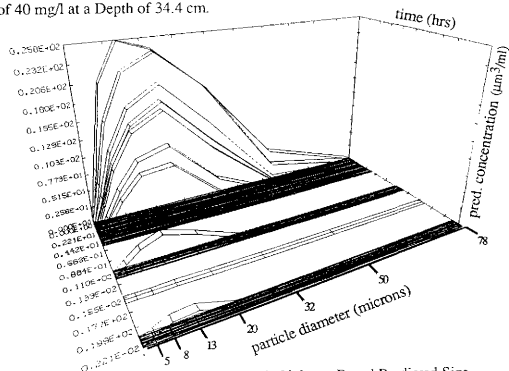


Fig. E64b.- Experiment 13: Heterogeneous Particle Volume-Based Predicted Size Distribution with Shear of 20 sec⁻¹, Salinity of 5 ppt, Type C Sediment, and Suspended Solids of 40 mg/l at a Depth of 141.8 cm.

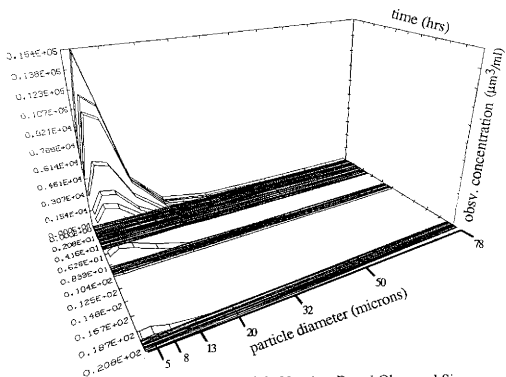


Fig. E65a.- Experiment 14: Heterogeneous Particle Number-Based Observed Size Distribution with Shear of 20 sec⁻¹, Salinity of 15 ppt, Type C Sediment, and Suspended Solids of 40 mg/l at a Depth of 34.4 cm.

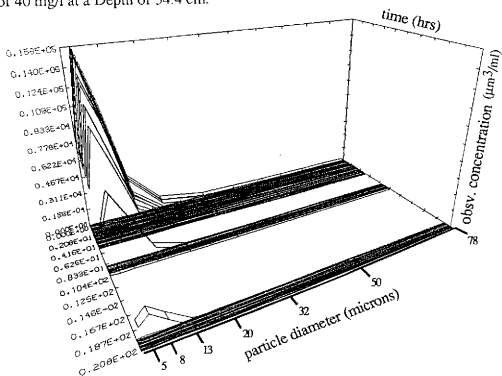


Fig. E65b.- Experiment 14: Heterogeneous Particle Number-Based Observed Size Distribution with Shear of 20 sec⁻¹, Salinity of 15 ppt, Type C Sediment, and Suspended Solids of 40 mg/l at a Depth of 141.8 cm.

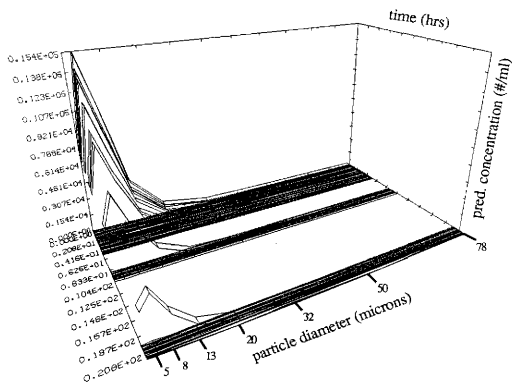


Fig. E66a.- Experiment 14: Heterogeneous Particle Number-Based Predicted Size Distribution with Shear of 20 sec^{-1} , Salinity of 15 ppt, Type C Sediment, and Suspended Solids of 40 mg/l at a Depth of 34.4 cm.

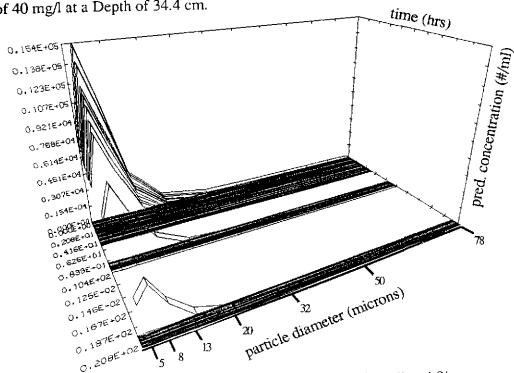


Fig. E66b.- Experiment 14: Heterogeneous Particle Number-Based Predicted Size Distribution with Shear of 20 sec^{-1} , Salinity of 15 ppt, Type C Sediment, and Suspended Solids of 40 mg/l at a Depth of 141.8 cm.

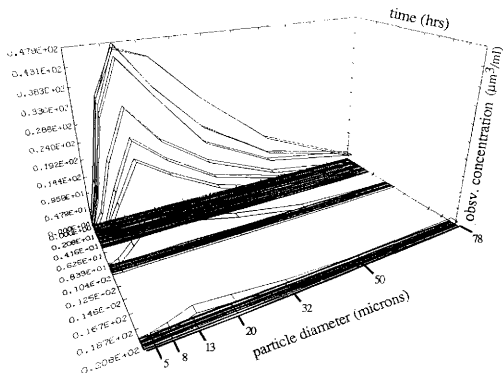


Fig. E67a.- Experiment 14: Heterogeneous Particle Volume-Based Observed Size Distribution with Shear of 20 sec^{-1} , Salinity of 15 ppt, Type C Sediment, and Suspended Solids of 40 mg/l at a Depth of 34.4 cm .

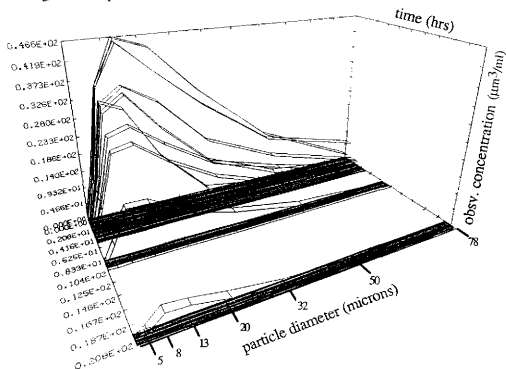


Fig. E67b.- Experiment 14: Heterogeneous Particle Volume-Based Observed Size Distribution with Shear of 20 sec^{-1} , Salinity of 15 ppt, Type C Sediment, and Suspended Solids of 40 mg/l at a Depth of 141.8 cm .

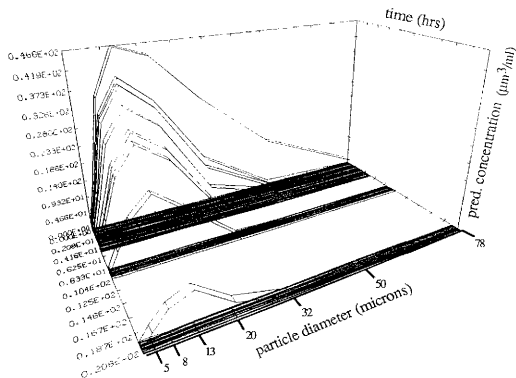


Fig. E68a.- Experiment 14: Heterogeneous Particle Volume-Based Predicted Size Distribution with Shear of 20 sec⁻¹, Salinity of 15 ppt, Type C Sediment, and Suspended Solids of 40 mg/l at a Depth of 34.4 cm.

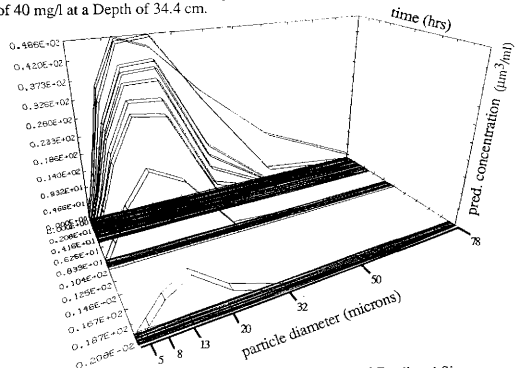


Fig. E68b.- Experiment 14: Heterogeneous Particle Volume-Based Predicted Size Distribution with Shear of 20 sec⁻¹, Salinity of 15 ppt, Type C Sediment, and Suspended Solids of 40 mg/l at a Depth of 141.8 cm.

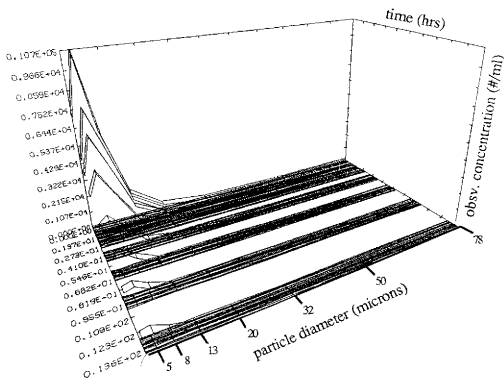


Fig. E69a.- Experiment 15: Heterogeneous Particle Number-Based Observed Size Distribution with Shear of 20 sec⁻¹, Salinity of 30 ppt, Type C Sediment, and Suspended Solids of 40 mg/l at a Depth of 34.4 cm.

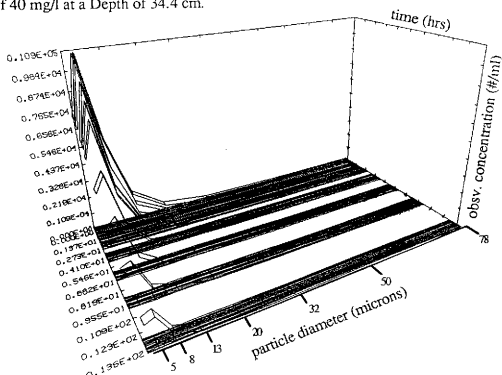


Fig. E69b.- Experiment 15: Heterogeneous Particle Number-Based Observed Size Distribution with Shear of 20 sec⁻¹, Salinity of 30 ppt, Type C Sediment, and Suspended Solids of 40 mg/l at a Depth of 141.8 cm.

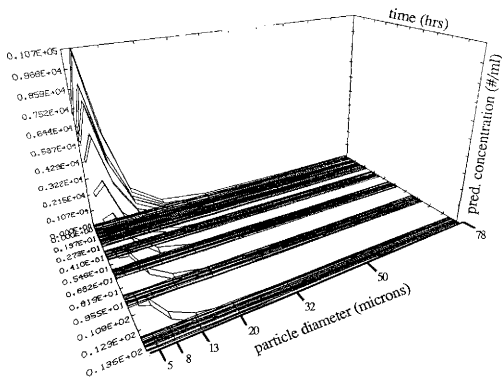


Fig. E70a.- Experiment 15: Heterogeneous Particle Number-Based Predicted Size Distribution with Shear of 20 sec⁻¹, Salinity of 30 ppt, Type C Sediment, and Suspended Solids of 40 mg/l at a Depth of 34.4 cm.

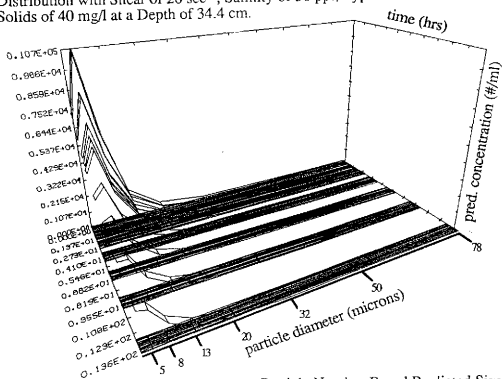


Fig. E70b.- Experiment 15: Heterogeneous Particle Number-Based Predicted Size Distribution with Shear of 20 sec⁻¹, Salinity of 30 ppt, Type C Sediment, and Suspended Solids of 40 mg/l at a Depth of 141.8 cm.

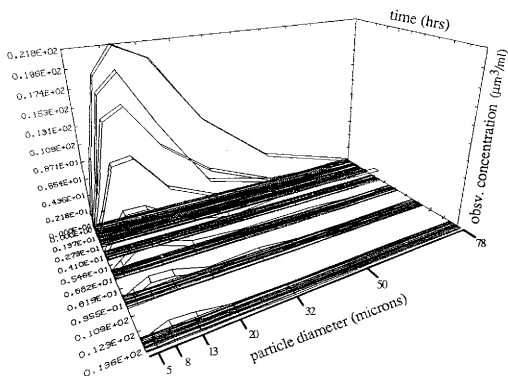


Fig. E71a.- Experiment 15: Heterogeneous Particle Volume-Based Observed Size Distribution with Shear of 20 sec⁻¹, Salinity of 30 ppt, Type C Sediment, and Suspended Solids of 40 mg/l at a Depth of 34.4 cm.

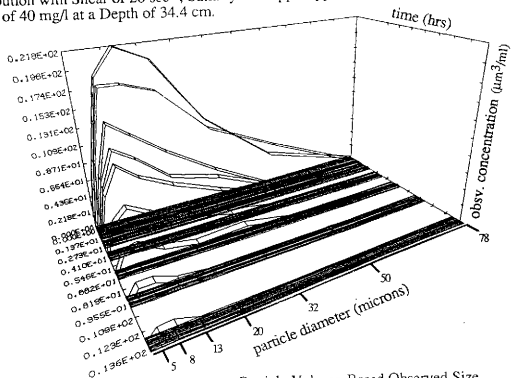


Fig. E71b.- Experiment 15: Heterogeneous Particle Volume-Based Observed Size Distribution with Shear of 20 sec⁻¹, Salinity of 30 ppt, Type C Sediment, and Suspended Solids of 40 mg/l at a Depth of 141.8 cm.

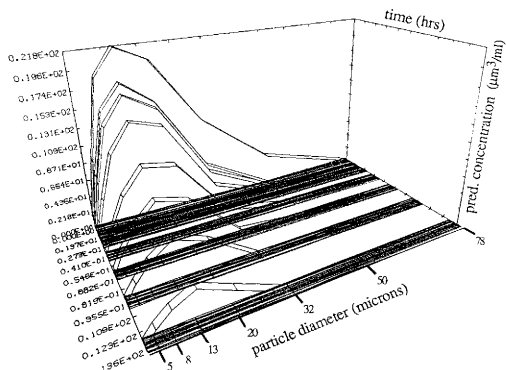


Fig. E72a.- Experiment 15: Heterogeneous Particle Volume-Based Predicted Size Distribution with Shear of 20 sec⁻¹, Salinity of 30 ppt, Type C Sediment, and Suspended Solids of 40 mg/l at a Depth of 34.4 cm.

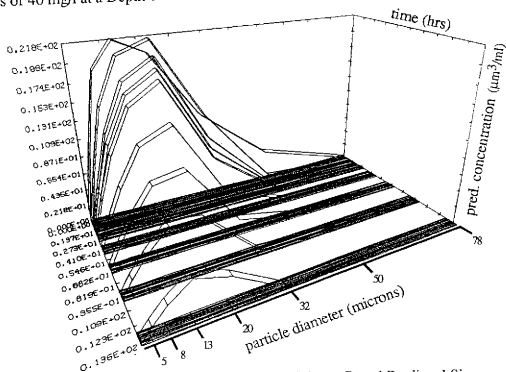


Fig. E72b.- Experiment 15: Heterogeneous Particle Volume-Based Predicted Size Distribution with Shear of 20 sec⁻¹, Salinity of 30 ppt, Type C Sediment, and Suspended Solids of 40 mg/l at a Depth of 141.8 cm.

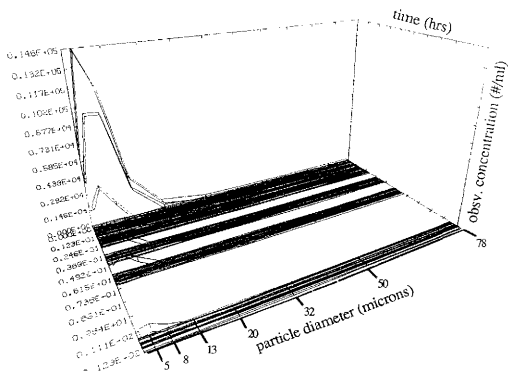


Fig. E73a.- Experiment 16: Heterogeneous Particle Number-Based Observed Size Distribution with Shear of 10 sec^{-1} , Salinity of 15 ppt, Type A Sediment, and Suspended Solids of 40 mg/l at a Depth of 34.4 cm.

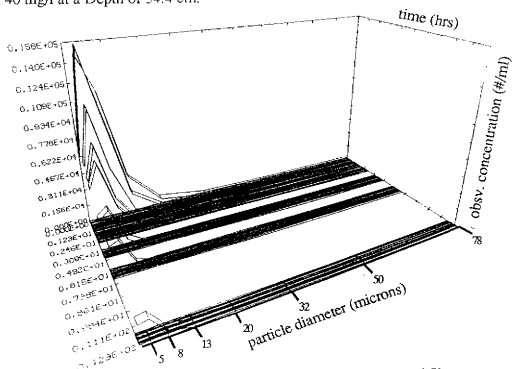


Fig. E73b.- Experiment 16: Heterogeneous Particle Number-Based Observed Size Distribution with Shear of 10 sec^{-1} , Salinity of 15 ppt, Type A Sediment, and Suspended Solids of 40 mg/l at a Depth of 141.8 cm.

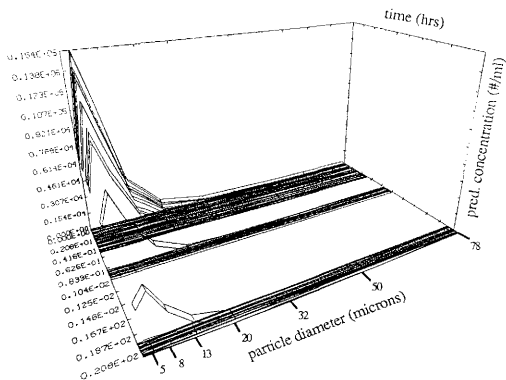


Fig. E74a.- Experiment 16: Heterogeneous Particle Number-Based Predicted Size Distribution with Shear of 10 sec^{-1} , Salinity of 15 ppt, Type A Sediment, and Suspended Solids of 40 mg/l at a Depth of 34.4 cm.

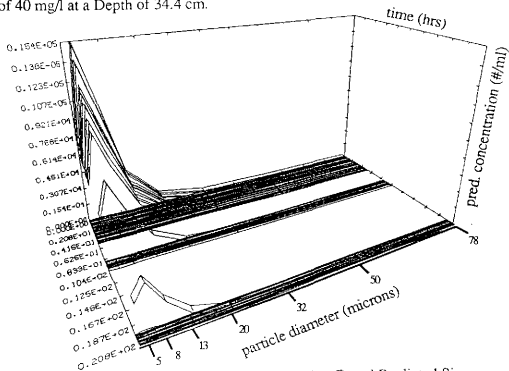


Fig. E74b.- Experiment 16: Heterogeneous Particle Number-Based Predicted Size Distribution with Shear of 10 sec^{-1} , Salinity of 15 ppt, Type A Sediment, and Suspended Solids of 40 mg/l at a Depth of 141.8 cm.

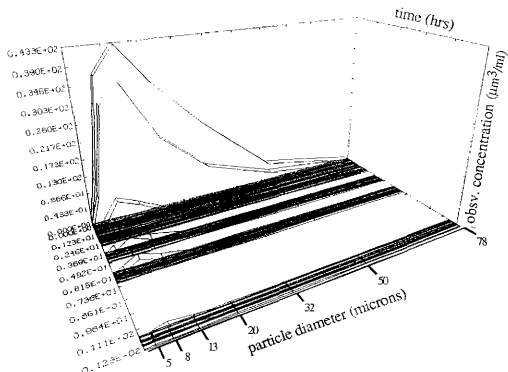


Fig. E75a.- Experiment 16: Heterogeneous Particle Volume-Based Observed Size Distribution with Shear of 10 sec^{-1} , Salinity of 15 ppt, Type A Sediment, and Suspended Solids of 40 mg/l at a Depth of 34.4 cm.

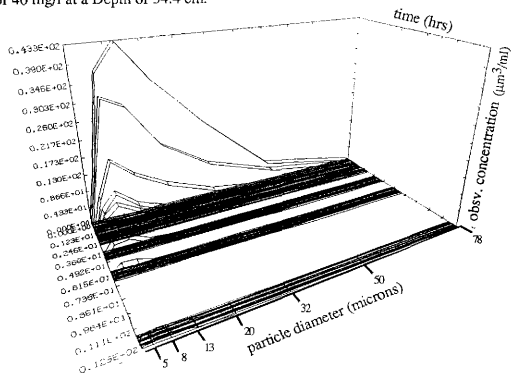


Fig. E75b.- Experiment 16: Heterogeneous Particle Volume-Based Observed Size Distribution with Shear of 10 sec^{-1} , Salinity of 15 ppt, Type A Sediment, and Suspended Solids of 40 mg/l at a Depth of 141.8 cm.

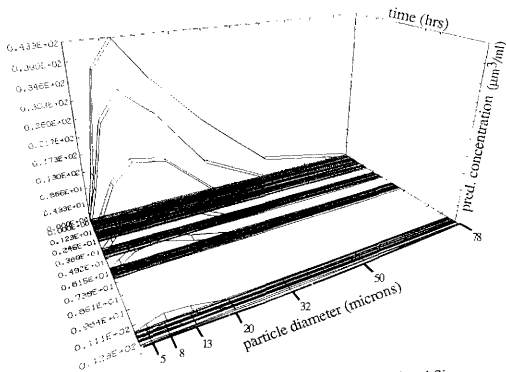


Fig. E76a.- Experiment 16: Heterogeneous Particle Volume-Based Predicted Size Distribution with Shear of 10 sec^{-1} , Salinity of 15 ppt, Type A Sediment, and Suspended Solids of 40 mg/l at a Depth of 34.4 cm.

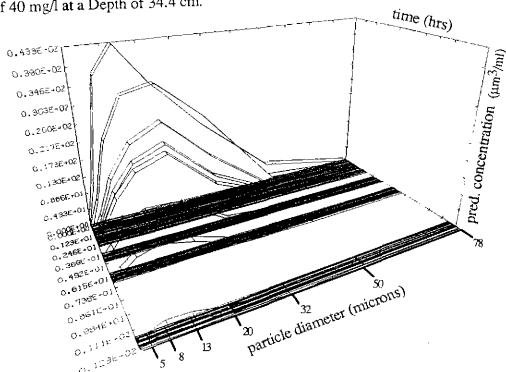


Fig. E76b.- Experiment 16: Heterogeneous Particle Volume-Based Predicted Size Distribution with Shear of 10 sec^{-1} , Salinity of 15 ppt, Type A Sediment, and Suspended Solids of 40 mg/l at a Depth of 141.8 cm.

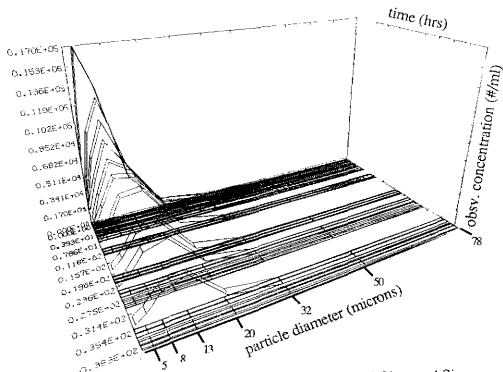


Fig. E77a.- Experiment 17: Heterogeneous Particle Number-Based Observed Size Distribution with Shear of 40 sec⁻¹, Salinity of 5 ppt, Type A Sediment, and Suspended Solids of 40 mg/l at a Depth of 34.4 cm.

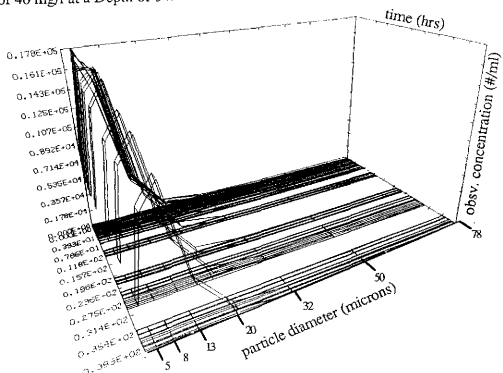


Fig. E77b.- Experiment 17: Heterogeneous Particle Number-Based Observed Size Distribution with Shear of 40 sec⁻¹, Salinity of 5 ppt, Type A Sediment, and Suspended Solids of 40 mg/l at a Depth of 141.8 cm.

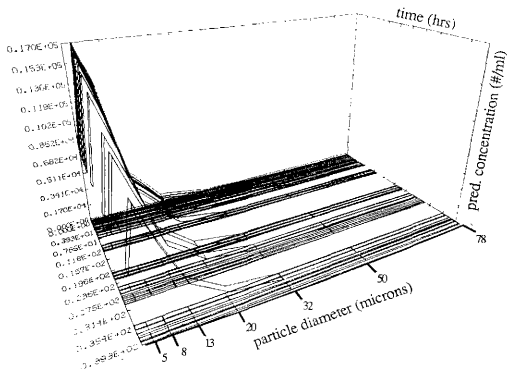


Fig. E78a.- Experiment 17: Heterogeneous Particle Number-Based Predicted Size Distribution with Shear of 40 sec⁻¹, Salinity of 5 ppt, Type A Sediment, and Suspended Solids of 40 mg/l at a Depth of 34.4 cm.

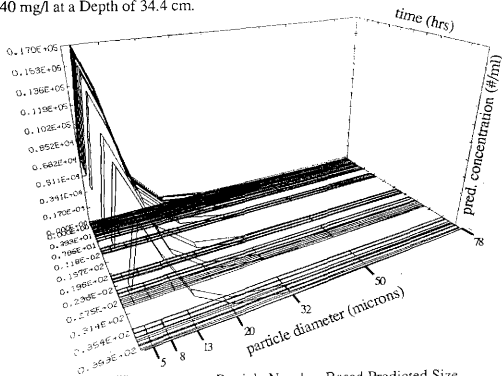


Fig. E78b.- Experiment 17: Heterogeneous Particle Number-Based Predicted Size Distribution with Shear of 40 sec⁻¹, Salinity of 5 ppt, Type A Sediment, and Suspended Solids of 40 mg/l at a Depth of 141.8 cm.

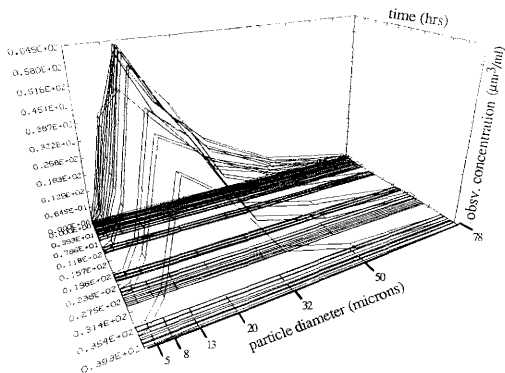


Fig. E79a.- Experiment 17: Heterogeneous Particle Volume-Based Observed Size Distribution with Shear of 40 sec⁻¹, Salinity of 5 ppt, Type A Sediment, and Suspended Solids of 40 mg/l at a Depth of 34.4 cm.

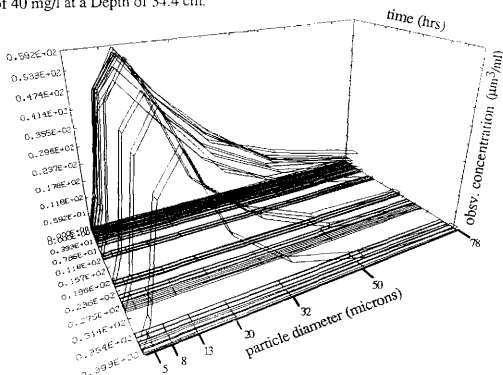


Fig. E79b.- Experiment 17: Heterogeneous Particle Volume-Based Observed Size Distribution with Shear of 40 sec⁻¹, Salinity of 5 ppt, Type A Sediment, and Suspended Solids of 40 mg/l at a Depth of 141.8 cm.

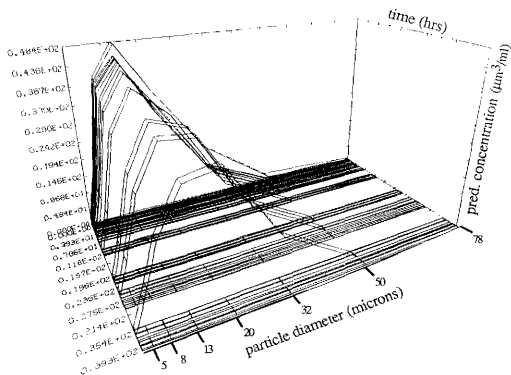


Fig. E80a.- Experiment 17: Heterogeneous Particle Volume-Based Predicted Size Distribution with Shear of 40 sec⁻¹, Salinity of 5 ppt, Type A Sediment, and Suspended Solids of 40 mg/l at a Depth of 34.4 cm.

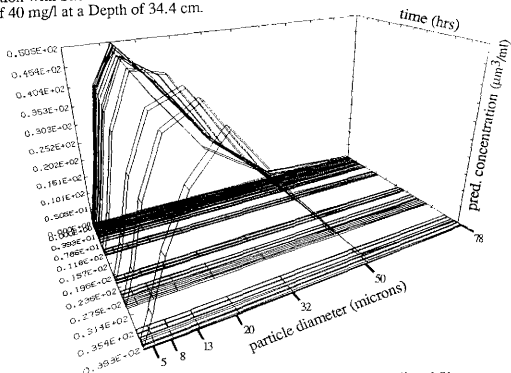


Fig. E80b.- Experiment 17: Heterogeneous Particle Volume-Based Predicted Size Distribution with Shear of 40 sec⁻¹, Salinity of 5 ppt, Type A Sediment, and Suspended Solids of 40 mg/l at a Depth of 141.8 cm.

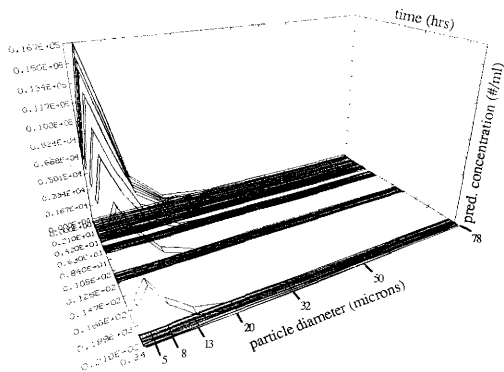


Fig. E81a.- Experiment 18: Heterogeneous Particle Number-Based Predicted Size Distribution with Shear of 20 sec⁻¹, Salinity of 15 ppt, Type A Sediment, and Suspended Solids of 40 mg/l at a Depth of 34.4 cm.

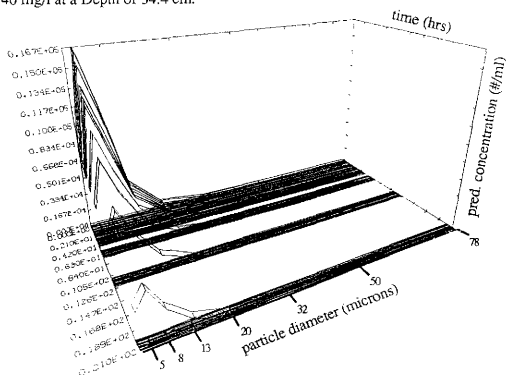


Fig. E81b.- Experiment 18: Heterogeneous Particle Number-Based Predicted Size Distribution with Shear of 20 sec⁻¹, Salinity of 15 ppt, Type A Sediment, and Suspended Solids of 40 mg/l at a Depth of 141.8 cm.

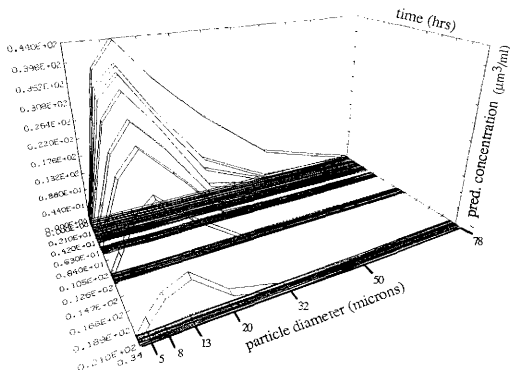


Fig. E82a.- Experiment 18: Heterogeneous Particle Volume-Based Predicted Size Distribution with Shear of 20 sec⁻¹, Salinity of 15 ppt, Type A Sediment, and Suspended Solids of 40 mg/l at a Depth of 34.4 cm.

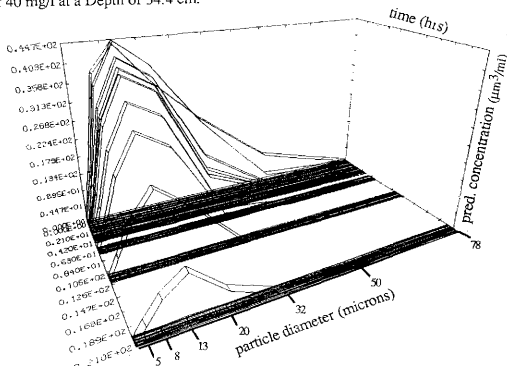


Fig. E82b.- Experiment 18: Heterogeneous Particle Volume-Based Predicted Size Distribution with Shear of 20 sec⁻¹, Salinity of 15 ppt, Type A Sediment, and Suspended Solids of 40 mg/l at a Depth of 141.8 cm.

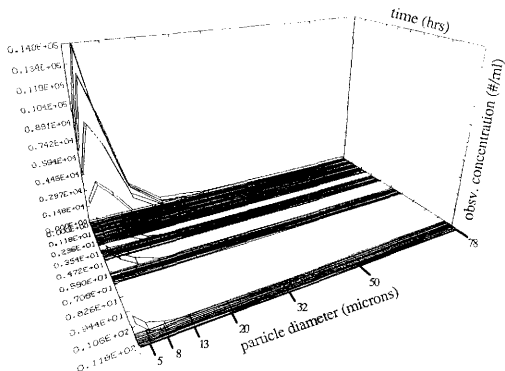


Fig. E83a.- Experiment 19: Heterogeneous Particle Number-Based Observed Size Distribution with Shear of 20 sec⁻¹, Salinity of 5 ppt, Type A Sediment, and Suspended Solids of 40 mg/l at a Depth of 34.4 cm.

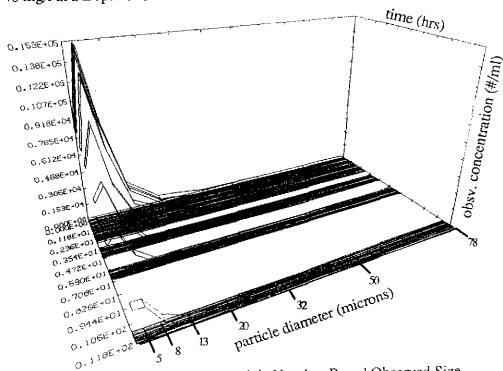


Fig. E83b.- Experiment 19: Heterogeneous Particle Number-Based Observed Size Distribution with Shear of 20 sec⁻¹, Salinity of 5 ppt, Type A Sediment, and Suspended Solids of 40 mg/l at a Depth of 141.8 cm.

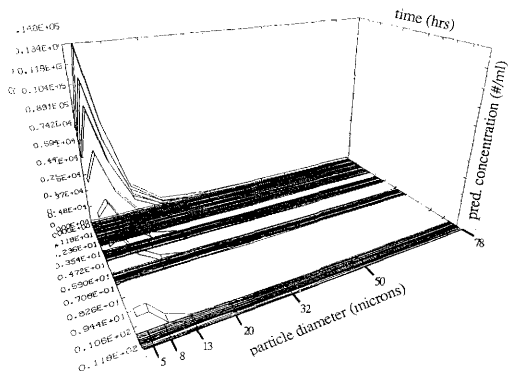


Fig. E84a.- Experiment 19: Heterogeneous Particle Number-Based Predicted Size Distribution with Shear of 20 sec-1, Salinity of 5 ppt, Type A Sediment, and Suspended Solids of 40 mg/l at a Depth of 34.4 cm.

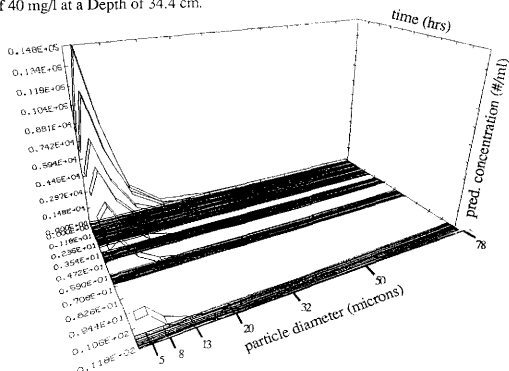


Fig. E84b.- Experiment 19: Heterogeneous Particle Number-Based Predicted Size Distribution with Shear of 20 sec-1, Salinity of 5 ppt, Type A Sediment, and Suspended Solids of 40 mg/l at a Depth of 141.8 cm.

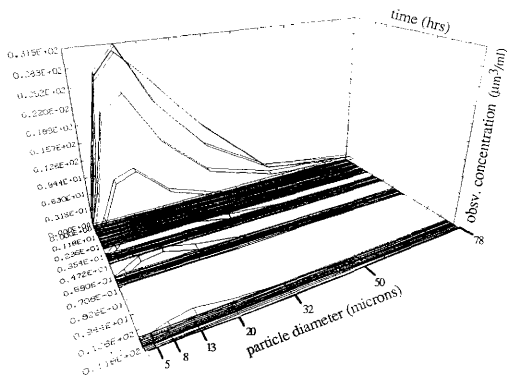


Fig. E85a.- Experiment 19: Heterogeneous Particle Volume-Based Observed Size Distribution with Shear of 20 sec⁻¹, Salinity of 5 ppt, Type A Sediment, and Suspended Solids of 40 mg/l at a Depth of 34.4 cm.

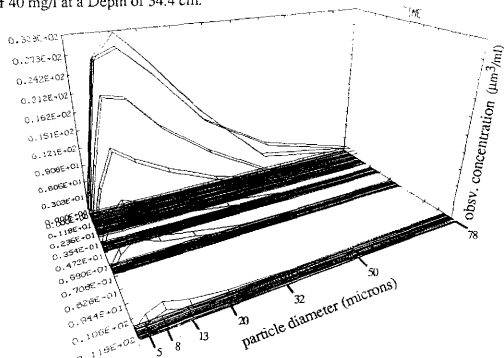


Fig. E85b.- Experiment 19: Heterogeneous Particle Volume-Based Observed Size Distribution with Shear of 20 sec⁻¹, Salinity of 5 ppt, Type A Sediment, and Suspended Solids of 40 mg/l at a Depth of 141.8 cm.

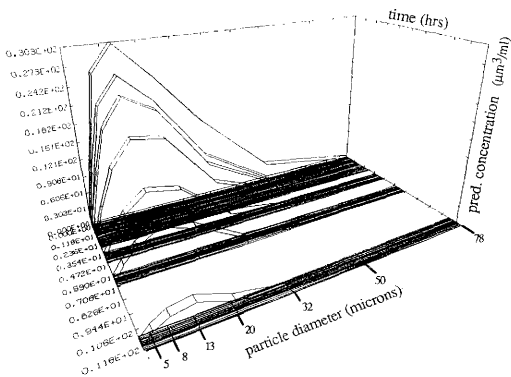


Fig. E86a.- Experiment 19: Heterogeneous Particle Volume-Based Predicted Size Distribution with Shear of 20 sec⁻¹, Salinity of 5 ppt, Type A Sediment, and Suspended Solids of 40 mg/l at a Depth of 34.4 cm.

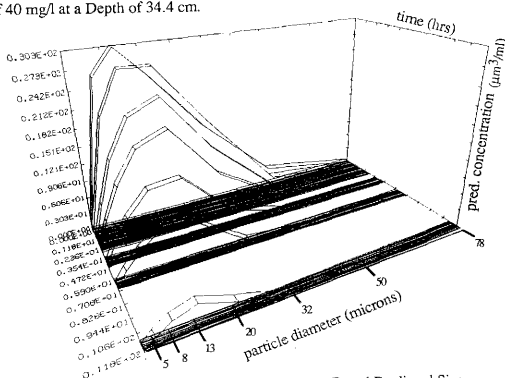


Fig. E86b.- Experiment 19: Heterogeneous Particle Volume-Based Predicted Size Distribution with Shear of 20 sec⁻¹, Salinity of 5 ppt, Type A Sediment, and Suspended Solids of 40 mg/l at a Depth of 141.8 cm.

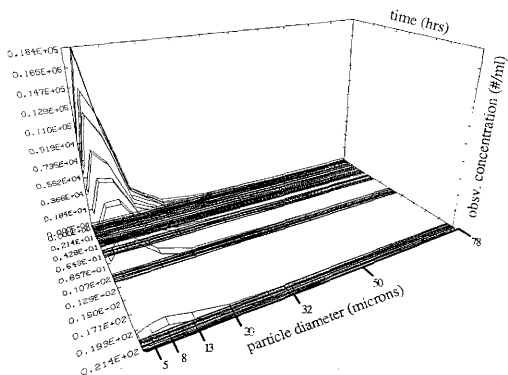


Fig. E87a.- Experiment 20: Heterogeneous Particle Number-Based Observed Size Distribution with Shear of 20 sec⁻¹, Salinity of 30 ppt, Type A Sediment, and Suspended Solids of 40 mg/l at a Depth of 34.4 cm.

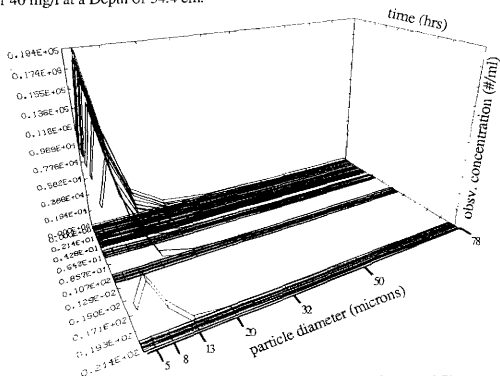


Fig. E87b.- Experiment 20: Heterogeneous Particle Number-Based Observed Size Distribution with Shear of 20 sec⁻¹, Salinity of 30 ppt, Type A Sediment, and Suspended Solids of 40 mg/l at a Depth of 141.8 cm.

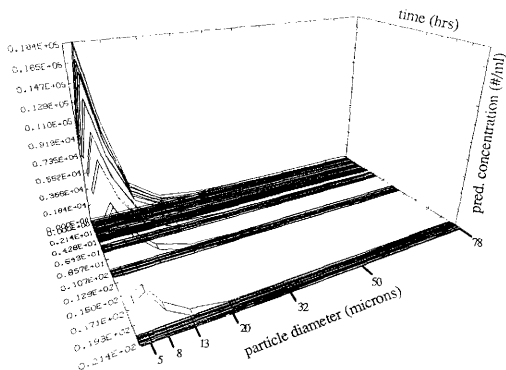


Fig. E88a.- Experiment 20: Heterogeneous Particle Number-Based Predicted Size Distribution with Shear of 20 sec⁻¹, Salinity of 30 ppt, Type A Sediment, and Suspended Solids of 40 mg/l at a Depth of 34.4 cm.

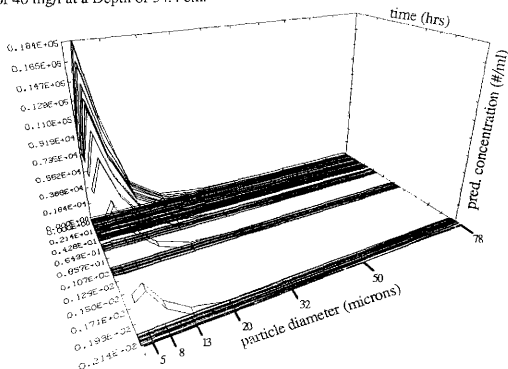


Fig. E88b.- Experiment 20: Heterogeneous Particle Number-Based Predicted Size Distribution with Shear of 20 sec⁻¹, Salinity of 30 ppt, Type A Sediment, and Suspended Solids of 40 mg/l at a Depth of 141.8 cm.

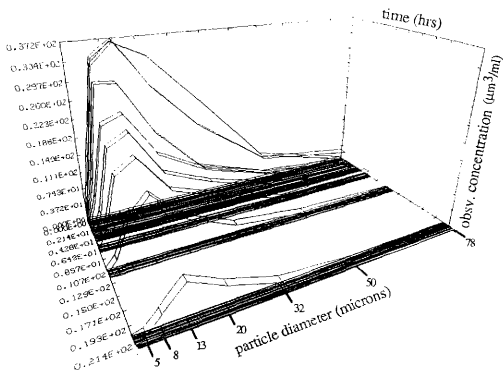


Fig. E89a.- Experiment 20: Heterogeneous Particle Volume-Based Observed Size Distribution with Shear of 20 sec⁻¹, Salinity of 30 ppt, Type A Sediment, and Suspended Solids of 40 mg/l at a Depth of 34.4 cm.

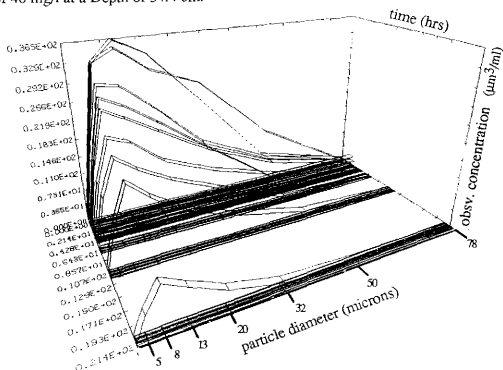


Fig. E89b.- Experiment 20: Heterogeneous Particle Volume-Based Observed Size Distribution with Shear of 20 sec⁻¹, Salinity of 30 ppt, Type A Sediment, and Suspended Solids of 40 mg/l at a Depth of 141.8 cm.

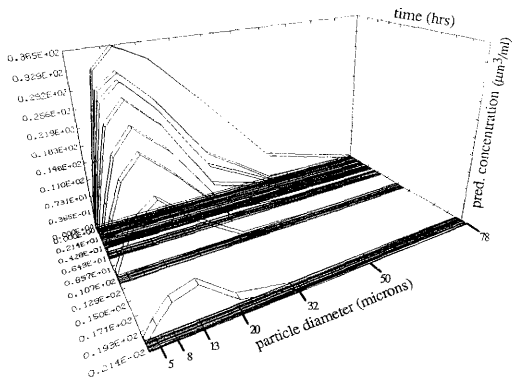


Fig. E90a.- Experiment 20: Heterogeneous Particle Volume-Based Predicted Size Distribution with Shear of 20 sec⁻¹, Salinity of 30 ppt, Type A Sediment, and Suspended Solids of 40 mg/l at a Depth of 34.4 cm.

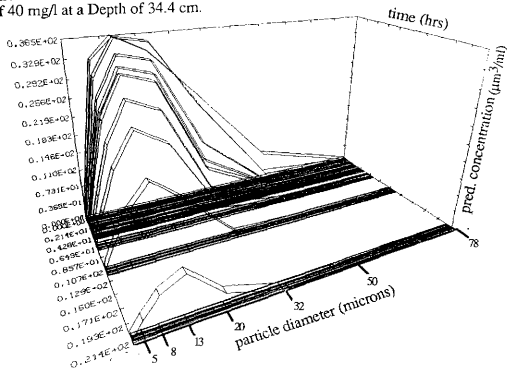


Fig. E90b.- Experiment 20: Heterogeneous Particle Volume-Based Predicted Size Distribution with Shear of 20 sec⁻¹, Salinity of 30 ppt, Type A Sediment, and Suspended Solids of 40 mg/l at a Depth of 141.8 cm.

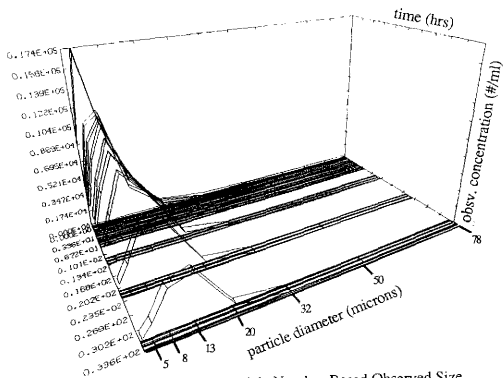


Fig. E91a.- Experiment 21: Heterogeneous Particle Number-Based Observed Size Distribution with Shear of 40 sec⁻¹, Salinity of 30 ppt, Type A Sediment, and Suspended Solids of 40 mg/l at a Depth of 34.4 cm.

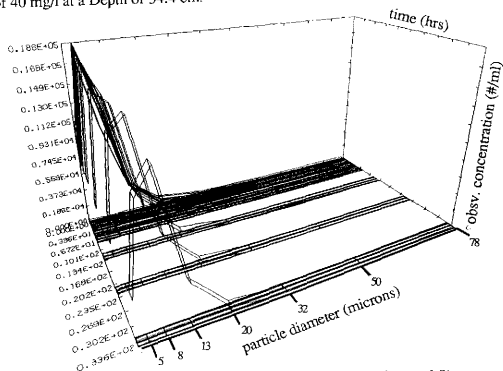


Fig. E91b.- Experiment 21: Heterogeneous Particle Number-Based Observed Size Distribution with Shear of 40 sec⁻¹, Salinity of 30 ppt, Type A Sediment, and Suspended Solids of 40 mg/l at a Depth of 141.8 cm.

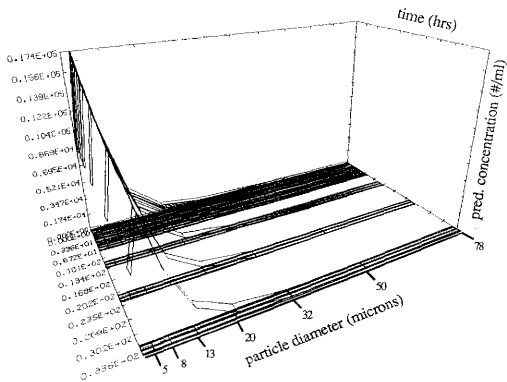


Fig. E92a.- Experiment 21: Heterogeneous Particle Number-Based Predicted Size Distribution with Shear of 40 sec^{-1} , Salinity of 30 ppt, Type A Sediment, and Suspended Solids of 40 mg/l at a Depth of 34.4 cm.

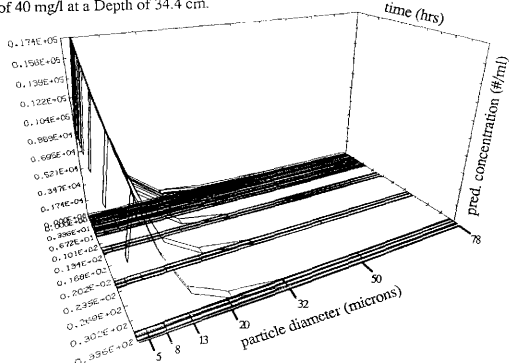


Fig. E92b.- Experiment 21: Heterogeneous Particle Number-Based Predicted Size Distribution with Shear of 40 sec^{-1} , Salinity of 30 ppt, Type A Sediment, and Suspended Solids of 40 mg/l at a Depth of 141.8 cm.

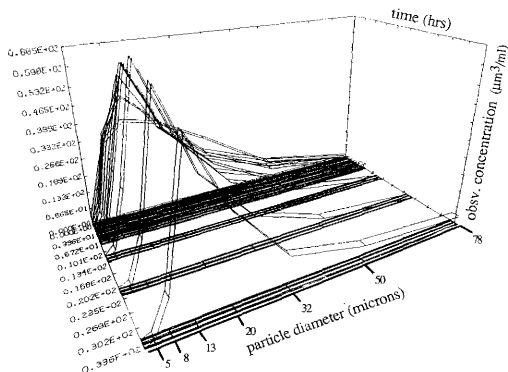


Fig. E93a.- Experiment 21: Heterogeneous Particle Volume-Based Observed Size Distribution with Shear of 40 sec⁻¹, Salinity of 30 ppt, Type A Sediment, and Suspended Solids of 40 mg/l at a Depth of 34.4 cm.

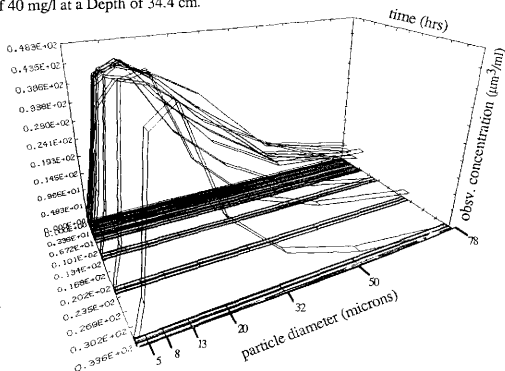


Fig. E93b.- Experiment 21: Heterogeneous Particle Volume-Based Observed Size Distribution with Shear of 40 sec⁻¹, Salinity of 30 ppt, Type A Sediment, and Suspended Solids of 40 mg/l at a Depth of 141.8 cm.

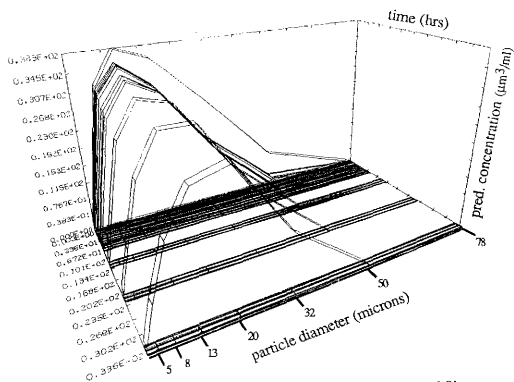


Fig. E94a.- Experiment 21: Heterogeneous Particle Volume-Based Predicted Size Distribution with Shear of 40 sec⁻¹, Salinity of 30 ppt, Type A Sediment, and Suspended Solids of 40 mg/l at a Depth of 34.4 cm.

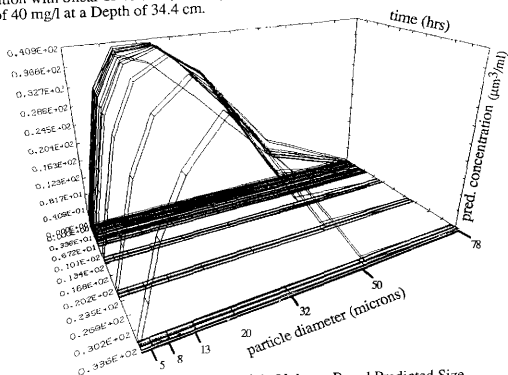


Fig. E94b.- Experiment 21: Heterogeneous Particle Volume-Based Predicted Size Distribution with Shear of 40 sec⁻¹, Salinity of 30 ppt, Type A Sediment, and Suspended Solids of 40 mg/l at a Depth of 141.8 cm.

APPENDIX F
STATISTICAL ANALYSIS

Statistical Analysis- Design 2

Alpha Values:

	I = 5	I = 15	I = 30	Totals
G = 20	0.30800	0.06830	0.09000	0.46630
G = 30	0.00180	0.01850	0.00800	0.02830
G = 40	0.00467	0.00468	0.00468	0.01403
Totals	0.31447	0.09148	0.10268	0.50863

Main interactions:

Shear rate: 0.01469

Salinity: 0.00351

Analysis of Variance:

	d.f.	s.s.	m.s.
Block (I)	2.00	0.01052	0.00526
Treatment (G)	8.00	0.04407	0.00551
Residual	16.00	0.02477	0.00155
Totals	26.00	0.07936	

Variance ratio: 3.56

'5 % level of significance based on 8/16 ratio: 2.59

Erosion Constant k:

	I = 5	I = 15	I = 30	Totals
G = 20	4.23E-09	3.27E-09	2.79E-09	1.03E-08
G = 30	1.66E-11	1.66E-09	1.74E-09	3.42E-09
G = 40	1.63E-10	1.63E-10	1.63E-10	4.89E-10
Totals	4.41E-09	5.09E-09	4.69E-09	1.42E-08

Main interactions:

Shear rate: 5.62E-18

Salinity: 2.62E-20

Analysis of Variance:

	d.f.	s.s.	m.s.
Block (I)	2.00	7.86E-20	3.93E-20
Treatment (G)	8.00	1.69E-17	2.11E-18
Residual	16.00	2.89E-18	1.81E-19
Totals	26.00	1.98E-17	

Variance ratio: 11.68

'5 % level of significance based on 8/16 ratio: 2.59

Geometric Mean:

	I = 5	I = 15	I = 30	Totals
G = 20	5.70E+01	5.40E+01	5.30E+01	1.64E+02
G = 30	8.60E+01	8.60E+01	8.30E+01	2.55E+02
G = 40	8.60E+01	8.60E+01	8.60E+01	2.58E+02
Totals	2.29E+02	2.26E+02	2.22E+02	6.77E+02

Main interactions:

Shear rate: 6.34E+02

Salinity: 2.74E+00

Analysis of Variance:

	d.f.	s.s.	m.s.
Block (I)	2.00	8.22E+00	4.11E+00
Treatment (G)	8.00	1.90E+03	2.38E+02
Residual	16.00	6.44E+00	4.03E-01
Totals	26.00	1.91E+03	

Variance ratio: 590.55

'5 % level of significance based on 8/16 ratio: 2.59

Geometric standard deviation:

	I = 5	I = 15	I = 30	Totals
G = 20	11.60	9.72	9.76	31.08
G = 30	11.60	11.62	11.43	34.65
G = 40	16.40	16.47	16.41	49.28
Totals	39.60	37.81	37.60	115.01

Main interactions:

Shear rate: 20.67

Salinity: 0.27

Analysis of Variance:

	d.f.	s.s.	m.s.
Block (I)	2.00	0.81	0.40
Treatment (G)	8.00	62.00	7.75
Residual	16.00	1.53	0.10
Totals	26.00	64.33	

Variance ratio: 81.23

'5 % level of significance based on 8/16 ratio: 2.59

Resuspension constant:

	I = 5	I = 15	I = 30	Totals
G = 20	0.615	0.025	0.018	0.657
G = 30	0.272	0.272	0.444	0.988
G = 40	1.490	1.490	1.490	4.470
Totals	2.377	1.787	1.952	6.115

Main interactions:
 Shear rate: 0.991
 Salinity: 0.021

Analysis of Variance:

	d.f.	s.s.	m.s.
Block (I)	2.00	0.062	0.031
Treatment (G)	8.00	2.974	0.372
Residual	16.00	0.193	0.012
Totals	26.00	3.229	

Variance ratio: 30.85

'5 % level of significance based on 8/16 ratio: 2.59

Statistical Analysis- Design 3

NOTE: The values for Type B, Salinity 30 were assumed to be the same as those for Type A and C at salinity 30 ppt.

Alpha Values:

	Type A	Type B	Type C	Totals
I = 5	0.30800	0.30800	0.30800	0.92400
I = 15	0.06800	0.06800	0.06800	0.20400
I = 30	0.08990	0.08990	0.08990	0.26970
Totals	0.46590	0.46590	0.46590	1.39770

Main interactions:

Salinity: 0.03522

Type: 0.00000

Analysis of Variance:

	d.f.	s.s.	m.s.
Block (T)	2.00	0.00000	0.00000
Treatment (I)	8.00	0.10565	0.01321
Residual	16.00	0.00000	0.00000
Totals	26.00	0.10565	

Variance ratio: -761268448999570.00

'5 % level of significance based on 8/16 ratio: 2.59

Erosion Constant k:

	Type A	Type B	Type C	Totals
I = 5	4.23E-09	4.23E-09	4.23E-09	1.27E-08
I = 15	3.27E-09	3.27E-09	3.27E-09	9.81E-09
I = 30	2.79E-09	2.79E-09	2.79E-09	8.37E-09
Totals	1.03E-08	1.03E-08	1.03E-08	3.09E-08

Main interactions:
 Salinity: 1.08E-18
 Type: 3.08E-32

Analysis of Variance:

	d.f.	s.s.	m.s.
Block (T)	2.00	7.40E-32	3.70E-32
Treatment (I)	8.00	3.23E-18	4.03E-19
Residual	16.00	0.00E+00	0.00E+00
Totals	26.00	3.23E-18	

Variance ratio: *****
 '5 % level of significance based on 8/16 ratio: 2.59

Geometric Mean:

	Type A	Type B	Type C	Totals
I = 5	5.70E+01	5.70E+01	5.70E+01	1.71E+02
I = 15	5.40E+01	5.40E+01	5.40E+01	1.62E+02
I = 30	5.30E+01	5.30E+01	5.30E+01	1.59E+02
Totals	1.64E+02	1.64E+02	1.64E+02	4.92E+02

Main interactions:
 Salinity: 8.67E+00
 Type: 0.00E+00

Analysis of Variance:

	d.f.	s.s.	m.s.
Block (T)	2.00	0.00E+00	0.00E+00
Treatment (I)	8.00	2.60E+01	3.25E+00
Residual	16.00	0.00E+00	0.00E+00
Totals	26.00	2.60E+01	

Variance ratio: *****
 '5 % level of significance based on 8/16 ratio: 2.59

Geometric standard deviation:

	Type A	Type B	Type C	Totals
I = 5	11.60	11.60	11.60	34.80
I = 15	9.72	9.72	9.70	29.14
I = 30	9.76	9.76	9.76	29.28
Totals	31.08	31.08	31.06	93.22

Main interactions:
 Salinity: 2.32
 Type: 0.00

Analysis of Variance:

	d.f.	s.s.	m.s.
Block (T)	2.00	0.00	0.00
Treatment (I)	8.00	6.95	0.87
Residual	16.00	0.00	0.00
Totals	26.00	6.95	

Variance ratio: 78157.00

'5 % level of significance based on 8/16 ratio: 2.59

Resuspension constant:

	Type A	Type B	Type C	Totals
I = 5	0.6148	0.0061	0.0061	0.6270
I = 15	0.0250	0.0250	0.0250	0.0750
I = 30	0.0175	0.0175	0.0175	0.0525
Totals	0.6573	0.0486	0.0486	0.7545

Main interactions:

Block (T)	0.024
Treatment (I)	0.027

Analysis of Variance:

	d.f.	s.s.	m.s.
Block (I)	2.00	0.082	0.041
Treatment (G)	8.00	0.071	0.009
Residual	16.00	0.165	0.010
Totals	26.00	0.318	

Variance ratio: 0.86

'5 % level of significance based on 8/16 ratio: 2.59

APPENDIX G

RECOMMENDATIONS

1. Increase particle concentration in the column. Develop a dilution procedure for these higher concentrations.
2. Improve the procedure for reproducing desired initial particle concentrations within the column. Investigate suspended solids relationship to particle size distributions.
3. Add a freshwater study to compare with salinity studies.
4. Perform studies in the 0 to 5 ppt salinity range. This range is the most dynamic and requires further investigation.
5. Decrease the shear rates , 5 to 10 sec^{-1} , and add a quiescent study.
6. Include porosity in modeling efforts.
7. Exclude resuspension term when working with low particle concentrations.
8. Use a taller column to test spatial scaling.

VITA

Stephanie Carol Sanders was born in Dallas, Texas on February 10, 1965. She grew up in Rosenberg, Texas where she attended B.F. Terry High School and graduated as valedictorian. She was a member of the Rangerettes Drill Team, student council, drama club, and National Honor Society. In 1983, she began a B.S. degree at Texas A&M University in Ocean Engineering which was completed in 1988. She was a member of the Opera and Performing Arts Society and the Omega Epsilon Honor Society. In 1988 she began working towards a M.S. degree in Civil Engineering, specializing in environmental engineering. Upon completion of this degree, she will begin a career as an Associate Environmental Engineer with the Environmental and Safety Department of Marathon Oil Company, P.O. Box 190168, Anchorage, Alaska, 99519.